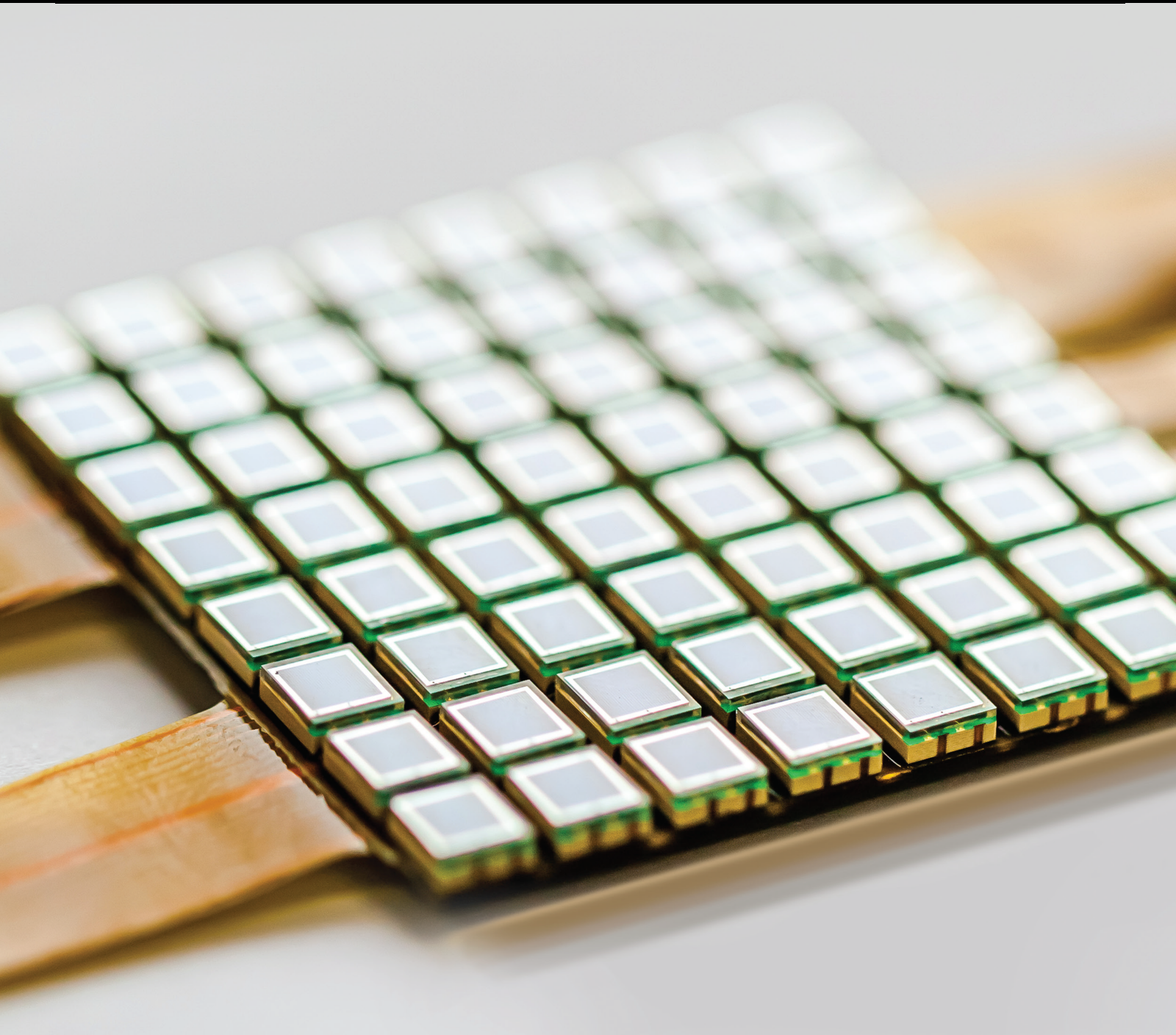


Green Wireless Sensor Networks

Lead Guest Editor: Mario E. Rivero-Angeles

Guest Editors: Ricardo Menchaca-Mendez, Rolando Menchaca-Mendez,
and Israel Leyva-Mayorga





Green Wireless Sensor Networks

Green Wireless Sensor Networks

Lead Guest Editor: Mario E. Rivero-Angeles
Guest Editors: Ricardo Menchaca-Mendez,
Rolando Menchaca-Mendez, and Israel Leyva-
Mayorga





Copyright © 2021 Hindawi Limited. All rights reserved.

This is a special issue published in "Journal of Sensors." All articles are open access articles distributed under the Creative Commons Attribution License, which permits unrestricted use, distribution, and reproduction in any medium, provided the original work is properly cited.

Chief Editor

Harith Ahmad , Malaysia

Associate Editors

Duo Lin , China
Fanli Meng , China
Pietro Siciliano , Italy
Guiyun Tian, United Kingdom

Academic Editors

Ghufran Ahmed , Pakistan
Constantin Apetrei, Romania
Shonak Bansal , India
Fernando Benito-Lopez , Spain
Romeo Bernini , Italy
Shekhar Bhansali, USA
Matthew Brodie, Australia
Ravikumar CV, India
Belén Calvo, Spain
Stefania Campopiano , Italy
Binghua Cao , China
Domenico Caputo, Italy
Sara Casciati, Italy
Gabriele Cazzulani , Italy
Chi Chiu Chan, Singapore
Sushank Chaudhary , Thailand
Edmon Chehura , United Kingdom
Marvin H Cheng , USA
Lei Chu , USA
Mario Collotta , Italy
Marco Consales , Italy
Jesus Corres , Spain
Andrea Cusano, Italy
Egidio De Benedetto , Italy
Luca De Stefano , Italy
Manel Del Valle , Spain
Franz L. Dickert, Austria
Giovanni Diraco, Italy
Maria de Fátima Domingues , Portugal
Nicola Donato , Italy
Sheng Du , China
Amir Elzwawy, Egypt
Mauro Epifani , Italy
Congbin Fan , China
Lihang Feng, China
Vittorio Ferrari , Italy
Luca Francioso, Italy





Libo Gao , China
Carmine Granata , Italy
Pramod Kumar Gupta , USA
Mohammad Haider , USA
Agustin Herrera-May , Mexico
María del Carmen Horrillo, Spain
Evangelos Hristoforou , Greece
Grazia Iadarola , Italy
Syed K. Islam , USA
Stephen James , United Kingdom
Sana Ullah Jan, United Kingdom
Bruno C. Janegitz , Brazil
Hai-Feng Ji , USA
Shouyong Jiang, United Kingdom
Roshan Prakash Joseph, USA
Niravkumar Joshi, USA
Rajesh Kaluri , India
Sang Sub Kim , Republic of Korea
Dr. Rajkishor Kumar, India
Rahul Kumar , India
Nageswara Lalam , USA
Antonio Lazaro , Spain
Chengkuo Lee , Singapore
Chenzong Li , USA
Zhi Lian , Australia
Rosalba Liguori , Italy
Sangsoon Lim , Republic of Korea
Huan Liu , China
Jin Liu , China
Eduard Llobet , Spain
Jaime Lloret , Spain
Mohamed Louzazni, Morocco
Jesús Lozano , Spain
Oleg Lupan , Moldova
Leandro Maio , Italy
Pawel Malinowski , Poland
Carlos Marques , Portugal
Eugenio Martinelli , Italy
Antonio Martinez-Olmos , Spain
Giuseppe Maruccio , Italy
Yasuko Y. Maruo, Japan
Zahid Mehmood , Pakistan
Carlos Michel , Mexico
Stephen. J. Mihailov , Canada
Bikash Nakarmi, China

Ehsan Namaziandost , Iran
Heinz C. Neitzert , Italy
Sing Kiong Nguang , New Zealand
Calogero M. Oddo , Italy
Tinghui Ouyang, Japan
SANDEEP KUMAR PALANISWAMY ,
India
Alberto J. Palma , Spain
Davide Palumbo , Italy
Abinash Panda , India
Roberto Paolesse , Italy
Akhilesh Pathak , Thailand
Giovanni Pau , Italy
Giorgio Pennazza , Italy
Michele Penza , Italy
Sivakumar Poruran, India
Stelios Potirakis , Greece
Biswajeet Pradhan , Malaysia
Giuseppe Quero , Italy
Linesh Raja , India
Maheswar Rajagopal , India
Valerie Renaudin , France
Armando Ricciardi , Italy
Christos Riziotis , Greece
Ruthber Rodriguez Serrezuela , Colombia
Maria Luz Rodriguez-Mendez , Spain
Jerome Rossignol , France
Maheswaran S, India
Ylias Sabri , Australia
Sourabh Sahu , India
José P. Santos , Spain
Sina Sareh, United Kingdom
Isabel Sayago , Spain
Andreas Schütze , Germany
Praveen K. Sekhar , USA
Sandra Sendra, Spain
Sandeep Sharma, India
Sunil Kumar Singh Singh , India
Yadvendra Singh , USA
Afaque Manzoor Soomro , Pakistan
Vincenzo Spagnolo, Italy
Kathiravan Srinivasan , India
Sachin K. Srivastava , India
Stefano Stassi , Italy

Danfeng Sun, China
Ashok Sundramoorthy, India
Salvatore Surdo , Italy
Roshan Thotagamuge , Sri Lanka
Guiyun Tian , United Kingdom
Sri Ramulu Torati , USA
Abdellah Touhafi , Belgium
Hoang Vinh Tran , Vietnam
Aitor Urrutia , Spain
Hana Vaisocherova - Lislalova , Czech
Republic
Everardo Vargas-Rodriguez , Mexico
Xavier Vilanova , Spain
Stanislav Vitek , Czech Republic
Luca Vollero , Italy
Tomasz Wandowski , Poland
Bohui Wang, China
Qihao Weng, USA
Penghai Wu , China
Qiang Wu, United Kingdom
Yuedong Xie , China
Chen Yang , China
Jiachen Yang , China
Nitesh Yelve , India
Aijun Yin, China
Chouki Zerrouki , France



Contents

A Binary Adaptive Clone Shuffled Frog Leaping Algorithm for Three-Dimensional Low-Energy Target Coverage Optimization in Environmental Monitoring Wireless Sensor Networks

Bao Liu , Rui Yang , Mengying Xu , and Jie Zhou 




Research Article (15 pages), Article ID 4510335, Volume 2021 (2021)

Elite Adaptive Simulated Annealing Algorithm for Maximizing the Lifespan in LSWSNs

Jie Zhou , Wenxian Jia, Menghan Liu, and Mengying Xu 


Research Article (11 pages), Article ID 9915133, Volume 2021 (2021)

An Adaptive Immune Ant Colony Optimization for Reducing Energy Consumption of Automatic Inspection Path Planning in Industrial Wireless Sensor Networks

Chaoqun Li , Jing Xiao, Yang Liu, Guohong Qi , Hu Qin, and Jie Zhou 






Research Article (11 pages), Article ID 9960043, Volume 2021 (2021)

Minimization of Energy Consumption for Routing in High-Density Wireless Sensor Networks Based on Adaptive Elite Ant Colony Optimization

Jing Xiao, Chaoqun Li, and Jie Zhou 






Research Article (12 pages), Article ID 5590951, Volume 2021 (2021)

Analysis and Design of a Wireless Sensor Network Based on the Residual Energy of the Nodes and the Harvested Energy from Mint Plants

Hassel Aurora Alcalá-Garrido , Víctor Barrera-Figueroa , Mario E. Rivero-Ángeles , Yunia Verónica García-Tejeda , and Hosanna Ramírez Pérez 

Research Article (26 pages), Article ID 6655967, Volume 2021 (2021)

An Improved Triggering Updating Method of Interest Message with Adaptive Threshold Determination for Directed Diffusion Routing Protocol

Jun Wang , Xiaohang Liu , Zhitao He , Yadan Zhang , and Song Gao 

Research Article (15 pages), Article ID 8814839, Volume 2021 (2021)

Research Article

A Binary Adaptive Clone Shuffled Frog Leaping Algorithm for Three-Dimensional Low-Energy Target Coverage Optimization in Environmental Monitoring Wireless Sensor Networks

Bao Liu , Rui Yang , Mengying Xu , and Jie Zhou 

College of Information Science and Technology, Shihezi University, Shihezi 832000, China

Correspondence should be addressed to Jie Zhou; jiezhou@shzu.edu.cn

Received 23 April 2021; Accepted 31 August 2021; Published 13 September 2021

Academic Editor: Mario E. Rivero-Angeles

Copyright © 2021 Bao Liu et al. This is an open access article distributed under the Creative Commons Attribution License, which permits unrestricted use, distribution, and reproduction in any medium, provided the original work is properly cited.

In recent years, more and more researchers have paid attention to the three-dimensional target coverage of environmental monitoring wireless sensor networks (EMWSNs) under real environmental conditions. However, the target coverage method studied in the traditional two-dimensional plane is full of loopholes when applied in the real three-dimensional physical world. Most coverage algorithms usually only optimize for a single problem of target coverage or network energy consumption and cannot reduce network energy consumption while improving coverage. This paper proposes a novel binary adaptive clone shuffled leapfrog algorithm (BACSFLA) suitable for EMWSNs. BACSFLA has an excellent performance in the coverage of three-dimensional nodes, which can significantly reduce the network energy consumption of ENWSNs in the coverage process, and greatly improve the coverage of nodes. Through simulation experiments, BACSFLA was compared with simulated annealing (SA) and genetic algorithm (GA) in the same conditional parameters. The coverage rate of BACSFLA in EMWSNs is 3.9% higher than that of GA and 5.4% higher than that of SA. The network energy consumption of BACSFLA is 36.0% lower than GA and 35.9% lower than SA. Moreover, BACSFLA can significantly reduce the calculation time and get better results in a shorter time.

1. Introduction

EMWSN is a self-organizing network composed of sensor nodes deployed in the environmental monitoring area. The nodes have the characteristics of small size, low cost, and low-power consumption. They can perceive, collect, and process the information of the monitored objects in real-time. Coverage optimization is a basic problem of EMWSNs. The proper coverage of EMWSN nodes will directly affect network performance and network life. Therefore, the coverage optimization of EMWSN nodes has always been a hot issue of concern and research by scholars. In recent years, some researchers have made breakthroughs in improving the energy efficiency and coverage of wireless sensor networks (WSNs) [1, 2].

The primary purpose of EMWSN coverage is to expand its monitoring range and increase the coverage of the target and secondly to ensure certain network performance. At

present, most of the research on covering this basic problem by researchers is carried out in an ideal two-dimensional environment [3]. However, most of the actual application scenarios of EMWSNs are in the three-dimensional environment, and the coverage method studied in the two-dimensional plane will have very bad performance when applied in the real three-dimensional physical world. Because the space and surface location of the target in the real world is mostly in the environment of agriculture, forestry, and wild [4]. It is urgent to design coverage perception models and corresponding algorithms that conform to three-dimensional scenes, to improve the practical applicability of EMWSNs. At the same time, EMWSNs need to further design more complete 3D perception models and effective coverage optimization algorithms. The impact of space size, target, and the number of sensor monitoring nodes on the coverage performance of wireless sensor networks is extremely important [5].

Target coverage is generally used to reflect the sensing ability of EMWSNs to the objective world and can also be used as a standard to measure the quality of network monitoring services [6]. The coverage of EMWSNs reflects the quality of EMWSNs' monitoring of target areas and target nodes and is the basis for providing perception services required by the system. Through the coverage control technology, the space allocation of the network can also be optimized, and the tasks of object perception, information acquisition, and data transmission can be completed more energy-saving and efficient [7]. Coverage optimization control is one of the key technologies for network construction and normal network operation. Target coverage optimization directly affects network performance indicators such as network energy consumption and network monitoring area [8].

Due to the particularity of the application environment of EMWSNs, in most cases, the staff cannot reach it on the spot. Sensor nodes can only be distributed in the target area reached by aircraft [9]. The throwing process is simple and random [10]. How to use a limited number of sensor nodes to monitor the coverage of the target area to the maximum extent, build a reliable sensor network, and maximize the network's monitoring efficiency of the target area has always been one of the research hotspots of EMWSN technology [11].

Based on the above background, this article is aimed at improving the 3D coverage of EMWSNs and saving network energy consumption in the real application environment. This article focuses on the 3D perception model close to the actual application environment and the corresponding 3D coverage deployment method. EMWSN coverage optimization method. By designing coverage perception models and corresponding algorithms that are closer to the real 3D application environment, the applicability of EMWSN coverage in real-life environments can be effectively improved. Besides, taking into account performance indicators such as network energy consumption based on meeting coverage requirements is also of practical significance in terms of improving network perceived service quality [12].

Literature [13] proposed a new coverage optimization algorithm for WSNs based on SA optimization. SA can significantly improve the global optimization capability of the algorithm and has the characteristics of fast convergence. The results show that SA can improve network coverage efficiency and reduce node energy consumption. However, the algorithm is simulated in a two-dimensional environment, and its robustness is poor, and it has little reference significance in the real environment.

Literature [14] proposed an improved GA to optimize the coverage efficiency of WSNs. The result is that the improved GA is better than other intelligent optimization algorithms in the coverage process of WSNs and has better performance than the immune algorithm and the whale optimization algorithm. The improved GA is better than the comparison algorithm in coverage, network overhead, and stability. However, the algorithm's convergence performance is poor, the convergence speed is slow, and the calculation complexity is relatively large. And because three-

dimensional environmental factors are not considered, the performance of the algorithm, in reality, cannot be evaluated.

Literature [15] proposed a new type of GA with efficient coverage, which has very good performance in WSNs. The algorithm combines an improved crossover operator, which can maintain high accuracy in the fitness function calculation. The result is that the quality and stability of the solution of this algorithm are better than that of the comparison algorithm. However, the algorithm does not consider the network energy consumption during the coverage process, and the network overhead cannot be estimated. Moreover, since the simulation environment of the algorithm is performed in a two-dimensional ideal plane, the performance in a three-dimensional real environment may be quite different from the ideal result.

Literature [16] proposed a new heuristic algorithm based on a GA to optimize the target coverage of WSNs. This algorithm can extend the life of the network to a large extent and has a faster convergence speed and better performance than the comparison algorithm. However, this algorithm greatly increases the complexity of the algorithm, and if it encounters a high-density three-dimensional network, poor results may occur.

Literature [17] proposed an improved greedy algorithm to extend the network lifetime of WSNs. A greedy algorithm has the characteristics of simple structure, easy implementation, fast convergence, and strong robustness. The results show that the algorithm can significantly improve the survival time of the network and has a faster convergence rate compared with the comparison algorithm. However, since only the network lifetime is considered, the optimal effect is not achieved in terms of coverage.

Literature [18] proposed an improved Bat algorithm to improve the coverage efficiency of 3D WSNs. The algorithm takes into account the harsh environment in the three-dimensional space and adopts a multiobjective optimization strategy to improve the coverage rate while reducing network energy consumption. The results show that compared with the comparison algorithm, this algorithm can reduce the energy consumption of nodes by a greater degree of uniform node energy. However, the global search of the algorithm is not strong, the convergence is also poor, and the implementation is relatively complicated.

The main contributions of this paper are as follows:

- (1) This paper proposes a new target coverage model for EMWSNs. The model uses a binary coding scheme, which can greatly reduce the computational complexity and speed up the calculation. And for the three-dimensional coverage of the nodes in EMWSNs, a 3D target coverage model was constructed to extend the traditional planar coverage to spatial coverage. Because the model has strong stability, it can also have excellent performance in real-world EMWSNs
- (2) This paper proposes an improved target coverage algorithm. Based on the selection of the optimal

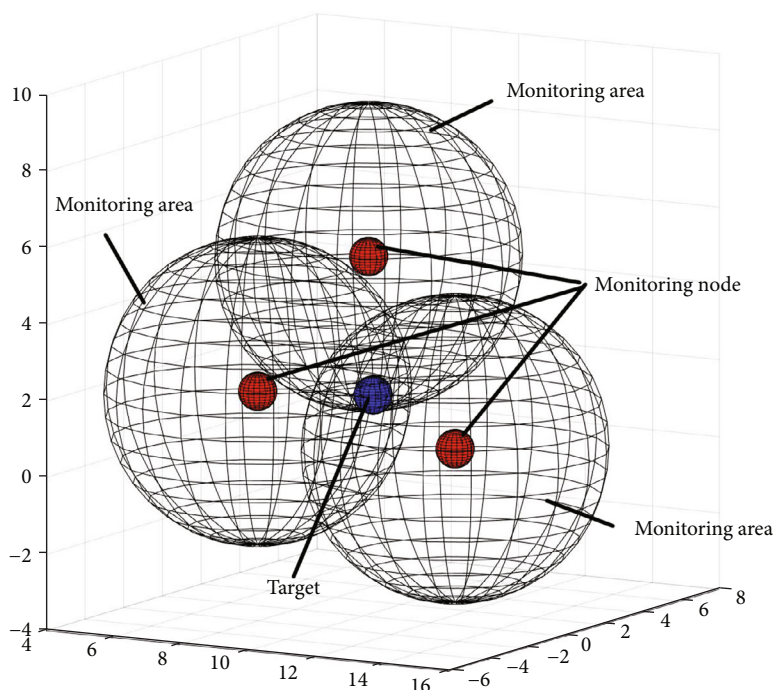


FIGURE 1: EMWSN target coverage.

target coverage node-set, BACSFLA considers the energy consumption of the nodes, which can greatly improve the coverage optimization performance and network energy consumption of EMWSNs. Because BACSFLA combines adaptive operators and clone operators, it has good global search performance and can get the optimal solution in a short time. Compared with the two-dimensional space, the three-dimensional space has an increase of an order of magnitude in both the complexity and the amount of calculation. Compared with the comparison algorithm, BACSFLA has a faster convergence speed, higher coverage, and lower network in three-dimensional space

- (3) This paper proposes an improved low-power clone selection operator. This operator is aimed at reducing network energy consumption. For individuals to be cloned, a certain cloning ratio is used to generate a new population according to the energy consumption. The results show that using this operator not only does not increase the amount of calculation of the algorithm but also can significantly reduce network energy consumption

The structure of this article is as follows. Section 2 introduces the target coverage model and binary coding scheme of EMWSNs. Section 3 uses BACSFLA to optimize the target coverage algorithm. Section 4 presents the results of simulation experiments and discusses the performance of BACSFLA in comparison with other algorithms in EMWSNs. Then, Section 5 concludes.

2. EMWSN Target Coverage Model

EMWSN is a network system composed of a large number of sensor nodes deployed in monitoring areas such as forests, grasslands, and oceans. It is self-organized through wireless communication. It mainly cooperatively senses, collects, and processes the information of the sensed objects in the network coverage area [19]. And send it to the monitor.

EMWSN node deployment methods can be divided into static deployment, dynamic deployment, and hybrid deployment. Considering that the environment of EMWSNs is usually more complicated and harsh, the simulation environment in this article is static deployment. In this case, sensor nodes can usually be deployed in the area to be monitored in a deterministic or random manner, and generally, no longer move after deployment [20].

According to the classification of application attributes, the coverage of EMWSNs can be divided into area coverage, target coverage, and barrier coverage, which, respectively, cover the entire area and certain fixed points or paths in the area [21]. This article uses the target coverage model. Target coverage studies the realization of the perception of special locations or monitoring points in the area to be covered. The model where the target is successfully covered in the 3D environment is shown in Figure 1.

In EMWSNs, the monitoring node must not only monitor the target but also estimate the area where the target is located, so when the target is covered by three or more sensor monitoring nodes, the target can be guaranteed to be successfully covered. When covering, energy-saving coverage should be considered. If sensor monitoring nodes are randomly distributed, to maximize the network survival

time and monitor reliability, this paper sets the goal of the minimum number of sensor monitoring nodes successfully covered to three.

This article uses a probabilistic perception model. Considering the complexity of the actual application environment, the probabilistic model can more reasonably represent the perception characteristics of sensor nodes [22]. In actual EMWSNs, the various sensing signals of the sensors will attenuate with the increase of the propagation distance, and the sensor nodes deployed in the field will also be interfered with by various environmental noises. When the target is very close to the sensor monitoring node, the sensor monitoring node can be sure to detect the target. As the distance between the target and the sensor monitoring node increases, the sensing signal strength gradually attenuates and is subject to various interferences [23]. And the detection ability of the target increases with the increase of the distance shows a gradual weakening trend, which affects the certainty of the target detection by the sensor monitoring node [24].

For any sensor node l_m , its maximum sensing radius is k_l , and the sensing area is divided into a definite sensing area and a probability sensing area according to the Euclidean distance from l_m , denoted as C_l^a and C_l^b , where the definite sensing radius of the area is k_l^a . For the target r_n in space, if the point is in C_l^a , the monitoring probability of the sensor monitoring node l_m when the target is located at the point r_n is 1. If the point is in C_l^b , the detection probability of the sensor when the target is located at r_n decreases as the Euclidean distance between the target and the sensor increases; if the target is located outside the sensing area, the target cannot be detected when the target is located at r_n . The sensor node l_m is detected. The coordinates of l_m are (t_m, w_m, v_m) , and the coordinates of r_n are (t_n, w_n, v_n) . In the probabilistic perception model, the probability $d(l_m, r_n)$ that is detected by the sensor l_m when the target is located at r_n is

$$d(l_m, r_n) = \begin{cases} 1, & u(l_m, r_n) \leq k_l^a, \\ e^{-\theta\rho^\beta}, & k_l^a \leq u(l_m, r_n) \leq k_l, \\ 0, & u(l_m, r_n) > k_l. \end{cases} \quad (1)$$

In equation (1), $u(l_m, r_n)$ is the Euclidean distance between sensor monitoring node l_m and target r_n , and its calculation formula is equation (2). $\rho = u(l_m, r_n) - k_l^a$. θ and β are the path loss indexes of the sensor's detection signal strength. Both parameters are determined by the physical characteristics of the sensor. In this paper, $\theta = \beta = 1$. It can be seen that when ρ is large enough, the value of $d(l_m, r)$ will quickly decay to close to zero.

$$u(l_m, r_n) = \sqrt{(t_m - t_n)^2 + (w_m - w_n)^2 + (v_m - v_n)^2}. \quad (2)$$

Assuming that there are M sensor monitoring nodes and N targets in EMWSNs, the target coverage relationship matrix P is obtained by equation (3) when the binary coding

scheme is adopted.

$$P = \begin{bmatrix} pma_{1,1} & pma_{m1,2} & \cdots & pma_{1,M-1} & pma_{1,M} \\ pma_{2,1} & pma_{22} & \cdots & pma_{2,M-1} & pma_{2,M} \\ \vdots & \vdots & pma_{n,m} & \vdots & \vdots \\ pma_{N-1,1} & pma_{N-1,2} & \cdots & pma_{N-1,M-1} & pma_{N-1,M} \\ pma_{N,1} & pma_{N,2} & \cdots & pma_{N,M-1} & pma_{N,M} \end{bmatrix}. \quad (3)$$

In equation (3), $pma_{n,m}$ represents the situation of the target being sensed by the sensor monitoring node, and its value formula is

$$pma_{n,m} = \begin{cases} 1, & d(l_m, r_n) > d_{\text{rand}}, \\ 0, & d(l_m, r_n) < d_{\text{rand}}. \end{cases} \quad (4)$$

In equation (4), d_{rand} represents the random probability. If the perceptual probability $d(l_m, r_n)$ is greater than the random probability d_{rand} , then the target is successfully covered by the monitoring node. At this time, $pma_{n,m} = 1$; otherwise, $pma_{n,m} = 0$.

To reduce the energy consumption of EMWSNs and at the same time limit the sensing performance of sensor monitoring nodes, this paper sets the maximum monitoring target number of a sensor as H . According to performance constraints, a new perception relationship matrix Q can be obtained as

$$Q = \begin{bmatrix} qma_{1,1} & qma_{1,2} & \cdots & qma_{1,M-1} & qma_{1,M} \\ qma_{2,1} & qma_{22} & \cdots & qma_{2,M-1} & qma_{2,M} \\ \vdots & \vdots & qma_{n,m} & \vdots & \vdots \\ qma_{N-1,1} & qma_{N-1,2} & \cdots & qma_{N-1,M-1} & qma_{N-1,M} \\ qma_{N,1} & qma_{N,2} & \cdots & qma_{N,M-1} & qma_{N,M} \end{bmatrix}. \quad (5)$$

In equation (5), $qma_{n,m}$ represents the condition of the target being sensed by the sensor monitoring node, and $qma_{n,m} = 1$ means that the target is sensed and monitored by the corresponding sensor node. If $qma_{n,m} = 0$, it means that the target is not sensed by the corresponding sensor node or sensed by the corresponding sensor node but not monitored. The Q matrix constraint relationship can be expressed as

$$\sum_{n=1}^N qma_{n,m} \leq H, \quad m = 1 \cdots M. \quad (6)$$

The target coverage matrix optimization model of EMWSNs described in this paper is the process of adding constraints to the P matrix to obtain the optimized Q matrix. BACSFLA has high-efficiency computing performance and excellent global search capabilities, which can solve the

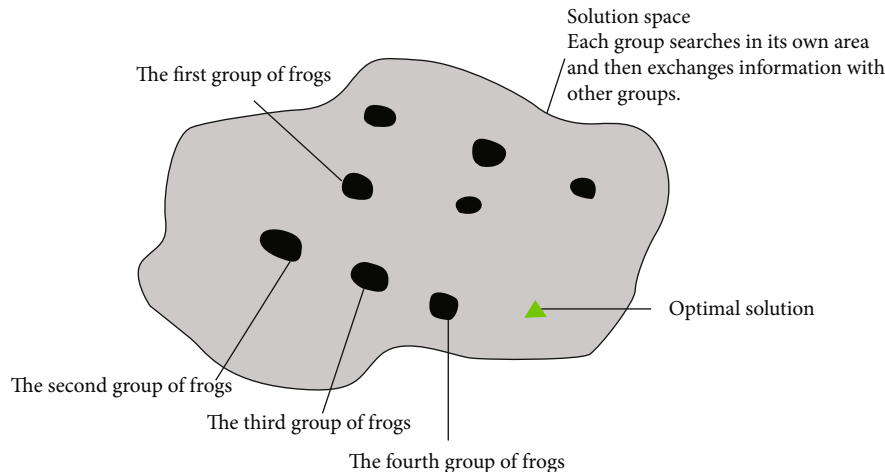


FIGURE 2: BACSFLA principle diagram.

optimization target coverage problem in EMWSNs with excellent performance.

3. BACSFLA for High-Coverage and Low-Energy Consumption in EMWSNs

In this paper, BACSFLA adopts a binary population coding scheme and produces two brand-new operators for EMWSNs. The adaptive operator improves the global search capability during the BACSFLA iteration process and at the same time prevents the algorithm from falling into the local optimal solution. The addition of the low-power selection feature to the clone operator is of great help in accelerating the iteration speed of BACSFLA and reducing the overall energy consumption. As a coevolutionary algorithm, BACSFLA combines stochastic and deterministic methods. The schematic diagram of BACSFLA is shown in Figure 2.

The principle of BACSFLA is to assume that there is a group of frogs in the pond, and there are a lot of rocks in the pond. The frogs can jump through these rocks and finally find food. First, the frog population is divided into several subgroups with the same number. Each subgroup starts to forage independently of each other, but the frogs within the subgroup can exchange information with each other to ensure that the frogs in each subgroup can be directed towards the subgroup. The excellent frogs in the group learn. After a certain period of food, the subgroups send their excellent frogs to communicate to ensure that the overall frogs learn from the best frogs. This process is also called memetic evolution. BACSFLA can be seen as a combination of local optimization and global optimization, that is, each subgroup is a process of local optimization, and the exchange of information between subgroups is a process of global optimization.

BACSFLA is based on the collective search for food by the frog population, focusing on grouping information exchange, and centering on the internal communication of subgroups and global information exchange to realize the whole process of optimizing, adding an improved adaptive operator, and low-power consumption. Clone the selection

operator, to achieve the purpose of searching and optimizing. The algorithm steps of BACSFLA are as follows:

Step 1. In the stage of randomly generating the initial population, a total of I frogs are generated.

Step 2. In the sorting stage, the fitness function is designed according to the target coverage rate, and the fitness value of the I frog is calculated and sorted from small to large.

Step 3. In the grouping stage, it is divided into I_1 subgroups and a single subgroup contains I_2 frogs. The grouping is carried out according to the alternating principle. After sorting, the frogs with serial numbers from 1 to I_1 are taken out, and each subgroup is placed in descending order. The frogs with serial numbers from $I_1 + 1$ to $2I_1$ are taken out and one for each subgroup in descending order. And so on, until all the frogs are divided.

Step 4. In the subgroup internal search stage, determine the number of searches within the subgroup, and then search for the next subgroup after completing one subgroup search, until all subgroups have been searched.

Step 5. In the mixed subgroup stage, after completing the evolution of I_1 subgroups, reorder all the subgroups in the mixture according to the method in step two.

Step 6. In the low-power cloning stage, a certain number of individuals are selected and placed in the cloning warehouse according to the sorting situation from good to bad. The individuals in the clone warehouse are set to different clone ratios according to the energy consumption. The smaller the energy consumption, the greater the clone ratio. Finally, a mutation operation is performed on the newly generated population after cloning to generate a new population.

Step 7. In the judgment stage, if the number of global information exchanges is reached or the set termination

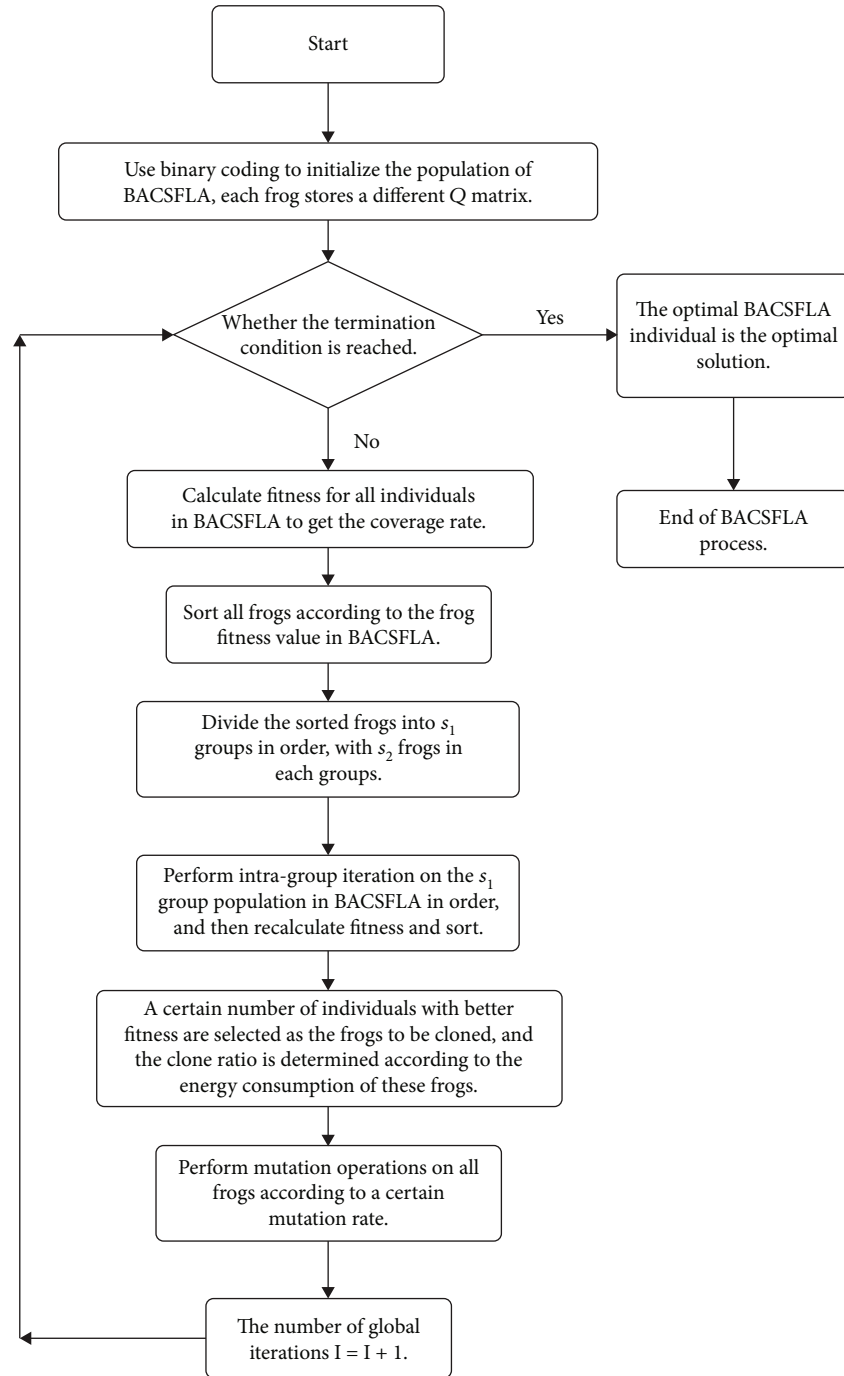


FIGURE 3: BACSFLA flow chart.

condition is reached, the optimal solution is output; otherwise, it returns to step 2.

The algorithm flow chart is shown in Figure 3.

3.1. The Population Initialization Operation and Binary Encoding of BACSFLA. The locations of sensor nodes in EMWSNs are distributed randomly and distributed according to specific areas. When the sensor nodes are randomly distributed, they are placed anywhere in the monitoring area, and the nodes are static and immovable

after they are placed. Since EMWSNs are affected by different environmental factors when monitoring the environment, the required area will show a certain distribution law. The simulated three-dimensional monitoring environment in this paper is divided into random distribution in the region, band distribution in the region, and spherical distribution in the region. The coordinate distribution of the target is the same as the coordinate distribution of the sensor node. The distribution of targets and sensors in the monitoring area is shown in Figure 4.

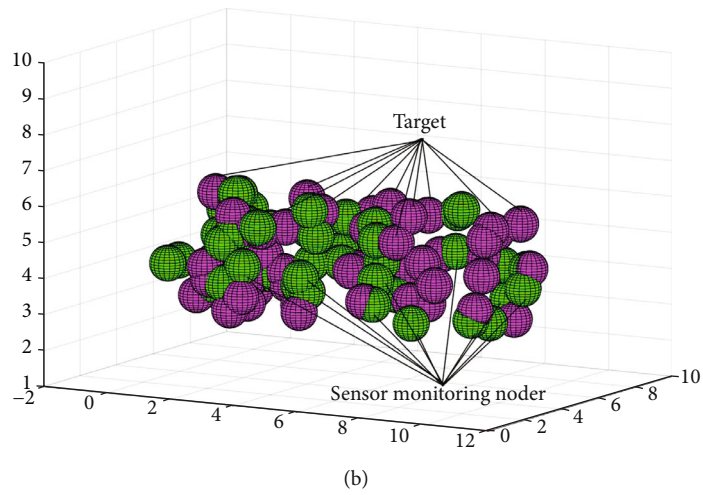
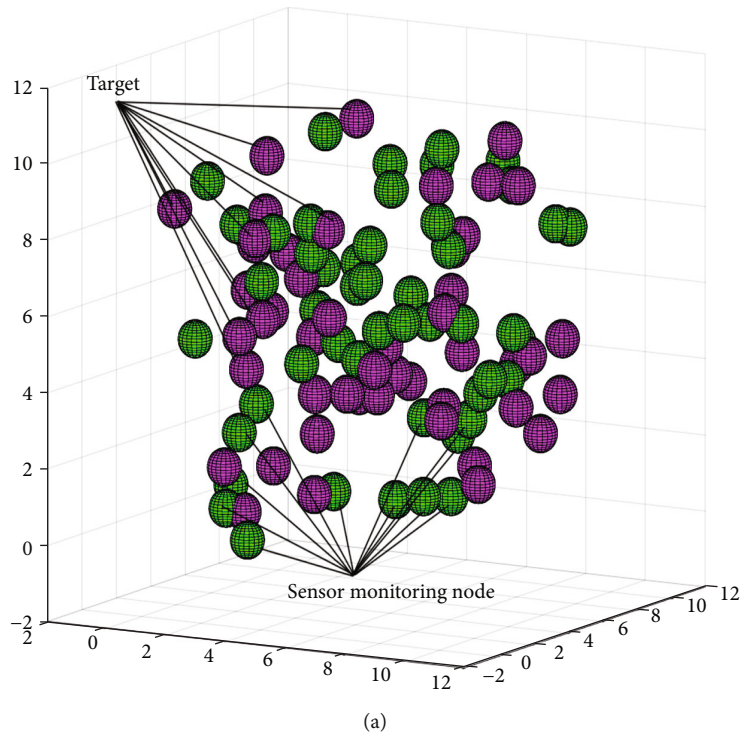


FIGURE 4: Continued.

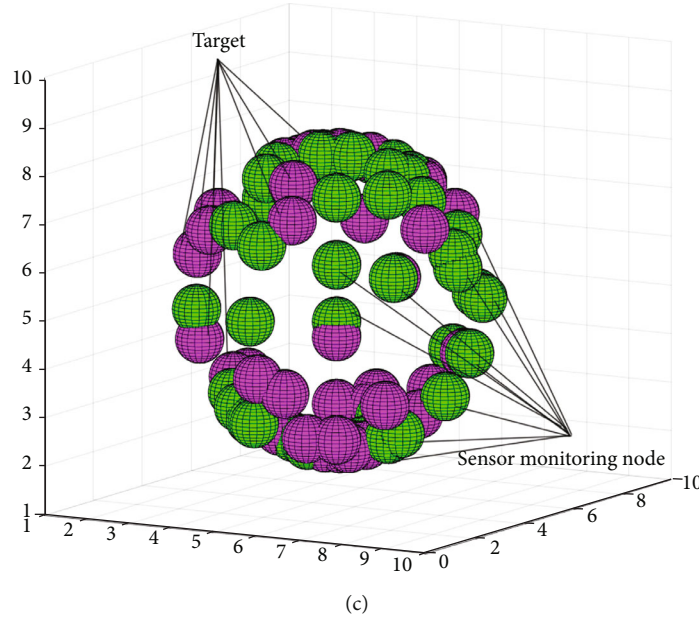


FIGURE 4: Schematic diagram of target and sensor node distribution: (a) random distribution; (b) banded distribution; (c) spherical distribution.

The population coding adopts a binary coding scheme, and the P matrix is obtained after the sensor monitoring node and the target position are successfully deployed. After adding constraints to the P matrix, i different Q matrices are generated, and each Q matrix is an individual frog.

3.2. The Fitness Function Design of BACSFLA. The fitness function plays an important role in BACSFLA. In EMWSN target coverage optimization, it is the core of optimized search. The choice of fitness function will directly affect the accuracy of the algorithm results and the final optimization results. This paper sets the target coverage rate $g(S_i)$ in the network as the fitness function of BACSFLA and adopts the principle that the bigger the better. The calculation formula is shown in

$$g(S_i) = \frac{\sum_{n=1}^N \left(\sum_{m=1}^M qma_{n,m} \geq h \right)}{N}. \quad (7)$$

In equation (7), h is the minimum number of sensor monitoring nodes that the target is successfully covered, which balances network energy consumption and coverage accuracy. In this paper, $h = 3$. S_i is denoted as the i_{th} frog in the population.

3.3. BACSFLA's Intragroup Frog Update Operation. Determine the best and worst frogs in the group after BACSFLA grouping. There must be good or bad frogs in the group. The best frog in all subgroups is denoted as S_j , the worst frog is denoted as S_o , and the best frog in the population is denoted as S_f . Improve the position of the worst frog, the worst frog S_o obtains the intermediate vector according to

$$\text{Temp} = \text{rand} \times (S_j - S_o). \quad (8)$$

TABLE 1: Simulation experiment parameter settings.

Parameter	Value
k_i^a	70 m
k_i	100 m
Temp _{max}	50
Temp _{min}	5
dt	4096 bits
nc_{elec}	50 nJ/bits

In equation (8), Temp is the intermediate vector between the best frog S_j in the middle group and the worst frog S_o in the group. rand represents a random number, $0 \leq \text{rand} \leq 1$. Then, a new frog is generated, which is obtained by

$$\begin{aligned} S_o(\text{new}) &= S_o + \text{Temp}, \\ \text{Temp}_{\min} &\leq \text{Temp} \leq \text{Temp}_{\max}. \end{aligned} \quad (9)$$

In equation (9), Temp_{min} is the minimum jump distance of the frog, and Temp_{max} is the maximum jump distance of the frog. The value of Temp must be between the two. If the value of Temp overflows, it will be processed according to

$$\text{Temp} = \begin{cases} \text{Temp}_{\min}, & \text{Temp} < \text{Temp}_{\min}, \\ \text{Temp}, & \text{Temp}_{\min} \leq \text{Temp} \leq \text{Temp}_{\max}, \\ \text{Temp}_{\max}, & \text{Temp} > \text{Temp}_{\max}. \end{cases} \quad (10)$$

In this process, the frog jumps to find a position better than S_o , and if it is found, it will update the worst frog, otherwise, proceed to the next step. Replace the best frog S_j in the subgroup with the best frog S_f in the subgroup. Repeat

equations (8), (9), and (10), if you still cannot find a better position to improve the worst in the subgroup frog S_o , proceed to the next step. Generate a random frog, no matter the frog is good or bad, use it instead of S_o .

3.4. BACSFLA's Low-Power Clone Selection Operation. After BACSFLA is updated within the group, the entire population is reordered according to fitness. The low-power clone selection operation first selects a certain number of individuals with adaptability from large to small and puts them into the clone warehouse. Assume that the number of frog individuals in the cloned warehouse is NUM. Therefore, the coverage of individual frogs in the warehouse must be greater than the coverage of the remaining unselected individuals. Then, calculate the energy consumption of individual frogs in the cloned warehouse, and the calculation of network energy consumption is shown in

$$EC(S_i) = \sum_{m=1}^M dt \times nc_{elec} + dt \times \varepsilon_{fs} \times u(l_m, r_n)^2. \quad (11)$$

In equation (11), dt represents the data size that the sensor monitoring node needs to send when monitoring the target. nc_{elec} represents the energy consumption during data transmission. ε_{fs} is a parameter in the signal transmission process, set $\varepsilon_{fs} = 1$. It can be seen that the closer the sensor monitoring node is to the target, the lower the network energy consumption. In this way, when the sensor node monitors the target, it will give priority to selecting the target close to itself, thereby reducing the energy consumption of the network communication of the entire EMWSNs.

After calculating the network energy consumption of individual frogs in the cloned warehouse, sort them in ascending order of energy consumption. The smaller the energy consumption, the greater the proportion of cloned individuals. The clone ratio selection is shown in

$$rate_1 + \dots + rate_{num} + \dots + rate_{NUM} = 1. \quad (12)$$

In equation (12), $rate_{num}$ represents the proportion of the num_{th} frog in the clone warehouse in the total population, $rate_1$ represents the proportion of frogs with the smallest energy consumption, and $rate_{NUM}$ represents the proportion of frogs with the largest energy consumption proportion. According to the energy consumption of individual frogs corresponding to the clone ratio, the clone ratio satisfies

$$rate_1 > rate_2 > \dots > rate_{num} > \dots > rate_{NUM}. \quad (13)$$

After selecting the new cloning ratio, the individual to be cloned is cloned according to the cloning ratio. After the cloning operation is completed, a new intermediate population is obtained. The degree of similarity of the intermediate population is too high to perform the global search performance of BACSFLA, so the next step is to perform an adaptive mutation operation.

3.5. Adaptive Mutation Operation of BACSFLA. After BACSFLA performs the low-power clone selection operation, it needs to perform adaptive mutation operations on the frogs in the population to obtain differentiated individuals. This operation is conducive to search in the vicinity of the global optimal solution, while ensuring that BACSFLA will not fall into the local optimal solution, increasing the diversity of the population, and has important significance for the rapid convergence of the algorithm.

BACSFLA will adaptively change the mutation probability BR of the population. The size of the mutation probability is affected by the fitness of the individual, and it is also affected by the speed of convergence in the iterative process. If the fitness of the individual frog is to be mutated, and the coverage rate of the frog is small, the probability of mutation will increase. In the iterative process, if the fitness of the optimal frog individual relative to the previous generation does not increase much, or no better individual is found, the mutation probability will gradually increase, and the mutation probability will not decrease until a better individual is found. The formula for changing the adaptive mutation probability is shown in

$$BR = \frac{1 - g(S_i)}{\sum_{i=1}^I g(S_i)} + LR(\text{gen}). \quad (14)$$

In equation (14), $LR(\text{gen})$ represents the driving variation factor of BACSFLA iteration to the gen_{th} generation. The calculation formula is shown in

$$LR(\text{gen}) = \begin{cases} LR(\text{gen}) + \delta, & g_{\text{gen}-1}(S_f) = g_{\text{gen}}(S_f), \\ 0, & g_{\text{gen}-1}(S_f) < g_{\text{gen}}(S_f), \\ 0, & \text{gen} = 1. \end{cases} \quad (15)$$

In equation (15), δ is the increment of mutation probability, set $\delta = 0.05$. It can be seen from the update equation of BR that the probability of mutation is affected by two factors. If in the iterative process, the global optimal individual has not been updated, there may be two situations, either the optimal solution has been found or the locally optimal solution is trapped. At this time, it is necessary to increase the mutation probability of all individuals, increase the global optimization ability, and judge whether the optimal solution has been found. The fitness of an individual also affects the probability of individual mutation. The greater the fitness, the smaller the probability of individual mutation. When the fitness value of an individual is large, it proves that the coverage rate of the individual is large, so it is only necessary to find the optimal solution in the close range of the individual. If the fitness value of an individual is small, it proves that the individual is far from the optimal solution, so increases the probability of mutation and expands the search range of the solution.

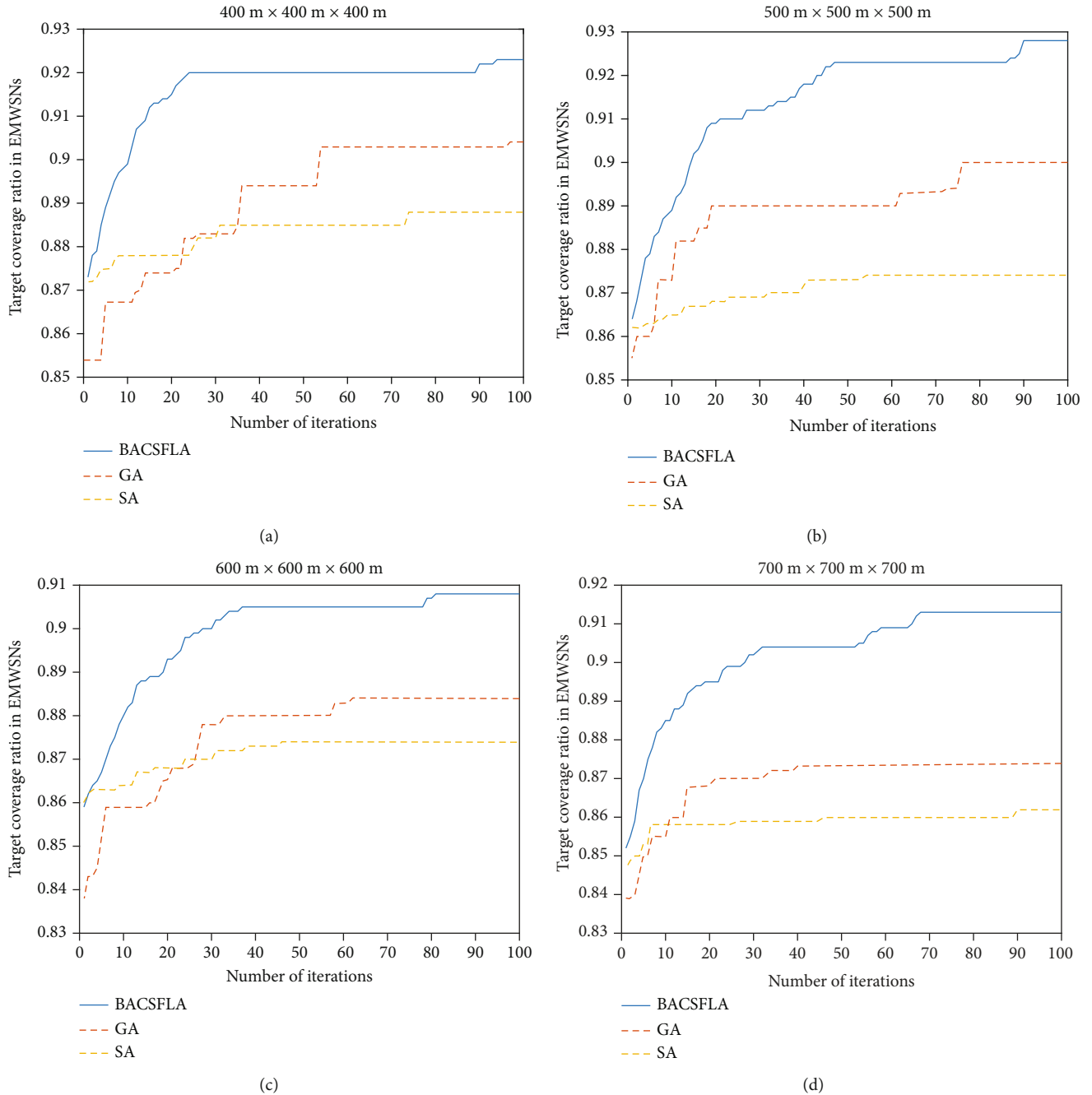


FIGURE 5: Algorithm coverage curve in different monitoring areas: (a) $400\text{ m} \times 400\text{ m} \times 400\text{ m}$; (b) $500\text{ m} \times 500\text{ m} \times 500\text{ m}$; (c) $600\text{ m} \times 600\text{ m} \times 600\text{ m}$; (d) $700\text{ m} \times 700\text{ m} \times 700\text{ m}$.

4. Results and Discussion

This section will verify the performance of BACSFLA through simulation experiments and select GA and SA as the comparison algorithm. All nodes in EMWSNs are composed of static nodes, and all sensor nodes have omnidirectional sensors, and their perception model is a probabilistic perception model. This article carries on the experiment simulation under the environment of MATLAB R2019a, and the simulation platform is the Intel Core I7 processor. After multiple tests on BACSFLA parameters, the optimal

TABLE 2: The coverage of the three algorithms in different areas.

	BACSFLA	GA	SA
$400\text{ m} \times 400\text{ m} \times 400\text{ m}$	92.3%	90.4%	88.8%
$500\text{ m} \times 500\text{ m} \times 500\text{ m}$	92.8%	90.0%	87.4%
$600\text{ m} \times 600\text{ m} \times 600\text{ m}$	90.8%	88.4%	87.4%
$700\text{ m} \times 700\text{ m} \times 700\text{ m}$	91.3%	87.4%	86.2%

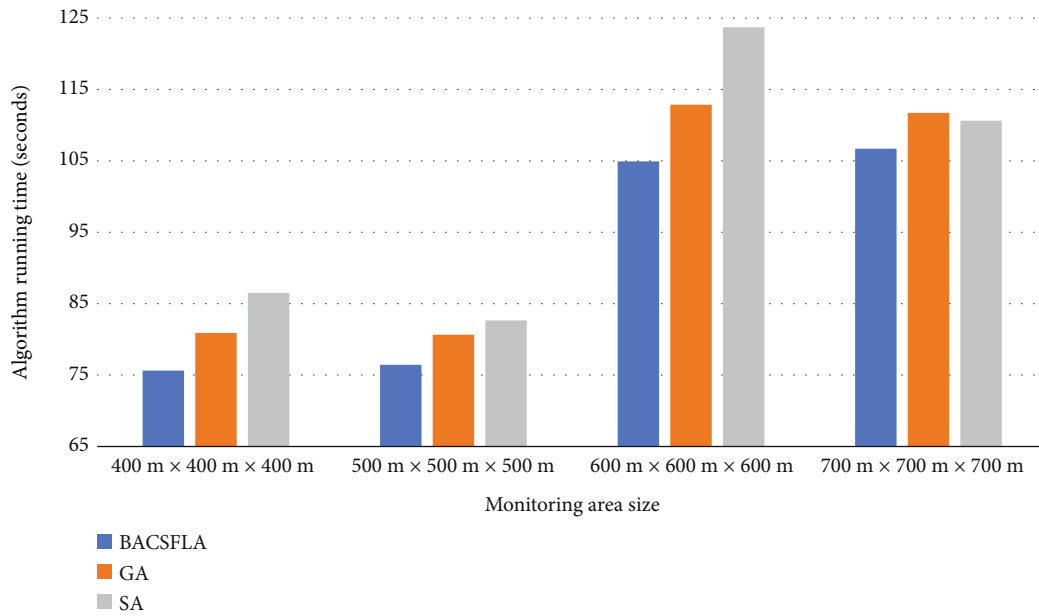


FIGURE 6: The running time of the algorithm in different monitoring area sizes.

value of each parameter was determined. The parameter values in the target coverage of EMWSNs are shown in Table 1.

In Table 1, the maximum jump distance $Temp_{max}$ is set to 50, which means that the maximum number of changes in the sensor monitoring node perception relationship in the Q matrix each time the worst frog individual is updated is 50. The maximum jump distance $Temp_{min}$ is set to 5, which means that each update cannot be less than 5 sensor monitoring nodes.

The target coverage methods of BACSFLA, GA, and SA are used in the simulation, and the sensor monitoring nodes and target distribution are randomly distributed. The selection operation in GA adopts the roulette method, the crossover operation is a single point crossover, and the mutation probability is 0.05. The initial temperature in SA is set to 1000 degrees Celsius, the lower bound of the temperature is a number close to zero, and the temperature drop rate is 0.98. The number of individuals in the population is set to 50, where the number of subpopulations in BACSFLA $I_1 = 10$, the number of frog individuals in each subpopulation $I_2 = 5$, and the number of iterations within the group is 5. The number of targets N is 1000, and the number of sensor monitoring nodes is 700. The maximum number of targets that the sensor can monitor is $H = 5$. When the monitoring area is $400\text{ m} \times 400\text{ m} \times 400\text{ m}$, $500\text{ m} \times 500\text{ m} \times 500\text{ m}$, $600\text{ m} \times 600\text{ m} \times 600\text{ m}$, and $700\text{ m} \times 700\text{ m} \times 700\text{ m}$, the simulation result curve is shown in Figure 5.

It can be seen from Figure 5 that when the monitoring area changes, the coverage of BACSFLA and the comparison algorithm are both affected. When the number of sensor monitoring nodes and the number of targets remain unchanged, as the monitoring area increases, the coverage of GA and SA will decrease to a large extent, while the decrease of BACSFLA is not large. This result shows that

BACSFLA has better performance than GA and SA when the dimensionality of the coverage problem increases. As the number of iterations of the algorithm increases, the coverage of BACSFLA, GA, and SA all increase rapidly at the beginning. However, the curve of SA tends to be flat in the subsequent optimization process, because SA's global optimization performance is poor, and the algorithm falls into premature convergence during operation, and the solution obtained is the local optimal solution instead of the global optimal solution. The result of GA is better than that of SA, and the convergence speed and the final solution are greatly improved compared to SA. However, the optimization process of GA is slow, which is reflected in the curve, which is that although the coverage rate increases with the increase of the number of iterations, the increase is smaller. Compared with GA and SA, BACSFLA has a significant improvement in both the convergence speed and the final result. This is because the clone operator of BACSFLA increases the global search performance, and the adaptive algorithm increases the local search performance. Therefore, BACSFLA can obtain the optimal solution with a faster convergence rate. In the iterative process, each iteration of BACSFLA in the early stage of the operation will greatly improve the results, so better results can be obtained in the early stage of algorithm operation. After getting the optimal result, BACSFLA can terminate the algorithm iteration process early. The coverage rates of BACSFLA, GA, and SA in three-dimensional monitoring areas of different sizes are shown in Table 2.

It can be seen from Table 2 that under the conditions of different monitoring areas and the same number of sensor nodes and targets, the coverage rate of BACSFLA is increased by 1.9% to 3.9% than that of GA and 3.4% to 5.4% than that of SA. Compared with the two-dimensional plane in the three-dimensional area, the complexity of the

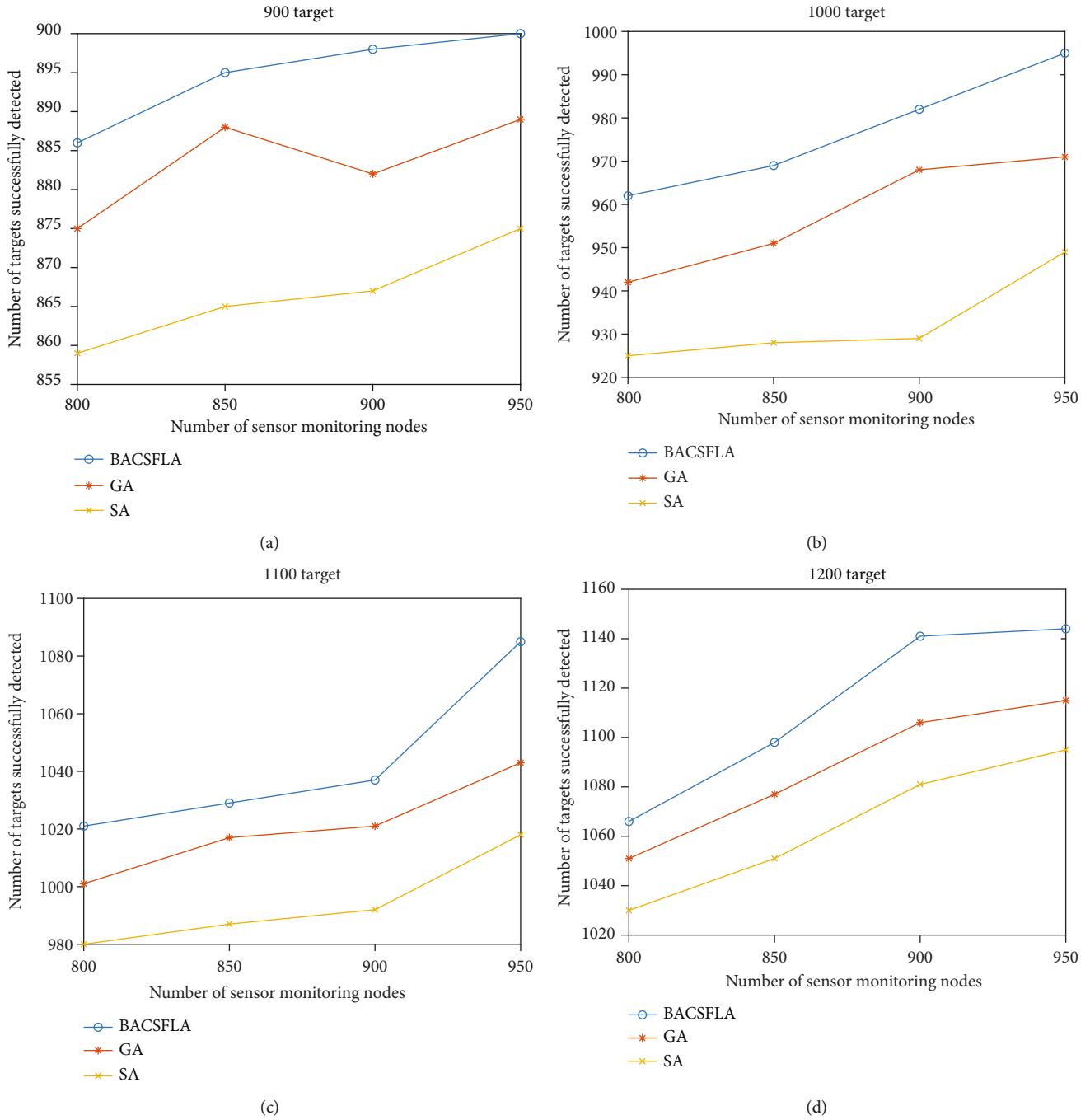


FIGURE 7: The influence of sensor monitoring node number and target number change on coverage: (a) targets 900; (b) targets 1000; (c) targets 1100; (d) targets 1200.

problem and the amount of calculation show an exponential increase. BACSFLA shows very good three-dimensional performance, and the optimal results can still be obtained in solving the covering problem. However, GA and SA cannot meet the performance requirements of EMWSNs facing the three-dimensional area and perform poorly in the process of solving the target coverage problem. The running time of the three algorithms is shown in Figure 6.

It can be seen from Figure 6 that the running time of the BACSFLA algorithm is shorter than that of GA and SA. This

TABLE 3: Network energy consumption in EMWSNs.

	BACSFLA	GA	SA
900 target	0.5870 J	0.9173 J	0.9163 J
1000 target	0.6169 J	0.9095 J	0.9077 J

shows that while BACSFLA improves the coverage performance of EMWSNs, it does not increase the time complexity of the algorithm compared to the comparison algorithm.

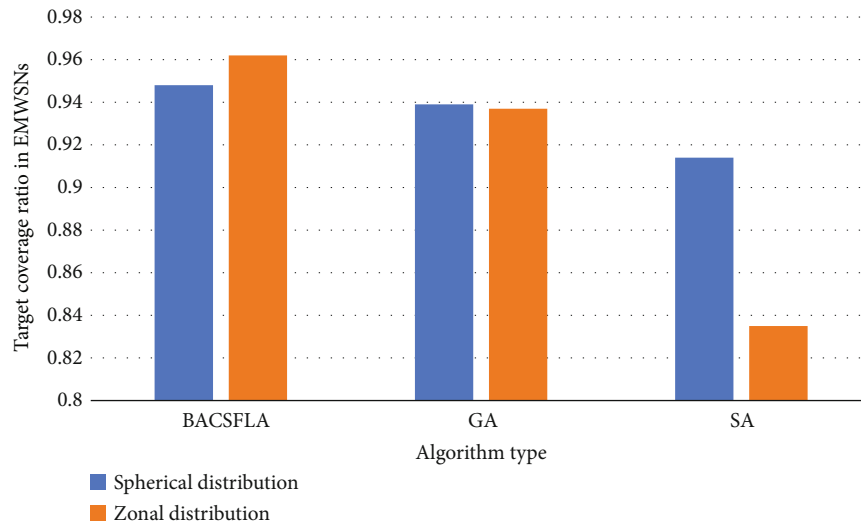


FIGURE 8: The coverage results of the three algorithms under spherical and zonal distributions.

BACSFLA can show better coverage in a shorter time. In real-world applications, the performance of nodes and networks in EMWSNs is limited. BACSFLA can consume less computing power and get better results.

It can be concluded from the results that monitoring areas of different sizes have a significant impact on BACSFLA. To analyze the influence of the number of sensor monitoring nodes and the number of targets on BACSFLA, the algorithm parameters will be adjusted next to obtain new simulation results. Set the monitoring area to be $400\text{ m} \times 400\text{ m} \times 400\text{ m}$, and the maximum monitoring number of sensors $H=7$. The number of targets is 900, 100, 1100, and 1200. The number of sensor nodes is 800, 850, 900, and 950. The simulation results are shown in Figure 7.

It can be seen from Figure 7 that with the increase of sensor nodes, the coverage rates of BACSFLA, GA, and SA all increase. The degree of increase in BACSFLA is greater than that of GA and SA. Although the number of sensor monitoring nodes increases, the number of monitored targets in EMWSNs will increase. However, the number of calculations required by the algorithm in a three-dimensional environment will increase greatly. GA and SA are limited by algorithm performance and cannot make rational use of the added sensors. When facing a large number of sensors and targets, BACSFLA can give full play to the performance of the algorithm, reasonably allocate target coverage relationships, and improve coverage. Compared with GA and SA, BACSFLA has more complex problems, more sensor nodes, and more targets, the more obvious the performance advantage will be. In EMWSNs, the environment that needs to be monitored is often huge, which means that more targets need to be monitored and the number of sensor monitoring nodes deployed. However, BACSFLA's excellent performance in handling a large number of nodes can meet the performance requirements of EMWSNs.

Although coverage is an important performance parameter of EMWSNs, network energy consumption also has an important impact on EMWSNs. The energy consumption of EMWSNs when the monitoring area is $400\text{ m} \times 400\text{ m} \times$

400 m , the number of sensor nodes is 800, and the target number is 900 and 1000 is shown in Table 3.

It can be seen from Table 3 that under the same conditions, the network energy consumption of BACSFLA is much smaller than that of GA and SA. The results show that the network energy consumption of BACSFLA is reduced by 36.0% compared with GA and 35.9% compared with SA. This is because BACSFLA's low-power clone selection operator promotes sensor monitoring nodes to preferentially cover targets that are close in the iterative process. However, GA and SA only optimize the target coverage of EMWSNs without considering the size of network energy consumption. Although GA and SA can also complete the target coverage, the huge energy cost is not acceptable.

The random distribution of node positions in EMWSNs can simulate most real-life scenarios. However, the target distribution in some areas will show certain rules. Therefore, this paper also adopts two distribution methods, belt-shaped distribution and spherical distribution, to simulate the environment in the real three-dimensional world. The parameter setting in the strip space is $400\text{ m} \times 300\text{ m} \times 300\text{ m}$ in the monitoring area. In the spherical space, the radius of the monitoring area is set to 200 m. The number of sensor monitoring nodes is 900, the target number is 1000, and the maximum number of sensors monitored is $H=6$. The simulation results are shown in Figure 8.

It can be seen from Figure 8 that compared with GA and SA, BACSFLA still has a higher target coverage after changing the distribution types of sensor monitoring nodes and targets. GA and SA are more affected under the band distribution, while the results of BACSFLA are better. This is because the adaptive operator of BACSFLA will quickly adjust the parameters of the algorithm when facing changes in the environment to obtain a higher coverage rate.

5. Conclusion

Coverage has always been a basic problem in the research of EMWSNs, and its purpose is to ensure a certain network

performance while maximizing the target coverage as much as possible. Because the traditional 2D perception model and its corresponding target coverage algorithm are difficult to directly apply to the real 3D environment, this paper mainly studies the low-energy target coverage optimization problem of 3D EMWSN nodes. A low-power target coverage algorithm BACSFLA suitable for the three-dimensional physical world is proposed. In a static network, the performance pros and cons of BACSFLA, GA, and SA are discussed. The results show that BACSFLA has better performance than the comparison algorithm in terms of target coverage, algorithm running time, and network energy consumption. BACSFLA combines cloning operators and adaptive operators, which can better adapt to changes in external parameters and obtain better results. The individual uses a binary coding scheme, which greatly reduces the calculation time of the algorithm and reduces the time complexity. Through simulation experiments, BACSFLA has shown good performance advantages in three-dimensional space and has less network energy consumption while maintaining high coverage. These results show that BACSFLA has a very good application prospect in EMWSNs.

However, the target coverage optimization method we proposed in this article has problems such as a small scale of sensor monitoring nodes and poor coordination among nodes. The design of distributed algorithms that are suitable for large-scale three-dimensional environments and cooperate among nodes can be used as the next research direction. Besides, the method proposed in this paper is static and immovable when the sensor monitors the node during the target coverage process. Future work can focus on moving the sensor to monitor the position of the node under dynamic conditions, balance the network energy consumption of EMWSNs, and extend the life of the network.

Data Availability

The data used to support the findings of this study are available from the corresponding author upon request.

Conflicts of Interest

The authors declare that they have no conflicts of interest.

Acknowledgments

This paper was funded by the Corps Innovative Talents Plan, grant number 2020CB001, the project of Youth and Middle Aged Scientific and Technological Innovation Leading Talents Program of the Corps, grant number 2018CB006, the China Postdoctoral Science Foundation, grant number 220531, the Funding Project for High Level Talents Research in Shihezi University, grant number RCZK2018C38, and the Project of Shihezi University, grant number ZZZC201915B. It is a postgraduate education innovation program of the Autonomous Region.

References

- [1] C. Duan, J. Feng, H. Chang, J. Pan, and L. Duan, "Research on sensor network coverage enhancement based on non-cooperative games," *Computers, Materials & Continua*, vol. 60, no. 3, pp. 989–1002, 2019.
- [2] J. He, Z. Xing, R. Hu et al., "Directional antenna intelligent coverage method based on traversal optimization algorithm," *Computers, Materials & Continua*, vol. 60, no. 2, pp. 527–544, 2019.
- [3] M. O. Ramkumar, "Intelligent fruit fly algorithm for maximization coverage problem in wireless sensor network," *7th international conference on smart structures and systems (ICSSS)*, 2020, pp. 1–6, Chennai, India, 2020.
- [4] L. Cao, Y. Yue, Y. Cai, and Y. Zhang, "A novel coverage optimization strategy for heterogeneous wireless sensor networks based on connectivity and reliability," *IEEE Access*, vol. 9, pp. 18424–18442, 2021.
- [5] Z. Wang, H. Xie, D. He, and S. Chan, "Wireless sensor network deployment optimization based on two flower pollination algorithms," *IEEE Access*, vol. 7, pp. 180590–180608, 2019.
- [6] A. K. Sangaiyah, M. Sadeghilalimi, A. A. R. Hosseinabadi, and W. Zhang, "Energy consumption in point-coverage wireless sensor networks via bat algorithm," *IEEE Access*, vol. 7, pp. 180258–180269, 2019.
- [7] X. Hui, W. Bailing, S. Jia, H. Haohan, and Z. Xiaolei, "An algorithm for calculating coverage rate of WSNs based on geometry decomposition approach," *Peer-to-Peer Networking and Applications*, vol. 12, no. 3, pp. 568–576, 2019.
- [8] Z. Hao, N. Qu, X. Dang, and J. Hou, "Node optimization coverage method under link model in passive monitoring system of three-dimensional wireless sensor network," *International Journal of Distributed Sensor Networks*, vol. 15, no. 8, 2019.
- [9] Y. Feng, S. Zhao, and H. Liu, "Analysis of network coverage optimization based on feedback K-means clustering and artificial fish swarm algorithm," *IEEE Access*, vol. 8, pp. 42864–42876, 2020.
- [10] L. Wang, W. Wu, J. Qi, and Z. Jia, "Wireless sensor network coverage optimization based on whale group algorithm," *Computer Science and Information Systems*, vol. 15, no. 3, pp. 569–583, 2018.
- [11] A. Anurag, R. Priyadarshi, A. Goel, and B. Gupta, "2-D coverage optimization in WSN using a novel variant of particle swarm optimisation," in *2020 7th international conference on signal processing and integrated networks (SPIN)*, pp. 663–668, Noida, India, 2020.
- [12] S. Karimi-Bidhendi, J. Guo, and H. Jafarkhani, "Energy-efficient node deployment in heterogeneous two-tier wireless sensor networks with limited communication range," *IEEE Transactions on Wireless Communications*, vol. 20, no. 1, pp. 40–55, 2021.
- [13] Y. Zhang, L. Cao, Y. Yue, Y. Cai, and B. Hang, "A novel coverage optimization strategy based on grey wolf algorithm optimized by simulated annealing for wireless sensor networks," *Computational Intelligence and Neuroscience*, vol. 2021, Article ID 6688408, 14 pages, 2021.
- [14] H. ZainEldin, M. Badawy, M. Elhosseini, H. Arafat, and A. Abraham, "An improved dynamic deployment technique based-on genetic algorithm (IDDT-GA) for maximizing coverage in wireless sensor networks," *Journal of Ambient Intelligence and Humanized Computing*, vol. 11, no. 10, pp. 4177–4194, 2020.

- [15] N. T. Hanh, H. T. T. Binh, N. X. Hoai, and M. S. Palaniswami, "An efficient genetic algorithm for maximizing area coverage in wireless sensor networks," *Information Sciences*, vol. 488, pp. 58–75, 2019.
- [16] S. D. Manju, S. Chand, and B. Kumar, "Genetic algorithm-based heuristic for solving target coverage problem in wireless sensor networks," in *Advanced Computing and Communication Technologies. Advances in Intelligent Systems and Computing*, R. Choudhary, J. Mandal, and D. Bhattacharyya, Eds., vol. 562, Springer, Singapore., 2018.
- [17] J. Sahoo and B. Sahoo, "Solving target coverage problem in wireless sensor networks using greedy approach," in *2020 International Conference on Computer Science, Engineering and Applications (ICCSEA)*, pp. 1–4, Gunupur, India, 2020.
- [18] X. Zhao, Y. Cui, C. Gao, Z. Guo, and Q. Gao, "Energy-efficient coverage enhancement strategy for 3-D wireless sensor networks based on a vampire bat optimizer," *IEEE Internet of Things Journal*, vol. 7, no. 1, pp. 325–338, 2020.
- [19] L. Wang, C. Li, H. Wang, Y. Zhang, and Z. Liu, "MEP-PSO algorithm-based coverage optimization in directional sensor networks," in *GLOBECOM 2020 - 2020 IEEE global communications conference*, pp. 1–6, Taipei, Taiwan, 2020.
- [20] E. Bonnah, S. Ju, and W. Cai, "Coverage maximization in wireless sensor networks using minimal exposure path and particle swarm optimization," *Sensing and Imaging*, vol. 21, no. 1, p. ???, 2020.
- [21] V. Kiani, "A greedy virtual force algorithm for target coverage in distributed sensor networks," in *2020 10th international conference on computer and knowledge engineering (ICCKE)*, pp. 317–322, Mashhad, Iran, 2020.
- [22] W. Wang, H. Huang, F. He, F. Xiao, X. Jiang, and C. Sha, "An enhanced virtual force algorithm for diverse k-coverage deployment of 3D underwater wireless sensor networks," *Sensors*, vol. 19, p. 3496, 2019.
- [23] Y. Sun, Y. Hu, L. Chen, H. Liu, J. Chen, and B. Lv, "The coverage optimization method for underwater sensor network based on VF-PSO algorithm," in *2020 Chinese control and decision conference (CCDC)*, pp. 2008–2013, Hefei, China, 2020.
- [24] M. Elhoseny, A. Tharwat, A. Farouk, and A. E. Hassanien, "K-coverage model based on genetic algorithm to extend WSN lifetime," *IEEE Sensors Letters*, vol. 1, no. 4, pp. 1–4, 2017.

Research Article

Elite Adaptive Simulated Annealing Algorithm for Maximizing the Lifespan in LSWSNs

Jie Zhou ^{1,2}, Wenxian Jia,¹ Menghan Liu,¹ and Mengying Xu ¹

¹College of Information Science and Technology, Shihezi University, Shihezi 832000, China

²Xinjiang Tianfu Information Technology Co., Ltd., China

Correspondence should be addressed to Jie Zhou; ziejzhou@shzu.edu.cn

Received 30 March 2021; Accepted 2 June 2021; Published 28 June 2021

Academic Editor: Mario E. Rivero-Angeles

Copyright © 2021 Jie Zhou et al. This is an open access article distributed under the Creative Commons Attribution License, which permits unrestricted use, distribution, and reproduction in any medium, provided the original work is properly cited.

Large-scale wireless sensor networks (LSWSNs) are currently one of the most influential technologies and have been widely used in industry, medical, and environmental monitoring fields. The LSWSNs are composed of many tiny sensor nodes. These nodes are arbitrarily distributed in a certain area for data collection, and they have limited energy consumption, storage capabilities, and communication capabilities. Due to limited sensor resources, traditional network protocols cannot be directly applied to LSWSNs. Therefore, the issue of maximizing the LSWSNs' lifetime by working with duty cycle design algorithm has been extensively studied in this paper. Encouraged by annealing algorithm, this work provides a new elite adaptive simulated annealing (EASA) algorithm to prolong LSWSNs' lifetime. We then present a sensor duty cycle models, which can make sure the full coverage of the monitoring targets and prolong the network lifetime as much as possible. Simulation results indicate that the network lifetime of EASA algorithm is 21.95% longer than that of genetic algorithm (GA) and 28.33% longer than that of particle swarm algorithm (PSO).

1. Introduction

Large-scale wireless sensor networks (LSWSNs) have broad application prospects in various fields, such as agriculture, industry, military, and environmental monitoring because of their real-time data collection and flexibility of deployment methods. The use of LSWSNs to detect harmful gas leaks is one of the research hotspots. Classical harmful gas detection mainly includes detection methods such as wired fixed devices and portable instruments. However, these ways have disadvantages such as poor flexibility, low real-time performance, and inaccurate location of leaks. LSWSNs rely on their low cost, high real-time performance, and good collaboration. It provides a new system for remote detection of harmful gases.

At present, traditional LSWSNs usually deploy dense static sensor nodes in industrial plants to obtain more accurate results. Nevertheless, in actual situations, since LSWSN is composed of a certain battery power and related sensor nodes within the sensor range, the sensing resources are limited. In addition, sensing, monitoring, and obtaining infor-

mation in the target monitoring area are the basic and ultimate goals of LSWSN deployment nodes. Sensing nodes are generally randomly deployed in the monitoring area, which is likely to cause uneven distribution of nodes and lead to problems such as coverage blind areas [1]. This will affect the coverage quality of LSWSN. Moreover, the quality of coverage will directly affect the quality of service of the network, so coverage optimization is a basic issue that needs to be studied and analyzed in the deployment of LSWSN nodes [2, 3]. Therefore, coverage optimization is a fundamental issue that needs to be studied and analyzed in the deployment of LSWSN nodes. The coverage optimization problem of LSWSN nodes is essential to use as few nodes as possible to achieve the maximum deployment of sensory coverage and communication coverage of the target monitoring area under the premise of ensuring the quality of network connectivity. In order to achieve this goal, it is necessary to design an appropriate deployment strategy, comprehensively consider the characteristics of the node itself, and allocate various resources rationally by optimizing the deployment of the LSWSN node. The traditional deployment method is to use

large-scale static nodes to complete the coverage of the target area. This method will cause problems such as high node redundancy. Therefore, in the case of full coverage, how to extend the network lifetime by deploying LSWSN nodes has become a research hotspot.

To cover all the predetermined targets, the research point of paper [4, 5] was from the perspective of the power limitation of LSWSNs. Paper [6] used the feature that the sensor can charge the battery, and the solar sensor was applied to extend the working life of the wireless sensors. Paper [4] also proposed a probabilistic perception model (PSM). In the paper, each sensor could switch between charging and working status and perform cooperative sensing. The timing of monitoring common targets was well arranged. Paper [5] proposed the target Q coverage rate, which used a greedy heuristic algorithm to restrict the use of sensors with poor coverage. However, the convergence effects of these three target coverage mechanisms were not satisfactory. When the number of iterations increases, the convergence speed became slowly.

Paper [7] proposed a node state prediction method based on hidden Markov model. Under the premise of full coverage, the sensor could monitor all target nodes by determining the working sequence of the nodes. However, in the solution obtained by the methods, the working life of LSWSNs was short.

In this paper, we propose a method EASA to solve the problem of duty cycle, while ensuring full coverage of the monitoring target, and extend the lifetime of the LSWSNs as much as possible to ensure the monitoring effect of the target.

To enhance the lifespan of LSWSNs, we first set up an objective function for evaluating the working life of LSWSNs. Then, ECSA is designed to maximize the lifetime of LSWSNs. Advanced operators such as elite operator and adaptive operator are also incorporated into the EASA to extra raise the explore ability. ECSA simultaneously generates a large number of results to investigate the search region and to prevent local optima. Perform data simulation to judge the performance of EASA. Simulation results indicate the proposed algorithm can achieve a higher working life of LSWSNs over GA and PSO [8–13].

2. Related Work

Tiny sensing units are widely used by sensor nodes, and at the same time, the sensing capabilities of sensor nodes are limited. Since LSWSNs are restricted in sensing capabilities, the duty cycle plays a vital role in maximizing the working life of LSWSNs. Most of the research on duty cycle design is related to heuristic algorithms, such as exhaustive exploit. However, its computational complexity is too high to be used in real-time applications [14]. GA, SA, and PSO were specially exploited for this kind of problem.

Paper [15] proposed GA to solve the problem of the sensor working in the monitored area with obstacles. The paper gave the correspondence between the evolution theory and the terms in GA, so that the sensor layout problem could be solved. It provided the coding scheme of the algorithm

and the solution of the sensor placement problem. Finally, the GA solution could be used as a map for identifying obstacles in the monitored area. But this kind of full-coverage sensor placement method tended to converge prematurely when the number of generations increased.

To achieve more coverage and the lower energy consumption, a nondominated sorting genetic algorithm (NSGA-II) was proposed in [16] to optimize the coverage. The paper used a multiobjective optimization method to extend LSWSNs' lifespan and coverage. The paper proposed not only increased the coverage area and lifetime of the wireless sensor, but also ensured the connectivity of the wireless sensor. But it tended to converge prematurely when the cyclic algebra became larger.

In [17], it proposed a combined algorithm of VF-PSO. In order to increase the coverage of the wireless network, it used virtual forces to move the sensor to a suitable location to solve the problem. In the paper, the accelerated convergence of particles was guided by virtual forces. The algorithm solved the problem of poor optimization ability of virtual force algorithm and also used PSO to maximize the coverage target area. But VF-PSO increased the complexity of the algorithm.

For extending the lifespan of WSN, paper [18] adopted the coverage model of VCH-PSO. It took into account the energy consumption and coverage of the sensor and extended the lifetime of the WSN so that each target was covered by a single sensor. It was also compared with the existing technology by simulation, and the conclusion showed that this model had great advantages in terms of sensor lifetime and the time of transition between different areas. But the model only considered the wireless networks' lifetime, and the coverage rate in the target detection area was easy to fall into the local optimum.

3. Duty Cycle Model of LSWSNs

Duty cycle is when there is redundancy in the node, in order to ensure that the monitoring task can be completed, a part of the nodes is put into a sleep state, and the remaining nodes are put into a working state. Completing the monitoring task in this way can reduce the overall energy consumption, thereby prolonging the network life cycle. We can also wake up sleeping nodes or set working nodes to sleep as needed. Sleeping nodes can generally turn off the sensing and communication modules in order to reduce energy consumption.

3.1. Plane Duty Cycle Model. Assume that there is a monitored area ψ in a two-dimensional planar area. The sensor nodes in the monitored area are randomly distributed. The area of the monitored area is S , and the number of nodes is n . The communication radius of the node is r_c , and the sensing radius is r_s .

In the monitored area ψ , the set of sensor nodes $\Gamma = \{N_1(x_1, y_1), N_2(x_2, y_2) \cdots N_i(x_i, y_i) \cdots\}$, where $N_i(x_i, y_i)$ represents the position coordinates of node i is (x_i, y_i) , ($i = 1, 2, \dots, n$). Any space ψ_j in the monitoring area ψ can be sensed by at least one sensor node, expressed as $\psi_j \subseteq \omega$.

The sensing range of the sensor can be represented as follows:

$$R(N_i) = \sqrt{(x_i - x)^2 + (y_i - y)^2} \leq r_s, \quad (1)$$

where (x, y) is the coordinate of the node, r_s is the perception radius, and the constraint is $(x, y) \in \psi$.

The set of neighbor nodes of sensor node N_i is expressed as

$$\Theta(N_i) = \sqrt{(x_i - x_j)^2 + (y_i - y_j)^2} \leq r_t, \quad (2)$$

where (x_i, y_i) is a neighbor node of (x_j, y_j) , r_t is the communication radius, and its constraints are $u_j \in w$ and $u_i \neq u_j$.

Each work cycle of LSWSNs is called a round. There are two stages in each round, which are divided into sleeping node stage and working stage.

As shown in the coverage relationship Figure 1, the sensor nodes N_1, N_2, N_3 , and N_4 are represented by four squares at the center of the circle. The circle represents the sensing radius of the sensor node, and the monitored targets M_1, M_2 , and M_3 are represented by three triangles, respectively. In Figure 1, four sensing nodes N_1, N_2, N_3 , and N_4 with a circular sensing radius are monitoring the targets M_1, M_2 , and M_3 . The requirement of monitoring is that each target is covered by at least one sensor node at the same time. That is, in the lifetime of the sensor network, it is necessary to maintain the network's full coverage of all three targets.

Through the above description, we can summarize the corresponding coverage relationship as follows: $N_1 \rightarrow \{M_1, M_2\}, N_2 \rightarrow \{M_2, M_3\}, N_3 \rightarrow \{M_1, M_3\}, N_4 \rightarrow \{M_1, M_2, M_3\}$.

We assume that each sensor can work for 2 rounds. If we turn on four sensors throughout the working time of the sensor, the coverage time is 2 rounds. That is, the sensor set turned on in the first round is $\{N_1, N_2, N_3, N_4\}$, and the sensor set turned on in the second round is $\{N_1, N_2, N_3, N_4\}$ too. Since the energy of the four sensors is exhausted after two rounds, the sensors can no longer work. If we divide the sensor set into different coverage sets, start only one coverage set in each round and ensure that each coverage set can complete full coverage of all three targets at the same time; then, the LSWSNs' working life can be extended by duty cycle. For example, we divide the sensor into a set $\{N_1, N_2\}$ and a set $\{N_3, N_4\}$. Through the coverage relationship, it can be concluded that the set $\{N_1, N_2\}$ can complete the full coverage of all three target sets $\{M_1, M_2, M_3\}$. Similarly, the set $\{N_3, N_4\}$ can also cover all three target sets $\{M_1, M_2, M_3\}$. Therefore, if the sensor $\{N_1, N_2\}$ is turned on in the first two rounds as shown in Figure 2, and the sensor $\{N_3, N_4\}$ is turned on after two rounds as shown in Figure 3, the life of the LSWSNs can reach four rounds.

However, four rounds are not the limit of the working time of the LSWSNs. If we allow the same sensor to belong to different coverage sets, we can further extend the lifetime

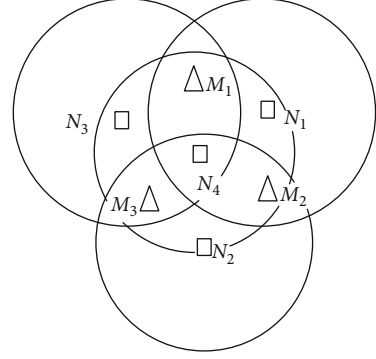


FIGURE 1: Coverage relationship between sensors and targets.

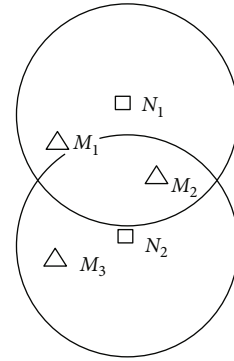


FIGURE 2: Schematic diagram of the working of sensors N_1 and N_2 .

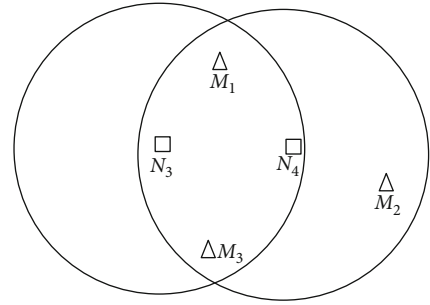


FIGURE 3: Schematic diagram of the working of sensors N_3 and N_4 .

of the LSWSNs. For example, turn on the sensor set $\{N_1, N_2\}$ in the first round, turn on the sensor set $\{N_2, N_3\}$ in the second round, and turn on the sensor set $\{N_1, N_3\}$ in the third round. Turning on the sensor set N_4 in the fourth and fifth rounds can extend the lifetime of the LSWSNs to 5 rounds while maintaining full coverage of the target.

3.2. Mathematical Model. In the two-dimensional target coverage model, not only must the detection rate be guaranteed, but also the average distance between the sensor node and the monitored target must be minimized. This monitoring effect is the best. Assuming that there are F monitoring targets and

E sensor nodes in the LSWSNs, matrix A represents a coverage relationship, the relationship between the sensor nodes in the monitoring range and the monitored target.

$$A = \begin{bmatrix} a_{1,1} & a_{1,2} & \cdots & a_{1,F-1} & a_{1,F} \\ a_{2,1} & a_{2,2} & \cdots & a_{2,F-1} & a_{2,F} \\ \vdots & \vdots & a_{e,f} & \vdots & \vdots \\ a_{E-1,1} & a_{E-1,2} & \cdots & a_{E-1,F-1} & a_{E-1,F} \\ a_{E,1} & a_{E,2} & \cdots & a_{E,F-1} & a_{E,F} \end{bmatrix} a_{e,f} \in \{0, 1\}. \quad (3)$$

In matrix A , the monitoring relationship between the e^{th} sensor node and the f^{th} monitored target is represented by $a_{e,f}$. The coverage of the e^{th} sensor node contains the f^{th} monitored target, and the value is expressed as $a_{e,f} = 1$. If it is 0, the opposite is true.

Due to energy limitations, among the E sensor nodes, round D represents each sensor's longest lifespan, and the maximum lifetime of the network is round ED , that is, the duty cycle order matrix of the sensors can be written as formula (4):

$$B = \begin{bmatrix} b_{1,1} & b_{1,2} & \cdots & b_{1,E-1} & b_{1,E} \\ b_{2,1} & b_{2,2} & \cdots & b_{2,E-1} & b_{2,E} \\ \vdots & \vdots & b_{i,e} & \vdots & \vdots \\ b_{ED-1,1} & b_{ED-1,2} & \cdots & b_{ED-1,E-1} & b_{ED-1,E} \\ b_{ED,1} & b_{ED,2} & \cdots & b_{ED,E-1} & b_{ED,E} \end{bmatrix} b_{i,e} \in \{0, 1\}. \quad (4)$$

In the formula, $b_{i,e} = 1$ means that the e^{th} sensor node is in the active state in the i^{th} round. Conversely, if the e^{th} sensor is in the sleeping state dormant in the i^{th} round, it will be expressed as $b_{i,e} = 0$.

If we multiply the two matrices, it can be obtained that the monitoring relationship between the e^{th} sensor node and the f^{th} monitored target in each round.

$$C = \begin{bmatrix} \sum_{e=1}^E b_{1,e} a_{e,1} & \sum_{e=1}^E b_{1,e} a_{e,2} & \cdots & \sum_{e=1}^E b_{1,e} a_{e,F-1} & \sum_{e=1}^E b_{1,e} a_{e,F} \\ \sum_{e=1}^E b_{2,e} a_{e,1} & \sum_{e=1}^E b_{2,e} a_{e,2} & \cdots & \sum_{e=1}^E b_{2,e} a_{e,F-1} & \sum_{e=1}^E b_{2,e} a_{e,F} \\ \vdots & \vdots & \sum_{e=1}^N b_{i,e} a_{e,f} & \vdots & \vdots \\ \sum_{e=1}^E b_{ED-1,e} a_{e,1} & \sum_{e=1}^E b_{ED-1,e} a_{e,2} & \cdots & \sum_{e=1}^E b_{ED-1,e} a_{e,F-1} & \sum_{e=1}^E b_{ED-1,e} a_{e,F} \\ \sum_{e=1}^E b_{ED,e} a_{e,1} & \sum_{e=1}^E b_{ED,e} a_{e,2} & \cdots & \sum_{e=1}^E b_{ED,e} a_{e,F-1} & \sum_{e=1}^E b_{ED,e} a_{e,F} \end{bmatrix}. \quad (5)$$

In matrix C , $\sum_{e=1}^E b_{i,e} a_{e,f} > 0$ indicates that the f^{th} target monitored in round i is monitored by at least one sensor.

And $\sum_{e=1}^E b_{i,e} a_{e,f} < 0$ means that the f^{th} monitored target in the i^{th} round is not monitored by any sensor. When LSWSN has completed all coverage in this round, the elements in this row are all positive numbers. The row number where the first zero element appears in matrix C is the round number than LSWSNs cannot complete the full coverage, and the round number minus one is the lifespan of LSWSN.

For the convenience of representation, we stipulate that the function row_{zero} represents the number of rows where the first zero element appears in the matrix C , and the duty cycle model of LSWSNs can be expressed as formulas (6) and (7):

$$\text{Objective : } f(C) = \text{row}_{\text{zero}(C)} - 1, \quad (6)$$

$$\text{Subject to : } \sum_{i=1}^{ND} b_{i,n} \leq D, n = 1 \cdots N. \quad (7)$$

4. EASA-Based Duty Cycle for Maximizing the Lifespan in LSWSNs

To solve the LSWSN target coverage problem, we propose a heuristic optimization algorithm EASA that combines elite selection and adaptive strategy. In this way, we can prevent the best individuals of the current group from being lost in the next generation, and the fitness value of each person can also be dynamically changed to improve the convergence speed. Different from traditional artificial intelligence GA, our proposed EASA takes SA as the framework and uses SA and GA to generate a new generation of individuals in the iterative process. When selecting new individuals, an adaptive selection strategy is adopted. According to the different fitness values of individuals in the current community, individuals are adaptively selected. It is ensured that every individual with low fitness in the community is eliminated, so that excellent individual genes can be preserved. In the subsequent steps, the crossover strategy is a multipoint crossover of the target individual rather than a single point. In order to ensure the diversity of individual genes, we have adopted a mutation strategy. But the mutation rate in this article is lower than that in the genetic algorithm. The process of EASA can be described as initializing population, calculating fitness, adaptive selection, crossover, mutation, temperature initialization, and termination condition.

4.1. Initializing Community. Unlike other evolutionary methods, EASA's solution competes for survival in evolutionary iterations. The EASA does not paper on a single variable but on a community with variables that undergoes an evolutionary process starting via the initial community. Additionally, a larger community size, when paired with an elitist adaptive selection method, allows the algorithm to reach a good solution more quickly than a smaller community size. In EASA, each target is randomly initialized by a random number generator. Because the random value has great discreteness, the accuracy of the solution will be lower if it is used directly. Therefore, EASA developed the best solution for improvement according to formula (10).

For the LSWSNs to solve the optimal coverage set selection problem, the working and sleeping state of the wireless sensor N_i are represented by the bit string $G = (g_1, g_2, \dots, g_h, \dots, g_H)$, through formula (1), and the actual space is converted into the corresponding coding space.

$$g_h = \begin{cases} 1, N_i \text{ was selected as a working node in round } h \\ 0, \text{ otherwise} \end{cases}, \quad (8)$$

where g_h represents any sensor node.

Assuming a total of 8 sensor nodes are placed in the monitoring area, the length of string G is 8. If the nodes $\{N_1, N_4, N_6\}$ are working, this string can be expressed as $\{1, 0, 0, 1, 0, 1, 0, 0\}$.

In order to convert the search for the genotype individual space into the problem of finding the optimal solution to the community, we set the sensor community to three dimensions. And all sensors are working within the number of working rounds. Then, the community code is as follows:

$$\text{Chrom}(D, E, \text{NUM}) = 1, \quad (9)$$

where matrix Chrom is the initial community and NUM is the number of initial communities. D represents the maximum number of rounds that the sensor can work, and E is the number of sensors.

4.2. Calculating Fitness. The fitness of an individual is directly corresponding to its objective value. In this paper, the objective value of a solution variable depends on the working life of sensor network. In this way, the longer the lifespan, the better the individual is. During each iteration, use formula (10) to evaluate individuals. The specific operation is as follows:

First, calculate the fitness value of the individual, then select the minimum fitness value in the community, and finally subtract the minimum fitness value from each individual in the community to obtain a new fitness value. We propose a three-dimensional community $\text{Chrom}(D, E, \text{NUM})$. The fitness value we proposed is to calculate the working life of the LAWSNs, that is, to calculate the number of positive numbers in each row of the matrix C in Chapter 3. The initial fitness value is DE . The existence of zero elements in matrix C means that the sensor network cannot complete the complete coverage in this round, so the applicability of formula (10) is modified. To increase the fitness value, we add an adaptive factor. This method can also optimize the group coverage problem. The adaptive selection formula is shown in formula (11).

$$\text{Fitness}(W_n) = \text{fitness}(W_n) - 1, \quad (10)$$

where W_n represents any network entity and $n \in [1, \text{NUM}]$.

$$\text{Fitness}(W_n) = \text{fitness}(W_n) - \min(\text{fitness}). \quad (11)$$

4.3. Adaptive Selection. Selection is a genetic operation, which is to select an individual from the current community and place it in the next generation's community. Individuals with low fitness values are generally discarded.

In result, the probability of premature convergence decreases relatively and the preservation of individual is improved. In this respect, it is important to note that not all individuals are chosen. The way to be selected is as in formulas (12), (13), and (14).

$$p(W_n) = \frac{\text{fitness}(W)}{\sum_{n=1}^{\text{NUM}} \text{fitness}(W_n)} \quad n = 1, 2, \dots, \text{NUM}, \quad (12)$$

$$P(n) = P(n-1) + p(W_n) \quad n = 1, 2, \dots, \text{NUM}, \quad (13)$$

$$P(W_{n-1}) < \text{rand} < P(W_n) \quad n = 1, 2, \dots, \text{NUM}. \quad (14)$$

W_n represents any network entity, $\text{fitness}(W_n)$ is the fitness value of the W_n^{th} sensor network, $p(W_n)$ represents the probability of the sensor network W_n being selected, and rand is a random number between 0 and 1.

Repeat the above steps until the iteration is complete. The new community generated is composed of members of the current self or the parent community. In this way, the community is constantly updated. After multiple iterations, the elimination of low fitness values can be achieved in the simulation, and the high retention can be achieved.

4.4. Crossover. After finishing the operation of selecting individuals from the current iteration community, the next step is to perform crossover and selection operations to generate the second iteration community. In the crossover operation, the children copy the parent's gene, and the point where the parent chromosome crosses is randomly generated. Each of these couples will have two children. The crossover operation is not static; there is one point, two points, and uniform crossover. In EASA, the multipoint crossover based on the target value is used to modify, and the expression is defined as formulas (15) and (16).

We set the parent matrix representing the individual as X_1 and X_2 , and the child matrixes are X'_1 and X'_2 . Assume that the number of sensors in each LSWSNs is 3, and the number of sensors working rounds is 4. Randomly generate a number U between 1 and 4 and cross all the numbers from 1 to U in matrix X_1 with the numbers from 1 to U in matrix X_2 . After crossover, child matrices X'_1 and X'_2 are generated.

$$X_1 = \begin{bmatrix} 1 & 1 & 11 & \\ 1 & 1 & 1 & 1 \\ 1 & 1 & 1 & 1 \end{bmatrix} \quad X_2 = \begin{bmatrix} 0 & 0 & 0 & 0 \\ 0 & 0 & 0 & 0 \\ 0 & 0 & 0 & 0 \end{bmatrix}. \quad (15)$$

After crossover,

$$X'_1 = \begin{bmatrix} 1 & 1 & 0 & 1 \\ 1 & 1 & 0 & 1 \\ 1 & 1 & 0 & 1 \end{bmatrix} \quad X'_2 = \begin{bmatrix} 0 & 0 & 1 & 0 \\ 0 & 0 & 1 & 0 \\ 0 & 0 & 1 & 0 \end{bmatrix}. \quad (16)$$

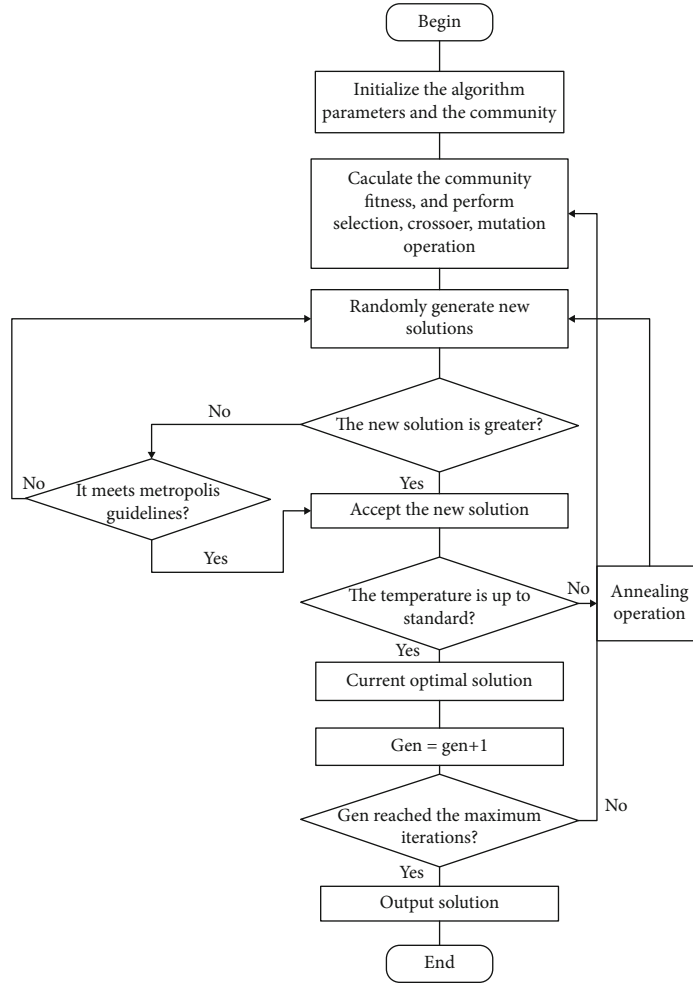


FIGURE 4: Steps of EASA.

4.5. Mutation. Sporadically, in biological systems, there will be unavoidable errors in copying random information, and mutations will occur. This kind of mutation puts it in the mutation operation. Therefore, the mutation operation is to randomly select an individual and randomly select the position of this individual to mutate. Mutation operation is to randomly select individuals in the community and then invert the values of some of its columns or mutate a certain gene of the individual to perform mutation operations. The mutation in this paper is to change the value of some bits of an individual from 1 to 0 or from 0 to 1. It is worth noting that the probability of mutation is very small.

4.6. Annealing Operator. The physical annealing process consists of the following three parts: heating process, isothermal process, and cooling process. The SA realizes a large-scale coarse search and a local fine search by controlling the initial value T_0 of the annealing temperature and its attenuation change process. Generally speaking, only a large enough T_0 can meet the algorithm requirements. Because when the problem scale is large, too small T_0 often makes it difficult for the algorithm to escape the local trap and fail to reach the global optimum. But in order to reduce the amount of

TABLE 1: Parameters of the GA.

	Iteration numbers	Community size	Crossover probability	Mutation probability
GA	100	50	0.9	0.05

TABLE 2: Parameters of the PSO.

	Iteration numbers	Community size	The maximum velocity	The cognitive and social parameters
PSO	100	50	4	2

TABLE 3: Parameters of the EASA.

	Iteration numbers	Community size	The initial temperature	Attenuation coefficient
EASA	100	50	200	0.9

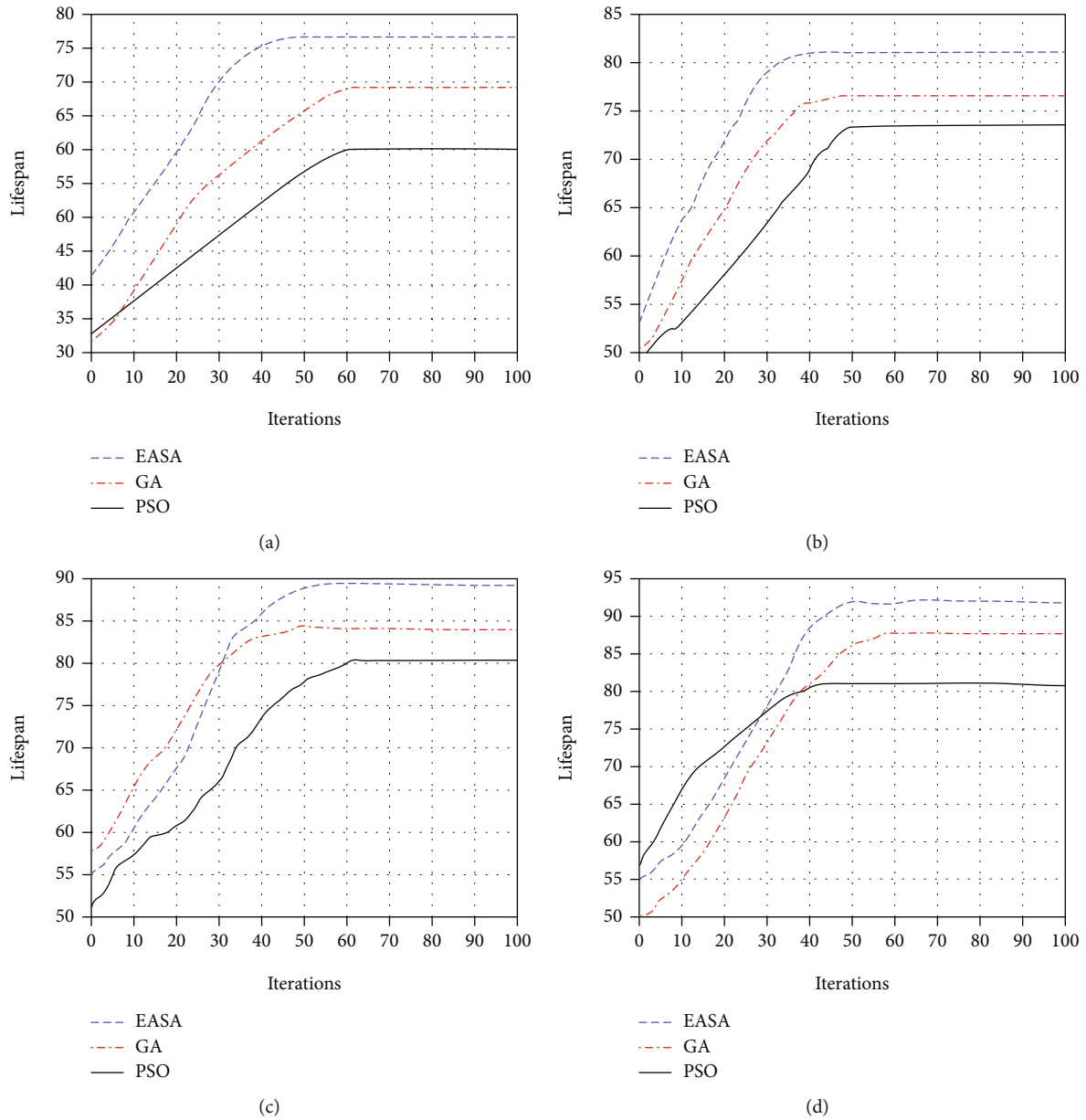


FIGURE 5: The lifespan of the three algorithms. (a) 80 sensors; (b) 90 sensors; (c) 100 sensors; (d) 110 sensors.

calculation, T_0 should not be too large. Set the number of cycles at the same temperature as count.

The steps of the annealing operator are as follows:

- (1) Set the fitness value of the current population as the initial optimal solution
- (2) Set the number of cycles count at the same temperature to 0
- (3) Perturb the population that currently generates the optimal solution, generate a new solution, and calculate a new fitness value U_u . According to formula (17), if the difference between the new solution U_u and the old solution U_{u-1} is greater than 0, the new

solution is accepted. Otherwise, the acceptance probability q of a new solution is generated. Then, compare q with the random number rand , and if q is greater than the random number, accept it; otherwise, do not accept it

$$q = \begin{cases} \exp\left(\frac{-(U_m - U_{m-1})}{T_k}\right), & \text{if } U_m < U_{m-1}, \\ 1 & \text{if } U_m \geq U_{m-1}. \end{cases} \quad (17)$$

- (4) If the cycle number is less than count, then add 1 and return to step (3). Otherwise, execute formula (17).

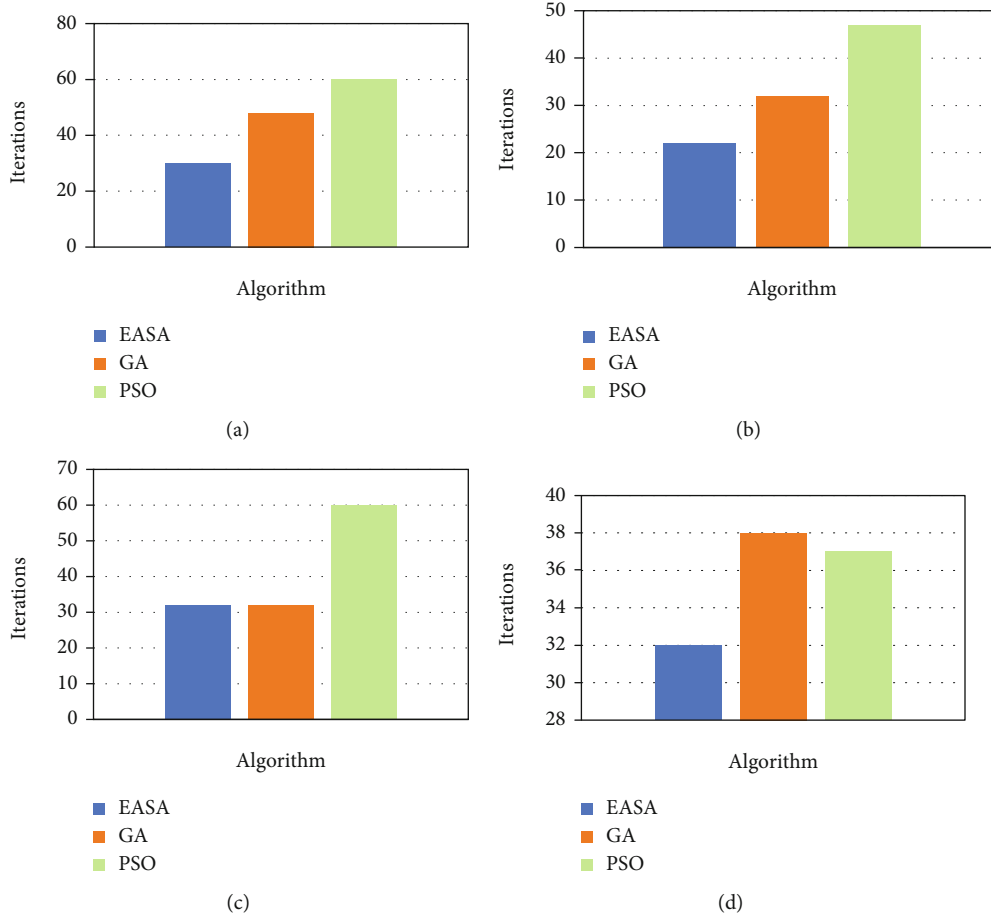


FIGURE 6: The number of iterations required for the three algorithms to reach 4 different network lifetimes, respectively. (a) The number of sensors is 80, and the solutions of the three algorithms reach 60; (b) the number of sensors is 90, and the solutions of the three algorithms reach 73; (c) the number of sensors is 100, and the solutions of the three algorithms reach 80; (d) the number of sensors is 110, and the solutions of the three algorithms reach 80.

α is the attenuation coefficient. T is the current temperature

$$T = \alpha T. \quad (18)$$

4.7. Termination Condition. Termination is the criterion by which EASA decides whether to continue the iteration or stop. In the process of repeating the iterative loop, until the solution of the predetermined number of iterations is reached. When the target value reaches a certain threshold, EASA will terminate according to the number of iterations. After the maximum number of iterations, the process is terminated, and the individual with the highest fitness in the community is the final solution.

4.8. Steps of the Algorithm. First, initialize the algorithm parameters and the community. Then, calculate the initial community fitness value and perform adaptive selection, crossover, and mutation. Next, an annealing operation is performed to determine the size of the new value and the old value in turn. Finally, determine whether the termination

condition is reached. The specific details of the EASA process are shown in Figure 4.

5. Simulation and Results

The EASA method we proposed to solve the sensor duty cycle problem will carry out a series of experiments and compare EASA with GA and PSO to prove its effectiveness. The comparison of algorithms is carried out under different number of sensors. In addition, all test cases are completed on a computer equipped with matlab2018a, and the applicability used in the algorithm is calculated according to formula (10).

In order to be able to compare these three algorithms under the same experimental conditions, we uniformly define the parameters commonly used in the sensor duty cycle problem in LSWSNs. The number of iterations is set to 100 generations, and the population size is 40. The surveillance area of LSWSNs is set as a square area with a side length of 200, and the coordinates of the sensor and target node are randomly generated in this area.

The comparison between the three algorithms uses the same number of iterations of 50 and community size of 50. And the coordinate parameters of the sensor nodes are the

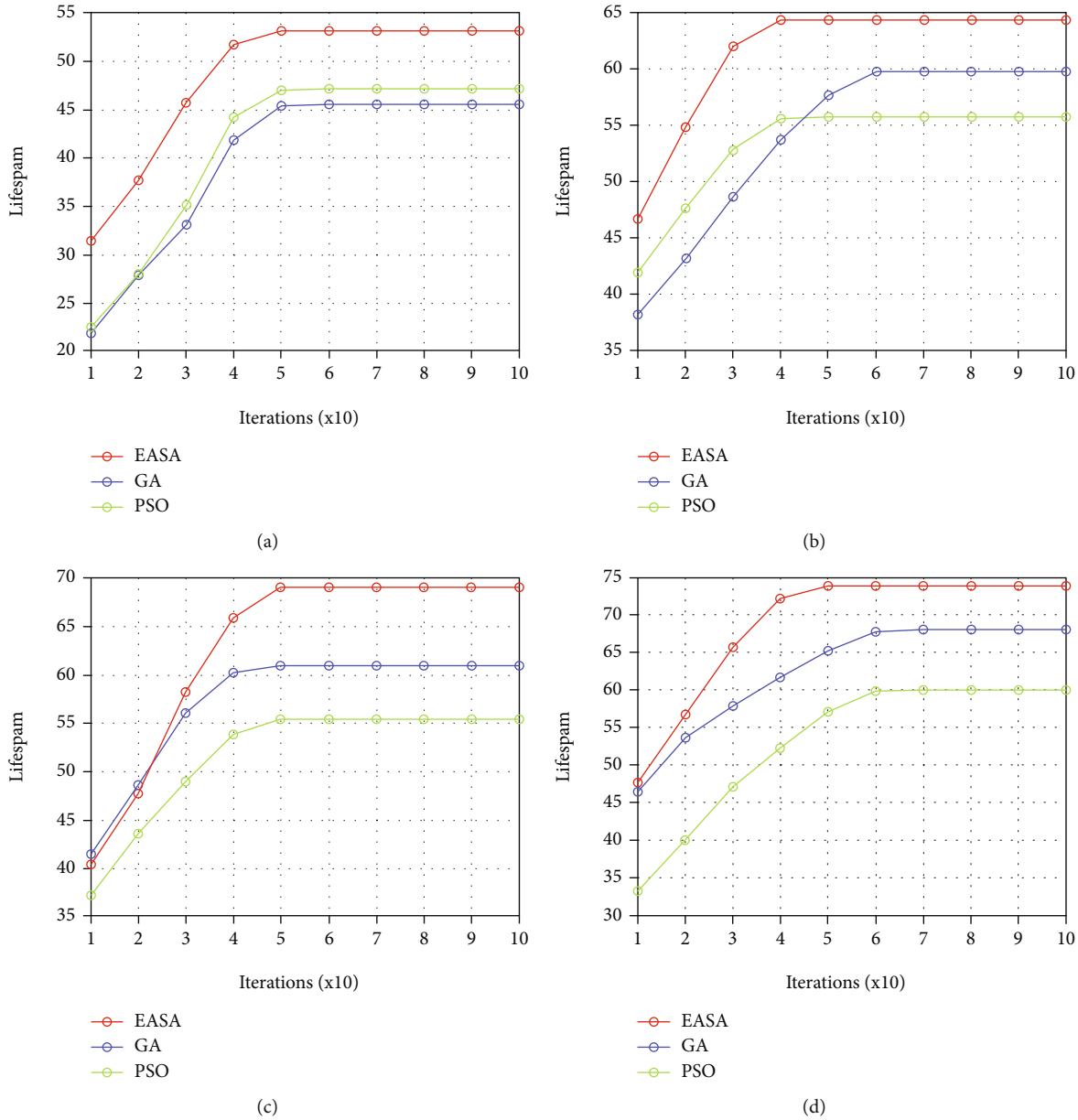


FIGURE 7: The lifespan of the three algorithms. (a) 40 sensors; (b) 50 sensors; (c) 60 sensors; (d) 70 sensors.

same, and each individual has the same number of genes. The specific parameters of GA, PSO, and EASA are in Tables 1–3.

The key to affecting the behavior and performance in GA is the probability of crossover and mutation. The greater the crossover probability, the faster the iteration speed of the new individual. And too much crossover probability will increase the risk of genetic model being destroyed. If the mutation probability is too small, too few new individuals will be produced. Therefore, in this simulation calculation, the crossover probability is set to 0.9, and the mutation probability is 0.05.

In PSO, the maximum speed determines the maximum moving distance of the particles in a cycle, which is set to 4. Both cognitive and social parameters are set to 2, namely, $c_1 = c_2$.

In EASA, the area where the global maximum fitness value is located can only be found in the initial large-scale search stage, and the search range can be gradually reduced. Therefore, only a sufficiently large initial temperature can meet the algorithm requirements, so the initial temperature is set to 200. The settings of crossover probability are 0.9. And mutation probability is 0.03. The attenuation coefficient determines the cooling process. If the attenuation coefficient is too large, it will slow down the temperature attenuation process, resulting in an increase in the number of iterations of the algorithm, so it should not be too large, and set it to 0.9.

Figure 5 shows the convergence speed and lifespan change of the three algorithms of EASA, GA, and PSO under different sensor numbers. It can be seen that EASA has a longer network life than GA and PSO. It is because when

selecting a new generation of individuals, EASA adopts an adaptive selection strategy. This will eliminate individuals with low fitness in each community and ensure the ability of the new community to find the best. And the mutation strategy of EASA increases the diversity of individuals in the community and prevents EASA from falling into local extremes. Although GA also uses a mutation strategy, the probability of mutation is lower than that of GA, which reduces the risk of model damage. In Figure 5(a), the GA and PSO solutions were not very different at the beginning and the sensor number is 80. Gradually, the 10th generation opened the gap. At the same time, EASA's solution has always been higher than the other two algorithms. When EASA converges, the final LSWSNs' lifetime is 76.65. The LSWSNs' lifetimes of the other two algorithms, GA and PSO, are 69.13 and 60, respectively.

In Figure 5(b), as the number of sensors is 90, the growth trends of the three solutions are roughly the same. Ultimately, the maximum lifespan of EASA is 81.35, GA is 76.85, and PSO is 73.38. In Figures 5(c) and 5(d), when the sensor number is 100 and 110, there are changes compared with the previous two simulation results. In Figure 5(c), at the beginning, the growth rate of GA is greater than that of EASA and PSO, until the situation changes when the number of iterations reaches 30. EASA's solutions continue to grow, while GA tends to be smooth, gradually converging to 83.85. Finally, EASA is 88.97, and PSO is 80. In Figure 5(d), under the condition that the sensor is 110, PSO's solutions are relatively flat, as well as EASA and GA continued to grow until EASA's solution is 91.97 and GA is 87.87. And PSO is 80.78.

Figure 6 is made to better show the convergence speed of the three algorithms. In Figure 6(a), we take the LSWSNs' lifetime as 60 and the number of sensors as 80. The solutions of the three algorithms are, respectively, 30, 48, and 60 iterations. The trend of the histograms in Figures 6(b) and 6(a) is the same, but the condition in Figure 6(b) is that the number of sensors is 90, and the common lifespan is 73. The iteration time required for the three solutions is 22, 32, and 60 in order. Figure 6(c) shows that when the number of sensors is 90, the number of iterations required for the three algorithms to reach a lifetime of 73 together is 32, 32, and 47. In Figure 6(d), as the sensor number is 110, and the lifespan is 80, EASA, GA, and PSO require 32 iterations, 38 iterations, and 37 iterations in turn.

Figures 7(a)–7(d) show the trend of the three algorithms more clearly in the form of line charts. Specifically, in Figure 7(a), it is shown that when the number of sensors is 40, the convergence speed of EASA is faster than the other two solutions, and EASA maintains a higher lifespan in the iterative process. From the beginning of the iterative process, the lifetime value of EASA is higher than GA and PSO, and EASA keeps a higher value until the algorithm convergence is reached. In Figure 7(a), the difference between PSO and GA is not very obvious, and their optimal solutions are 47.14 and 45.56, respectively. On the contrary, the lifespan of EASA can reach 53.14.

In Figure 7(b), although the solutions of EASA and PSO converge at the same time, the network lifetime of EASA is

TABLE 4: Improvement percentage of network lifespan by EASA compared with GA and PSO.

Sensor number	40	50	60	70
GA	16.55%	7.81%	13.34%	8.50%
PSO	12.73%	15.54%	24.63	22.95%

significantly higher than that of PSO. As the number of iterations increases, EASA's solution has been higher than the other two algorithms until all three algorithms converge. Before the 41st generation, the solution of PSO is higher than that of GA, but PSO tends to converge to 55.78, and GA continues to increase until the lifespan is 59.78. Finally, the maximum lifespan reached by EASA is 64.45.

Other than that, there is little difference between the trends in Figures 7(c) and 7(d). EASA's solutions are all the highest, but the iteration in which the three solutions tend to converge is different. In Figure 7(c), the maximum lifetimes of EASA, GA, and PSO are 68.97, 60.85, and 55.34, respectively. Similarly, in Figure 5(d), the values of the three solutions are 73.77, 67.99, and 60.00.

In order to better illustrate the advantages of EASA, in Table 4, EASA is compared with GA and PSO, and the percentage increase in network lifespan is shown.

Table 4 shows that when the number of sensors is 40, 50, 60, and 70, EASA has a higher lifetime percentage than GA and PSO. It can be seen that EASA can be up to 16.55% higher than GA and 24.63% higher than PSO.

6. Conclusions

In this paper, we propose an elite adaptive simulated algorithm (EASA) to settle the target coverage problem in LSWSNs. We first formulate our aim function as formula (10) to maximize the working life of sensor network under multiple constraints. To demonstrate the advantages of EASA, the target coverage problem was simulated. And we used GA and PSO for performance comparison. Simulation experiments show that our proposed EASA solution has a longer lifespan of LSWSNs than GA and PSO, and its complexity is lower than previous methods.

Data Availability

The data presented in this study are available on request from the corresponding author. The data are not publicly available due to privacy.

Disclosure

The funders had no role in the design of the study, in the collection, analyses, or interpretation of data, in the writing of the manuscript, or in the decision to publish the results.

Conflicts of Interest

The authors declare no conflict of interest.

Acknowledgments

This paper was funded by the Corps innovative talents plan, grant number 2020CB001, the project of Youth and Middle-aged Scientific and Technological Innovation Leading Talents Program of the Corps, grant number 2018CB006, the China Postdoctoral Science Foundation, grant number 220531, the Funding Project for High Level Talents Research in Shihezi University, grant number RCZK2018C38, the Project of Shihezi University, grant number ZZZC201915B, and the Postgraduate Education Innovation Program of the Autonomous Region.

References

- [1] M. L. Umashankar, M. V. Ramakrishna, and S. Mallikarjunaswamy, "Design of high speed reconfigurable deployment intelligent genetic algorithm in maximum coverage wireless sensor network," in *2019 International Conference on Data Science and Communication (IconDSC)*, pp. 1–6, Bangalore, India, 2019.
- [2] R. Elhabyan, W. Shi, and M. St-Hilaire, "Coverage protocols for wireless sensor networks: review and future directions," *Journal of Communications and Networks*, vol. 21, no. 1, pp. 45–60, 2019.
- [3] M. O. Ramkumar, "Intelligent fruit fly algorithm for maximization coverage problem in wireless sensor network," in *2020 7th International Conference on Smart Structures and Systems (ICSSS)*, pp. 1–6, Chennai, India, 2020.
- [4] S. Najjar-Ghabel, L. Farzinavash, and S. N. Razavi, "Mobile sink-based data gathering in wireless sensor networks with obstacles using artificial intelligence algorithms," *Ad Hoc Networks*, vol. 106, p. 12, 2020.
- [5] G. S. Gandhi, K. Vikas, V. Ratnam, and K. S. Babu, "Grid clustering and fuzzy reinforcement-learning based energy-efficient data aggregation scheme for distributed WSN," *IET Communications*, vol. 14, no. 16, pp. 2840–2848, 2020.
- [6] W. Liao, B. Dande, C. Chang, and D. S. Roy, "MMQT: maximizing the monitoring quality for targets based on probabilistic sensing model in rechargeable wireless sensor networks," *IEEE Access*, vol. 8, pp. 77073–77088, 2020.
- [7] S. S. Manju, S. Kumar, A. Nayyar, F. Al-Turjman, and L. Mostarda, "Proficient QoS-based target coverage problem in wireless sensor networks," *IEEE Access*, vol. 8, pp. 74315–74325, 2020.
- [8] P. Chaturvedi and A. K. Daniel, "Hidden Markov model based node status prediction technique for target coverage in wireless sensor networks," in *2017 International Conference on Intelligent Communication and Computational Techniques (ICCT)*, pp. 223–227, Jaipur, 2017.
- [9] P. Chaturvedi and A. K. Daniel, "Trust aware node scheduling protocol for target coverage using rough set theory," in *2017 International Conference on Intelligent Computing, Instrumentation and Control Technologies (ICICT)*, pp. 511–514, Kanpur, 2017.
- [10] S. E. Bouzid, Y. Seresstou, K. Raoof, M. N. Omri, M. Mbarki, and C. Dridi, "MOONGA: multi-objective optimization of wireless network approach based on genetic algorithm," *IEEE Access*, vol. 8, pp. 105793–105814, 2020.
- [11] J. Li, Z. Luo, and J. Xiao, "A hybrid genetic algorithm with bidirectional mutation for maximizing lifetime of heterogeneous wireless sensor networks," *IEEE Access*, vol. 8, pp. 72261–72274, 2020.
- [12] J. Wang, Y. Cao, B. Li, H. J. Kim, and S. Lee, "Particle swarm optimization based clustering algorithm with mobile sink for WSNs," *Future Generation Computer Systems*, vol. 76, pp. 452–457, 2017.
- [13] S. C. Manju and B. Kumar, "Genetic algorithm-based meta-heuristic for target coverage problem," *IET Wireless Sensor Systems*, vol. 8, no. 4, pp. 170–175, 2018.
- [14] Z. Jiao, L. Zhang, M. Xu, C. Cai, and J. Xiong, "Coverage control algorithm-based adaptive particle swarm optimization and node sleeping in wireless multimedia sensor networks," *IEEE Access*, vol. 7, pp. 170096–170105, 2019.
- [15] T. Qasim, M. Zia, Q. A. Minhas et al., "An ant colony optimization based approach for minimum cost coverage on 3-D grid in wireless sensor networks," *IEEE Communications Letters*, vol. 22, no. 6, pp. 1140–1143, 2018.
- [16] N. Nguyen and B. Liu, "The mobile sensor deployment problem and the target coverage problem in mobile wireless sensor networks are NP-hard," *IEEE Systems Journal*, vol. 13, no. 2, pp. 1312–1315, 2019.
- [17] I. N. Dziubenko and T. M. Tatarnikova, "Algorithm for solving optimal sensor devices placement problem in areas with natural obstacles," in *2018 Wave electronics and its application in information and telecommunication systems (WECONF)*, pp. 1–5, St. Petersburg, 2018.
- [18] N. Meena and B. Singh, "Coverage maximization using multi-objective optimization approach for wireless sensor network in real time environment," in *2018 IEEE 8th International Advance Computing Conference (IACC)*, pp. 333–337, Greater Noida, India, 2018.

Research Article

An Adaptive Immune Ant Colony Optimization for Reducing Energy Consumption of Automatic Inspection Path Planning in Industrial Wireless Sensor Networks

Chaoqun Li ¹, Jing Xiao,¹ Yang Liu,¹ Guohong Qi ¹, Hu Qin,¹ and Jie Zhou ^{1,2}

¹College of Information Science and Technology, Shihezi University, Shihezi, China

²Xinjiang Tianfu Information Technology Co., Ltd., China

Correspondence should be addressed to Jie Zhou; jiezhou@shzu.edu.cn

Received 4 March 2021; Revised 27 March 2021; Accepted 3 April 2021; Published 23 April 2021

Academic Editor: Mario E. Rivero-Angeles

Copyright © 2021 Chaoqun Li et al. This is an open access article distributed under the Creative Commons Attribution License, which permits unrestricted use, distribution, and reproduction in any medium, provided the original work is properly cited.

Industrial wireless sensor networks (IWSNs) are usually fixedly deployed in industrial environments, and various sensor nodes cooperate with each other to complete industrial production tasks. The efficient work of each sensor node of IWSNs will improve the efficiency of the entire network. Automated robots need to perform timely inspection and maintenance of IWSNs in an industrial environment. Excessive inspection distance will increase inspection costs and increase energy consumption. Therefore, shortening the inspection distance can reduce production energy consumption, which is very important for the efficient operation of the entire system. However, the optimal detection path planning of IWSNs is an N-P problem, which can usually only be solved by heuristic mathematical methods. This paper proposes a new adaptive immune ant colony optimization (AIACO) for optimizing automated inspection path planning. Moreover, novel adaptive operator and immune operator are designed to prevent the algorithm from falling into the local optimum and increase the optimization ability. In order to verify the performance of the algorithm, the algorithm is compared with genetic algorithm (GA) and immune clone algorithm (ICA). The simulation results show that the inspection distance of IWSNs using AIACO is lower than that of GA and ICA. In addition, the convergence speed of AIACO is faster than that of GA and ICA. Therefore, the AIACO proposed in this paper can effectively reduce the inspection energy consumption of the entire IWSN system.

1. Introduction

Intelligent manufacturing has emerged with the rapid development of information technology. IWSNs are one of the key technologies of intelligent manufacturing, and they are a combination of IWSNs and the Internet of Things [1–3]. Compared with traditional wired industrial sensor networks, it has the characteristics of fast deployment, high flexibility, and self-organization. It has broad application prospects in intelligent dispatching, industrial monitoring, and other fields. However, the battery-powered sensor node limits the overall performance of IWSNs [4–7]. Therefore, the inspection of IWSNs can effectively ensure the healthy operation of the system. Due to the large scale of IWSNs, the cost of

an entire network inspection is very high. Therefore, planning an optimal inspection path is an effective way to reduce inspection costs [8–10].

At this stage, there are many path planning algorithms that can be used for automated robot inspections of IWSNs, such as rapidly exploring random tree (RRT) algorithm, Dijkstra algorithm, A* algorithm, GA, and ICA [11–15]. These algorithms can find a relatively good path, but they also have various disadvantages. Dijkstra is not suitable for optimizing combinatorial optimization problems. The RRT algorithm performs random point connection search, and it is difficult to find the optimal path. Although A* has added heuristic ideas, there is a problem that the optimal path cannot be guaranteed. Compared with the first three algorithms,

GA and ICA have improved, but due to the slow convergence speed, it is easy to fall into the local optimum, and the algorithm performance is not very good.

Regarding the problems of the above algorithms, this article designs a new AIACO to overcome the above shortcomings. Aiming at the problem of minimizing the inspection overhead faced by IWSNs, applying path planning optimization technology to IWSNs can effectively reduce the overall inspection overhead of the network. AIACO's inspection path optimization can provide a low-cost, high-efficiency letter inspection method for IWSNs. The simulation proves AIACO's ability to optimize the inspection path of IWSNs.

The main contributions are as follows:

- (1) First, this paper proposes an adaptive immune ant colony optimization (AIACO) to solve the optimization problem of automated inspection path planning, design a path planning model for IWSNs, and design a new fitness function to evaluate the performance of the algorithm
- (2) Secondly, new adaptive operator and immune operator are designed in this paper to enhance the optimization ability of the algorithm. AIACO, which combines adaptive operators and immune operators, has better performance, enhances global search capabilities, and avoids falling into local optimum
- (3) Finally, we compare the simulation results of AIACO with GA and ICA in the inspection path planning of IWSNs to prove the superior performance of AIACO in path planning and optimization and give detailed data and demonstrations. More importantly, it also provides a new method for the research field of automated inspection path planning

The remaining structure of the paper is shown below. Section 2 introduces related research on the optimization of inspection path planning in the field of IWSNs. Section 3 shows the path planning model. Section 4 proposes an adaptive immune ant colony optimization to solve the inspection path planning problem in IWSNs. Section 5 demonstrates the effectiveness of AIACO in solving the task assignment problem through simulation experiments and discusses it. Section 6 is the conclusion part.

2. Related Work

In recent years, the research on the optimization of inspection path planning of IWSNs has attracted a large number of scholars [16, 17]. In IWSNs, an effective inspection program can obtain lower inspection time and lower cost and improve industrial production efficiency [18, 19]. There are also many optimization algorithms for path planning, which are basically divided into heuristic algorithms and nonheuristic algorithms.

The paper [20] proposed a weighted pigeon swarm algorithm for UAV trajectory planning in a complex environment and introduced weight coefficients to calculate the

speed and position of individuals in the population to improve the quality and efficiency of route planning. However, this algorithm has the problems of being easy to fall into local optimum, slow and unstable convergence speed.

In [21], the authors aimed at the rapid planning of the optimal trajectory of the intelligent aircraft, considering the error constraints and the correction probability constraints, constructing the trajectory planning model of the intelligent aircraft under multiple constraints, and proposed a global search algorithm based on Dijkstra to solve the model. The algorithm proposed by the author improves the basic Dijkstra algorithm by calculating the residual error and constrained flight distance, so that it has better adaptability when solving the trajectory planning problem under multiple constraints. However, Dijkstra is not suitable for solving path planning problems.

In [22], the authors aimed at the problem of low node utilization and large calculation amount in the traditional RRT algorithm. Based on the fast RRT algorithm, they optimized the strategy of reselecting the parent node and pruning range, improved the sampling method, and introduced adaptive Step size; the fast RRT algorithm is improved, making the algorithm time-consuming and path length shorter. At the same time, the node connection screening strategy is added to eliminate the excessive turning angle in the path, and a path can be searched in a high-dimensional environment. However, the fast RRT algorithm still has a large amount of calculation and slow convergence speed, and it is difficult to find the optimal path.

In [23], the authors proposed an improved A* algorithm. The improved algorithm extends the traditional 8-neighborhood search to 24 neighborhoods and uses guidance vectors to optimize the number of neighborhoods, eliminate redundant nodes, improve search efficiency, and optimize smooth paths. However, this algorithm has low search freedom, and the planned path length is still very long.

In [24], the authors proposed a mobile robotic arm picking path optimization method based on an improved GA. Through the analysis of the position of the picked items, the mobile robotic arm sorting path model and multistation at a single station are established. Point's traveling salesman (TSP) problem model, using an improved GA to optimize the position coordinates of each station point in the workspace, and plan the shortest path captured by the mobile robot arm and the shortest movement between multistation point path. However, this algorithm still has the problems of premature and slow convergence.

In [25], the author simulated the optimization path planning problem of the biological immune process and established the mathematical model of the ICA. Using the random process theory, the convergence of the Markov chain of the population sequence formed by the ICA is proved. The author verifies that the algorithm's ability to maintain diversity is stronger than general genetic algorithms in searching for local and global solutions. However, this algorithm is easy to fall into the local optimum, and there is a problem of insufficient convergence accuracy.

Aiming at the shortcomings in the above literature, we propose a new solution to solve the problem of IWSN

inspection path planning optimization, improve the overall inspection speed of the IWSN system, increase the automation efficiency, reduce the cost of industrial production, and improve the industrial production effectiveness.

3. System Model

In a complex IWSN environment, regarding the network control range and path planning constraints, in order to minimize the inspection path, a mathematical model is designed based on two-dimensional coordinates. This model can realize automatic inspection of sensor nodes in an industrial environment, so that the path of inspection of IWSNs is the shortest. This model can be simply abstracted into an undirected complete graph $G(V, E)$. V represents a node set composed of N sensor nodes, and E represents a set of distances between every two nodes. Assume that N industrial sensor nodes have been installed in the industrial detection environment, represented by integer codes $(1, 2, \dots, N-1, N)$, and the two-dimensional coordinates of each sensor node are known. The distance between node i and node j is $d_{i,j}$ which can be calculated by formula (1), where i_x and j_x represent the abscissa of nodes i and j , respectively, and i_y and j_y represent the ordinate of nodes i and j , respectively. The ultimate goal of this paper is to find the shortest inspection path to reduce inspection overhead.

$$d_{i,j} = \sqrt{(i_x - j_x)^2 + (i_y - j_y)^2} \quad (i, j = 1, 2, \dots, N). \quad (1)$$

Suppose S_n is a set of randomly generated solutions for the inspection path planning, and s represents one of the arbitrary N sensor node sets. The robot inspection starts from s_1 , inspects to s_N , and then returns to s_1 . A group of inspection paths is represented by formula (2). The distance between every two nodes of the inspection path is represented by $d_{s_n, s_{n+1}}$. The total inspection path length is represented by d_{sum} , which can be calculated by formula (3). $\sum_{n=1}^N d_{s_n, s_{n+1}}$ represents the distance from s_1 through all nodes to s_N ; d_{s_N, s_1} represents the distance from s_N to s_1 .

$$S = [s_1 s_2 \cdots s_n \cdots s_{N-1} s_N] (s_n \in [1, N]), \quad (2)$$

$$d_{\text{sum}} = d_{s_N, s_1} + \sum_{n=1}^N d_{s_n, s_{n+1}}. \quad (3)$$

In order to explain the model more clearly, suppose there are 8 industrial sensor nodes in total, and a random inspection path is planned. This path is expressed in formula (4). The distance between two of the 8 nodes can be calculated sequentially in vector order, and the total path length can be calculated according to formula (3).

$$S = [6 \ 2 \ 4 \ 3 \ 1 \ 5 \ 8 \ 7]. \quad (4)$$

The inspection path planning of IWSNs must not only meet the actual production requirements but also reduce

the inspection cost of the entire IWSNs. The shorter the path, the higher the inspection efficiency of the system. The inspection path refers to the trajectory that the robot traverses in one-time inspection of each sensor node in the system. Especially in large-scale IWSNs, the difficulty of inspection increases exponentially as the number of nodes increases. Therefore, an excellent inspection path planning program can achieve lower network inspection costs and higher network operation efficiency.

4. AIACO for Reducing Energy Consumption of Automatic Inspection Path Planning in IWSNs

Aiming at the problem of inspection path planning in IWSNs, a new optimization algorithm of AIACO is proposed. In the proposed AIACO strategy, new adaptive operators and immune operators are designed. Operators can enable AIACO to plan the shortest inspection path and find the best solution.

Basic ant colony optimization often has insufficient convergence accuracy and is easy to fall into local optimum. Therefore, this article proposes an innovative adaptive strategy in AIACO. In the pheromone update stage, the pheromone update can be adjusted in time according to the operation of the algorithm, thereby increasing the global search capability of the entire AIACO. A new clonal immune strategy is designed to accelerate the algorithm convergence. In the ant-cycle model, after evaluating the fitness of each ant in the ant colony, a clone immune method is adopted to clone the elite ants and form a new colony according to the immune mechanism. Therefore, the two new strategies can improve AIACO's ability to solve the inspection path planning problem in IWSNs.

The execution steps of AIACO are shown in Figure 1.

Use the following detailed steps to illustrate the algorithm flow chart shown in Figure 1.

Step 1. Design coding rules. Use integer encoding.

Step 2. Initialize the ant colony. Construct an ant colony that meets the path planning model conditions. The ant colony can be abstracted as an integer matrix. Set M ants and N sensor nodes. The matrix can be expressed as $\text{mat}\{MN\}$.

Step 3. Cycle each ant. Generate a set of ant colony solutions.

Step 4. Adjust the volatilization factor. Use an adaptive mechanism to change the exponential factor.

Step 5. Update pheromone. Use dynamically changing volatilization factor to update.

Step 6. Calculate the fitness of the ants. According to the fitness of each individual to evaluate the quality of the program.

Step 7. Clone the elite ants. Clone the most adaptable ants and use immunity to regenerate a new colony. Repeat Step 6.

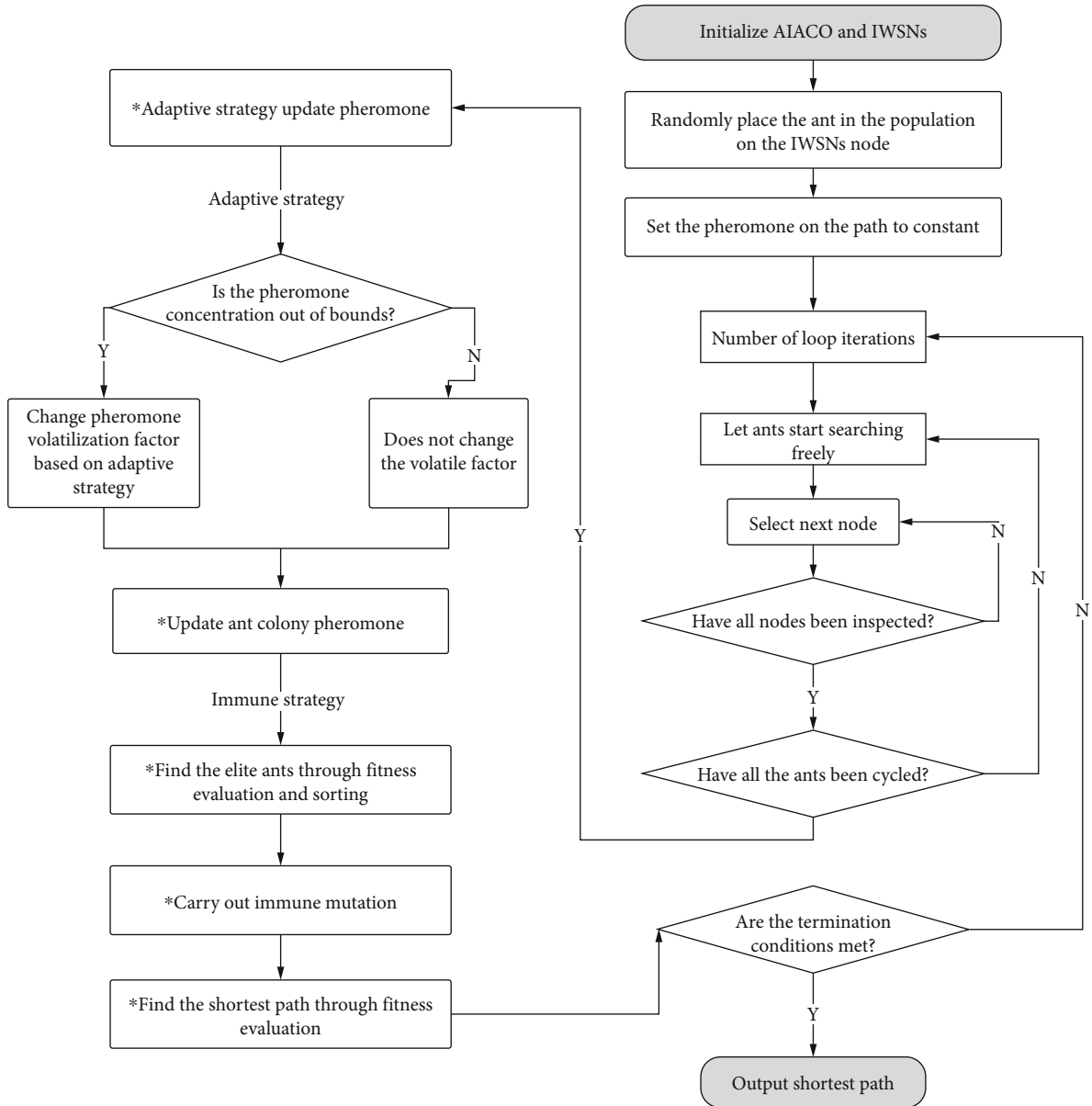


FIGURE 1: The flow chart of AIACO.

Step 8. Repeat Steps 3, 4, 5, 6, and 7. Stop when the upper limit of iteration is met.

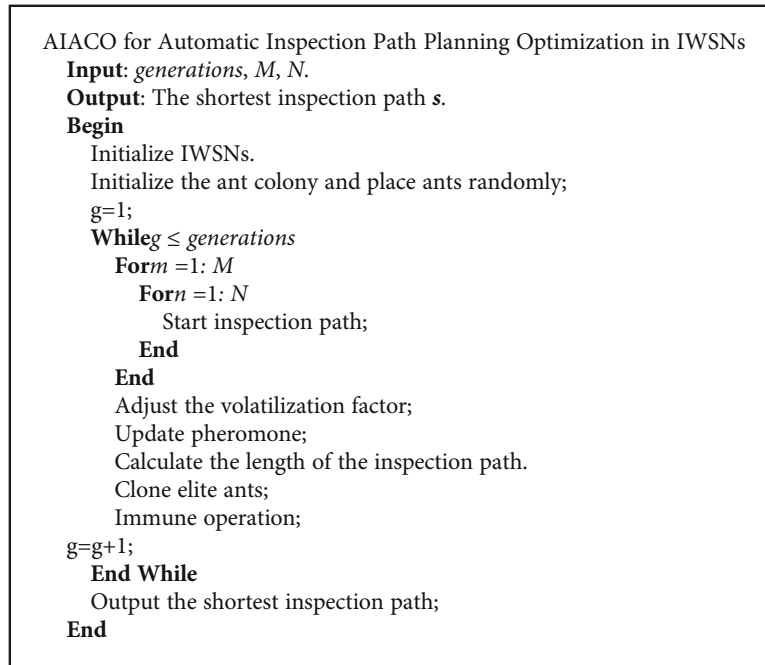
Step 9. Output the shortest inspection path.

In Algorithm 1, we show the entire IACGA algorithm flow in pseudo code.

This article discusses in detail the process of the proposed AIACO to solve the inspection path planning problem in IWSNs in the following sections. Respectively, explain from the aspects of initialization, calculation of fitness, path selection, new operators, and update pheromone.

4.1. Coding Scheme. One of the first steps to use AIACO to solve IWSN inspection path planning is to design the coding scheme according to the system model. The problem of the

inspection path of the wireless sensor network is that the automated robot starts from a sensor node randomly, inspects all nodes, and cannot check repeatedly. Finally, return to the starting point. The ultimate goal of solving the problem is to make the path of the robot the shortest, that is, to minimize the inspection cost. The coding scheme will directly affect the efficiency of the algorithm. This article uses integer coding to improve the performance of the program. The coding design is to use multiple ants of the ant colony to search for paths in parallel and use the intelligence of the group to plan the shortest path. Each path traversed by an ant represents a solution, and $S_{(M,N)}$ represents a set of inspection path plans generated by the ant colony. A single ant is represented by m , and the number of ant colonies is represented by M . N represents all sensor nodes of IWSNs. $s_{m,n}$ represents the sensor node selected by



ALGORITHM 1: AIACO algorithm program.

the m_{th} ant in the n_{th} step. The coding scheme is expressed in formula (5).

$$S_{(M,N)} = \begin{bmatrix} s_{1,1} & s_{1,2} & \cdots & s_{1,N-1} & s_{1,N} \\ s_{2,1} & s_{2,2} & \cdots & s_{2,N-1} & s_{2,N} \\ \cdots & \cdots & s_{m,n} & \cdots & \cdots \\ s_{M-1,1} & s_{M-1,2} & \cdots & s_{M-1,N-1} & s_{M-1,N} \\ s_{M,1} & s_{M,2} & \cdots & s_{M,N-1} & s_{M,N} \end{bmatrix} \quad (5)$$

$\cdot (s_{m,n} \in [1, N], m \in [1, M], n \in [1, N]).$

Regarding the intuitive representation of the coding scheme, and set M to 3 and N to 8. The ant colony scheme is represented by formula (6). The three ants represent three different inspection schemes.

$$S_{(3,8)} = \begin{bmatrix} 2 & 5 & 4 & 7 & 6 & 1 & 8 & 3 \\ 4 & 2 & 3 & 8 & 1 & 5 & 6 & 7 \\ 7 & 1 & 6 & 8 & 3 & 5 & 2 & 4 \end{bmatrix}. \quad (6)$$

4.2. Initial Ant Colony. The ant colony is initialized and coded according to the model of inspection path planning. Coding mainly solves the abstract connection problem between inspection planning and AIACO and uses mathematics and computer programs to solve it. Ant colony initialization is the first encoding when the pheromone is the initial value. We assume that the first search is not affected by pheromone differences, and the free search method can be used to better simulate the natural ant colony looking for food. Therefore, the path planning scheme is generated

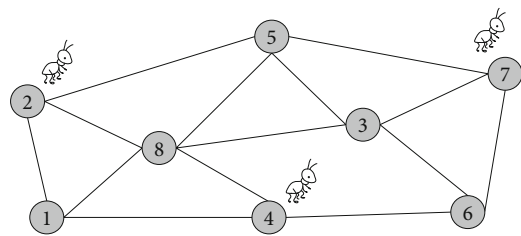


FIGURE 2: Initialization diagram of 8 sensor nodes and 3 ants.

for M ants. The initial ant colony scheme can be simply described as $S = \{S_1, S_2, \dots, S_M\}$. The path of the m_{th} ant can be expressed as $S_m = \{s_{m,1}, s_{m,2}, \dots, s_{m,N}\}$. For example, the specific codes of 3 ants and 8 nodes are reflected in formula (5).

Combined with the data of formula (5), Figure 2 shows the initialization scene. The 8 sensor nodes are initialized as a wireless sensor network. The three ants were randomly placed at the sensor nodes 2, 4, and 7 during initialization, began to plan their respective inspection paths, and finally completed the inspection task. Evaluate the quality of the inspection route plan by calculating the path length.

4.3. Fitness Evaluation. The fitness function is the criterion for evaluating the quality of the inspection path. The fitness function designed in this paper is designed to evaluate the shortest path found by the ant colony. The fitness function basically determines the direction of AIACO's program operation. The shorter the inspection path, the greater the probability of being selected by the ants. Each ant in the ant colony has its own evaluation value. AIACO embodies the search process of natural ants, through the search path, and then leave pheromone on the path. In this article, the evaluation of ants is based on the length of the inspection path. The goal

of the research is to minimize the inspection path of IWSNs. The evaluation value of the inspection path can be calculated by formula (3).

4.4. Select Path. When the ants in an ant colony start to search for a path, the visibility and pheromone content on the path are important factors. These two factors determine the ant's choice to go to the next sensor node. In formula (7), τ is the sum of pheromone on the path between two sensor nodes. u represents the visibility between the two sensor nodes. In addition, the inspection rules of the ants in this article are as follows: each ant randomly selects a node and searches from the current node until it has traversed all the nodes and returned to the node where it started. During this search, the ants will leave pheromone on the path they pass. In the algorithm initialization, set the pheromone content in the path to a constant. $P_{ij}(m)$ represents the probability that ant m chooses from node i to the next node j . Λ represents the remaining node set. α and β are the pheromone index constant and the visibility index constant, respectively. In formula (7), the roulette method is used to determine the direction of the ant to the next node.

$$P_{ij}(m) = \frac{\tau_{ij}^\alpha(m) u_{ij}^\beta(m)}{\sum_{j \in \Lambda} \tau_{ij}^\alpha(m) u_{ij}^\beta(m)} \quad (i, j \in [1, N], \Lambda \subseteq [1, N], m \in [1, M]). \quad (7)$$

4.5. Pheromone Update. Pheromone update is an important step for AIACO to solve the problem of inspection path planning. When looking for the best path, the path needs to be selected by calculating pheromone. When ants visit each sensor node, they release pheromone on the path from node i to node j . As the algorithm runs, the entire ant colony will have an impact on the entire sensor network path. During the period, the pheromone content will also volatilize part of the evolution process. In AIACO, after each ant completes an inspection, the pheromone on the path it passes will be updated. The modification method is determined by formulas (8), (9), and (10).

$$\tau_{ij}(g, g+1) = \rho \cdot \tau_{ij}(g) + \Delta\tau_{ij}(g, g+1), \quad (8)$$

$$\Delta\tau_{ij}(g, g+1) = \sum_{m=1}^M \Delta\tau_{ij}^m(g, g+1), \quad (9)$$

$$\tau_{ij}^m = \frac{Q}{d_{ij}}, \quad (10)$$

where g represents the number of iterations of the loop and ρ represents the volatilization factor of the pheromone. $\tau_{ij}(g, g+1)$ represents the updated pheromone result after the end of the g_{th} generation. $\Delta\tau_{ij}$ represents the pheromone change produced by M ants after the search is over. $\Delta\tau_{ij}^m$ represents the pheromone result updated by the m_{th} ant. However, the result of pheromone update on each path is determined by the pheromone constant Q and the path dis-

tance d_{ij} . The longer the path length, the smaller the release of pheromone.

4.6. Adaptive Strategy. In the case of large-scale nodes, the traditional ant colony optimization gradually becomes the choice of ants with the accumulation of pheromone, but this path may not be the shortest path. Moreover, the traditional ant colony optimization is often easy to fall into the local optimum. There are two problems with the fixed setting of the volatilization factor. If the setting is too large, the pheromone content will be less after the cycle of the g generation, and it will not be able to be truly fed back to the subsequent ants to choose. If the setting is too small, there will be a large accumulation of pheromone, and the pheromone difference on the path will become larger, leading to premature algorithm.

The purpose of the new adaptive strategy designed in this paper is to prevent premature programs and increase the search space of the ant colony. In the inspection process, the adaptive strategy judges whether to adjust the pheromone volatilization factor according to the concentration of the pheromone in the current network, which affects the path selection probability of the ants, thereby guiding AIACO to a better solution. Therefore, the adaptive mechanism of the proposed algorithm can show better performance when the problem is more complicated. The adaptive update method is determined by formulas (11) and (12).

$$\begin{cases} \tau_{ij}(g, g+1) = \rho^{1+\varphi(\theta)} \cdot \tau_{ij}(g) + \Delta\tau_{ij}(g, g+1) & \tau > \tau_{\max}, \\ \tau_{ij}(g, g+1) = \rho^{1-\varphi(\theta)} \cdot \tau_{ij}(g) + \Delta\tau_{ij}(g, g+1) & \tau < \tau_{\min}, \end{cases} \quad (11)$$

$$\varphi(\theta) = \frac{\theta}{c}, \quad (12)$$

where c represents a constant and $\varphi(\theta)$ is directly proportional to the convergence factor θ and inversely proportional to c . An increase in the number of convergences of θ will result in an increase in $\varphi(\theta)$. τ_{\max} represents the upper limit of the pheromone concentration, and τ_{\min} represents the lower limit of the pheromone concentration. With the operation of the algorithm, AIACO adaptively adjusts the pheromone concentration so that the ant inspection path will not be concentrated quickly. Therefore, AIACO avoids local optima and enhances global search capabilities.

4.7. Immune Strategy. In AIACO, improving the convergence speed of the algorithm is an important task. This paper designs a clonal immune strategy for the stage of population change. When the immune system solves the problem of IWSN inspection path planning, it uses the immune advantage in immunology to respond to antigen stimulation in a timely manner, thereby changing antibodies. The clonal immune strategy better simulates the clone process of the ant colony immune system. The clonal immune strategy can greatly improve the optimization speed of inspection path planning. Immunization can increase the diversity of ant colony programs. After the ant colony search is over,

TABLE 1: The main parameter of AIACO.

Algorithm	Number of generations	Population size	Pheromone volatilization factor	Information heuristic factor	Pheromone weight
AIACO	100	100	0.95	1	2.5

TABLE 2: The main parameter of ICA.

Algorithm	Number of generations	Population size	Probability of antibody recombination	Probability of antibody mutation	Elite clone percentage
ICA	100	100	0.75	0.55	10%

TABLE 3: The main parameter of GA.

Algorithm	Number of generations	Population size	Crossover probability	Mutation probability
GA	100	100	0.69	0.04

the existing ant colony codes are used to find a number of elite ants by evaluating the fitness ranking of the ant colony. These elites are randomly cloned to form a new population for immune mutation operation. Mutation may lead to new schemes, and there is a chance to produce more adaptable ants, which accelerates the algorithm convergence.

5. Simulation and Discussion

5.1. Experimental Setup. This section will verify the performance of AIACO, ICA, and GA in IWSN inspection path planning through simulation. The experimental hardware equipment is Intel(R) Core (TM) i5 @2.40GHz CPU DELL computer. The simulation software is MATLAB R2018a. The operating system is Windows 10 version 1909. The experimental termination conditions of the three algorithms are all 100 generations, and the two-dimensional coordinate area is $100 \times 100 \text{ m}^2$.

In order to compare the problem-solving capabilities of AIACO with ICA and GA, we set the population size of AIACO, ICA, and GA to 100. In AIACO, set pheromone volatilization factor to 0.95, information heuristic factor to 1, and pheromone weight is 2.5. In ICA, we set the antibody recombination probability to 0.75, the antibody mutation probability to 0.55, and the percentage of clone elites to 10%. In GA, we set the crossover probability to 0.69 and the mutation probability to 0.04. The main experimental parameters of the three algorithms of AIACO, ICA, and GA are listed in Tables 1–3.

5.2. Discussion of Experimental Results. Figures 3(a)–3(d) show the inspection path optimization results of AIACO, ICA, and GA under the experimental conditions of four different sensor node numbers. In Figures 3(a)–3(d), AIACO optimizes the inspection path better than ICA and GA. When the algorithm is in the 20th generation, AIACO has basically converged and found a short path relative to ICA and GA. ICA converges faster than GA. In 100 generations,

all three algorithms found their shortest paths. From the optimization trend, AIACO's performance is the best compared to ICA and GA. This point proves that the immune cloning operator can improve the convergence speed of the algorithm. In Figure 3(d), the number of sensor nodes is 80, and the trend of AIACO's optimization path is more obvious. It is verified that the new adaptive strategy and immune strategy can make AIACO better solve the problem of minimizing the inspection path of IWSNs.

Figures 4(a)–4(d) compare the shortest path lengths of the three algorithms in 100 generations, and the number of sensor nodes is 20, 40, 60, and 80, respectively. Use the histogram to directly compare the gaps. As can be seen in Figures 4(a)–4(d), in the four cases, the length of the inspection path optimized by AIACO is less than that of ICA and GA. When the sensor node increases, the shortest path length also increases. At the same time, AIACO has better path optimization performance than ICA and GA. When the number of nodes is 60 and 80, the gap between AIACO and ICA and GA is greater. This point illustrates AIACO's network optimization capabilities for large-scale nodes. Therefore, compared with ICA and GA, AIACO has better ability to optimize inspection paths.

Figures 5(a)–5(d) show the path optimization percentages when the number of sensor nodes is 30, 50, 60, and 80, respectively. From the pie chart, we can intuitively see the comparison between AIACO, ICA, and GA on the improvement of the optimization degree of the inspection path. In the case of four different numbers of nodes, the path length optimized by AIACO is larger than that of ICA and GA, accounting for 41%, 44%, 48%, and 49%, respectively. ICA accounts for 34%, 35%, 32%, and 32%, respectively. GA accounts for 25%, 21%, 20%, and 19%, respectively. As the number of nodes increases, AIACO performance will also improve. The adaptive strategy can prevent AIACO from falling into the local optimum, increase the algorithm's global optimization ability, and find a shorter path. Overall, the performance of AIACO in IWSNs is always better than the other two algorithms.

Figure 6 shows a comparison of reduced path lengths with sensor nodes of 20, 30, 40, 50, 60, 70, and 80. The data comes from Table 4. It can be seen from Figure 6 that in the seven cases, as the number of nodes increases, the degree of reduction of the path length by the three algorithms increases. From the overall trend, AIACO's optimization performance for inspection paths is better than ICA and

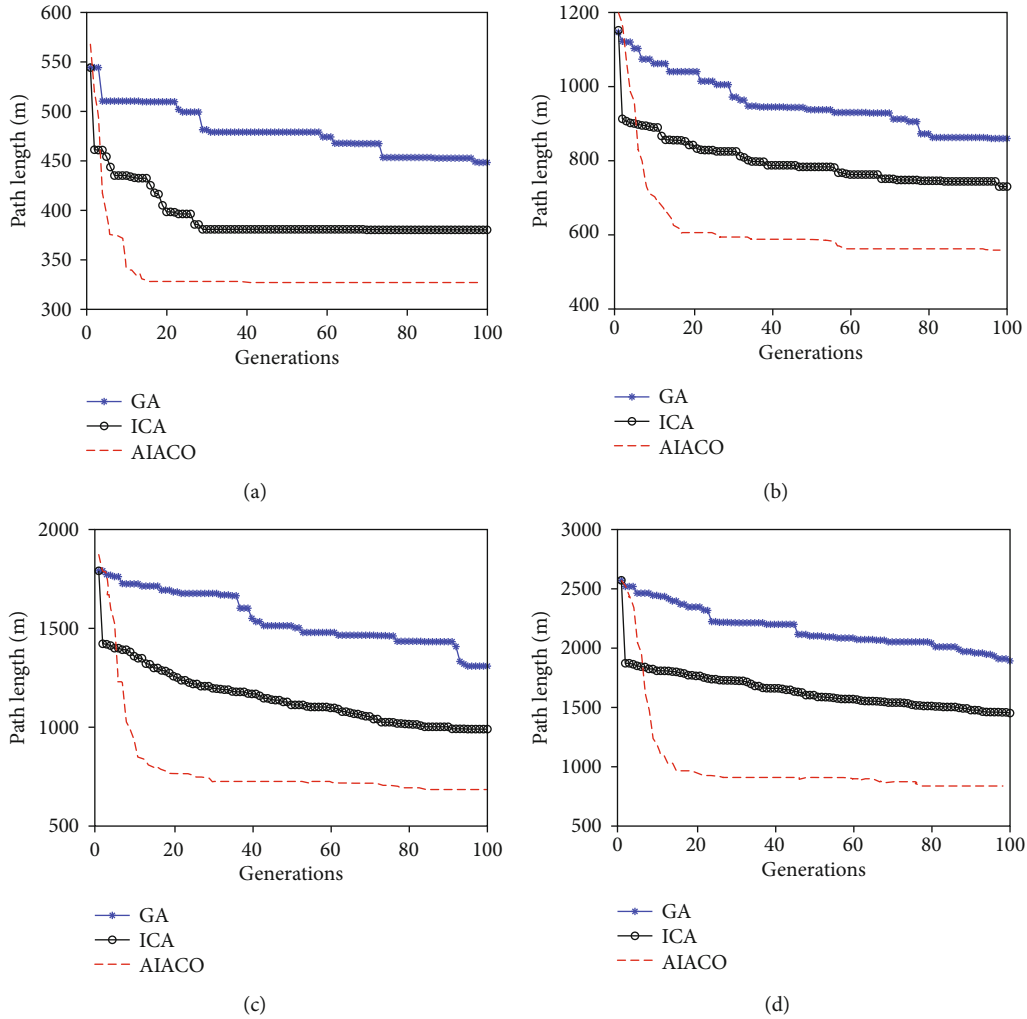


FIGURE 3: The path planning optimization trends of the three algorithms are compared within 100 generations: (a) 20 sensor nodes; (b) 40 sensor nodes; (c) 60 sensor nodes; (d) 80 sensor nodes.

GA. The line graph shows an upward trend. Especially when the number of nodes is 70 and 80, AIACO's performance is better than ICA and GA. Better than self-adjusting the volatilization of pheromone, it promotes AIACO's ability to find the best. The immune clone method makes the new ant colony recombined by elite ants have a higher diversity, which is conducive to finding the shortest path. Overall, AIACO's performance is very superior.

Table 4 shows that AIACO, ICA, and GA reduce the length of the inspection path. It can be seen from the data in Table 4 that as the number of sensor nodes increases for each algorithm, the shortened path length also increases. Combining Figure 6 to see similar conclusions more intuitively. Based on Table 4, Table 5 shows the optimized performance of AIACO, ICA, and GA under different node parameter settings in percentage form. The proportion of AIACO's shortened path length is always greater than that of ICA and GA. The highest percentage is 49%, and the corresponding node numbers are 70 and 80, respectively. The percentage of ICA ranks second in total, and GA is the smallest. The factor of AIACO's high

performance is that the new operator adjusts the pheromone concentration in real time when the algorithm is running to prevent premature convergence. Compared with AIACO, ICA and GA are easy to fall into the local optimum, and the performance of finding the shortest inspection path is poor.

Suppose the population size is m , and the number of sensor nodes is n . It can be seen from Table 6 that the algorithm complexity of AIACO is $O(m \times n^2)$, and the algorithm complexity of ICA and GA is $O(m \times n^2 + n)$. In AIACO, ants need to search for each node and then update the pheromone, forming a double cycle. ICA and GA have similar selection and mutation processes, and both are double cycles. Therefore, compared with ICA and GA, AIACO has lower complexity. More importantly, as can be seen from Figure 3, AIACO's convergence speed and optimization performance are better than ICA and GA.

Through the comparison and discussion of simulation results, the effectiveness of the proposed AIACO in solving the problem of automatic inspection path planning in inspection IWSNs is verified. Successfully solve the problem of

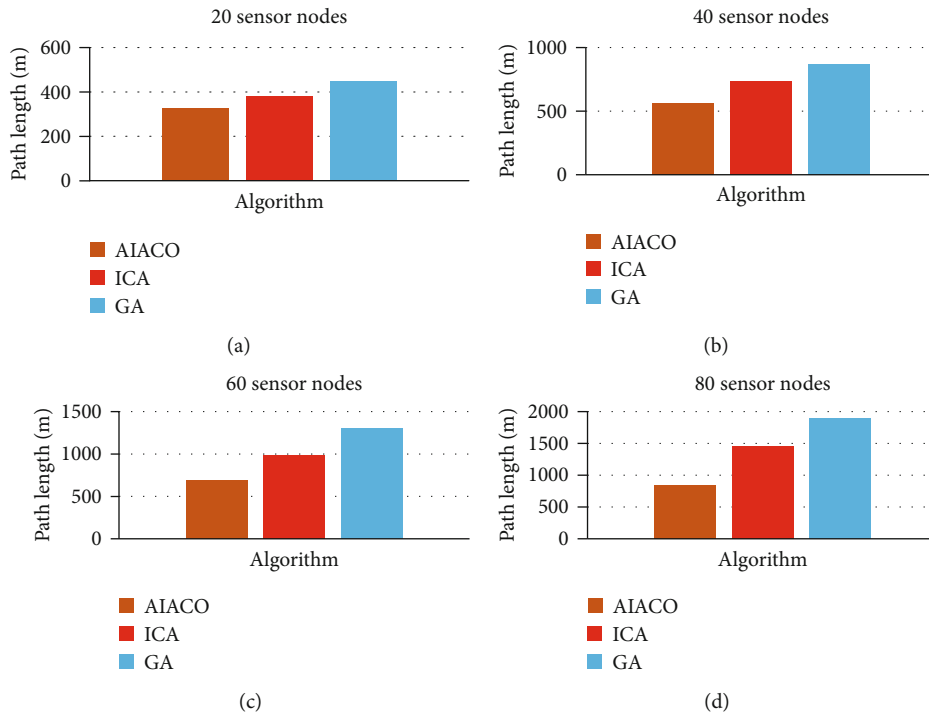


FIGURE 4: The comparison of the shortest paths of the three algorithms with different sensor nodes is in 100 generations: (a) 20 sensor nodes; (b) 40 sensor nodes; (c) 60 sensor nodes; (d) 80 sensor nodes.

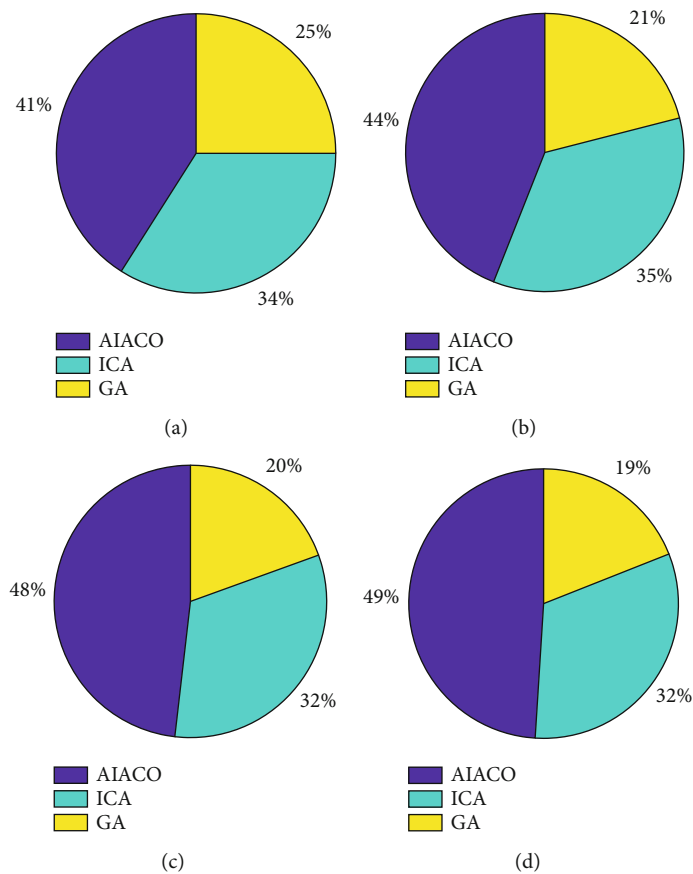


FIGURE 5: The three algorithms shorten the percentage of path length in 100 generations: (a) 30 sensor nodes; (b) 50 sensor nodes; (c) 60 sensor nodes; (d) 80 sensor nodes.

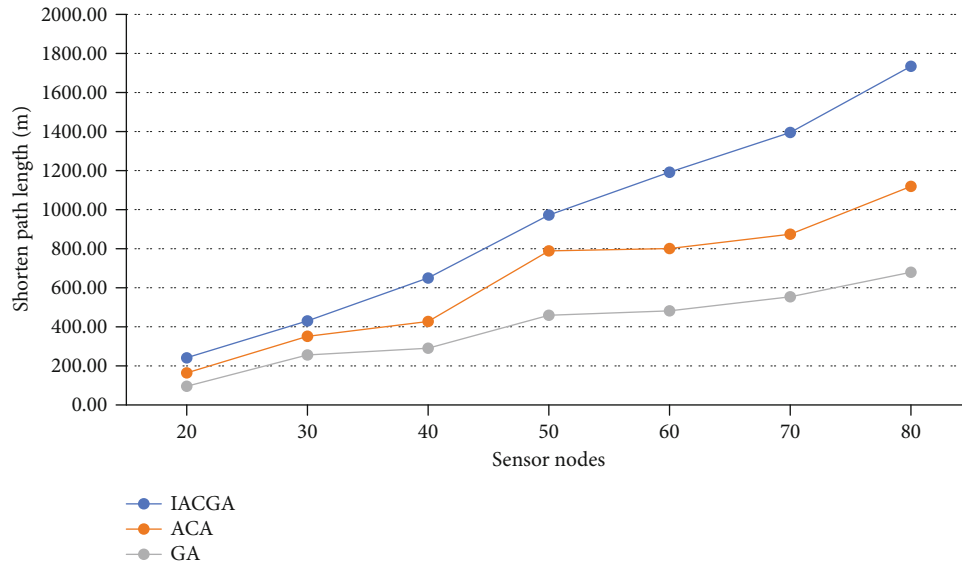


FIGURE 6: Comparison of the optimization degree of the three algorithms as the number of sensors increases.

TABLE 4: Three algorithms improve the path length (m).

Number of sensor nodes	AIACO	ICA	GA
20 nodes	241.33	163.76	95.79
30 nodes	430.15	351.16	255.65
40 nodes	649.76	426.85	290.31
50 nodes	972.25	788.68	458.99
60 nodes	1191.56	800.35	481.80
70 nodes	1395.07	874.00	553.94
80 nodes	1733.67	1118.91	679.24

TABLE 5: The three algorithms improve the proportion of path length.

Number of sensor nodes	AIACO	ICA	GA
20 nodes	48%	33%	19%
30 nodes	41%	34%	25%
40 nodes	48%	31%	21%
50 nodes	44%	35%	21%
60 nodes	48%	32%	20%
70 nodes	49%	31%	20%
80 nodes	49%	32%	19%

TABLE 6: The computational complexity of the three algorithms is compared.

Algorithm	AIACO	ICA	GA
Complexity	$O(m \times n^2)$	$O(m \times n^2 + n)$	$O(m \times n^2 + n)$

minimizing inspection path planning in two-dimensional coordinates. Future research will involve inspection path planning in three-dimensional space and more complex industrial environments.

6. Conclusion

Aiming at the problem of minimizing the inspection path planning of industrial wireless sensor networks (IWSNs), this paper proposes a new adaptive immune ant colony optimization (AIACO). Before the algorithm is executed, the inspection path planning model of IWSNs is established. A new adaptive strategy is designed to dynamically adjust the volatilization of pheromone to prevent the algorithm from premature convergence. A new immune strategy is designed to select elite ants to reorganize new colonies. The immune strategy increases the optimization speed of the algorithm and the diversity of the inspection plan. In addition, we compare the performance of AIACO with ICA and GA in solving IWSN path planning through simulation results and discussed in detail. The result proves that the performance of AIACO is better than that of ICA and GA. This algorithm effectively solves the problem of automatic inspection path planning in IWSNs, can find the shortest path, and reduce the energy consumption of industrial inspection tasks.

Data Availability

The data presented in this study are available on request from the corresponding author. The data are not publicly available due to privacy.

Disclosure

The funders had no role in the design of the study; in the collection, analyses, or interpretation of data; in the writing of the manuscript, or in the decision to publish the results.

Conflicts of Interest

The authors declare no conflict of interest.

Acknowledgments

This paper was funded by the Corps innovative talents plan, grant number 2020CB001; the project of Youth and mid-dleaged Scientific and Technological In-novation Leading Talents Program of the Corps, grant number 2018CB006; the China Postdoctoral Science Foundation, grant number 220531; the Funding Project for High Level Talents Research in Shihezi University, grant number RCZK2018C38; and the Project of Shihezi University, grant number ZZZC201915B.

References

- [1] S. Sun, J. Zhao, X. Feng, J. Zhang, and J. Luo, "Mobile multi-sink nodes path planning algorithm concerned with energy balance in wireless sensor networks," *IEEE Access*, vol. 7, pp. 96942–96952, 2019.
- [2] Q. Yang and S. Yoo, "Optimal UAV path planning: sensing data acquisition over IoT sensor networks using multi-objective bio-inspired algorithms," *IEEE Access*, vol. 6, pp. 13671–13684, 2018.
- [3] Z. Lyu, Z. Wei, X. Wang, Y. Fan, C. Xia, and L. Shi, "A periodic multinode charging and data collection scheme with optimal traveling path in WRSNs," *IEEE Systems Journal*, vol. 14, no. 3, pp. 3518–3529, 2020.
- [4] A. Alomari, W. Phillips, N. Aslam, and F. Comeau, "Swarm intelligence optimization techniques for obstacle-avoidance mobility-assisted localization in wireless sensor networks," *IEEE Access*, vol. 6, pp. 22368–22385, 2018.
- [5] S. Zhang, S. Shi, S. Gu, and X. Gu, "Power control and trajectory planning based interference management for UAV-assisted wireless sensor networks," *IEEE Access*, vol. 8, pp. 3453–3464, 2020.
- [6] G. Han, X. Yang, L. Liu, W. Zhang, and M. Guizani, "A disaster management-oriented path planning for mobile anchor node-based localization in wireless sensor networks," *IEEE Transactions on Emerging Topics in Computing*, vol. 8, no. 1, pp. 115–125, 2020.
- [7] P. Tsai, G. Shih, W. Cheng, and R. Tsai, "Sigma-scan: a mobile beacon-assisted localization path-planning algorithm for wireless sensor networks," *IEEE Sensors Journal*, vol. 19, no. 23, pp. 11492–11502, 2019.
- [8] X. Liu, T. Qiu, X. Zhou, T. Wang, L. Yang, and V. Chang, "Latency-aware path planning for disconnected sensor networks with mobile sinks," *IEEE Transactions on Industrial Informatics*, vol. 16, no. 1, pp. 350–361, 2020.
- [9] W. Xia, C. Di, H. Guo, and S. Li, "Reinforcement learning based stochastic shortest path finding in wireless sensor networks," *IEEE Access*, vol. 7, pp. 157807–157817, 2019.
- [10] H. J. Na and S. Yoo, "PSO-based dynamic UAV positioning algorithm for sensing information acquisition in wireless sensor networks," *IEEE Access*, vol. 7, pp. 77499–77513, 2019.
- [11] J. Wang, W. Chi, C. Li, C. Wang, and M. Q. Meng, "Neural RRT*: learning-based optimal path planning," *IEEE Transactions on Automation Science and Engineering*, vol. 17, no. 4, pp. 1748–1758, 2020.
- [12] D.-D. Zhu and J. -Q. Sun, "A new algorithm based on Dijkstra for vehicle path planning considering intersection attribute," *IEEE Access*, vol. 9, pp. 19761–19775, 2021.
- [13] Y. Li, H. Zhang, H. Zhu, J. Li, W. Yan, and Y. Wu, "IBAS: index based A-star," *IEEE Access*, vol. 6, pp. 11707–11715, 2018.
- [14] K. Okamoto and P. Tsiotras, "Optimal stochastic vehicle path planning using covariance steering," *IEEE Robotics and Automation Letters*, vol. 4, no. 3, pp. 2276–2281, 2019.
- [15] W. A. Shutnan and T. Y. Abdalla, "Artificial immune system based optimal fractional order PID control scheme for path tracking of robot manipulator," in *2018 International Conference on Advance of Sustainable Engineering and its Application (ICASEA)*, pp. 19–24, Wasit-Kut, Iraq, 2018.
- [16] R. Fareh, M. Baziyad, T. Rabie, and M. Bettayeb, "Enhancing path quality of real-time path planning algorithms for mobile robots: a sequential linear paths approach," *IEEE Access*, vol. 8, pp. 167090–167104, 2020.
- [17] C. Liu, S. Zhang, and A. Akbar, "Ground feature oriented path planning for unmanned aerial vehicle mapping," *IEEE Journal of Selected Topics in Applied Earth Observations and Remote Sensing*, vol. 12, no. 4, pp. 1175–1187, 2019.
- [18] X. Chen, L. Yu, T. Wang et al., "Artificial intelligence-empowered path selection: a survey of ant colony optimization for static and mobile sensor networks," *IEEE Access*, vol. 8, pp. 71497–71511, 2020.
- [19] G. Han, H. Guan, J. Wu, S. Chan, L. Shu, and W. Zhang, "An uneven cluster-based mobile charging algorithm for wireless rechargeable sensor networks," *IEEE Systems Journal*, vol. 13, no. 4, pp. 3747–3758, 2019.
- [20] B. Zhang and H. Duan, "Three-dimensional path planning for uninhabited combat aerial vehicle based on predator-prey pigeon-inspired optimization in dynamic environment," *IEEE/ACM Transactions on Computational Biology and Bioinformatics*, vol. 14, no. 1, pp. 97–107, 2017.
- [21] M. Luo, X. Hou, and J. Yang, "Surface optimal path planning using an extended Dijkstra algorithm," *IEEE Access*, vol. 8, pp. 147827–147838, 2020.
- [22] H. Zhang, Y. Wang, J. Zheng, and J. Yu, "Path planning of industrial robot based on improved RRT algorithm in complex environments," *IEEE Access*, vol. 6, pp. 53296–53306, 2018.
- [23] Z. Cai, X. Cui, X. Su, Q. Mi, L. Guo, and Z. Ding, "A novel vector-based dynamic path planning method in urban road network," *IEEE Access*, vol. 8, pp. 9046–9060, 2020.
- [24] K. P. Cheng, R. E. Mohan, N. H. Khanh Nhan, and A. V. Le, "Multi-objective genetic algorithm-based autonomous path planning for hinged-tetro reconfigurable tiling robot," *IEEE Access*, vol. 8, pp. 121267–121284, 2020.
- [25] Z. Tang, L. Xu, and H. Xie, "Picking trajectory planning of citrus based on improved immune algorithm and binocular vision," in *2020 IEEE international conference on artificial intelligence and computer applications (ICAICA)*, pp. 6–10, Dalian, China, 2020.

Research Article

Minimization of Energy Consumption for Routing in High-Density Wireless Sensor Networks Based on Adaptive Elite Ant Colony Optimization

Jing Xiao,¹ Chaoqun Li,¹ and Jie Zhou ^{1,2}

¹College of Information Science and Technology, Shihezi University, Shihezi, China

²Xinjiang Tianfu Information Technology Co., Ltd., China

Correspondence should be addressed to Jie Zhou; jiezhou@shzu.edu.cn

Received 7 January 2021; Revised 2 February 2021; Accepted 28 February 2021; Published 18 March 2021

Academic Editor: Mario E. Rivero-Angeles

Copyright © 2021 Jing Xiao et al. This is an open access article distributed under the Creative Commons Attribution License, which permits unrestricted use, distribution, and reproduction in any medium, provided the original work is properly cited.

High-density wireless sensor networks (HDWSNs) are usually deployed randomly, and each node of the network collects data from complex environments. Because the energy of sensor nodes is powered by batteries, it is basically impossible to replace batteries or charge in the complex surroundings. In this paper, a QoS routing energy consumption model is designed, and an improved adaptive elite ant colony optimization (AEACO) is proposed to reduce HDWSN routing energy consumption. This algorithm uses the adaptive operator and the elite operator to accelerate the convergence speed. So, as to validate the efficiency of AEACO, the AEACO is contrast with particle swarm optimization (PSO) and genetic algorithm (GA). The simulation outcomes show that the convergence speed of AEACO is sooner than PSO and GA. Moreover, the energy consumption of HDWSNs using AEACO is reduced by 30.7% compared with GA and 22.5% compared with PSO. Therefore, AEACO can successfully decrease energy consumption of the whole HDWSNs.

1. Introduction

Nowadays, emerging high-density wireless sensor network (HDWSNs) technologies have attracted a large number of scholars to study new QoS routing optimization algorithms in this field. With the further development and popularization of wireless communication technology, HDWSNs have been used in many application fields such as community monitoring, smart home, military, traffic control, environmental and detection [1]. HDWSNs combine computing technology with wireless mobile communication technology and sensor node technology to revolutionize the architecture and mode of traditional networks [2, 3]. However, due to the constraints of the sensing environment, in HDWSNs, a lot of nodes only provide restricted energy through batteries. Therefore, effectively cut down the energy consumption of nodes and realize energy-saving routing and data transmission have important research and application value for improving the performance and stability of HDWSNs [4, 5].

For multicondition restricted QoS routing optimization problems, the purpose is to find the best path from beginning to end for specific problems in HDWSNs, rather than the shortest path. And this path should meet multiple QoS constraint requirements such as delay jitter, delay, packet loss rate, and link bandwidth. These QoS routing conditions are used as the criteria for QoS routing considerations [6]. Due to energy limitations, how to maximize the reduction of routing energy consumption and extend the lifetime of sensor networks have become a bottleneck problem faced by HDWSNs.

Generally speaking, the volume and mass of sensors are very small. It is necessary to take into account the completion of specific communication tasks and to ensure that the internal energy utilization rate is increased [7]. The QoS routing optimization algorithm is an efficient way to cut down energy consumption within the network [8].

In this paper, a QoS routing optimization based upon AEACO is recommended to minimize the energy consumption

of HDWSNs. In order to assess the effectiveness of the AEACO, the model of QoS routing is first given. To improve the execution effectiveness of the algorithm, the routing fitness function is designed. Moreover, the adaptive and elite mechanisms are introduced into the ant colony optimization. We designed a new adaptive mechanism to improve the global search ability in the pheromone update phase and avoid falling into local optimum. A new elite mechanism is designed to retain the optimal ants and improve the optimization ability of the algorithm.

In the simulation, AEACO showed a good ability to find the best individual. It speeds up the convergence of the algorithm. The simulation results show that implementing AEACO in HDWSNs has higher performance than the particle swarm optimization (PSO) and genetic algorithm (GA). The consequence also shows that the adaptive and elite strategies proposed in this paper improve the global search capability of ant colony optimization.

The main contributions are as follows:

- (1) First, we propose an improved adaptive elite ant colony optimization (AEACO), which can effectively minimize the routing energy consumption in HDWSNs. After several iterations, the energy consumption of routing optimized by AEACO is reduced by 22.5% and 30.7%, respectively, compared with PSO and GA under the same experimental conditions. In addition, when the number of nodes increases, a similar conclusion can be drawn by comparing the experimental results with the other two algorithms. Therefore, the AEACO-based routing method can effectively improve energy utilization
- (2) Secondly, the AEACO that combines adaptive operators and elite operators has better performance in the absence of premature convergence. Increased global search capabilities. When the number of sensor nodes is 50 and 70, respectively, AEACO has a higher convergence speed than PSO and GA. Compared with the other two algorithms, the fitness after AEACO optimization converges to a small value after iteration
- (3) Finally, the total routing energy consumption of HDWSNs depends on the transmission and reception energy consumption of all nodes. Under the algorithm's adaptive mechanism, the overall energy consumption will be reduced. With the increase in the number of sensors in HDWSNs, the demand for data transmission increases, and the effect of AEACO in optimizing routing energy consumption also increases accordingly

The continuation of this paper is shown below. Section 2 discusses the author's related work for this article. Section 3 describes the QoS routing model. In Section 3, AEACO is used to optimize the QoS routing algorithm process. Section 5 presents the simulation results and comparison. The conclusion is given in Section 6.

2. Related Work

In HDWSNs, there is a direct relationship between lifetime and performance. Appropriate and efficient routing algorithms can decrease the energy consumption in the sensor networks, which is of excellent meaning to extend the HDWSN life span. Therefore, in [9], the author proposed a multimobile trajectory scheduling method based on coverage, using PSO and GA for optimal scheduling. The paper [10] combined the PEGASIS algorithm and Hamilton loop algorithm together, designed the best route, and effectively reduced energy consumption. The paper [11] proposed an enhanced high-performance aggregation algorithm, determine the best communication distance, set thresholds, and use mobile technology to reduce energy consumption between nodes. The paper [12] proposed a maximum data generation rate routing algorithm based on data flow control technology, which greatly reduced the time synchronization energy consumption. The paper [13] proposed a new coverage control algorithm based on PSO, by dividing the entire network into multiple A grid to increase coverage and reduce energy consumption.

Research on optimization of energy consumption in sensor networks has attracted scholars recently. The paper [14] proposed an energy-conscious green opponent model used in a green industrial environment, which can improve the hardware and software of the electronic physical system to reduce its energy consumption. The paper [15] uses the bat algorithm to select the best monitoring sensor node and the best path to reduce energy consumption. The paper [16] uses the whale optimization algorithm to solve the RA problem, achieves the best RA, and reduces the total communication cost. The paper [17] uses linear adaptive congestion control to improve the situation of greedy routing and data distribution.

HDWSNs has developed speedily in recent years, and it can well solve the problems of physical control and sensing. Based on the performance of the routing scenario used, computing and processing power is minimal considering the limited battery power [18]. For this reason, in paper [19], the author uses the genetic algorithm (GA) for simulation experiments in multihop QoS routing wireless networks, and the performance of the algorithm is analyzed from the aspects of scalability, energy consumption, and HDWSN life cycle. It can maximize the activity of the sensor by saving energy, thereby extending the service life of the network.

For QoS problems in high-quality wireless sensor networks, the simulated annealing algorithm is first found in [20], and the performance of SA is evaluated through routing energy consumption. Routing optimization for wireless sensor networks is with limited resources and computing power. The results show that the computational complexity increases with the rise of the quantity of network nodes in the case of limited computing capacity.

Paper [21] analyses a wireless powered sensor network, where the energy efficiency maximization problem is developed as a nonlinear fractional problem, which is hard to address for global best due to the absence of convexity. To prolong the life span of the network and reduce energy loss,

TABLE 1: The key parameter of AEACO.

Algorithm	Number of generations	Population size	Pheromone volatilization factor	Information heuristic factor	Pheromone weight
AEACO	100	50	0.98	1	3

TABLE 2: The key parameter of PSO.

Algorithm	Number of generations	Population size	Maximum speed	Social factor	Individual factor
PSO	100	50	10	2	2

a PSO routing strategy is proposed. With the PSO method, routing and forwarding can be performed quickly and directly. In this way, the algorithm searched for the optimal solution to the energy optimization problem. Results show the stability and fast convergence of the suggested algorithm. However, the algorithm is very easy to fall under premature convergence.

In [22], an SFLA sensor network routing scheme is put forward to cut down the total energy consumption of the network system. The SFLA is applied to resolve QoS routing issues of wireless sensor networks with mobile receivers. The authors describe the above problem as an optimization problem. To solve the NP-hard problem, the authors propose an improved shuffled frog-leap algorithm with delay constraints. The algorithm uses chaos technology to obtain a diverse group of frogs and gives an adaptive operator to speed up the algorithm. Operating speed: the author also proposes a new task scheduling algorithm which takes surplus energy into account to balance the network load. Finally, a large number of simulation experiments validate the efficiency of the algorithm. By this means, the best route delivery path can be selected to reduce network delay and energy consumption. However, the execution speed of the SFLA is still slow and cannot satisfy the requirements of QoS routing.

In [23], the QoS routing algorithm determines the lowest energy consumption path for information transmission from the start point to the endpoint. Because wireless sensor network nodes lack sufficient energy, energy efficiency utilization is an essential sign of wireless sensor network data transmission. The basic significance of HDWSNs in the current scene is to decrease the energy consumption of nodes in the network, improve data transmission effectiveness and availability, and extend entire network lifetime. In this regard, author demands to find the best route for data transmission in HDWSNs. To resolve this problem, authors put forward to an energy-saving routing algorithm for HDWSNs based on ant colony optimization (ACO). The improved low-energy routing method selects the cluster head by considering the energy and the distance between nodes. In order to decrease the energy consumption between nodes, the remaining energy is taken as a factor to extend the network life and improve the efficiency of routing data transmission. However, due to the high complexity of the algorithm, the efficiency of the program is not ideal.

In [24], in the design of HDWSNs, the energy consumption of HDWSNs has become a serious problem due to the limited battery energy. Therefore, a fast and robust algorithm is needed to optimize QoS routing in HDWSNs. Battery

TABLE 3: The key parameter of GA.

Algorithm	Number of generations	Population size	Crossover probability	Mutation probability
GA	100	50	0.75	0.06

power is needed to run the network. In order to extend the life cycle of the network, it is necessary to optimize the energy consumption. Energy consumption and QoS are two important factors. In HDWSNs based on low-energy consumption standard, energy consumption lies in activities such as data collection, data forwarding, and exchange with the gateway. Therefore, improving the routing efficiency of HDWSNs is an important task to extend the network life cycle. In the process of solving the problem, the author improved the hybrid leap-frog algorithm and modified the number of leap-frog and the population size appropriately. The author carried out extensive simulations on the proposed routing algorithm according to various performance parameters. However, the algorithm has poor robustness and cannot meet the requirements of HDWSN's QoS routing algorithm.

In this research, the key parameters of AEACO, PSO, and GA are listed in Tables 1–3.

3. System Model

This section introduces the QoS routing optimization model with multiple constraints. The mathematical model of HDWSNs can be expressed as the path set between each node in the sensor network, which is represented by $G(V, E)$. Graph theory is used to represent the source, destination, and multiple relay nodes and links. The node set includes the source node v_1 , terminal node v_n , and numerous intermediate nodes $v_2 \rightarrow \dots \rightarrow v_{n-1}$. The source node is the No.1 node, the intermediate nodes are No.2 to No.($n-1$) nodes, and the terminal node is the No. n node. Therefore, the route from the starting node to the terminal node can be expressed as $r(v_1, v_n) = \{v_1 \rightarrow v_2 \rightarrow \dots \rightarrow v_{n-1} \rightarrow v_n\}$.

Two nodes form a link. In this way, the sequence numbers of the adjacent 2 nodes are a and b , which can be expressed as $e = \{v_a \rightarrow v_b\} (a \neq b)$. Transmission performance over links is restricted by 4 parameters of link bandwidth, packet loss rate, delay jitter, and delay. The energy consumption in every path may be expressed as $LS(e)$, the jitter may be expressed as $D(e)$, the link bandwidth may be expressed as $BW(e)$, the packet loss rate may be expressed as $PL(e)$, and the delay jitter may be expressed as $DJ(e)$.

3.1. Radio Energy Model. Before the algorithm starts, we assume that constraints such as jitter, delay jitter, bandwidth, and packet loss rate in QoS routing already exist, and sensor nodes are randomly distributed in a two-dimensional coordinate.

On a link consisting of two conjoining nodes a and b , the energy consumption is consisting of data transmission and data reception energy consumption, and the total energy consumption $LS(e)$ between the two adjacent nodes can be expressed as

$$LS(e) = LS_s + LS_r, \quad (1)$$

where LS_s can denote energy consumption of data transmission between neighboring nodes, and LS_r can denote the energy consumption of data receiving between neighboring nodes.

Suppose the distance between two conjoining nodes is l and the bits of transmitted data can denote q , and the energy cost of data transmission over a link can be expressed as

$$LS_s(q, l) = E_e \cdot q + \eta_{amp} \cdot q \cdot l^3, \quad (2)$$

where E_e is the electronics energy parameter. LS_s is the transmitter dissipated energy. The power amplification parameter for multipath fading η_{amp} determine the energy of the amplifier. The distance between two nodes is l , and the length of bits is q . The receiving energy consumption can be shown as

$$LS_r(q) = E_e \cdot q. \quad (3)$$

We can assume some parameters under constraints. For example, suppose when two sensor nodes are $0.5m$ apart and $q = 1 Mbit$. We can set $\eta_{amp} = 10pJ/bit/m^3$. According to Equation (3), $LS_r(q) = E_e \cdot q = 50nJ/bit \cdot 10^6 bit = 0.05J$ can be obtained.

3.2. Route Functions

3.2.1. Energy Consumption Functions. Assume that the data is from v_1 to v_n , the energy consumption of link $r(v_1, v_n)$ can be calculated by formula (4).

$$LS(r(v_1, v_n)) = \sum_{e \in r(v_1, v_n)} LS(e). \quad (4)$$

3.2.2. Delay Functions. The whole delay of data from node v_1 to node v_n can be calculated by formula (5):

$$D(r(v_1, v_n)) = \sum_{e \in r(v_1, v_n)} D(e), \quad (5)$$

where $D(r(v_1, v_n))$ is the total delay time of routing, $r(v_1, v_n)$ is a routing from v_1 to v_n , and e is a link on the route $r(v_1, v_n)$. The delay of link e can be expressed as $D(e)$.

3.2.3. Bandwidth Functions. The whole link bandwidth from node v_1 to v_n can be expressed as formula (6)

$$BW(r(v_1, v_n)) = \min \{BW(e)\}, \quad (6)$$

where $BW(r(v_1, v_n))$ is the bottleneck bandwidth of routing $r(v_1, v_n)$, and e is a link on routing $r(v_1, v_n)$. The bandwidth on the routing e can be represented as $BW(e)$.

3.2.4. Delay Jitter Functions. The whole delay jitter of data from node v_1 to v_n can be expressed by formula (7).

$$DJ(r(v_1, v_n)) = \sum_{e \in r(v_1, v_n)} DJ(e). \quad (7)$$

3.2.5. Packet Loss Rate Functions. The whole packet loss rate of data from node v_1 to v_n can be expressed by formula (8).

$$PL(r(v_1, v_n)) = 1 - \prod_{e \in r(v_1, v_n)} (1 - PL(e)), \quad (8)$$

where $PL(r(v_1, v_n))$ is the whole packet loss rate of routing $r(v_1, v_n)$, e is a link on routing $r(v_1, v_n)$, and $PL(e)$ is the packet loss rate of link e .

3.3. Objective Function. In HDWSNs, many restrictions of the QoS routing model can be formed by the graph model. According to the delay energy loss model based on the conditions, the goal of QoS routing of is to find a route from the start node to the end node with the lowest energy consumption.

Fitness (fitness) is a parameter of all individuals based on the degree of adaptation of organisms to the natural environment. The fitness function refers to the one-to-one correspondence between all basic units in the actual problem and their own fitness. Normally, it is a constant function. In this paper, fitness is used to represent the energy consumption of HDWSNs QoS routing, and the fitness function can be shown by equation (9).

$$\text{fitness} = \min \{LS(p(v_1, v_n))\}. \quad (9)$$

3.4. Restrictions. Finding the best route with minimum energy consumption is the main goal of QoS routing model. Data transmission begins at source node v_1 and ends at terminal node v_n . Links between adjacent nodes on this route need to meet the following restrictions ((10), (11), (12), (13)).

$$D(r(v_1, v_n)) \leq D_{\max}, \quad (10)$$

$$BW(r(v_1, v_n)) \geq BW_{\min}, \quad (11)$$

$$DJ(r(v_1, v_n)) \leq DJ_{\max}, \quad (12)$$

$$PL(r(v_1, v_n)) \leq PL_{\max}, \quad (13)$$

where D_{\max} represents the maximum delay acceptable on the route, BW_{\min} represents the minimum link bandwidth, PL_{\max} represents the maximum packet loss rate, and DJ_{\max} represents the maximum delay jitter.

4. AEACO-Based Routing Minimizes Energy Consumption in HDWSNs

Aiming at QoS routing problem in HDWSNs, an optimization algorithm based on AEACO is put forward. The idea comes from the ant creature [25, 26]. In our AEACO strategy, a significant improvement is to add adaptive strategy and elite strategy on the basis of traditional ant colony optimization. These strategies enable AEACO to route well and direct search to the best solution.

Ant is a kind of social insect with the characteristics of social life, which has strict social structure and division of labor. In addition to harmonious division of labor, the highly complex “ant colony” system also has a mechanism of information transmission among ants, which makes the system operate orderly and efficiently. According to research, ants in nature are able to self-organize and choose the best route from nest to food source and can spontaneously find new good choices based on their surroundings [27, 28]. Ants can use pheromone as a medium to interact with each other.

The original ant colony optimization is an intelligent algorithm proposed by Italian Dorigo M. in 1992 and was successfully applied to solve TSP and QAP [29, 30] and then gradually developed by many scholars. At present, ACO has been applied to various fields, such as coloring problem, vehicle scheduling problem, and job scheduling problem [31, 32].

AEACO is a group intelligence approximate optimization technology. The process of evolution can be divided into two stages: adaptation stage and cooperation stage. In the initial stage of search route adaptation, pheromones accumulate with the increase of evolution time, and the more times ants pass, the higher the pheromone content in the route is, and the route is more likely to be selected by other ants. Therefore, the number of ants choosing this route is increasing. Finally, all ants will concentrate on the best route with positive feedback. At this time, the corresponding route is the optimal route of the routing problem.

This paper discusses several parts of AEACO from the aspects of parameters and population initialization, fitness calculation, path selection, operator optimization, pheromone change, and condition termination.

4.1. Coding Scheme. The first task of AEACO to solve routing problem is program coding. In the implementation of AEACO, coding will greatly affect the routing, fitness evaluation, and pheromone change. There are many coding methods, including real number and binary number. In order to increase the search space, real numbers are used to encode. Suppose there are K ants and s nodes. Each ant generates a route after it reaches the destination. In the restriction QoS routing optimization problem, the route of data transmission is expressed as $p(v_1, v_n)$. The whole number of nodes on the route can be expressed as n , which satisfies the formula (14)

$$n \leq s. \quad (14)$$

The population can be described formula (15), $x_{K,s}$ represents the single node passed by the $No.k$ ant, and $(x_{k,1}, x_{k,2}, x_{k,3} \dots x_{k,s})$ represents the route of the $No.k$ ant.

$$X = \begin{bmatrix} x_{1,1} & x_{1,2} & x_{1,3} & \dots & x_{1,s} \\ x_{2,1} & x_{2,2} & x_{2,3} & \dots & x_{2,s} \\ \dots & \dots & \dots & \dots & \dots \\ x_{k,1} & x_{k,2} & x_{k,3} & \dots & x_{k,s} \\ \dots & \dots & \dots & \dots & \dots \\ x_{K,1} & x_{K,1} & x_{K,3} & \dots & x_{K,s} \end{bmatrix} \quad (x_{K,s} \in [0, s], k \in [1, K]). \quad (15)$$

4.2. Ant Colony Initialization. Ant colony is based on routing model coding. Its purpose is to establish a link between routing issues and AEACO. So, before stimulation, K ants were randomly generated as the initial ant colony. The initial ant colony holds K ants can be described as $X = \{X_1, X_2, \dots, X_K\}$. The $No.i$ ant can be expressed as $X_i = \{x_{i,1}, x_{i,2}, \dots, x_{i,s}\}$.

4.3. Fitness Evaluation. Each ant has its own fitness value and has a path selection solution. Therefore, the fitness function will greatly affect the performance of the algorithm. In the multicondition constrained QoS routing optimization issue, when the delay, link bandwidth, packet loss rate and jitter delay conditions are met, the fitness value can be calculated by formula (9); thus, the routing energy consumption of every one ant in the population in the process of data transmission is got. The lesser the energy consumption is, the better the route is.

Therefore, the criterion of evaluating each ant's path is the value of energy consumption. The less energy consumption of a route, the better the route.

4.4. Select Path. The K ants in the colony have the following characteristics: the energy consumption and pheromone content on the route determine which node the ant will choose. τ_{ij} is the summation number of pheromones in the adjacency link between the 2 nodes. Moreover, the search rules of ants are as follows: each ant need complete a walk from the source to the destination, but it does not necessarily traverse all nodes and cannot access the nodes that have been traversed. Each ant will leave a certain amount of pheromone on its routing after completing the journey. In the initial stage of the algorithm, the pheromone content in the path between adjacent points is the same. At this moment, the $No.k$ ant chooses the next node, and the number of pheromones and the energy consumption value determines which node the ant will choose. $P_{d,e}^{j,j+1}$ represents the probability that ants choose the next node link $No.j$ to $No.(j+1)$. d and e are adjacent to each other.

The amount of pheromone on the path and the energy consumption benefit can be calculated to select the probability of other nodes, so as to select the next routing node. Assuming conditions are met, ants can choose routing nodes. The chance p of the $No.t$ generation ant accessing node d

from node e is calculated by formula (16). In formula (16), the Roulette method can be routed nodes on the route that ants have not passed.

$$P_{d,e}^{i,j+1}(t) = \frac{\tau_{de}^\alpha(t) u_e^\beta(t)}{\sum_{l=1}^s \tau_{dl}^\alpha(t) u_{l,j+1}^\beta(t)} \quad (d \in [1, s], e \in [1, s], u_e \in u_{ij}, u_{l,j+1} \in u_{ij}), \quad (16)$$

$$C_{ij} = \begin{bmatrix} c_{11} & c_{12} & c_{13} & \cdots & c_{1(s-1)} \\ c_{21} & c_{22} & c_{23} & \cdots & c_{2(s-1)} \\ c_{31} & c_{32} & c_{33} & \cdots & c_{3(s-1)} \\ \cdots & \cdots & \cdots & \cdots & \cdots \\ c_{K1} & c_{K2} & c_{K3} & \cdots & c_{K(s-1)} \end{bmatrix} \quad (i \in [1, K], j \in [1, s-1]), \quad (17)$$

$$u_{ij} = \frac{1}{C_{ij}}. \quad (18)$$

In formula (16), t is the iteration time. $\tau_{de}(t)$ is the pheromone content of the $No.t$ generation link (d, e) . u_{ij} represents the reciprocal of the energy consumption value from the $No.j$ node to the $No.(j+1)$ node, which is called energy consumption benefit, which is calculated by formula (18). α and β on behalf of the weighted value of pheromone and energy consumption correspondingly, which affects pheromone concentration and energy consumption. With the value of α increases, the probability of ant selecting nodes increases. With the value of β increases, ants will also increase the chance to select other nodes according to j nodes.

In formula (16), With the increase pheromone concentration and energy efficiency, the probability of ant selecting routing node increases.

C_{ij} represents the energy consumption value of the ant's route, and it is made up of K the same matrixes, which can be expressed as $[c_1 \ c_1 \ c_1 \ \cdots \ c_{s-1}]$. u_{ij} is a matrix of fitness of energy consumption, which can be calculated by formulas ((17) and (18)).

4.5. Pheromone Update. In search of the best route, the pheromone needs to be calculated and updated. When ants visit each routing node, they leave pheromone from the $No.d$ node to the $No.e$ node. With the continuous evolution of the algorithm, the content of pheromone will volatilize in the process of evolution. In AEACO, after each ant completes a walk from the origin node to the end node, the pheromone on the route is updated. The pheromone content on the link (d, e) during $(g, g+1)$ round is modified in

$$\tau_{de}(g, g+1) = \rho \cdot \tau_{de}(g) + \Delta\tau_{de}(g, g+1), \quad (19)$$

$$\Delta\tau_{de}(g, g+1) = \sum_{k=1}^m \Delta\tau_{de}^k(g, g+1). \quad (20)$$

In equation (19), $\Delta\tau_{de}(g, g+1)$ represents the pheromone content that the ant remaining on the link (d, e) during

$(g, g+1)$ round. ρ represents the volatility factor of pheromone, which is used to reduce the accumulated pheromone on the link. According to formula (20), $\Delta\tau_{de}^k(g, g+1)$ means the content of pheromone that the $No.k$ ant remaining on the link (d, e) during $(g, g+1)$ round.

The ant colony pheromone value update calculation of AEACO is represented by equation (21).

$$\tau_{de}^k = u_e Q. \quad (21)$$

In equation (21), Q represents a constant and represents the pheromone unit concentration left by ants on the path to complete the search. u_e is the energy consumption revenue value between two nodes. In this model, when the ant finds the optimal route, the ant releases pheromone. Therefore, the ant colony uses the overall pheromone environment.

4.6. Termination Condition. During the execution of the AEACO, When the algorithm runs to the stop condition statement, it will automatically judge whether it meets the condition. If it meets the upper limit value, it will end the algorithm and output the result.

4.7. Adaptive Operator. In the process of AEACO, the algorithm adopts an adaptive operator, which reduces the speed of the algorithm in the iterative evolution process. The main function of the positive feedback mechanism is to accelerate the algorithm convergence and make the algorithm have good performance, but it is very easy to lead the algorithm to be too premature. Therefore, in the selection operator, an adaptive method can be used. The purpose of the adaptive operator is to flexibly adjust the probability of choosing other paths during the search process. Through multiple loop iterations, the evolution direction of the ant colony can be basically determined, and the pheromone on the path completed by the ants can be dynamically adjusted.

Adaptive strategy is a new information update strategy. When the problem is more complicated, if the pheromone volatilization factor exists, then the pheromone content on the path that ants choose less or has not chosen will be exhausted. Therefore, it will reduce AEACO's global search capabilities. However, if the pheromone content in other paths is very high, then the amount of information in these paths will increase again, so the chance of finding these high-content paths again increases. The path traversed by the previous generation of ants is likely to be selected again by the next generation of ants, which will lead to local optimal search and reduce global search performance. Therefore, AEACO's global search capability can be increased by changing the pheromone volatilization factor. The adaptive strategy proposes an adaptive method to change the pheromone, and the pheromone update formula (22) is expressed as

$$\begin{cases} \tau_{de}(g, g+1) = (1 - \rho)^{1+\varphi(w)} \cdot \tau_{de}(g) + \Delta\tau_{de}(g, g+1) & \tau \geq \tau_{\max} \\ \tau_{de}(g, g+1) = (1 - \rho)^{1-\varphi(w)} \cdot \tau_{de}(g) + \Delta\tau_{de}(g, g+1) & \tau < \tau_{\max} \end{cases} \quad (22)$$

$$\varphi(w) = w/c. \quad (23)$$

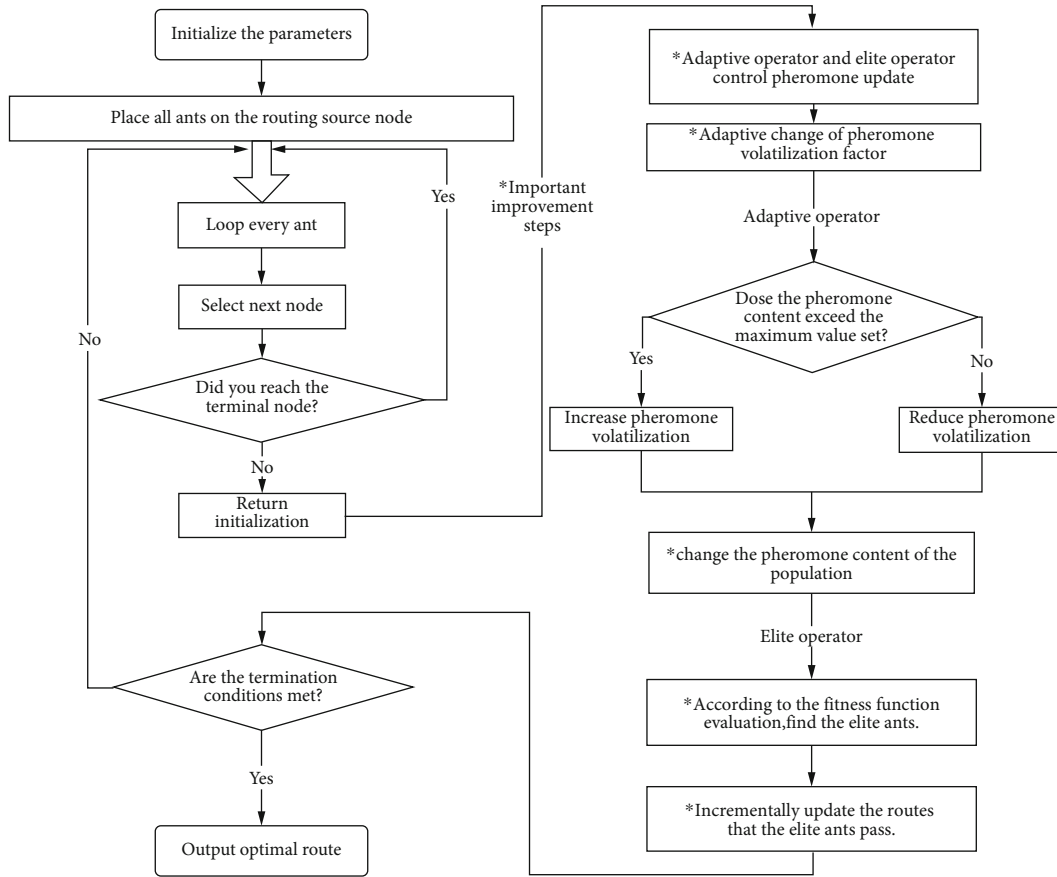


FIGURE 1: The flow chart of AEACO.

Improved adaptive elite ant colony optimization based on routing energy consumption

Begin

Step 1. Set the parameters and QoS constraints of each node and each edge in the model, and the relevant parameters in the algorithm are set. Set the pheromone volatilization coefficient, initialize pheromone value, and energy consumption revenue value. The upper limit of iterations is N_{g_max} . The primary value is $N_g = 0$. The colony size is K .

Set pheromone initial value of τ_{de} on the link (d, e) , $\tau_{de}(0) = 1$.

While the algorithm has not reached the maximum number of iterations.

Step 2. Increase iteration times, $N_g = N_g + 1$.

Step 3. Increase the number of ants, $k = k + 1$.

Step 4. Calculate the selection probability of the next node j , according to Equation (16).

Step 5. If $j \neq s$, continue *step 4*; otherwise, perform *step 6*.

Step 6. If $k \geq K$, go to *step 7*; otherwise, go to *step 3*.

Step 7. Update pheromone adaptive adjustment, according to equation ((16), (22)).

Step 8. Find elite ants and update pheromone incrementally, according to Equation (9).

Step 9. When the condition meets the number of cycles $N_g > N_{g_max}$, then output the result; otherwise, go to *step 2*.

End while

End

ALGORITHM 1: Algorithm flow.

In formula (23), $\varphi(w)$ represents a functional formula proportional to the convergence factor w . The more the times w , the greater the value of $\varphi(w)$, and c represents a constant. According to the evolution of the algorithm, adaptive update pheromone, thereby dynamically adjusting the intensity of the amount of information on each path, so that the ants are neither

too concentrated nor too scattered, thereby avoiding premature and local convergence and improving the global search ability.

4.8. Elite Operator. The elite ant operator is an improvement of the basic ACO. Its design idea is to give the optimal path extra pheromone after each cycle. The ant that finds the best

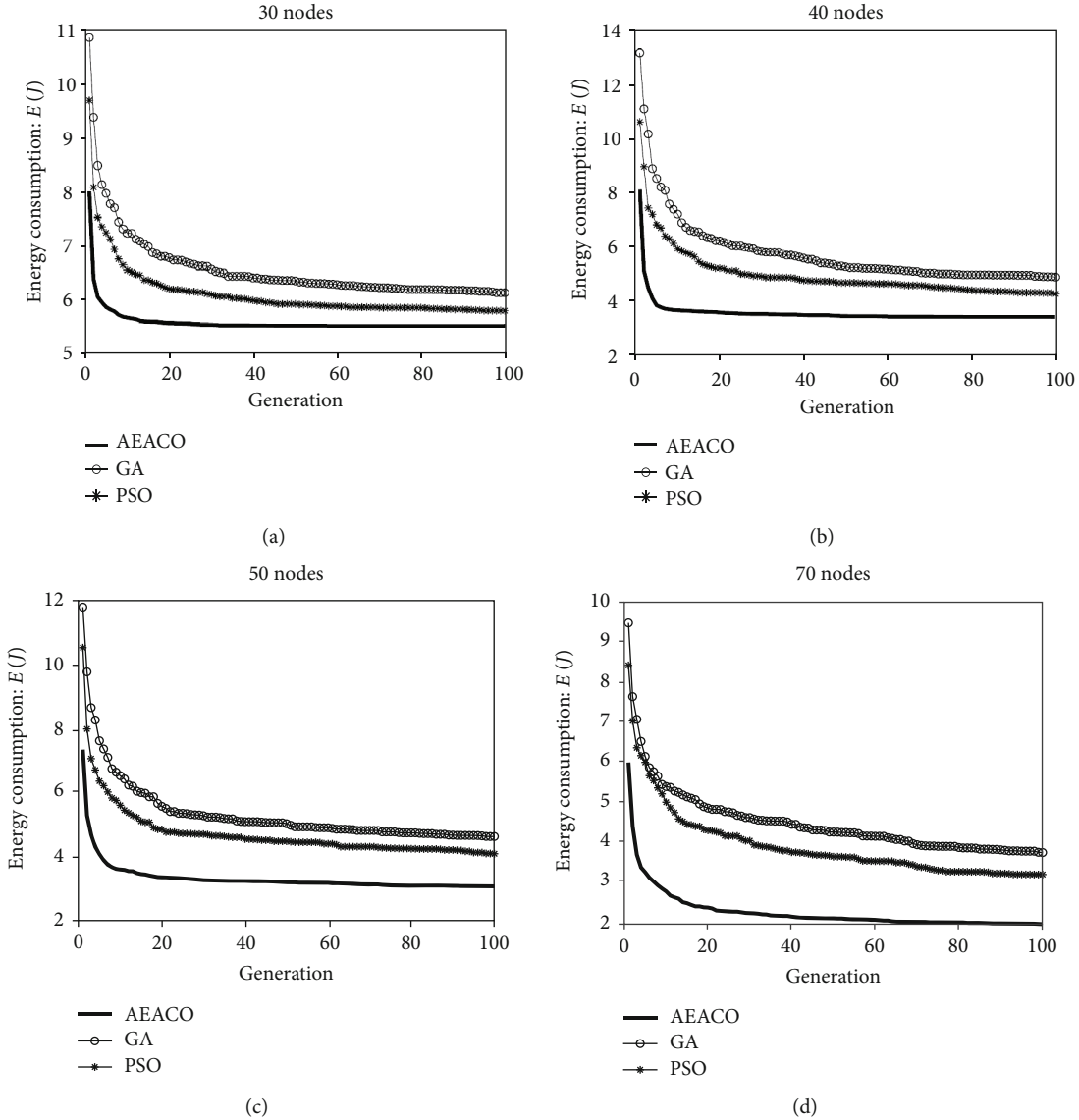


FIGURE 2: Comparison of energy consumption of three algorithms. (a) The energy consumption comparison of three algorithms after 100 generations of 30 nodes. (b) The energy consumption comparison of three algorithms after 100 generations of 40 nodes. (c) The energy consumption comparison of three algorithms after 100 generations of 50 nodes. (d) The energy consumption comparison of three algorithms after 100 generations of 30 nodes.

route is called the elite ant. Denote this optimal route as R_{best} . The additional enhancement for route R_{best} is obtained by adding pheromone to each edge in R_{best} . The update formula of pheromone can be expressed as ((24), (25))

$$\tau_{de}(g, g+1) = \rho \cdot \tau_{de}(g) + \Delta\tau_{de}(g, g+1) + \Delta\tau_{de}^*, \quad (24)$$

$$\Delta\tau_{de}^* = \partial \cdot Q \cdot u_e^*, \quad (25)$$

where ∂ is a parameter that defines the weight given to route R_{best} , and $\Delta\tau_{de}^*$ shows the change of pheromone on the link (d, e) according to the ant that completes the best path. u_e^* shows the benefit value of energy consumption.

4.9. AEACO Steps. As shown in Figure 1, the whole execution process of the AEACO algorithm is visually displayed.

In Figure 1, we can see the overall flow chart. The first is to initialize the parameters, place the ants at the source point of the route, and loop each ant to search. Each ant selects the next node in turn during its own search. After the entire population cycle is over, the next most important process is pheromone update. We propose an adaptive mechanism to determine whether the pheromone content on the current path exceeds the set maximum value, so as to adjust the volatilization factor to control pheromone update. When the entire population is updated, we evaluate the population according to the fitness function and find the elite ants with the least energy consumption for routing. Pheromone is incrementally updated on this path of elite ants. When the predetermined termination condition is reached, the algorithm ends, and the best route is output.

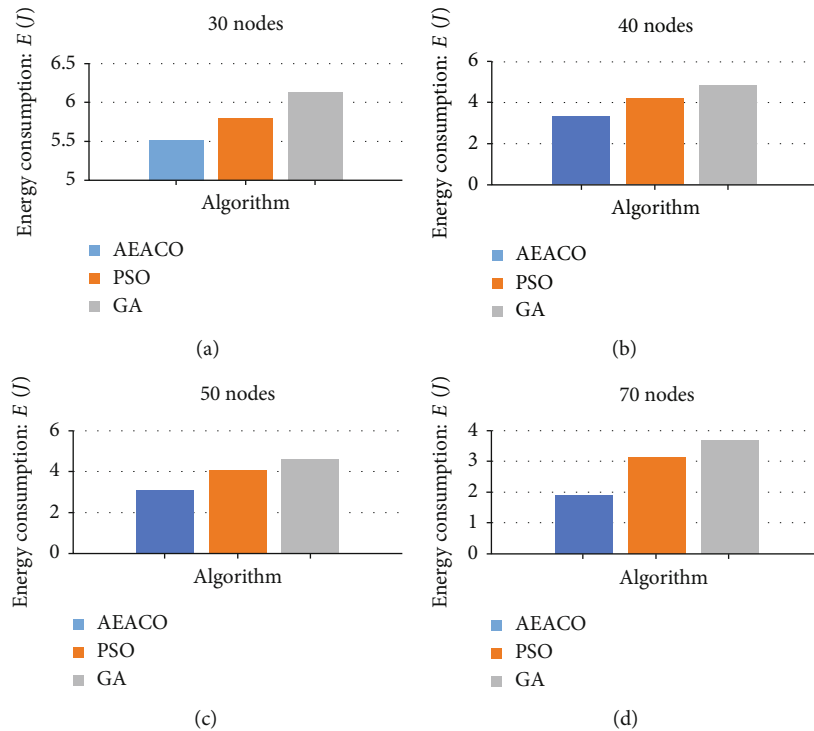


FIGURE 3: Compare the energy consumption of the three algorithms in the form of a histogram. (a) Comparison of energy consumption of three algorithms with 30 nodes. (b) Comparison of energy consumption of three algorithms with 40 nodes. (c) Comparison of energy consumption of three algorithms with 50 nodes. (d) Comparison of energy consumption of three algorithms with 70 nodes.

Through the detailed explanation of the above flowchart, we give the specific algorithm pseudo code of the specific AEACO as shown in Algorithm 1.

5. Discussion on Simulation Results

In the simulation part, we will test the algorithm performance of AEACO in HDWSN routing optimization and compare the results with the simulation results of GA and PSO for HDWSN routing optimization. Under the condition that other conditions are the same, HDWSNs of different numbers of nodes are used for comparison. The software and hardware environment are uniformly equipped with Intel (R) Core (TM) i5 2.40GHz CPU computers and the same version of Windows 10, and the programming language is MATLAB. On this basis, to prove AEACO's superior performance in optimizing QoS routing.

In the simulation, the performance of AEACO is compared with PSO and GA. The three of AEACO, PSO, and GA output results after 100 iterations of the loop and sets the population size to 50 individuals. In AEACO, set the pheromone volatilization factor to 0.98, the energy consumption gain coefficient to 2, the information heuristic factor to 1, the expected heuristic factor to be 4, and the pheromone intensity to 3. The crossover probability of genetic algorithm is 0.75, and the mutation probability is 0.06. In PSO, the value of the social learning factor is defined as 2, the value of the individual learning factor is defined as 2, and the absolute value of the upper and lower speed limits is defined as 10. These parameter settings are given in Tables 1–3.

Figures 2(a)–2(d) shows the simulation results of AEACO, PSO, and GA at four different node scales. It can be clearly seen from Figures 2(a)–2(d) that AEACO has superior performance than PSO and GA under four different node scales. Especially when the number of nodes is 70, AEACO's performance is more obvious. In the first 20 iterations, the energy consumption of AEACO has changed greatly, and the convergence speed has increased significantly after 20 generations. From 20 iterations to 100 iterations, the energy consumption of AEACO is close to 1.8986 J. At this time, PSO and GA are 3.1489 J and 3.7012 J, respectively, using adaptive operators and elite operators to improve AEACO's global search capability and convergence speed. In 100 iterations, the energy consumption of PSO is lower than that of the GA algorithm, while the convergence speed of the AEACO algorithm is faster and the energy consumption is the lowest. In Figures 2(a)–2(c), when the number of nodes is 30, 40, and 50, AEACO performs better than PSO and GA in solving routing energy consumption problems, and the convergence speed of PSO and GA algorithms is slower and easier to fall into a local optimal solution. In general, under the same algebra, AEACO has a faster convergence rate, better effect, and better performance than PSO and GA in terms of routing optimization.

Compare the performance of AEACO, PSO, and GA with the histogram in Figure 3. In Figure 3(d), when the number of nodes is 70 and when iterates 100 times, the energy consumption cost of AEACO is significantly lower than that of PSO and GA. At this time, the energy consumption cost of GA is greater than that of PSO, while the energy

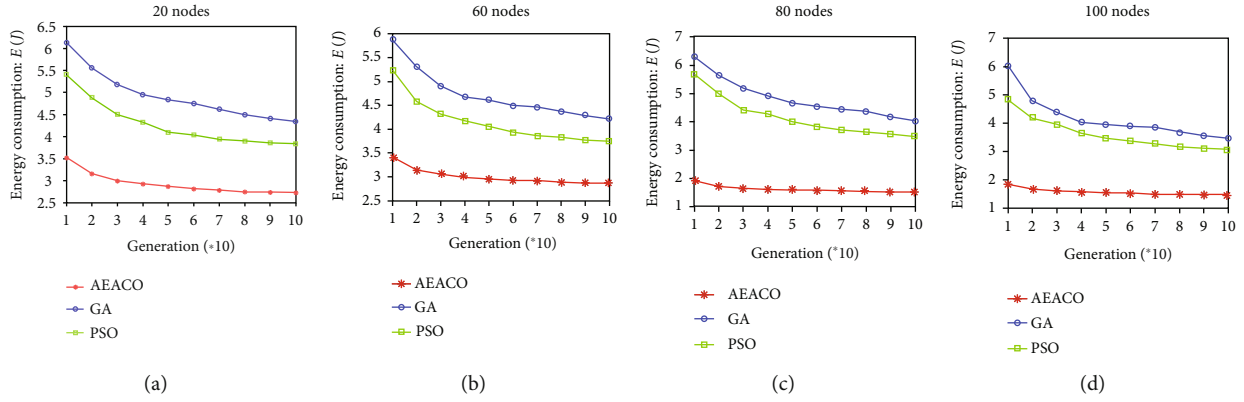


FIGURE 4: The energy consumption of the three algorithms is compared every ten generations. (a) Comparison of 20 nodes every 10 generations. (b) Comparison of 60 nodes every 10 generations. (c) Comparison of 80 nodes every 10 generations. (d) Comparison of 100 nodes every 10 generations.

TABLE 4: Energy consumption values of different node sizes.

Algorithm	30 nodes	40 nodes	50 nodes	70 nodes
AEACO	5.5195	3.3449	3.0690	1.8986
PSO	5.7957	4.2094	4.0883	3.1489
GA	6.1329	4.8302	4.6283	3.7012

consumption cost of AEACO is relatively the lowest and the performance is the best. In Figures 3(a)–3(c), when the number of nodes is 30, 40, and 50, respectively, the same conclusion can be drawn as in Figure 3(d). The performance of AEACO is always better than PSO and GA.

In Figure 4, 20 nodes, 60 nodes, 80 nodes and 100 nodes are set up, respectively. Data comparison is performed every 10 generations. In Figures 4(a)–4(d), it can be seen that in the 10th iteration, the energy consumption of AEACO is much lower than that of PSO and GA, and it quickly converges and stabilizes in the next 90 iterations. At this time, the convergence speed of PSO and GA is slower, PSO performance is better than GA, and AEACO performance is the best. In Figures 4(c) and 4(d), AEACO is basically close to the optimal solution at the 10th generation, while PSO and GA dissociate to the optimal solution, and the difference is great. The results show that AEACO is more effective than PSO and GA, and its performance is always better than PSO and GA.

Aiming at the QoS routing problem with different numbers of sensors, the same number of iterations is adopted. Table 4, respectively, lists the correlation between the energy consumption and node scale of AEACO, PSO, and GA.

The data in Table 5 shows the percentage improvement in energy consumption of AEACO compared with the other two algorithms. When the number of nodes is 30, AEACO's improvement in reducing routing energy consumption is 4.76% and 10.00% higher than that of PSO and GA. Especially when the number of nodes is 70, AEACO's improvement in reducing routing energy consumption is 39.71% and 48.70% higher than that of PSO and GA. It can be seen from Tables 4 and 5 that as the scale of nodes increases, the degree of optimization of the algorithm proposed in this paper is more obvious, which is suitable for dense networks

TABLE 5: Compared with the other 2 algorithms, the percentage of improvement in energy consumption is optimized by AEACO.

Number of nodes	PSO	GA
30	4.76%	10.00%
40	20.54%	30.75%
50	24.93%	33.69%
70	39.71%	48.70%

TABLE 6: Convergence time comparison of three algorithms.

Number of nodes	AEACO	PSO	GA
30	9.63 s	14.26 s	18.95 s
40	15.64 s	20.53 s	25.12 s
50	19.37 s	24.47 s	28.96 s
70	35.49 s	48.37 s	55.83 s

such as HDWSNs. The data shows that this method can effectively reduce routing energy consumption.

The data in Table 6 shows the calculated convergence time of the three algorithms under the conditions of 30, 40, 50, and 70 nodes, respectively. It can be seen from the data that the convergence time of AEACO's algorithm is shorter than that of PSO and GA. Especially as the number of nodes increases, the performance of AEACO's algorithm is more obvious than that of PSO and GA. Therefore, it is proved that the method has better performance.

Based on the above result data analysis, the AEACO we proposed has superior performance in reducing energy consumption and algorithm convergence. This is due to the strategy of combining adaptive and elite design we designed to control the volatilization of pheromone in the algorithm flow to increase the algorithm's global search capability. Add extra pheromone to the elite ants to increase the ability of the algorithm to quickly find the best. Simulation results show that this method can effectively reduce routing energy consumption.

In this research, for the energy consumption optimization method of high-density wireless sensor network under multiple constraints, this paper proposes an optimization method for the network model under the constraints of delay, jitter, bandwidth, and packet loss rate and only considers two nonmovable situations in the dimensional coordinates. We did not consider more complex situations, such as three-dimensional space, movable sensors, and other factors. In the future, it will be further studied under the combined effect of environmental interference, movable deployment conditions, and other influencing factors and expanded into three-dimensional space to optimize network energy consumption. Therefore, these issues are the content of this article that needs further research.

6. Conclusion

In order to optimize routing selection, an improved adaptive elite ant colony optimization (AEACO) is proposed, which combines the advantages of traditional ant colony optimization and adaptive strategy and elite strategy. The process of AEACO evolution, population coding, and population initialization calculates fitness, selects path, and updates pheromone. By adding an elite operator, additional pheromone will be added to the path taken by the individual ant with lower energy consumption to accelerate the algorithm convergence. AEACO after adding adaptive operator evolution has a more comprehensive global search capability. We compared this algorithm with PSO and GA in simulation. The outcomes show that the proposed AEACO has a quicker convergence speed and can be more effective find a data transmission path with minimum energy consumption.

Data Availability

The data presented in this study are available on request from the corresponding author. The data are not publicly available due to privacy.

Disclosure

The funders had no role in the design of the study in the collection, analyses, or interpretation of data in the writing of the manuscript, or in the decision to publish the results.

Conflicts of Interest

The authors declare no conflict of interest.

Authors' Contributions

Jie Zhou and Jing Xiao performed the conceptualization. Jie Zhou performed the methodology. Chaoqun Li performed the software. Jie Zhou, Jing Xiao, and Chaoqun Li contributed to the validation. Jing Xiao and Chaoqun Li contributed to the formal analysis. Jie Zhou contributed to the investigation. Jie Zhou performed the resources. Chaoqun Li performed the data curation. Jing Xiao and Chaoqun Li performed the writing—original draft preparation. Jie Zhou contributed to the writing—review and editing. Chaoqun Li

performed the visualization. Jie Zhou and Jing Xiao performed the supervision. Jie Zhou contributed to the project administration. Jie Zhou performed the funding acquisition. All authors have read and agreed to the published version of the manuscript.

Acknowledgments

This paper was funded by the Project of Youth and Middle Aged Scientific and Technological Innovation Leading Talents Program of the Corps, grant number 2018CB006, the China Postdoctoral Science Foundation, grant number 220531, Corps Innovative Talents Plan, grant number 2020CB001, Funding Project for High Level Talents Research in Shihezi University, grant number RCZK2018C38, and Project of Shihezi University, grant number ZZZC201915B.

References

- [1] J. W. Guck, A. Van Bemten, M. Reisslein, and W. Kellerer, "Unicast QoS routing algorithms for SDN: a comprehensive survey and performance evaluation," *IEEE Communications Surveys & Tutorials*, vol. 20, no. 1, pp. 388–415, 2018.
- [2] N. Varyani, Z. Zhang, and D. Dai, "QROUTE: an efficient quality of service (QoS) routing scheme for software-defined overlay networks," *IEEE Access*, vol. 8, pp. 104109–104126, 2020.
- [3] Y. Jin, K. S. Kwak, and S.-J. Yoo, "A novel energy supply strategy for stable sensor data delivery in wireless sensor networks," *IEEE Systems Journal*, vol. 14, no. 3, pp. 3418–3429, 2020.
- [4] N. Qi, K. Dai, F. Yi, X. Wang, Z. You, and J. Zhao, "An adaptive energy management strategy to extend battery lifetime of solar powered wireless sensor nodes," *IEEE Access*, vol. 7, pp. 88289–88300, 2019.
- [5] R. Du, L. Gkatzikis, C. Fischione, and M. Xiao, "On maximizing sensor network lifetime by energy balancing," *IEEE Transactions on Control of Network Systems*, vol. 5, no. 3, pp. 1206–1218, 2018.
- [6] B. O. Ayinde and A. Y. Barnawi, "Energy conservation in wireless sensor networks using partly-informed sparse auto-encoder," *IEEE Access*, vol. 7, pp. 63346–63360, 2019.
- [7] F. Afsana, M. Asif-Ur-Rahman, M. R. Ahmed, M. Mahmud, and M. S. Kaiser, "An energy conserving routing scheme for wireless body sensor nanonetwork communication," *IEEE Access*, vol. 6, pp. 9186–9200, 2018.
- [8] H. Mostafaei, "Energy-efficient algorithm for reliable routing of wireless sensor networks," *IEEE Transactions on Industrial Electronics*, vol. 66, no. 7, pp. 5567–5575, 2019.
- [9] J. Wang, Y. Gao, C. Zhou, R. S. Sherratt, and L. Wang, "Optimal coverage multi-path scheduling scheme with multiple mobile sinks for WSNs," *Computers, Materials & Continua*, vol. 62, no. 2, pp. 695–711, 2020.
- [10] J. Wang, X. Gu, W. Liu, A. K. Sangaiah, and H. J. Kim, "An empower Hamilton loop based data collection algorithm with mobile agent for WSNs," *Human-centric Computing and Information Sciences*, vol. 9, no. 1, pp. 1–14, 2019.
- [11] J. Wang, Y. Gao, X. Yin, F. Li, and H.-J. Kim, "An enhanced PEGASIS algorithm with mobile sink support for wireless sensor networks," *Wireless Communications and Mobile Computing*, vol. 2018, Article ID 9472075, 9 pages, 2018.

- [12] D. Gao, S. Zhang, F. Zhang, X. Fan, and J. Zhang, "Maximum data generation rate routing protocol based on data flow controlling technology for rechargeable wireless sensor networks," *Computers, Materials & Continua*, vol. 59, no. 2, pp. 649–667, 2019.
- [13] J. Wang, C. Ju, Y. Gao, A. K. Sangaiah, and G. J. Kim, "A PSO based energy efficient coverage control algorithm for wireless sensor networks," *Computers, Materials & Continua*, vol. 56, no. 3, pp. 433–446, 2018.
- [14] A. K. Sangaiah, D. V. Medhane, G.-B. Bian, A. Ghoneim, M. Alrashoud, and M. S. Hossain, "Energy-aware green adversary model for cyberphysical security in industrial system," *IEEE Transactions on Industrial Informatics*, vol. 16, no. 5, pp. 3322–3329, 2020.
- [15] A. K. Sangaiah, M. Sadeghilalimi, A. A. R. Hosseinabadi, and W. Zhang, "Energy consumption in point-coverage wireless sensor networks via bat algorithm," *IEEE Access*, vol. 7, pp. 180258–180269, 2019.
- [16] A. K. Sangaiah, A. A. R. Hosseinabadi, M. B. Shareh, S. Y. Bozorgi Rad, A. Zolfagharian, and N. Chilamkurti, "IoT resource allocation and optimization based on heuristic algorithm," *Sensors*, vol. 20, no. 2, p. 539, 2020.
- [17] A. K. Sangaiah, J. S. Ramamoorthi, J. J. P. C. Rodrigues, M. A. Rahman, G. Muhammad, and M. Alrashoud, "LACCVoV: linear adaptive congestion control with optimization of data dissemination model in vehicle-to-vehicle communication," *IEEE Transactions on Intelligent Transportation Systems*, pp. 1–10, 2020.
- [18] A. K. Sangaiah, D. V. Medhane, T. Han, M. S. Hossain, and G. Muhammad, "Enforcing position-based confidentiality with machine learning paradigm through Mobile edge computing in real-time industrial informatics," *IEEE Transactions on Industrial Informatics*, vol. 15, no. 7, pp. 4189–4196, 2019.
- [19] J. Li, Z. Luo, and J. Xiao, "A hybrid genetic algorithm with bidirectional mutation for maximizing lifetime of heterogeneous wireless sensor networks," *IEEE Access*, vol. 8, pp. 72261–72274, 2020.
- [20] Z. Ye, K. Xiao, Y. Ge, and Y. Deng, "Applying simulated annealing and parallel computing to the mobile sequential recommendation," *IEEE Transactions on Knowledge and Data Engineering*, vol. 31, no. 2, pp. 243–256, 2019.
- [21] M. Song and M. Zheng, "Energy efficiency optimization for wireless powered sensor networks with nonorthogonal multiple access," *IEEE Sensors Letters*, vol. 2, no. 1, pp. 1–4, 2018.
- [22] X. Gu, X. Zhou, B. Yuan, and Y. Sun, "A Bayesian compressive data gathering scheme in wireless sensor networks with one mobile sink," *IEEE Access*, vol. 6, pp. 47897–47910, 2018.
- [23] X. Li, B. Keegan, F. Mtenzi, T. Weise, and M. Tan, "Energy-efficient load balancing ant based routing algorithm for wireless sensor networks," *IEEE Access*, vol. 7, pp. 113182–113196, 2019.
- [24] D. R. Edla, A. Lipare, R. Cheruku, and V. Kuppili, "An efficient load balancing of gateways using improved shuffled frog leaping algorithm and novel fitness function for WSNs," *IEEE Sensors Journal*, vol. 17, no. 20, pp. 6724–6733, 2017.
- [25] D. Zhang, X. You, S. Liu, and H. Pan, "Dynamic multi-role adaptive collaborative ant colony optimization for robot path planning," *IEEE Access*, vol. 8, pp. 129958–129974, 2020.
- [26] Q. Song, Q. Zhao, S. Wang, Q. Liu, and X. Chen, "Dynamic path planning for unmanned vehicles based on fuzzy logic and improved ant colony optimization," *IEEE Access*, vol. 8, pp. 62107–62115, 2020.
- [27] A. M. Abdelbar and K. M. Salama, "Parameter self-adaptation in an ant colony algorithm for continuous optimization," *IEEE Access*, vol. 7, pp. 18464–18479, 2019.
- [28] M. Liu, X. You, X. Yu, and S. Liu, "KL divergence-based pheromone fusion for heterogeneous multi-colony ant optimization," *IEEE Access*, vol. 7, pp. 152646–152657, 2019.
- [29] E. Liao and C. Liu, "A hierarchical algorithm based on density peaks clustering and ant colony optimization for traveling salesman problem," *IEEE Access*, vol. 6, pp. 38921–38933, 2018.
- [30] X. Xia and Y. Zhou, "Performance analysis of ACO on the quadratic assignment problem," *Chinese Journal of Electronics*, vol. 27, no. 1, pp. 26–34, 2018.
- [31] D. Liang, Z.-H. Zhan, Y. Zhang, and J. Zhang, "An efficient ant colony system approach for new energy vehicle dispatch problem," *IEEE Transactions on Intelligent Transportation Systems*, vol. 21, no. 11, pp. 4784–4797, 2020.
- [32] Y. Wan, T.-Y. Zuo, L. Chen, W.-C. Tang, and J. Chen, "Efficiency-oriented production scheduling scheme: an ant colony system method," *IEEE Access*, vol. 8, pp. 19286–19296, 2020.

Research Article

Analysis and Design of a Wireless Sensor Network Based on the Residual Energy of the Nodes and the Harvested Energy from Mint Plants

Hassel Aurora Alcalá-Garrido , Víctor Barrera-Figueroa , Mario E. Rivero-Ángeles ,
Yunia Verónica García-Tejeda , and Hosanna Ramírez Pérez 

Instituto Politécnico Nacional, Mexico

Correspondence should be addressed to Hassel Aurora Alcalá-Garrido; b151135@sagitario.cic.ipn.mx

Received 21 October 2020; Revised 13 January 2021; Accepted 30 January 2021; Published 2 March 2021

Academic Editor: Xavier Vilanova

Copyright © 2021 Hassel Aurora Alcalá-Garrido et al. This is an open access article distributed under the Creative Commons Attribution License, which permits unrestricted use, distribution, and reproduction in any medium, provided the original work is properly cited.

Nowadays, the use of sensor nodes for the IoT is widespread; nodes that compose these networks must possess self-organizing capabilities and communication protocols that require less energy consumption during communication procedures. In this work, we propose the design and analysis of an energy harvesting system using bioelectricity harvested from mint plants that aids in powering a particular design of a wireless sensor operating in a continuous monitoring mode. The system is based on randomly turning nodes ON (active nodes) and OFF (inactive nodes) to avoid their energy depletion. While a node is in an inactive state, it is allowed to harvest energy from the surroundings. However, while the node is harvesting energy from its surroundings, it is unable to report data. As such, a clear compromise is established between the amount of information reported and the lifetime of the network. To finely tune the system's parameters and offer an adequate operation, we derive a mathematical model based on a discrete Markov chain that describes the main dynamics of the system. We observe that with the use of mint plants, the harvested energy is of the order of a few Joules; nonetheless, such small energy values can sustain a wireless transmission if correctly adapted to drive a wireless sensor. If we consider the lowest mean harvested energy obtained from mint plants, such energy can be used to transmit up to 259,564 bits or can also be used to receive up to 301,036 bits. On the other hand, if we consider the greatest mean harvested energy, this energy can be used to transmit up to 2,394,737 bits or can also be used to receive up to 2,777,349 bits.

1. Introduction

Internet of Things (IoT) are becoming popular due to the so-called three *anys*-, namely, *any* person, *anywhere*, and *anytime*. These networks are composed of a large number of sensor nodes, which are densely located nearby a phenomenon of interest, which is a major part of the next generation communication systems that provide and support the *anys* paradigm. Usually, can be deployed in inaccessible terrains or during disaster relief operations. The position of sensor nodes may not be previously designed or predetermined. Such randomness implies that protocols and algorithms must possess self-organizing capabilities.

Sensor nodes share information with each other and with the network administrator to provide different services to end users [1]. This represents a significant improvement over traditional sensors. Nodes are expected to operate during long periods without human intervention. The cooperative efforts of sensor nodes are necessary for the correct functioning of the network. For extending the lifetime of the network, the design of protocols must require less energy consumption during communication procedures [2].

Recent advances in wireless communications and electronics have enabled the development of low-cost, low-power, multifunctional wireless sensor nodes. Such nodes can reliably communicate in (relatively) short distances. Wireless

sensor nodes are fitted with an on-board processor for carrying out simple computations and to transmit only the required and partially processed data [3]. Thus, nodes are not always required to send all the acquired information to the sink node. This allows nodes to be working in a low energy consumption mode (*sleep* mode), during which their energy levels can be replenished if energy harvesting is enabled [4, 5].

Green self-sustainable operation is one of the most important issues in today's low-power electronics for smart environments (IoT, smart skins, smart cities, etc.) [6]. Energy harvesting technologies from ambient power sources—mainly radio frequency (RF) ambient energy—have recently attracted significant attention since the operation time of devices can be extended or even the energy depletion of batteries can completely be avoided. In this sense, numerous energy harvesting systems, devices, topologies, and circuitries have been developed [7].

The design of this networks is influenced by many factors such as fault tolerance, scalability, production costs, operating environment, network topology, hardware constraints, and transmission media [1]. Energy consumption is also a critical factor in the design, and the use of batteries with finite energy levels entails a finite operation time. In some scenarios, power recharging or battery replacement can be a very challenging task. Ongoing research is aimed at providing energy harvesting solutions for powering wireless sensor which can offer a significant advantage as these provide sustainable solutions to their power needs [8].

The main tasks of a wireless sensor node are sense environmental phenomena, perform quick local data processing, and then transmit the data. Each task implies a corresponding power consumption. If energy harvesting is implemented, a transducer is responsible for harvesting energy from the surroundings. Before its usage, harvested electrical energy should be conditioned by specialized circuitry. Conditioned electricity can be used directly or stored in rechargeable batteries or supercapacitors.

Power consumption of a wireless sensor is of great importance because it is functioning entirely depends on the energy supplied to the wireless nodes. Indeed, the failure of a few nodes due to lack of energy would result in significant topological changes that imply rerouting packets and reorganizing the network. Hence, the conservation and management of power take major importance. For these reasons, current researches are focusing on the design of power-aware protocols and algorithms for wireless sensors [9].

In the present work, we propose the design, analysis, and study of a Wireless Sensor Network (WSN) that allows its nodes to be turned ON and OFF, i.e., nodes are not required to transmit all the acquired information. When nodes are in the low energy consumption mode, data is neither acquired nor transmitted to the sink node. Specifically, we focus on extending the system's lifetime by taking advantage of energy harvesting techniques. Hence, we include the energy harvesting capabilities in our analysis where energy levels of nodes in the OFF mode are replenished.

Furthermore, we focus on a scheme that extends the lifetime of the system by assigning a higher (lower) packet transmission probability to nodes with high (low) residual energy

levels. This also entails that low energy nodes report fewer data to the sink node. Applications for the proposed scheme can be found in the cases where the network must operate for long times even if data reporting is reduced after long operation periods. For instance, when nodes are not accessible or placed in dangerous or remote locations like polar regions, radioactive zones, wildfire monitoring in forests, or even space exploration missions where the objective is to obtain as much information as possible from the environment for as long as possible, and if energy is scarce, conserve it as much as possible even if only occasional reports are available. We study the performance of such a system and the limitations of our proposal. Our main contributions are:

- (i) We developed our design of a card compatible with the Arduino IDE
- (ii) The card is designed for very low power consumption and has all in one: radio, microcontroller, antenna, and sensor ports
- (iii) A protocol based on residual energy available in the network to power the nodes
- (iv) A mathematical analysis based on Markov chains to determine the lifetime of the network
- (v) A detailed study to determine very accurately how much energy is needed to send a single bit. \hat{A}°
- (vi) An efficient electronic design without the need of a very sophisticated antenna for radio links. However, the simple wire was measured and characterized to determine the optimal length
- (vii) An open hardware architecture design where all card details are provided
- (viii) Low cost and reliable card design that, compared to Zig-Bee, is very cheap

2. Related Work

A wireless sensor is an electronic device equipped with certain characteristics of sensing and elementary functions for establishing wireless communication. These characteristics are governed by a basic computing system usually implemented in a microcontroller or a small microprocessor. In addition, a wireless sensor must possess capacities for efficient energy management and maybe the ability to harvest the energy from the surroundings, including solar, electromagnetic, or the energy from plants, see Figure 1.

In general, a wireless sensor is equipped with a small amount of energy stored in a battery or supercapacitor. The correct usage of this energy may lead to extending the lifetime of the wireless sensor. Eventually, such finite energy gets depleted, and the wireless sensor will be off the network until it acquires more energy in some way, for instance, by changing its batteries with new ones. This could be challenging if the wireless sensor is located in a difficult-to-reach position. In such cases, the network will lose nodes and eventually will be useless. Hence, determining the necessary power for

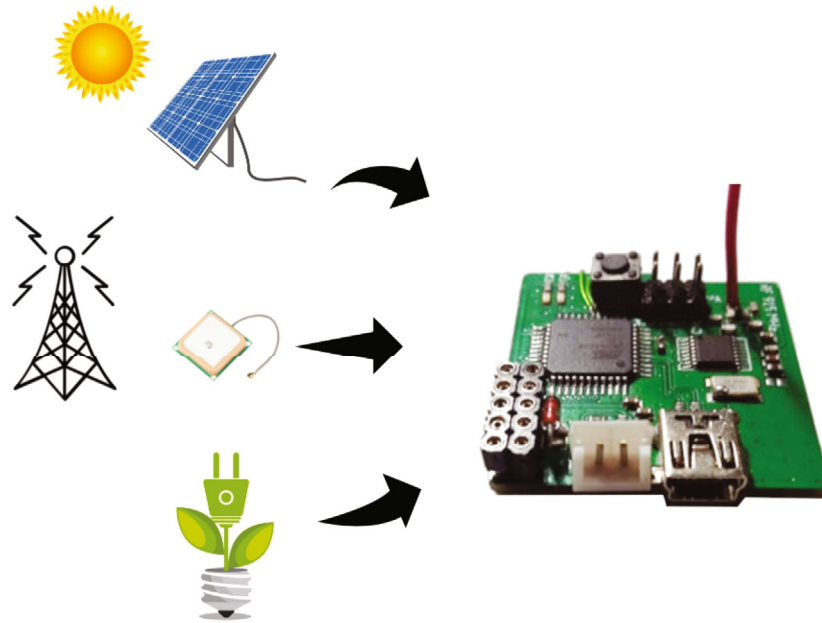


FIGURE 1: Simplified architecture of a wireless sensor.

transmitting or receiving data is important for estimating the lifetime of the WSN. An estimation of the lifetime of a WSN can be obtained from a stochastic point of view, for instance, by using Markov chains [10–14], or from an energetic point of view [15–17] [18, 19].

To estimate the energetic cost of transmitting/receiving data, we consider the following. By definition, the instantaneous electric power $p(t)$ is the rate at which electric energy $e(t)$ as a function of time is transferred to or from a part of an electric circuit [20, 21], that is

$$p(t) = \frac{de(t)}{dt}. \quad (1)$$

Cumulative energy E over a period of time $T = [t_i, t_f]$ is the integral of the instantaneous power,

$$E = \int_{t_i}^{t_f} p(t) dt. \quad (2)$$

Let us suppose that the instantaneous power p is a continuous function over the period T , then there exists an instant $t_m \in T$ such that

$$E = p(t_m)(t_f - t_i) = p(t_m)\Delta t, \quad (3)$$

where $\Delta t = t_f - t_i$ is the duration of T and $p(t_m)$ has the physical sense of mean power in that period, which is denoted by \bar{W} , hence

$$E = \bar{W}\Delta t. \quad (4)$$

Note that the mean power in T can be calculated from formulas (1) and (2),

$$E = \int_{t_i}^{t_f} d(e(t)) = e(t_f) - e(t_i) = \Delta e, \quad (5)$$

where Δe denotes the change of energy at the ends of period T , thereby $\bar{W} = \Delta e/\Delta t$.

By a unit of energy, we mean the energy necessary to perform a work by the wireless sensor (either transmit, receive, or sleep) during certain time. This includes, of course, the energetic cost of running some code by the microcontroller to control the communication tasks and to perform the corresponding networking functions. Let us assume that a wireless sensor performs a single operation of transmission or reception during a time slot of duration Δt_{slot} seconds. Formula (4) provides a simple way to estimate the energy $E_{\text{Tx,slot}}$, $E_{\text{Rx,slot}}$, or $E_{\text{Sleep,slot}}$ per slot to perform such an operation

$$E_{\text{Tx,slot}} = W_{\text{Tx}}\Delta t_{\text{slot}}, \quad (6)$$

$$E_{\text{Rx,slot}} = W_{\text{Rx}}\Delta t_{\text{slot}}, \quad (7)$$

$$E_{\text{Sleep,slot}} = W_{\text{Sleep}}\Delta t_{\text{slot}}, \quad (8)$$

where W_{Tx} , W_{Rx} , and W_{Sleep} are the representative values of the power consumed during transmission, reception, or sleep, respectively.

The rest of the paper is organized as follows: first, Section 3 describes the design of a wireless sensor; Section 4 presents the power and energy analysis in the wireless sensor; Section 5 is an analysis of the energy used by the WSN and the harvesting energy from mint plants; Section 6 develops the

mathematical model used to describe the system. The results are presented in Section 7 and finally our main conclusions.

3. Design of a Wireless Sensor

In this section, we show the design of a wireless sensor, including some simulations and related measurements. The objective is not to design a sophisticated device or to rival with some wireless sensors available in the market but to provide simple guidelines of design and to perform the measurements of energy and power necessary to evaluate its performance in a WSN.

3.1. Microcontroller Selection. For the design of a wireless sensor, we employ the chip ATmega32U4, which is a low-power CMOS 8-bit microcontroller, with an advanced RISC architecture. This microcontroller possesses 32 KBytes of in-system self-programmable flash program memory, 1 KByte EEPROM, 2.5 KBytes internal SRAM, and USB 2.0 full-speed/low-speed device module with interrupt on transfer completion, see Figure 2(a). Also, it possesses six sleep modes, namely, idle, ADC noise reduction, power-save, power-down, standby, and extended standby.

The microcontroller is set up in a stand-alone configuration, running with a 16 MHz crystal oscillator, see Figure 2(b). The configuration provides a set of pins that serve as I/O ports. These ports can be used for interfacing some sensors for sensing physical variables such as temperature, pressure, gases, presence, and light. If ports are configured as analog inputs, they internally use the analog-to-digital converter (ADC), which results in higher power consumption by the microcontroller.

The microcontroller can be programmed either by using the USB or SPI interface. USB programming requires a bootloader to enable built-in USB support. SPI programming does not require a bootloader, and well-known utilities such as AVRDUDE are available for programming the chip. For burning (*flashing*) a bootloader in the microcontroller, the SPI interface should be used as well.

3.2. Radio Chip Selection. The air interface of a wireless sensor involves a radio circuit for establishing wireless communications with other sensors of the network. There exist several commercial options that provide integrated solutions for configuring a wireless network like XBee, see Figure 3(a). XBee modules use the IEEE 802.15.4 networking protocol for fast point-to-multipoint or peer-to-peer networking; however, these modules have some drawbacks concerning the objectives of the present work. In the first place, they usually employ the 2.4 GHz ISM band for world-wide compatibility purposes. In this band of frequency, a wireless link reaches distances of some tens of meters in indoor environments [22, 23] with some improvement in outdoors [24]. Some XBee modules improve their coverage range by transmitting with a higher power, like the XBee Pro that reaches up to 1.6 km in line-of-sight at 63 mW (18 dBm) [25], thereby increasing the overall power consumption of the module.

On the other hand, the 2.4 GHz ISM band is populated by the radiation of Wi-Fi and Bluetooth devices, as well as microwave ovens among others. These behave as interfering sources resulting in higher packet error rates [27–29], lower throughput [30, 31], higher path loss, and fading [32]. For these reasons, some protocols and devices are moving to lower frequencies, which are less populated and offer higher coverage ranges. One example is found in the IEEE 802.11ah WLAN protocol, which uses the sub-1 GHz license-free ISM bands [33]. The XBee-PRO 900HP module works on the band of 902–928 MHz and reaches up to 15.5 km in line-of-sight by transmitting 250 mW (24 dBm) at 10 kb/s, [34]. Though the range of this module is quite broad, its power consumption is relatively high ($290 \text{ mA}_{\text{max}} \times 3.6 \text{ V}_{\text{max}} = 1.044 \text{ W}_{\text{max}}$).

Another drawback of the XBee modules is the impossibility to write custom firmware for specific applications. Though XBee modules are highly configurable, it is not possible to modify the way they transmit a single byte, not to mention his high price. On the opposite side, some RF modules are very cheap and lack firmware, thereby the user needs to write custom software to operate the modules via microcontrollers. An example is the RF modules of Figure 3(b), which can work in the ISM band of 315 MHz or 433 MHz. The transmitter (TX) module is indeed a simple Colpitts oscillator that is turned on/off by a transistor configured as a switch, which results in OOK modulation. The receiver (RX) module is a simple super-regenerative receiver equipped with an op-amp as a comparator for detecting digital symbols. RX and TX modules consume up to 20 mW and 10 mW, respectively, [35]. Even without antennas, the wireless link can be established with a range of some meters, but a single strand of wire as an antenna in the TX module may increase the coverage range to some tens of meters. Indeed, the coverage range can be extended to a few kilometers by using high gain well-matched antennas in both modules. Unfortunately, the PCBs of these modules are not designed to accommodate a proper RF connector for plugging external antennas. Another drawback is the large amount of source code for equipping the link with the essential functionality for deploying a basic WSN, thus occupying most of the microcontroller's program memory.

At the midpoint, we found commercial wireless modules based on the chips of the nRF24 Series from Nordic, which work in the 2.4 GHz ISM band, see Figure 3(c). Other popular wireless modules based on the CC1101 chip from Texas Instrument work in the sub-1 GHz ISM bands [36] at low-powers. Such modules are highly configurable, and custom software can be written from standard libraries. Furthermore, their coverage range is quite high when using high-gain well-matched antennas and transmitting at the maximum output power (up to 0 dBm for the nRF24L01+ at 2.4 GHz and up to 11 dBm for the CC1101 at 915 MHz).

For designing the wireless sensors, we have chosen the MRF49XA chip from Microchip [37], see Figure 3(d). This is a sub-1 GHz RF transceiver that can work in the 433, 868, and 915 MHz ISM bands. In particular, we opted for the 915 MHz ISM band for designing the wireless sensors. Few external components are needed for designing a

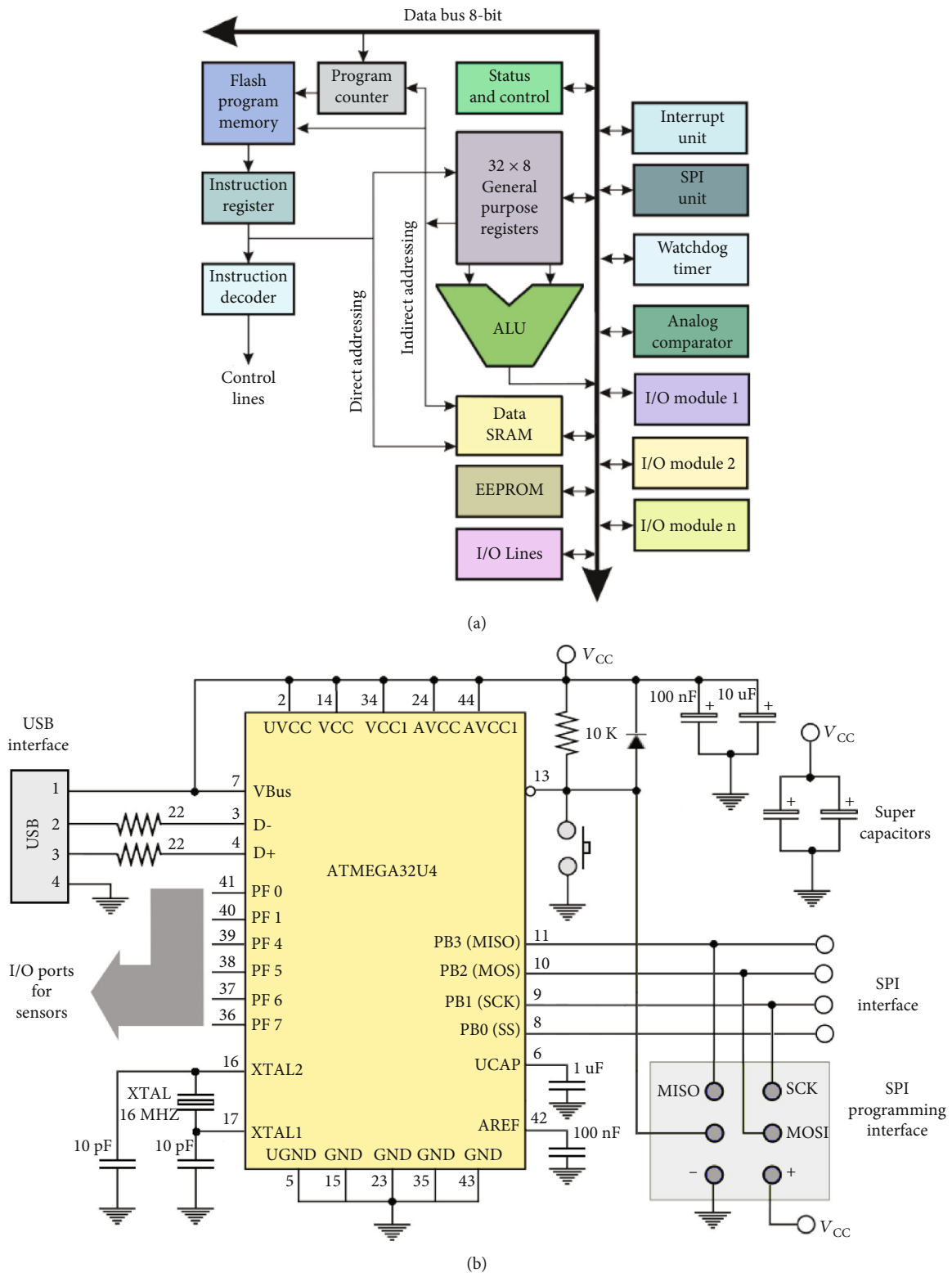


FIGURE 2: (a) CPU architecture of the ATmega32U4 (adapted from [[26], p. 9]). (b) Stand-alone configuration for the ATmega32U4.

completely integrated RF transceiver. The chip employs FSK modulation with a data rate ranging from 1.2 kbps to 256 kbps. Since the chip can rapidly settle the carrier to the desired frequency, it can perform frequency-hopping and

implement multichannel. The receiver is quite sensitive, with an increased receiving sensitivity of -110 dBm. The above allows the wireless link to be robust enough to surpass multipath fading and interference.

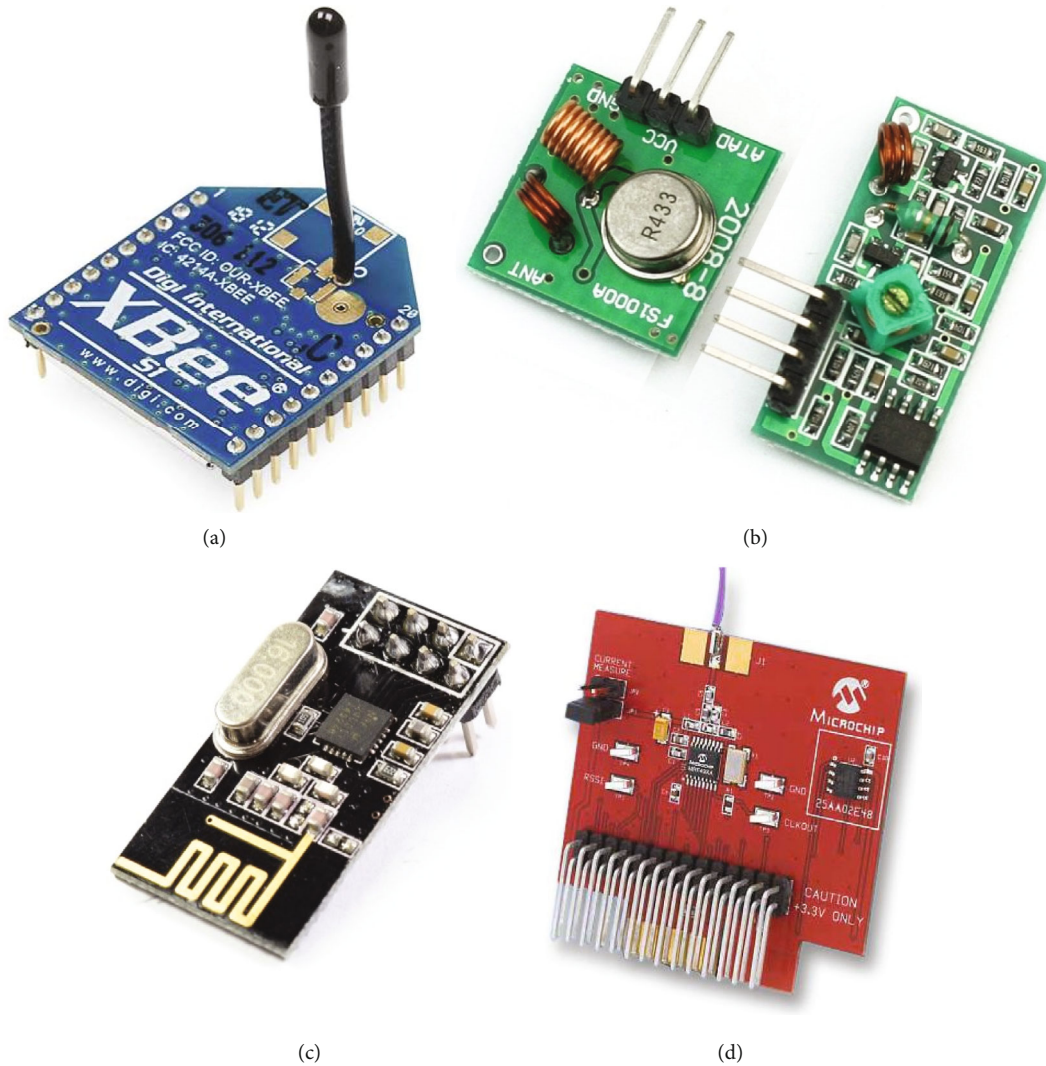


FIGURE 3: Some examples of commercial RF modules: (a) Xbee module; (b) 433 MHz TX/RX modules; (c) NRF24L01+ transceiver; (d) MRF49XA transceiver.

The MRF49XA chip is configured via a SPI interface, see Figure 4(a), and needs few extra signals from the microcontroller to handling interruptions and other functionalities of the transceiver. The chip allows different sleep modes for a reduced overall current consumption. The RF interface (RFN and RFP pins of the chip) consists of an open-collector differential output that can drive a 50Ω antenna using a suitable balun, see Figure 4(b). The output impedance of the RF interface at 915 MHz is $9 + i77\Omega$, which must be the input impedance of the balun. The datasheet of the chip [37] provides the appropriate values of the components the balun.

3.3. Design of a Simple Antenna. For simplicity, the antenna for the wireless sensor is made of a single strand of 24 AWG wire ($= 0.5106 \text{ mm}$). Its length ℓ was experimentally determined by successively shortening the wire up to observing the resonance at $f_0 = 915 \text{ MHz}$. This was performed by using a vector network analyzer (VNA) MS46121B from Anritsu. Resonance is determined from the parameter s_{11} , which is the reflection coefficient Γ at the input port of the antenna. In the

logarithmic scale, the quantity $10 \log |s_{11}| \text{ (dB)}$ is often called return loss RL. Recall that the reflection coefficient at a load is defined as the ratio of the amplitude B of the reflected wave and the amplitude A of the incident wave, that is $\Gamma = B/A$. The lower the value of $|\Gamma|$, the smaller the reflected power as well as the return losses. This implies that most of the power supplied to a load can be used to perform electric work. Resonance in the antenna is determined by the frequency at which s_{11} reaches its minimum value. We determined two candidates of resonant lengths, namely, $\ell_1 = 10.3 \text{ cm}$ and $\ell_2 = 25.8 \text{ cm}$. Other resonant lengths are indeed possible, but they are larger than ℓ_2 . In Figure 5, we observe the frequency response of the antenna for both resonant lengths.

The VNA performs a frequency sweep over a given bandwidth, and the measurements of $s_{11} = s_{11}(\omega)$ in the function of the frequency $\omega = 2\pi f$ are plotted on a Smith chart, see Figure 5(a). The central point of this diagram corresponds to $s_{11} = 0$, which implies the best coupling. In the vicinity of this point, we have a region with an optimal coupling, which is indicated in the figure by a gray disc. As we approach the

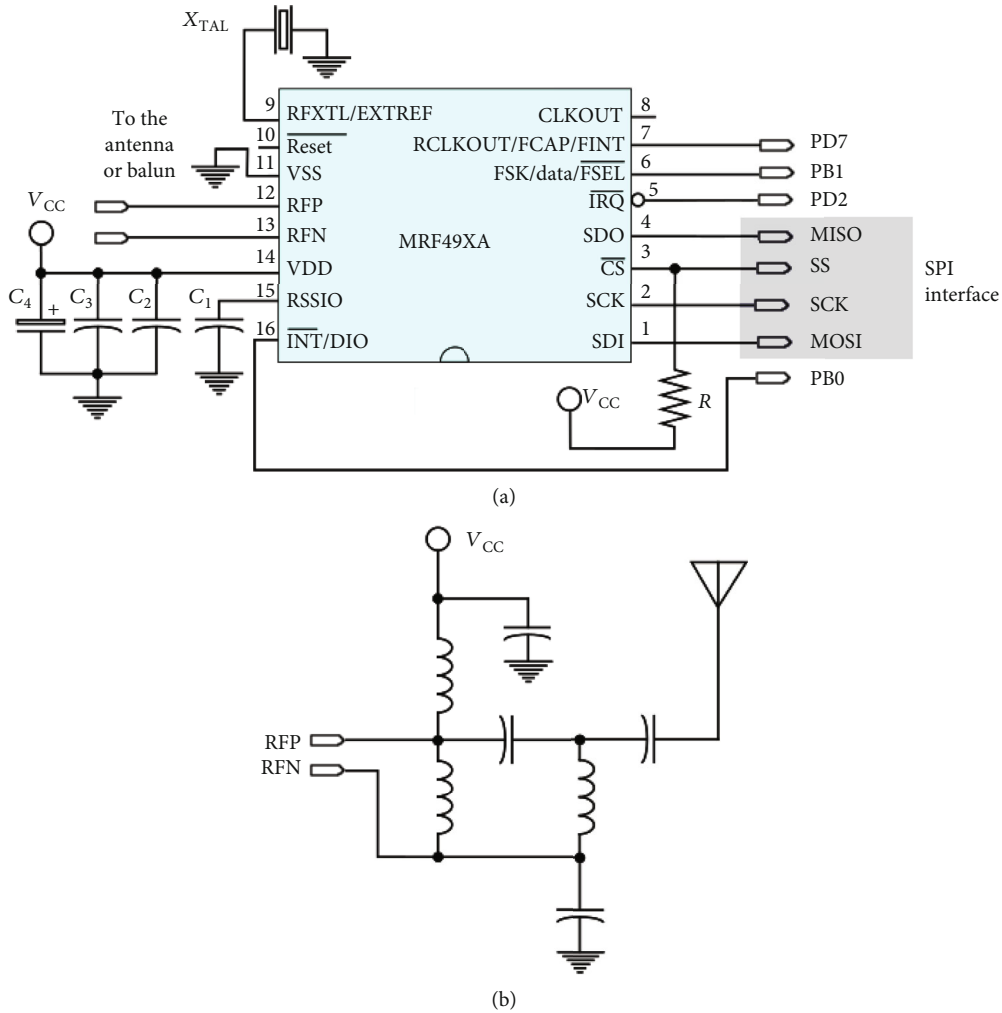


FIGURE 4: (a) Circuitry for the radio chip: C_1 – C_4 are decoupling capacitors, XTAL is a 10 MHz crystal, and R is a 10 k Ω resistor. (b) Balun for 50 Ω antenna.

outer circle, the coupling gets lost since $|s_{11}| \rightarrow 1$; thereby, all of the energy is reflected. The measurements corresponding to ℓ_1 and ℓ_2 are closer to the central point at 915 MHz. In Figure 5(b), the same information is plotted on Cartesian axes. The band of frequencies at which $|s_{11}(\omega)|$ reaches lower values is indicated by a gray stripe in the figure. We can see that the carrier frequency of 915 MHz indeed lies in this region. The plot corresponding to $\ell_2 = 25.8$ cm has another resonance frequency of about 400 MHz but is not useful in the present design.

The working wavelength at $f_0 = 915$ MHz is $\lambda_0 = 0.3278$ m. An antenna of the kind considered here is often called monopole or Marconi antenna [38]. Its ideal resonant lengths are given by $l_n = (2n - 1)\lambda/4$, $n = 1, 2, \dots$. This formula applies for an ideal filamentary antenna, that is, an antenna in which $\beta = 0$. The real resonant lengths ℓ_1 and ℓ_2 are comparable to the ideal resonant lengths $l_1 = \lambda_0/4 = 8.195$ cm and $l_2 = 3\lambda_0/4 = 24.585$ cm, respectively. The differences are due to the circumferential currents established around the wire as well as the end effects. Finally at $f_0 = 915$ MHz, the antenna shows an impedance of $Z_{in} = 37.858 + i10.101\Omega$ for the length ℓ_1 and $Z_{in} = 46.405 + i7.702\Omega$ for

the length ℓ_2 , which are closer to the impedance $Z_0 = 50\Omega$ at which the balun was designed.

3.4. Assembling a Prototype of Wireless Sensor. Based on the design considerations of previous subsections, a prototype for a wireless sensor was assembled in a PCB board with SMD components. The layout of the resulting PCB is shown in Figure 6. After soldering all of the components and burning a bootloader in the microcontroller, the prototype was proved both as a TX and RX by loading some testing programs via USB with the Arduino IDE. The spectrum of the prototype as TX was measured with a spectrum analyzer DSA710 of RIGOL, as is shown in Figure 7. Several units of the prototype were assembled and tested accordingly for the posterior deployment of a WSN.

4. Power and Energy Analysis in the Wireless Sensor

According to the previous design of the wireless node, in this section, we estimate the power used in the TX, RX, and OFF modes.

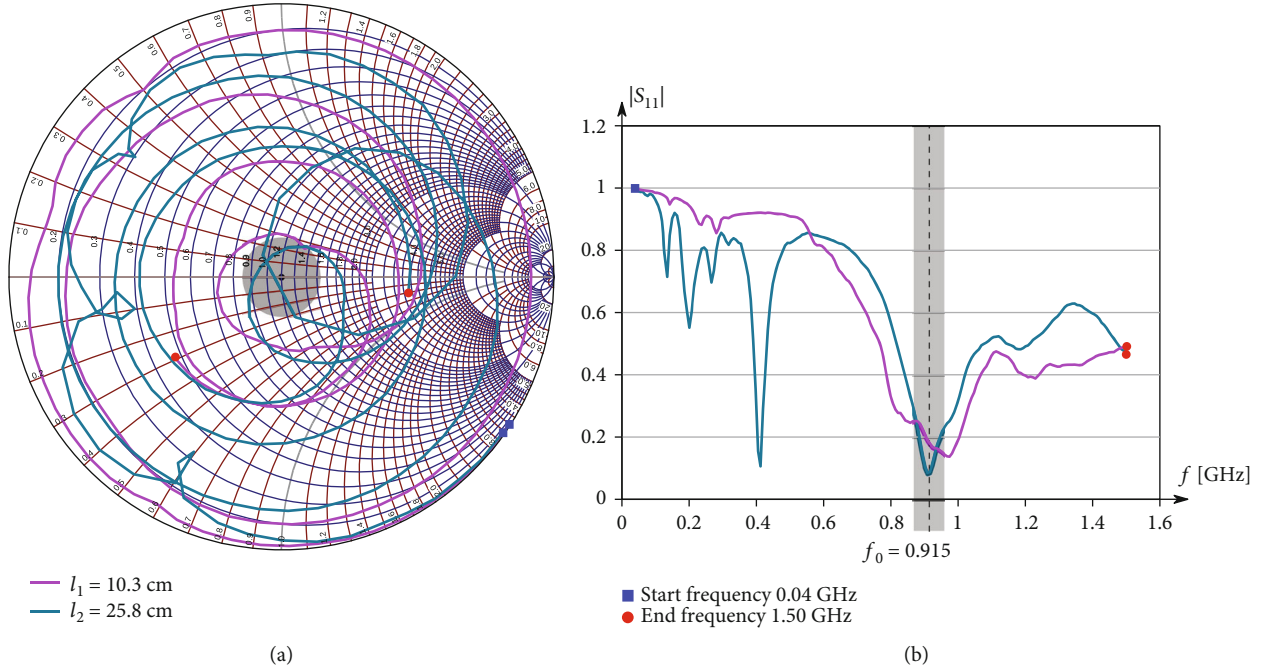


FIGURE 5: Frequency response of the resonant antenna: (a) plot of $s_{11}(\omega) = |s_{11}(\omega)|e^{i\theta(\omega)}$ on a Smith chart; (b) plot of $|s_{11}(\omega)|$.

4.1. Powering a Wireless Sensor with a Supercapacitor. Using supercapacitors instead of batteries in the wireless sensors would lead to a quasi-autonomous operation mode. Indeed, a bank of supercapacitors could be charged continuously by harvesting energy from the surroundings while the microcontroller is in sleep mode. A wireless sensor will awake only if it needs to transmit or receive data so that it will use some of the stored energy. Once TX/RX operations have finished, the wireless sensor will return to the sleep mode, and the supercapacitors will continue their charging process up to the next event.

Data transmission to the sink node is performed with slotted ALOHA protocol so that nodes with packets ready to transmit must wait for the beginning of the time slot and transmit with a probability τ . To further reduce the energy consumption, we let the probability τ to depend on the residual energy of each node. This is based on the fact that the highest energy consumption comes from transmission operations. Hence, nodes with the highest residual energy would perform more packet transmissions than those with the lowest residual energy levels. When nodes have low energy levels after long operation periods, this scheme would conserve energy by reporting very few events when nodes are in the active (ON) mode. Specifically, τ is determined by

$$\tau(e_i) = \gamma e^{-\gamma E_o/e_i}, \quad (9)$$

where E_o is the initial energy of the node, which can also be considered as the maximum energy stored in the supercapacitor, e_i is its residual energy, and γ is a parameter defined by the network administrator that controls the number of packet transmissions and consequently the system's lifetime.

For the considered wireless sensor, we have that $E_o = 139J$. This value is estimated as follows.

Figure 8 shows the behavior of a single supercapacitor of 15 F @ 4.3 V that feeds a wireless sensor that is continuously transmitting. The supercapacitor has the number part MAL219691203E3 from Vishay BCcomponents. Ideally, this supercapacitor can store up to $U_E = 1/2CV^2 = 138.67J$, though this energy cannot entirely be exploited by the wireless sensor. As can be seen in the figure, when the voltage of the capacitor is below 1.83 V neither the radio chip nor the microcontroller can work adequately. If this point is reached, the wireless sensor is unable to operate in the network unless the supercapacitor increases its energy in some way. Supercapacitors show an equivalent series resistance (ESR) that may consume some of the stored energy even if no load is connected to their ends. To reduce such power leakage, the value of ESR should be as close as possible to zero.

It is worth noticing that in a continuous transmission mode, a single supercapacitor can feed one wireless sensor for 40 min at the minimum transmitting power of -17.5 dBm and about 10 min at the maximum transmitting power of 0 dBm. Hence, a strategy must be to transmit small amounts of data and then send the wireless sensor to a sleep mode once its communication duties have finished and repeat this process if necessary. While the wireless sensor is in sleep mode the supercapacitor can be charged by harvesting energy from the surroundings. Furthermore, the sleeping of the wireless sensor favors the supercapacitor to "refresh" its available charge, as was observed in the experiments, which may be due to certain physicochemical processes that take place inside the supercapacitor [39, 40]. Otherwise, the uninterrupted usage of the wireless sensor leads to the "drying" of the supercapacitor, and the point of 1.83 V will be

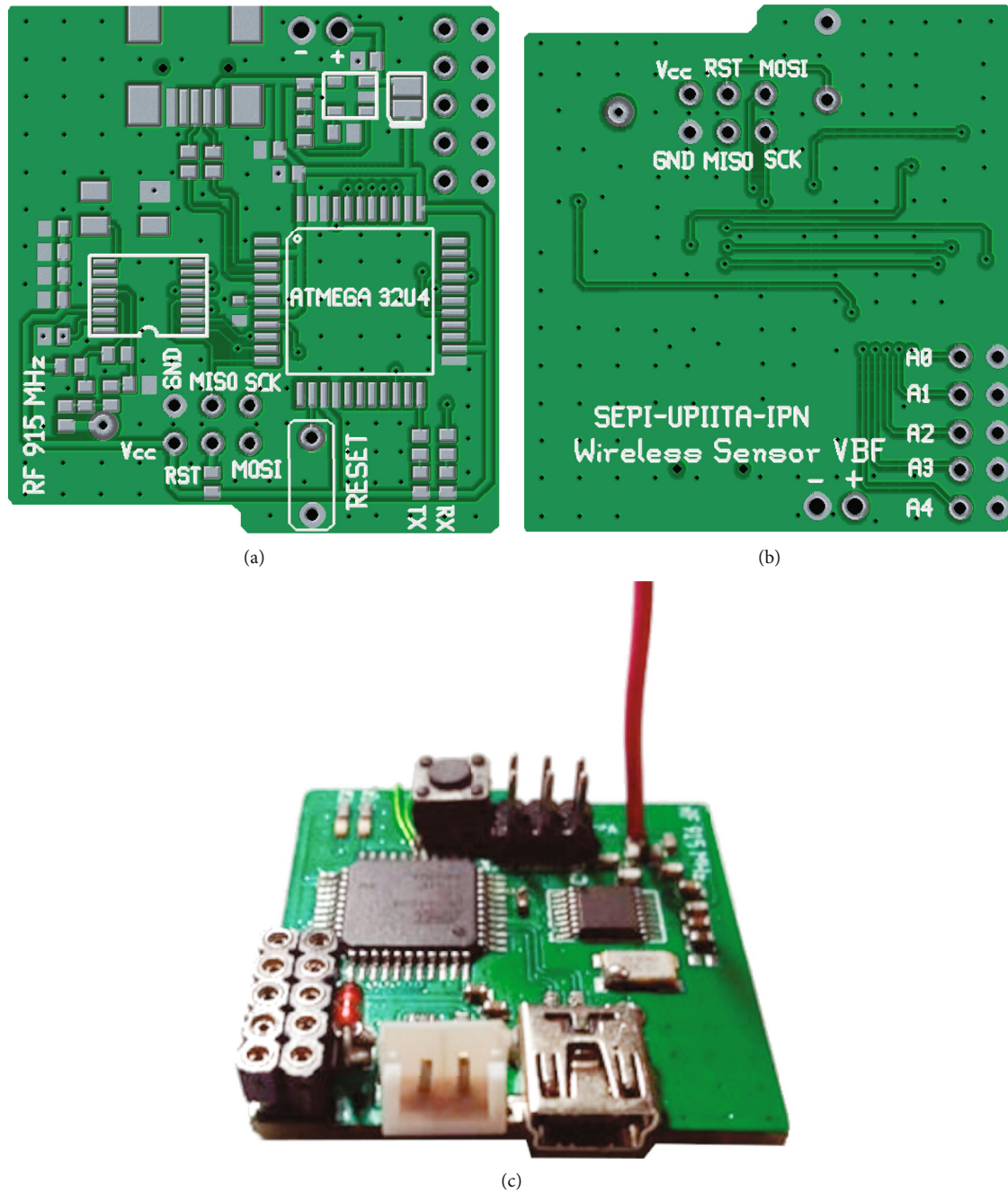


FIGURE 6: Layout of the prototype of a wireless sensor: (a) upper view of the PCB; (b) lower view of the PCB; (c) assembled prototype.

reached more rapidly. The *refreshing* and *drying* of the capacitors should be studied more rigorously in the laboratory.

4.2. Power Budget in the Designed Wireless Sensor. In this subsection, we report the power consumption of the wireless sensor in the TX, RX, and sleep modes. This is performed by measuring the current I_T consumed by the wireless sensor, which is fed by a voltage V_{sensor} applied at x the sensor's feeding terminals. Let $I_{\mu\text{C}}$ and I_{radio} denote the current consumed by the microcontroller and the radio chip, respectively, so that $I_T = I_{\mu\text{C}} + I_{\text{radio}}$. The power consumption of the sensor

denoted by W_{sensor} is calculated by the customary formula $W_{\text{sensor}} = I_T V_{\text{sensor}}$. Tables 1 and 2 show the results of the power consumption of the wireless sensor in TX mode at $V_{\text{sensor}} = 5\text{ V}$ and $V_{\text{sensor}} = 3.3\text{ V}$, respectively. In both cases, the wireless sensor is operating in a continuous form. The first columns of these tables show the available transmitting powers in the radio chip, being -17.5 dBm and 0 dBm the lowest and highest available powers, respectively. On the other hand, Tables 3 and 4 show the power consumption of the wireless sensor in RX and sleep modes, respectively, for $V_{\text{sensor}} = 5\text{ V}$ and $V_{\text{sensor}} = 3.3\text{ V}$. In the RX case, the wireless sensor is operating in a continuous form.

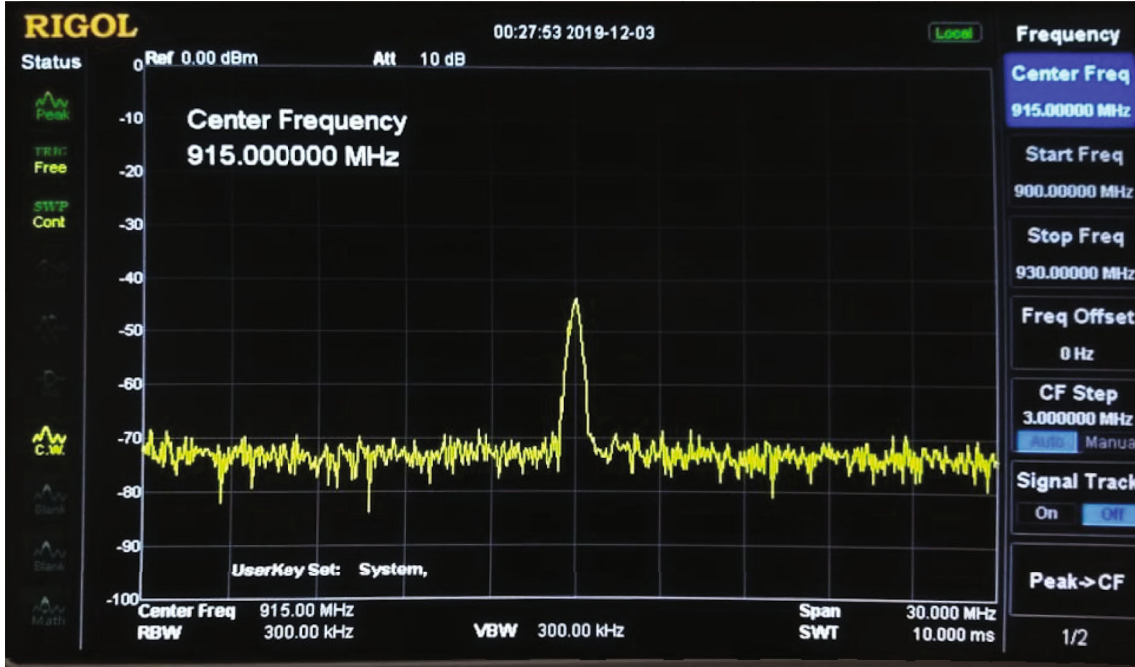


FIGURE 7: Spectrum of the prototype as transmitter, with the frequency of the carrier centered at 915 MHz.

According to the results shown in Tables 1–4, we observe that using a feeding voltage of $V_{\text{sensor}} = 5\text{ V}$ is energetically more expensive than using $V_{\text{sensor}} = 3.3\text{ V}$. Hence, the supercapacitors must be chosen to work in a regime close to 3.3 V. On the other hand, the average current consumption of the microcontroller in TX mode is $I_{\mu\text{C},\text{TX}} = 11.13\text{ mA}$ (4.37 mA) at $V_{\text{sensor}} = 5\text{ V}$ (3.3 V); in RX mode, the consumption is $I_{\mu\text{C},\text{RX}} = 11.6\text{ mA}$ (4.1 mA) at $V_{\text{sensor}} = 5\text{ V}$ (3.3 V); finally, the consumption in the sleep mode is $I_{\mu\text{C},\text{Sleep}} = 11.2\text{ mA}$ (3.94 mA) at $V_{\text{sensor}} = 5\text{ V}$ (3.3 V). These values agree with the values specified in the datasheet of the ATmega32U4, namely, $I_{\mu\text{C},\text{typ}} = 10\text{ mA}$ at 8 MHz and $V_{\text{CC}} = 5\text{ V}$ and $I_{\mu\text{C},\text{max}} = 5\text{ mA}$ at 4 MHz and $V_{\text{CC}} = 3\text{ V}$.

With respect to the radio, the average current consumption is $I_{\text{radio},\text{TX}} = 14.78\text{ mA}$ (13.6 mA) at $V_{\text{CC}} = 5\text{ V}$ (3.3 V) in TX mode and $I_{\text{radio},\text{RX}} = 13.9\text{ mA}$ (12.8 mA) at $V_{\text{CC}} = 5\text{ V}$ (3.3 V) in RX mode. These values do not show substantial differences regarding the operation mode or feeding voltage and are below the typical value indicated in the datasheet of the radio chip, of about 17 mA. However, a substantial reduction is observed in the sleep mode, with a current consumption of $I_{\text{radio},\text{Sleep}} = 726\text{ }\mu\text{A}$ (552 μA) at $V_{\text{CC}} = 5\text{ V}$ (3.3 V). In other words, a reduction in the overall power consumption of the wireless sensor mainly depends on reducing the current in the microcontroller. There exist several strategies to achieve this including setting the clock frequency to a value lower than 1 MHz or less, disabling the brown-out detector (BOD), disabling the ADC if not used by sensors, and among others. Also, it is possible to choose another microcontroller with a lower current consumption without altering the design of the wireless sensor too much.

In Table 5, we show the values that are used to model our mathematical proposal.

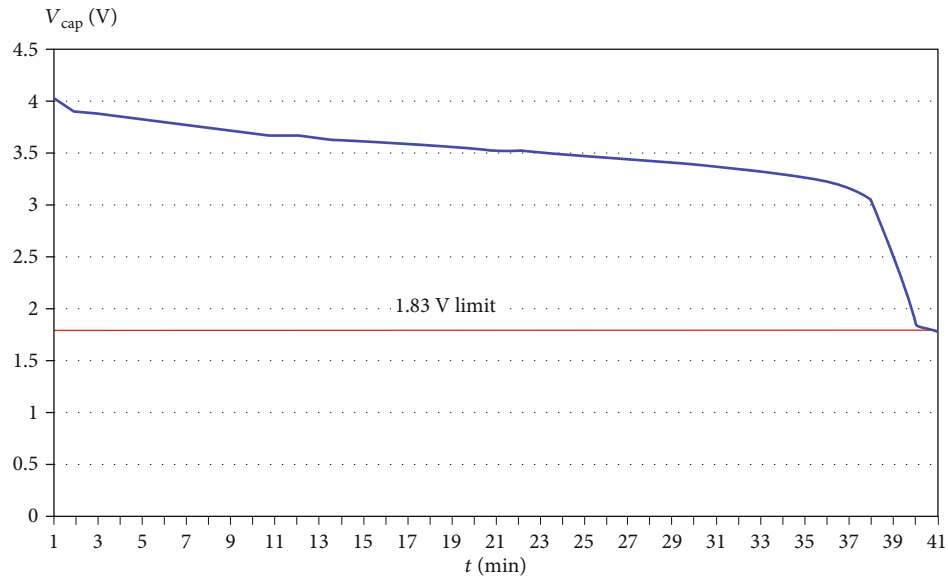
5. An Analysis of the Energy Used by the WSN and the Harvesting Energy from Mint Plants

In this section, we estimate the energetic cost of transmitting/receiving data by the designed wireless sensor from an empirical point of view based on the measurements of Section 4. Then, we consider recharging the supercapacitors of the wireless sensors by harvesting energy from mint plants. From the obtained results, we establish the viability of such a harvesting configuration for a real WSN.

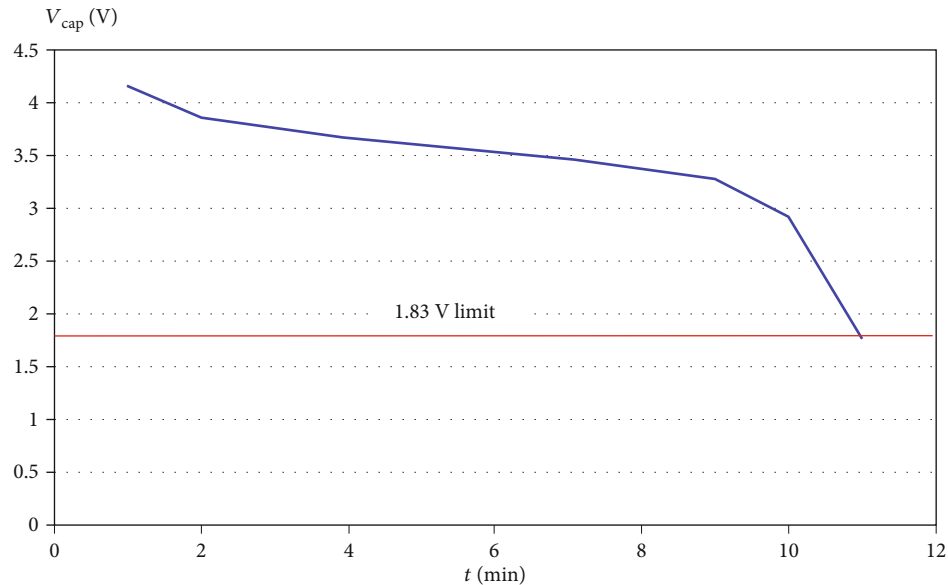
5.1. Power and Energy Estimates in the Wireless Sensor. As a numerical example and using formulas (6)–(8), let us assume that the wireless sensor is fed by $V_{\text{sensor}} = 3.3\text{ V}$, and let $\Delta t_{\text{slot}} = 5\text{ ms}$, which is a typical value for a time slotted communication system, see e.g., [41]. From Tables 2–4, we take as representative values $W_{\text{Tx}} = 64.68\text{ mW}$, $W_{\text{Rx}} = 55.77\text{ mW}$, and $W_{\text{Sleep}} = 14.85\text{ mW}$, being the first one the corresponding to a transmitting power of 0 dBm. On the basis of these values, we obtain

$$\begin{aligned} E_{\text{Tx},\text{slot}} &= 323.4\text{ }\mu\text{J}/\text{slot}, \\ E_{\text{Rx},\text{slot}} &= 278.85\text{ }\mu\text{J}/\text{slot}, \\ E_{\text{Sleep},\text{slot}} &= 74.25\text{ }\mu\text{J}/\text{slot}. \end{aligned} \quad (10)$$

We can also estimate the energy needed to transmit/receive a single bit or byte. For instance, assume that the data rate of the radio is 256 kbps. This implies that a 5 ms slot has 768 bits or equivalently 96 bytes. Therefore, the energy for a single byte is



(a)



(b)

FIGURE 8: Voltage of a 15 F @ 4.3 V supercapacitor in a function of time as the wireless sensor continuously transmit at (a) -17.5 dBm and (b) 0 dBm.

TABLE 1: Power consumption in transmission mode at $V_{\text{sensor}} = 5$ V.

TX power (dBm)	I_{radio} (mA)	$I_{\mu\text{C}}$ (mA)	I_T (mA)	W_{sensor} (mW)
0	16.4	11.4	27.8	139.0
-2.5	15.5	11.3	26.8	134.0
-5.0	15.0	11.4	26.4	132.0
-7.5	14.7	11.6	26.3	131.5
-10.5	14.4	11.0	25.4	127.0
-12.5	14.2	10.9	25.1	125.5
-15.0	14.1	10.8	24.9	124.5
-17.5	14.0	10.7	24.7	123.5

$$E_{\text{Tx,byte}} = 3.368 \mu\text{J}/\text{byte}, \quad (11)$$

$$E_{\text{Rx,byte}} = 2.904 \mu\text{J}/\text{byte},$$

and the energy needed to transmit or receive a single bit is

$$E_{\text{Tx,bit}} = 421.09 \text{ nJ}/\text{bit}, \quad (12)$$

$$E_{\text{Rx,bit}} = 363.08 \text{ nJ}/\text{bit}.$$

All these values can be used for specifying units of energy in WSN. The above values indeed depend on the data rate of the radio and on the duration of the time slot Δt_{slot} .

TABLE 2: Power consumption in transmission mode at $V_{\text{sensor}} = 3.3$ V.

TX power (dBm)	I_{radio} (mA)	$I_{\mu\text{C}}$ (mA)	I_T (mA)	W_{sensor} (mW)
0	15.2	4.4	19.6	64.68
-2.5	14.2	4.6	18.8	62.04
-5.0	13.9	4.3	18.2	60.06
-7.5	13.5	4.0	17.5	57.75
-10.5	13.3	4.2	17.5	57.75
-12.5	13.0	4.4	17.4	57.42
-15.0	12.9	4.5	17.4	57.42
-17.5	12.8	4.6	17.4	57.42

TABLE 3: Power consumption in reception mode.

I_{radio} (mA)	$I_{\mu\text{C}}$ (mA)	I_T (mA)	W_{sensor} (mW)
$V_{\text{sensor}} = 5$ V			
13.9	11.6	25.5	127.5
$V_{\text{sensor}} = 3.3$ V			
12.8	4.1	16.9	55.77

TABLE 4: Power consumption in sleep mode.

I_{radio} (μA)	$I_{\mu\text{C}}$ (mA)	I_T (mA)	W_{sensor} (mW)
$V_{\text{sensor}} = 5$ V			
726	11.2	12	60
$V_{\text{sensor}} = 3.3$ V			
552	3.94	4.5	14.85

5.2. *Harvesting Energy from Mint Plants.* Energy conversion performed by living organisms is intrinsically sustainable and essentially relevant for future biohybrid technologies and green energy sources [42]. Researchers are finding ways to tap into the power of photosynthesis to generate small amounts of electricity from microalgae [43], cyanobacteria [44], and living plants [42]. The plant cells generate electrical potentials, which can propagate along the plasma membrane on long distances in vascular bundles and short distances in plasmodesmata and protoxylem [45]. Plants translate external stimuli into electrical signals, e.g., to regulate a variety of physiological functions, to mediate defense reactions [46], and to communicate with other plants [45].

Peppermint or mint (*Mentha piperita* L.), a perennial aromatic herb belonging to the Lamiaceae (*Labiatae*) family, is a natural hybrid between spearmint (*Mentha spicata* L.) and water mint (*Mentha aquatic* L.) [47]. Peppermint oil is of great economic value due to its uses in medicine [48], cosmetics [49], and food industry [50]. Indeed, for these reasons, peppermint is extensively cultivated both in temperate and tropical countries. Mint grows particularly well in lands with high water-holding capacity soil [51]. In 2014, world production of peppermint was 92,296 tonnes [52].

There exist three main pathways of carbon assimilation by plants, namely, C3, C4, and CAM. During the CO_2 fixation, when the photosynthetic plant produces 3-carbon acid

as the first product, it is classified as C3 pathway. When the photosynthetic plant produces a 4-carbon compound as the first stable product, it is classified as C4. If the plant absorbs the energy of the sunlight at the day time and uses this energy for the assimilation or fixing of the CO_2 at night time, it is classified as crassulacean acid metabolism or CAM. Plants that use the C3 pathway tend to thrive in areas where sunlight intensity and temperatures are moderate, with CO_2 concentrations around 200 mg/l or higher and plentiful groundwater. Contrarily, C4 and CAM pathways are adaptations to arid conditions due to their improved water use efficiency [53]. On this basis, mint is classified as a C3 plant.

Photorespiration is an important process for energy dissipation for protecting plants against high light intensity to prevent excess water loss [54]. It consists of the uptake of molecular oxygen O_2 concomitant with the release of CO_2 from organic compounds. The gas exchange resembles respiration and is the reverse of photosynthesis where CO_2 is fixed and O_2 released [55]. The C4 pathway is an adaptation to the effects of photorespiration that can occur in response to ecological pressures in C3 photosynthesis [56]. The first product of photorespiration is the phosphoglycolate, which is produced by enzyme Ribulose-1,5-bisphosphate carboxylase/oxygenase, and the final product of photorespiration is NH_4^+ in the roots. Ammonia (NH_4^+) is oxidized to nitrite (NO_2^-) and subsequently to nitrate (NO_3^-) for bacterial ammonia oxidizers in a microbially catalyzed process called nitrification. This behavior generates an increase of electrons and protons in the system, resulting in a decrease of system internal electric resistance and the increasing of electric generation [57]. Excessive loss of N due to NO_3^- leaching is a serious problem in peppermint cultivation [58]; however, this disadvantage for plant growth can be exploited in energy harvesting.

In this work, we report the energy harvested from mint plants and evaluate the possibility of using this microsource of energy for recharging the supercapacitors of a wireless sensor. The experiment was carried out as follows. In a small plastic pot of $9 \times 10^{-4} \text{ m}^3$, we place a 7-turn helix made of 25 AWG copper wire, with a length of $\ell_{\text{helix}} = 0.9$ m. This will be the cathode of the microsource. Next, near the helix but without touching, we place a zinc-plated wire mesh with a surface of 0.010 m^2 , which will act as the anode of the source, see Figure 9(a). These electrodes are connected to female banana plugs that traverse the pot, see Figure 9(b). In the inner space of the helix, the roots of a mint plant (*mentha spicata*) are located, and then, the pot is filled with potting soil mix such that the electrodes and the roots get covered. This plant pot generates bioelectricity because of the microbial oxidative metabolism of the soil (see, e.g., [59–62]), which is measured externally at the female banana plugs by means of a multimeter, see Figure 9(c).

The experiment was carried out during four days from 10:00 to 18:00 Hrs. In the first day, the plant pot was watered at 9:00 Hrs. During sunning, the bioelectricity was measured hourly in each pot as follows: open-circuit voltage $v_{\text{open}}(t_n)$ was measured with a multimeter as voltmeter, and short-circuit current $i_{\text{short}}(t_n)$ was measured with a multimeter as ammeter, where $t_n = 3.6 \times 10^3(n + 10)$ s, $n = 0, \dots, 8$. The

TABLE 5: Energy values and variables use to model our mathematical proposal.

Energy variables	Definition	Values
E_0	Initial energy available in the node	We consider 500,000 units of energy
E_i	Residual energy available in every node. $i = 1, 2, 3, 4 \dots N$	The initial value that we consider is E_0 ; however, this value changes depending the node mode
E_{T_x}	Amount of energy that is use to transmit a packet	We consider that when a node transmits a packet, consume 5 units of energy
E_{R_x}	Amount of energy that is use to receive a packet	When a node receives a packet, consume 4 units of energy
E_{sleep}	Energy that is consume when the node is on sleep mode	If a node is on sleep mode, we consider that consume 1 unit of energy
E_{min}	Minimum value of energy necessary in the node to work	We consider that the minimum value of energy necessary to work is 5% of initial energy E_0
E_{max}	It is the maximum energy stored in the node	$E_{\text{max}} = E_0$



FIGURE 9: (a) Internal setup of the experiment inside the pot of the mint plant. (b) Electrodes of the mint plant. (c) A series of mint plants and the measured open-circuit voltage at the ends of the series.

instantaneous electric power $p(t_n)$ was calculated as $p(t_n) = v_{\text{open}}(t_n) i_{\text{short}}(t_n)$. Finally, the experiment was carried out seven-fold, thereby seven plant pots were individually measured during the experiment.

From the set of data points $(t_n, p(t_n))$, we construct an interpolating function $\tilde{p}(t)$ depending on the time $t \in [t_0, t_8]$. In Figure 10, we observe the plots of the instantaneous power $\tilde{p}_m(t)$ for each mint pot ($m = 1, \dots, 7$) as functions

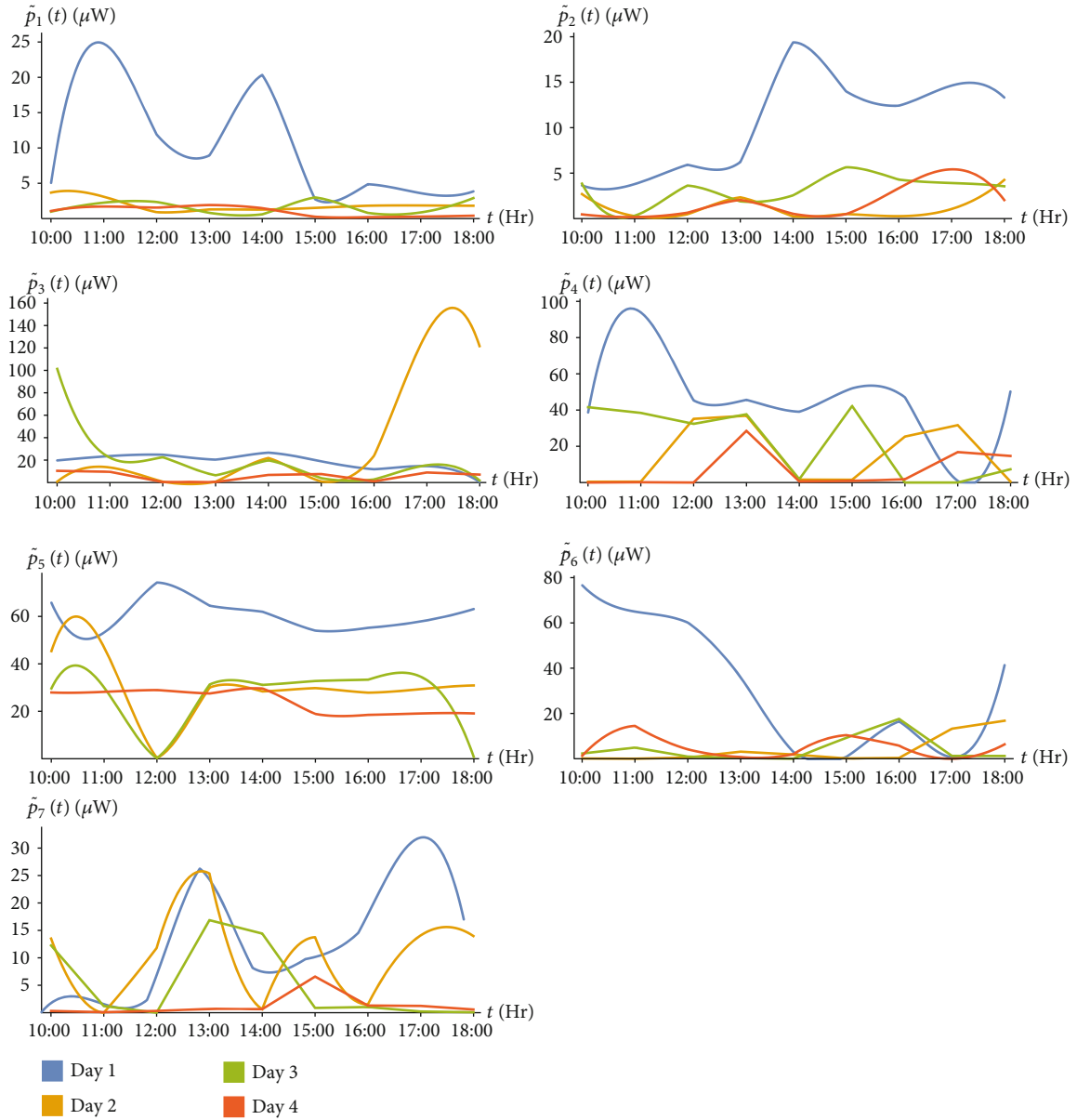


FIGURE 10: Instantaneous power measured in each plant pot.

of the time t , for each day. We can see that the harvested power is of the order of μW , with open-circuit voltages of the order of some volts and short-circuit currents of the order of μA .

In general, the highest measurements of power occurred on the day when the plants were watered. Was observed a strong correlation between the solar irradiation and the generated electric power, as was expected. On the other hand, during the afternoon hours, electric power was also generated, reaching even higher values than during the morning hours. This electric power is due to other chemical processes previously described. Nonetheless, such small power levels will not be able to drive a small device or even a single LED. However, these small powers can replenish a supercapacitor of a wireless sensor while it is in sleep mode. Accord-

ing to (2), the cumulative energy harvested from the plant pot is given approximately by

$$\tilde{E}_m = \int_{t_0}^{t_s} \tilde{p}_m(t) dt, m = 1, \dots, 7. \quad (13)$$

The integration can be calculated directly from the interpolating function \tilde{p}_m . In Table 6, we observe the values of the cumulative harvested energy calculated from this integral. Also, we observe the mean and total harvested energy, the total being calculated by summing the energy values from the four days. Plots of the energy as functions of the number of days can be seen in Figure 11. We observe that energy tends to decrease. This may be because the plants were only

TABLE 6: Cumulative harvested energy from mint plants.

	\tilde{E}_1 (J)	\tilde{E}_2 (J)	\tilde{E}_3 (J)	\tilde{E}_4 (J)	\tilde{E}_5 (J)	\tilde{E}_6 (J)	\tilde{E}_7 (J)
Day 1	0.3096	0.3066	0.5546	1.3314	1.7272	0.8267	0.3935
Day 2	0.0529	0.0283	0.9884	0.4790	0.8571	0.0995	0.2912
Day 3	0.0451	0.0898	0.4847	0.6371	0.7502	0.1300	0.1468
Day 4	0.0297	0.0522	0.1565	0.2020	0.6991	0.1491	0.0405
Mean	0.1093	0.1192	0.5460	0.6624	1.0084	0.3013	0.2180
Total	0.4375	0.4770	2.1843	2.6497	4.0337	1.2055	0.8722

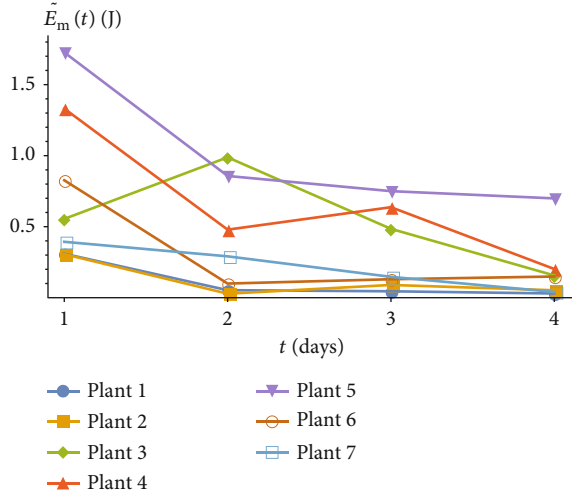


FIGURE 11: Cumulative energy for each plant pot.

watered the first day of the experiment, and no other water was supplied daily for not to flood the plants. Also, during days 2, 3, and 4, the experiment was carried out in cloudy conditions so that irradiation greatly diminished compared to day 1.

6. Mathematical Model

In this section, we develop a mathematical analysis based on a discrete-time Markov chain (DTMC) that models the main dynamics of the system, i.e., the nodes turning ON and OFF, the transmission of packets with probability τ , reception of packets, and collisions.

The time slot duration will serve as the reference time structure for the proposed DTMC. Changes in the system may occur only at the beginning of the time slot, and no events can occur in between slots. The valid state space of the Markov chain is

$$\Omega = \left\{ \left(e_1^{(S_1)}, e_2^{(S_2)}, \dots, e_n^{(S_n)} \right) : 0 \leq e_i^{(S_i)} \leq E_o; \quad S_i = \{0, 1\}; \quad i = 1, \dots, n \right\}, \quad (14)$$

where n is the number of nodes in the system, e_i is the residual energy of the i -th node, and the state S_i indicates whether the node is OFF ($S_i = 0$) or ON ($S_i = 1$). We assume that nodes change from state ON (OFF) to OFF (ON) with prob-

ability ρ . It implies that nodes remain an average time of $1/\rho$ seconds in each state. As such, the valid state transitions are as follows:

- (i) From the state $(e_1^{(1)}, e_2^{(1)}, \dots, e_n^{(1)})$ to the state

$$\left(e_1^{(1)} - \Delta_{R_x}, e_2^{(1)} - \Delta_{R_x}, \dots, e_n^{(1)} - \Delta_{R_x} \right) \quad (15)$$

with a probability $(1 - \rho)^n (1 - \tau)^n$. This transition corresponds to the case where all nodes are in the ON state ($S_i = 1$ for $1 \leq i \leq n$) but none of them transmit packets. In this way, each node consumes an amount of energy Δ_{R_x} corresponding to be active (listening and receiving) but not transmitting.

- (ii) From the state $(e_1^{(1)}, e_2^{(1)}, \dots, e_n^{(1)})$ to the state

$$\left(e_1^{(1)} - \Delta_{R_x}, \dots, e_i^{(1)} - \Delta_{T_x}, \dots, e_n^{(1)} - \Delta_{R_x} \right), \quad (16)$$

with probability $(1 - \rho)^n \tau (1 - \tau)^{n-1}$. This transition corresponds to the case where all nodes are in the ON state ($S_i = 1$ for $1 \leq i \leq n$) but only the node i ($i = 1, 2, \dots, n$) transmitted one packet. As such, the transmitting node i consumes an energy Δ_{T_x} , and the other nodes consume the energy Δ_{R_x} corresponding to be active (listening and receiving) but not transmitting.

- (iii) From the state $(e_1^{(1)}, e_2^{(1)}, \dots, e_n^{(1)})$ to the state

$$\left(e_1^{(1)} - \Delta_{R_x}, \dots, e_i^{(1)} - \Delta_{T_x}, e_{i+1}^{(1)} - \Delta_{R_x}, \dots, e_j^{(1)} - \Delta_{T_x}, e_{j+1}^{(1)} - \Delta_{R_x}, \dots, e_n^{(1)} - \Delta_{R_x} \right), \quad (17)$$

with a probability $(1 - \rho)^n \tau^2 (1 - \tau)^{n-2}$. This transition corresponds to the case where all nodes are in the ON state ($S_i = 1$ for $1 \leq i \leq n$) and only the nodes i and j ($i, j = 1, 2, \dots, n$) transmitted one packet each one. As such, the transmitting nodes i and j consume an amount of energy Δ_{T_x} , and the other nodes consume the energy Δ_{R_x} corresponding to be active (listening and receiving) but not transmitting and so on.

- (iv) From the state $(e_1^{(1)}, e_2^{(1)}, \dots, e_n^{(1)})$ to the state

$$\left(e_1^{(1)} - \Delta_{T_x}, e_2^{(1)} - \Delta_{T_x}, \dots, e_n^{(1)} - \Delta_{T_x} \right), \quad (18)$$

with a probability $(1 - \rho)^n \tau^n$, in which all nodes transmit. In this way, each transmitting node consumes an amount of energy Δ_{T_x} .

- (v) From the state $(e_1^{(1)}, e_2^{(1)}, \dots, e_n^{(1)})$ to the state

TABLE 7: Possible transitions in the case $n = 2$.

Initial state	Final state ¹	Probability of changing state	Notes
	$\begin{pmatrix} e_1^{(S'_1)} \\ e_2^{(S'_2)} \end{pmatrix} \begin{pmatrix} e_1^{(S_1)} \\ e_2^{(S_2)} \end{pmatrix}$	$\rho(1 - \rho)$	Only one node changes from state S_i to the state S'_i ²
$\begin{pmatrix} e_1^{(S_1)} \\ e_2^{(S_2)} \end{pmatrix}$	$\begin{pmatrix} e_1^{(S'_1)} \\ e_2^{(S'_2)} \end{pmatrix}$	ρ^2	The two nodes change from state S_i to the state S'_i ²
	$\begin{pmatrix} e_1^{(S_1)} \\ e_2^{(S_2)} \end{pmatrix}$	$(1 - \rho)^2$	The two nodes remain in the same state.

¹If $S_i = 0 \implies S'_i = 1$, then $P_{T_x} = \tau$, and $P_{R_x} = 1 - \tau$. If $S_i = 1 \implies S'_i = 0$, then $P_{T_x} = 0$, and $P_{R_x} = 0$. ²If a node changes from OFF to ON state, it can transmit or receive data and consume an amount of energy related to being active (listening or receiving) or transmitting, respectively. If a node changes from ON to OFF state, it harvests energy.

TABLE 8: Possible transitions in the case $n = 4$.

Initial state	Final state ³	Probability of changing state	Notes
	$\begin{pmatrix} e_1^{(S'_1)} \\ e_2^{(S'_2)} \\ e_3^{(S_3)} \\ e_4^{(S_4)} \end{pmatrix} \begin{pmatrix} e_1^{(S_1)} \\ e_2^{(S_2)} \\ e_3^{(S_3)} \\ e_4^{(S_4)} \end{pmatrix}$	$\rho(1 - \rho)^3$	Only one node changes from state S_i to the state S'_i ⁴
	$\begin{pmatrix} e_1^{(S_1)} \\ e_2^{(S_2)} \\ e_3^{(S'_3)} \\ e_4^{(S_4)} \end{pmatrix} \begin{pmatrix} e_1^{(S_1)} \\ e_2^{(S_2)} \\ e_3^{(S_3)} \\ e_4^{(S'_4)} \end{pmatrix}$	$\rho^2(1 - \rho)^2$	Two nodes change from state S_i to the state S'_i ⁴
$\begin{pmatrix} e_1^{(S_1)} \\ e_2^{(S_2)} \\ e_3^{(S_3)} \\ e_4^{(S_4)} \end{pmatrix}$	$\begin{pmatrix} e_1^{(S'_1)} \\ e_2^{(S'_2)} \\ e_3^{(S'_3)} \\ e_4^{(S_4)} \end{pmatrix}$	$\rho^3(1 - \rho)$	Three nodes change from state S_i to the state S'_i ⁴
	$\begin{pmatrix} e_1^{(S_1)} \\ e_2^{(S_2)} \\ e_3^{(S_3)} \\ e_4^{(S'_4)} \end{pmatrix} \begin{pmatrix} e_1^{(S_1)} \\ e_2^{(S_2)} \\ e_3^{(S_3)} \\ e_4^{(S_4)} \end{pmatrix}$	ρ^4	The four nodes change from state S_i to the state S'_i ⁴
	$\begin{pmatrix} e_1^{(S_1)} \\ e_2^{(S_2)} \\ e_3^{(S_3)} \\ e_4^{(S_4)} \end{pmatrix}$	$(1 - \rho)^4$	The four nodes remain in the same state.

³If $S_i = 0 \implies S'_i = 1$, then $P_{T_x} = \tau$, and $P_{R_x} = 1 - \tau$. If $S_i = 1 \implies S'_i = 0$, then $P_{T_x} = 0$, and $P_{R_x} = 0$. ⁴If a node changes from OFF to ON state, it can transmit or receive data and consume an amount of energy related to being active (listening or receiving) or transmitting, respectively. If a node changes from ON to OFF state, it harvests energy.

$$\left(e_1^{(1)} - \Delta_{R_x}, e_2^{(1)} - \Delta_{R_x}, \dots, e_k^{(0)} - \Delta_{\text{Sleep}}, \dots, e_n^{(1)} - \Delta_{R_x} \right), \quad (19)$$

with a probability $\rho(1 - \rho)^{(n-1)}(1 - \tau)^n$. This transition corresponds to the case where the node k ($k = 1, 2, \dots, n$) goes to the OFF state while the rest remain active (listening and receiving) but not transmitting, each of which consumes the energy Δ_{R_x} . As such, the sleeping node k consumes the energy

$$\Delta_{\text{Sleep}} := E_{\text{Sleep}} - E_H, \quad (20)$$

where E_H is the harvested energy from the surroundings and E_{Sleep} is the energy consumption during the sleep mode, both during a time slot. The condition $E_H > E_{\text{Sleep}}$ means that the energy employed during the sleep period is actually replenished and not drained. For the case in which two or more nodes go to the OFF state, the transition probability is calculated accordingly.

(vi) All possible combinations of nodes going to the ON (OFF) state and transmitting or receiving while being active are derived similarly.

As examples, Tables 7 and 8 show the possible transitions in the case where the network is formed by two and four nodes, respectively. In the case of two nodes, Figure 12 shows the corresponding Markov chain where nodes are assumed to be in the OFF state and can change to nine different states.

The aforementioned chain corresponds to an irreducible Markov chain. As such, the steady-state probabilities can be calculated by solving the linear system $\Pi = \Pi P$, where P is the transition probability matrix formed by calculating all possible valid transitions among states and Π is the steady-state vector $\Pi = \pi_{(e_1^{(S_1)}, \dots, e_n^{(S_n)})}$ for all possible values of S_i and e_i for $i = 1, 2, \dots, n$. Due to the intricacy of this Markov chain, we solve the linear system by numerical methods.

7. Results

In this section, numerical results are presented to evaluate the performance of the WSN when we use the harvesting energy

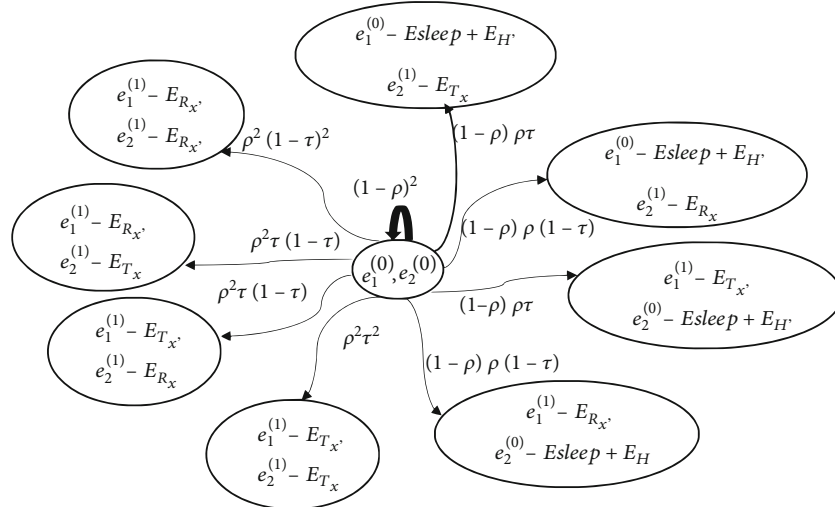


FIGURE 12: Markov chain corresponding to $n = 2$ and initial state in OFF mode.

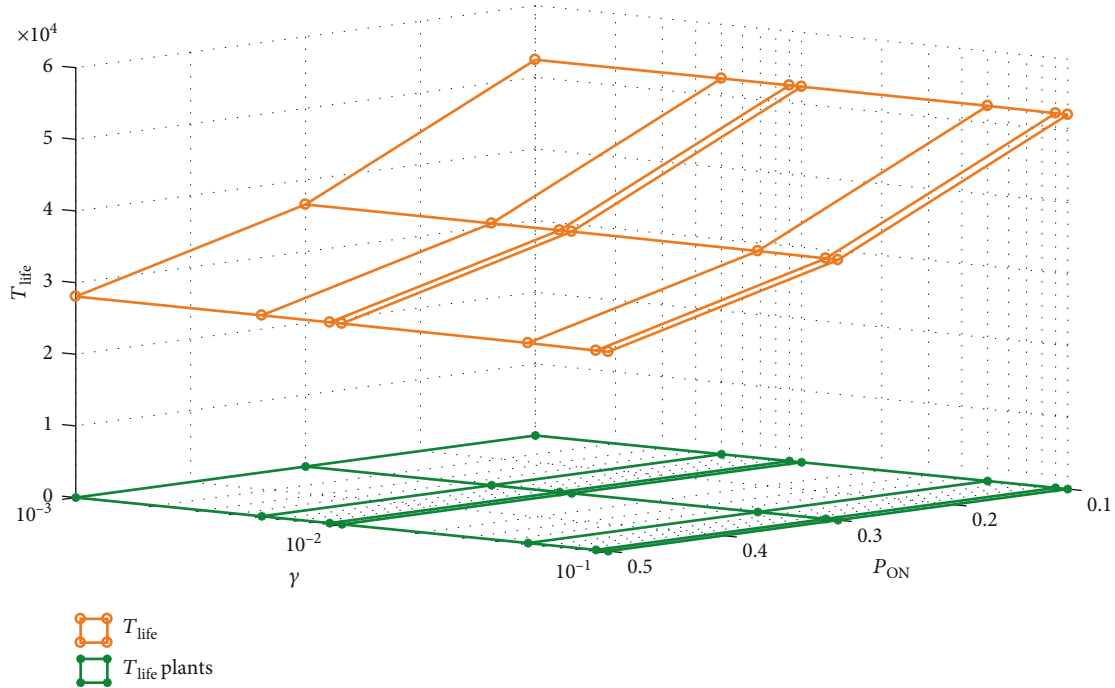


FIGURE 13: System lifetime for the system with no energy harvesting and node harvesting energy from plants. We consider that $\tau < 0.1$, so we use the values of $\gamma = 0.001, 0.005, 0.009, 0.01, 0.05, 0.09$, and 0.1 and $P_{on} = 0.1, 0.3$, and 0.5 .

obtained from mint plants. We study six main parameters: lifetime, active time, offline time, and the probability of successful transmission, free slot, and collision.

- (i) Lifetime is the time it takes for the first node of the WSN to die
- (ii) Active time is the time when all nodes have their energy above the energy threshold, i.e., nodes have enough energy to operate adequately in the network
- (iii) Offline time is the time when at least one node is harvesting energy

- (iv) Probability of successful transmission is the probability that one node of active nodes transmits a packet
- (v) Probability of idle slot is the probability that none of the active nodes transmits a packet
- (vi) Probability of collision is the probability that more than one of the active nodes transmits a packet

First, we study the system lifetime for different numbers of nodes in the network and P_{ON} of 0.1, 0.3, and 0.5. In Figure 13, we show the system lifetime when the energy harvesting

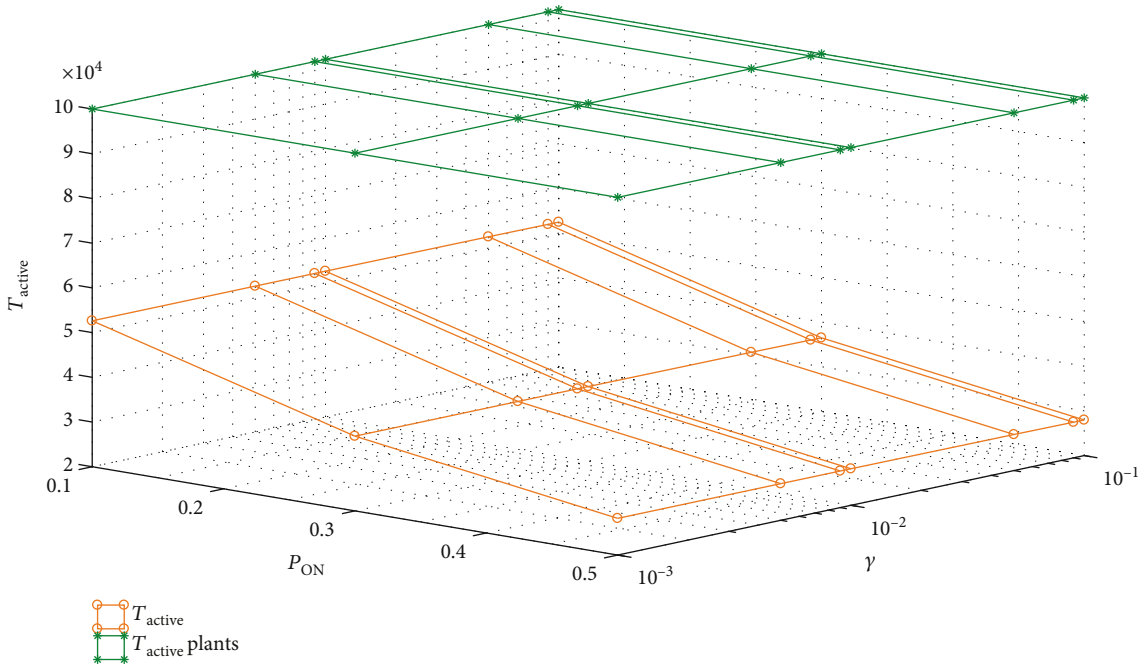


FIGURE 14: Active time. We consider that $\tau < 0.1$, so we use the values of $\gamma = 0.001, 0.005, 0.009, 0.01, 0.05, 0.09$, and 0.1 and $P_{on} = 0.1, 0.3$, and 0.5 .

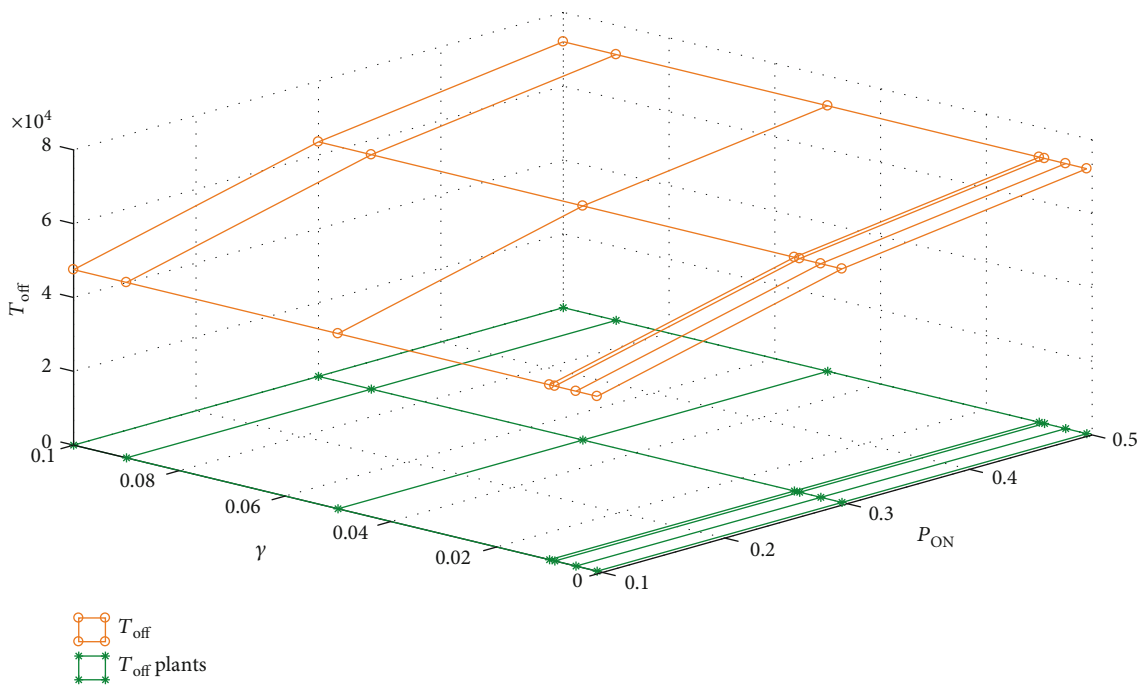


FIGURE 15: Offline time. We consider that $\tau < 0.1$, so we use the values of $\gamma = 0.001, 0.005, 0.009, 0.01, 0.05, 0.09$, and 0.1 and $P_{on} = 0.1, 0.3$, and 0.5 .

system is not considered and when the nodes harvest the energy from mint plants. As we expected, when the energy harvesting system is not considered and P_{ON} increases, the operational time decreases. However, when the energy obtained from plants is considered, the node never runs out of energy. Indeed, the energy obtained from either the plants is sufficient to power the nodes indefinitely. In the figure, we represent this with the value 0, since in fact, the system lifetime goes to infinity which is difficult to represent in the figure.

In Figure 14, we show the system active time. In this case, when there is no energy harvested and P_{ON} increases, the active time decreases because there is more probability that a node change from the OFF state to the ON state and consumes more energy. However, when we consider the energy obtained from the mint plants, we observe that active time increases. This is because the energy harvested in the system is enough to regenerate the energy consumed in the process of transmission and reception of packets providing

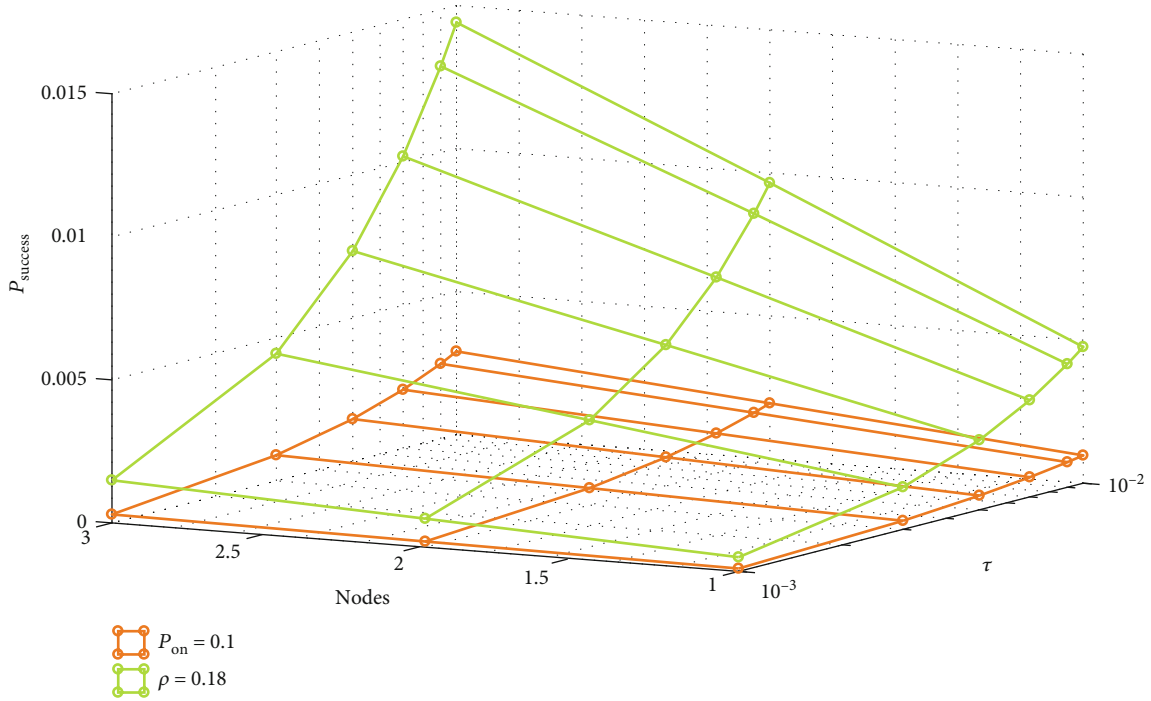


FIGURE 16: Probability of successful transmission with $P_{on} = 0.1$ and $\rho = 0.18$.

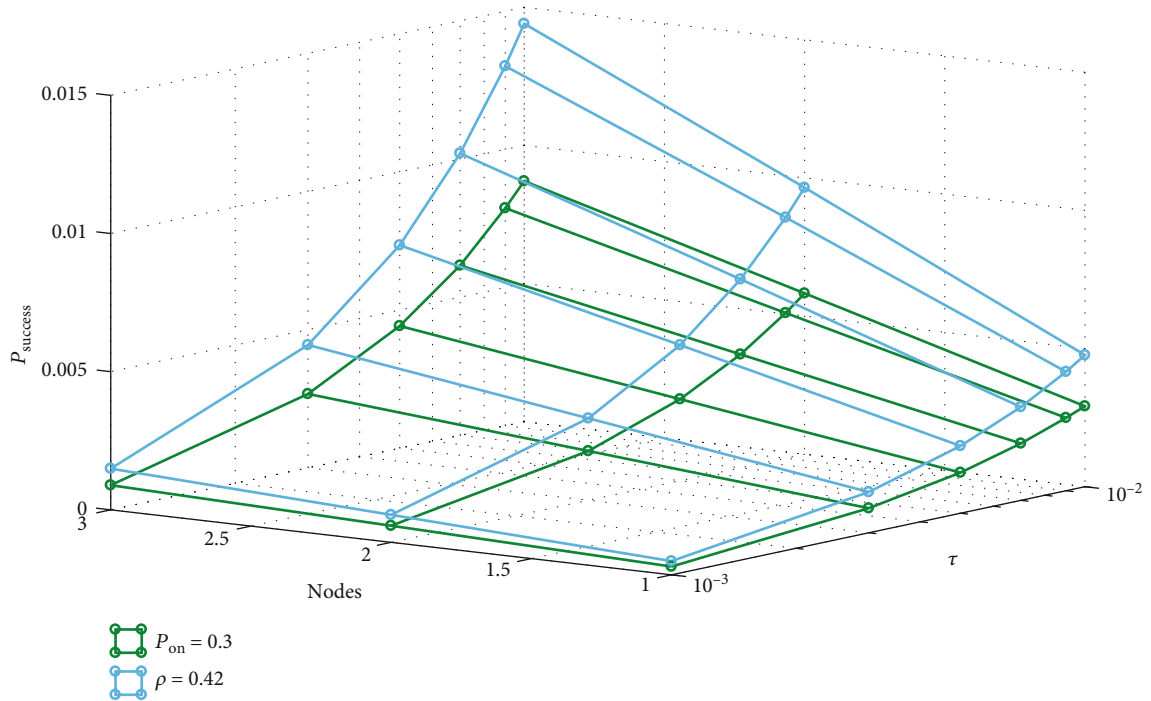


FIGURE 17: Probability of successful transmission with $P_{on} = 0.3$ and $\rho = 0.42$.

nodes with more functional time and transmitting more data to the sink.

This behavior is reflected in the offline as shown in Figure 15. When the system has no energy harvesting capabilities and P_{ON} increases, the offline time increases because there is a higher probability that a node change from the

OFF state to the ON state and consume more energy. When energy harvesting is enabled, the node never enters the offline mode, which, for simplicity, we represent by 0 in the figure.

In Figures 16–18, we show the probability of successful packet transmission for different numbers of nodes in the network and $P_{ON} = 0.1, 0.3,$ and $0.5,$ respectively, and

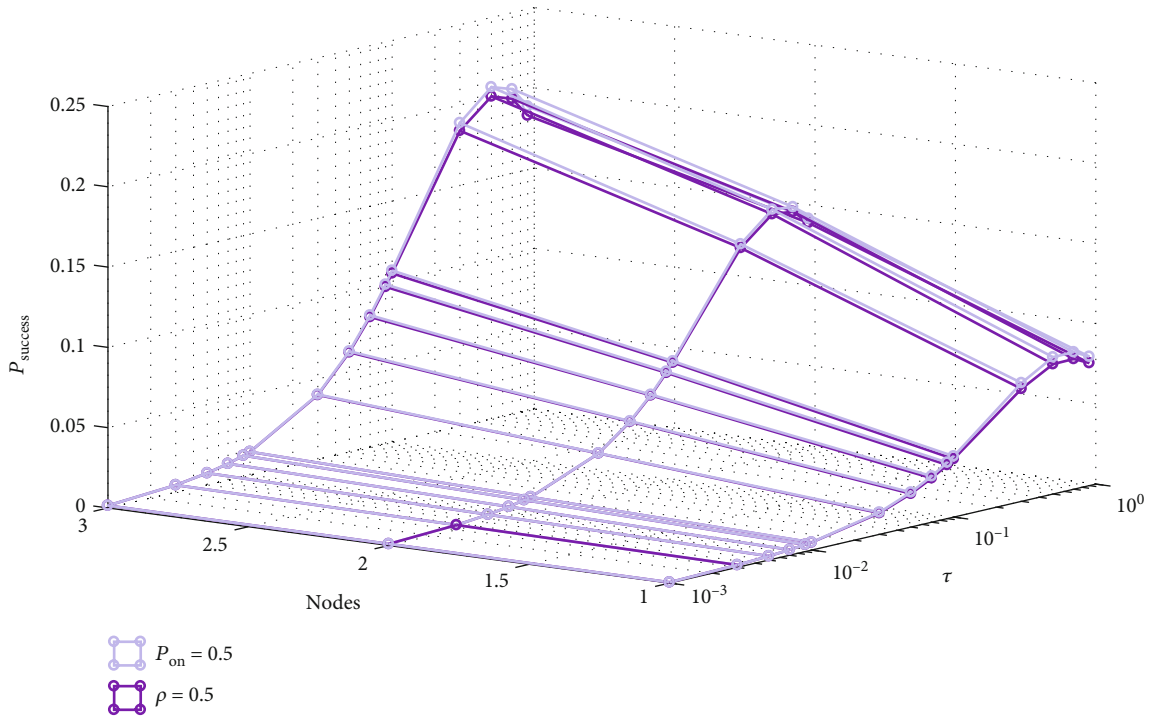


FIGURE 18: Probability of successful transmission with $P_{\text{on}} = 0.5$ and $\rho = 0.5$.

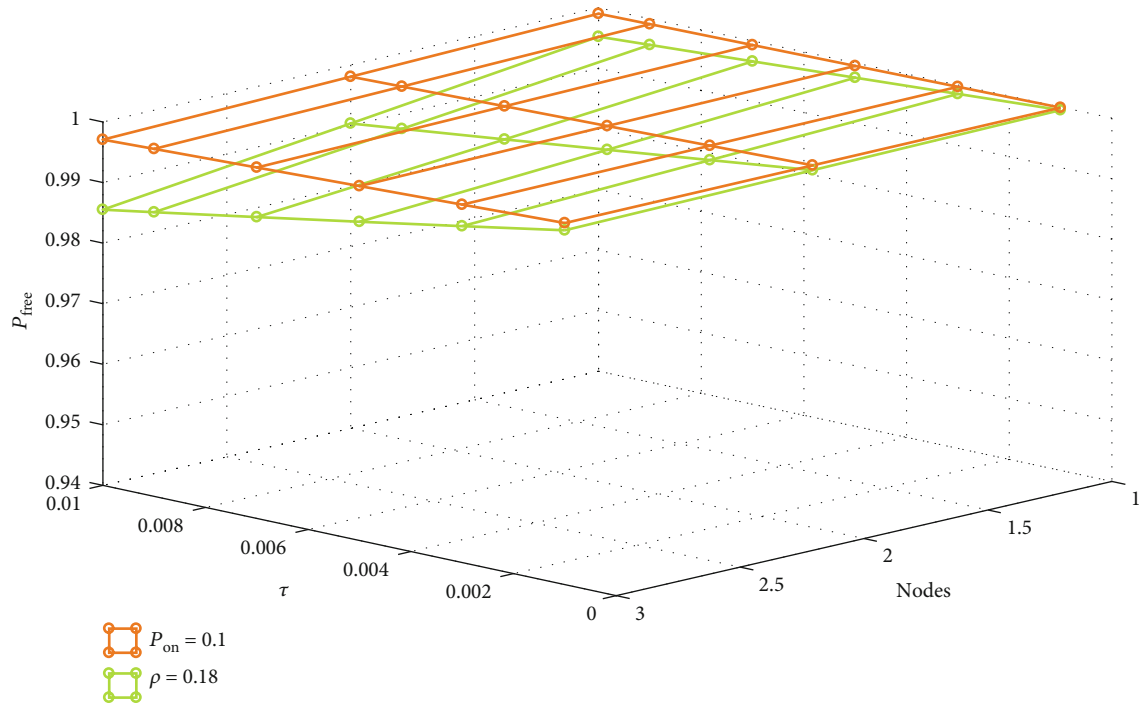


FIGURE 19: Probability of idle slot with $P_{\text{on}} = 0.1$ and $\rho = 0.18$.

different probability that a node can transmit a packet (τ). As expected, when τ increases, also the probability of successful transmission increases. This is because the probability that a node going from the OFF state to the ON state and transmits a packet is higher.

In Figures 19–21, we show the probability of idle slot for different number of nodes in the network and $P_{\text{ON}} = 0.1, 0.3,$

and 0.5, respectively, and different probability that a node can transmit a packet (τ). When the τ value increases, the probability of free slot decreases because it is more likely that a node transmits a packet.

In Figures 22–24, we show the probability of packet collision for different number of nodes in the network and $P_{\text{ON}} = 0.1, 0.3,$ and 0.5, respectively, and different probability

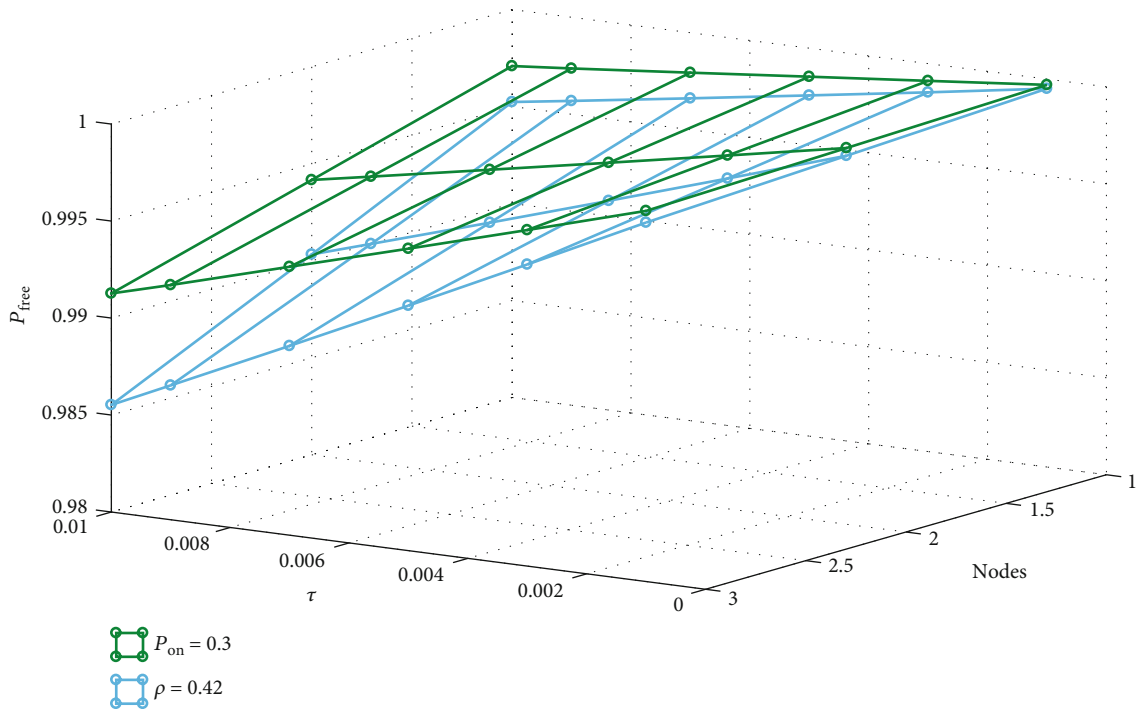


FIGURE 20: Probability of idle slot with $P_{on} = 0.3$ and $\rho = 0.42$.

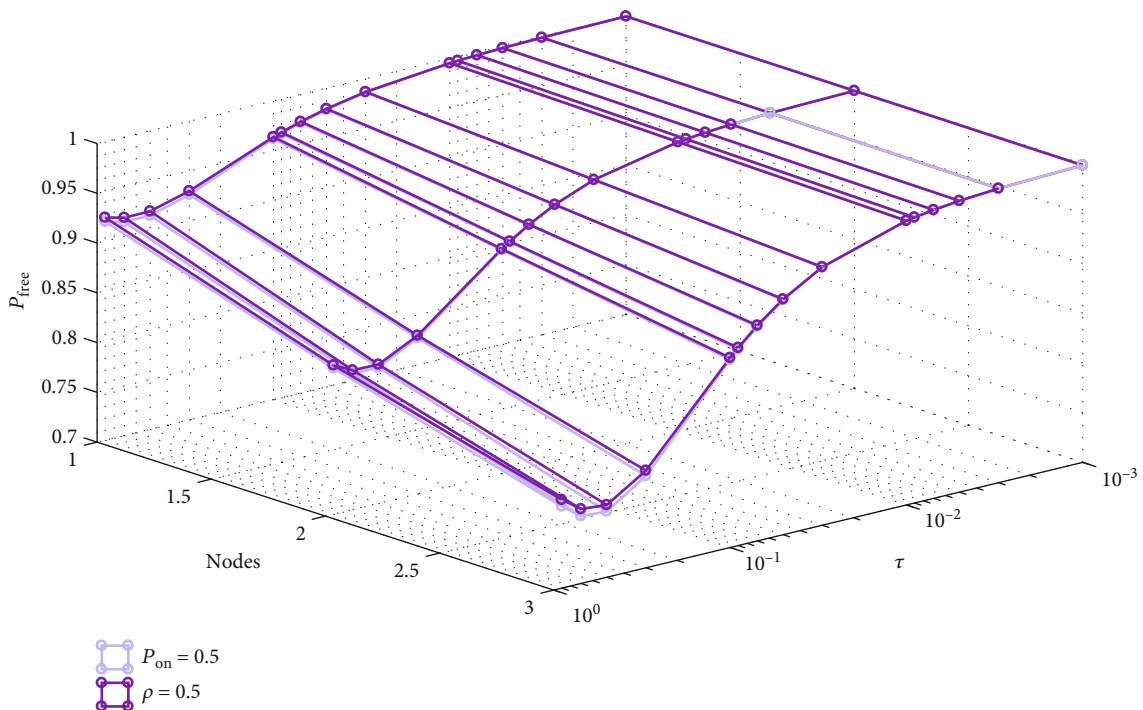


FIGURE 21: Probability of idle slot with $P_{on} = 0.5$ and $\rho = 0.5$.

that a node can transmit a packet (τ). As expected, when the probability that a node changes from the OFF state to the ON state and transmits a packet increases, also the probability of collision increases.

In Figure 25, we show the available nodes in the network over time when we consider a value of $\tau_{fixed} = 0.05$ and a value of $\tau_{variable}$ depending of residual energy of the network. As we expected, the lifetime of the network increases when

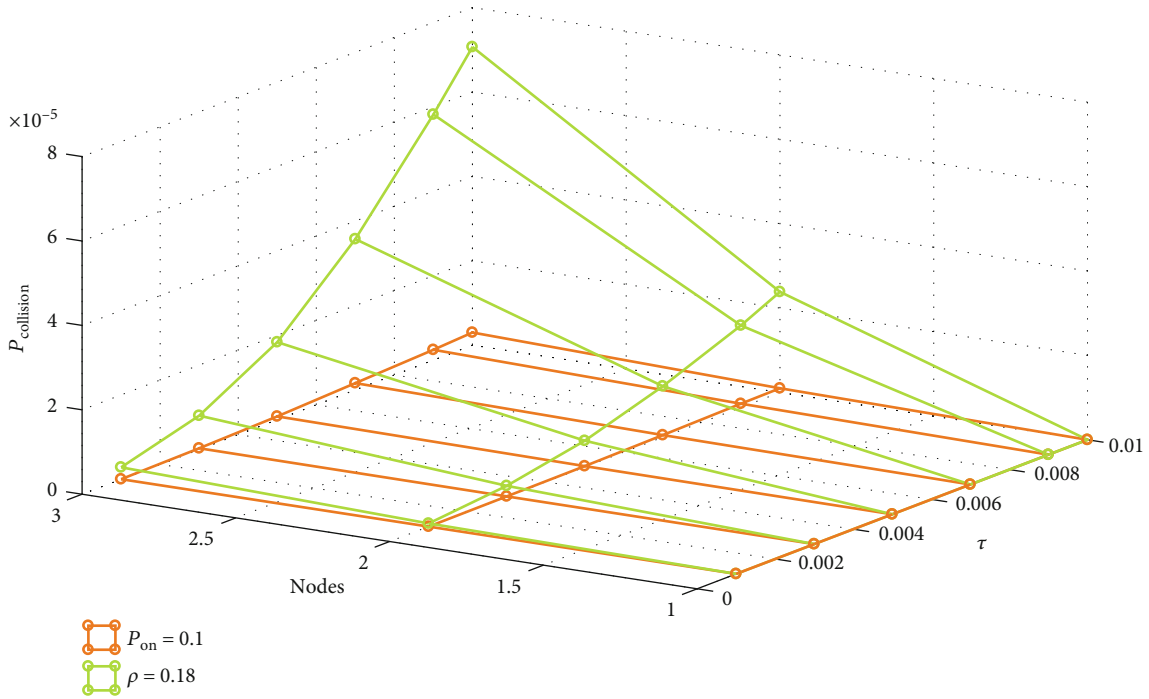


FIGURE 22: Probability of collision with $P_{\text{on}} = 0.1$ and $\rho = 0.18$.

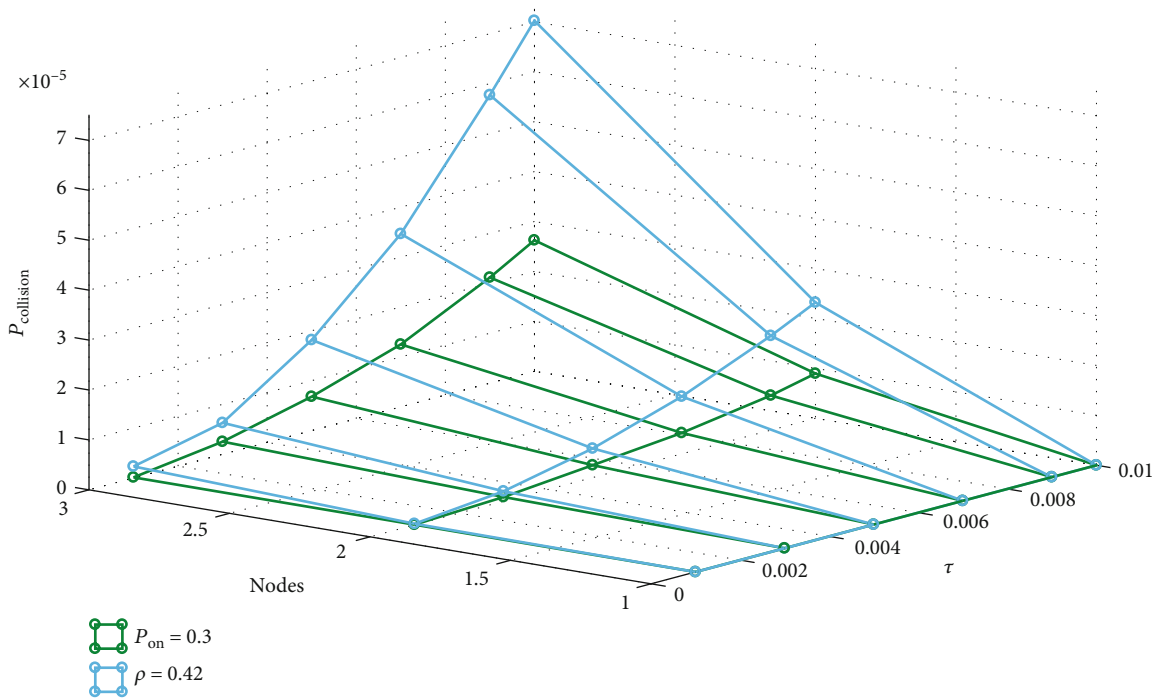


FIGURE 23: Probability of collision with $P_{\text{on}} = 0.3$ and $\rho = 0.42$.

we consider a value of tau which depends on the energy available on the node.

8. Conclusions

In this work, we study, analyze, and design a WSN that can operate indefinitely by harvesting energy from two separate

sources. In the first case, an antenna is used to capture energy from pervasive electromagnetic sources, i.e., radio frequency signals, in urban and suburban areas. In the second case, we consider the energy that can be extracted from plants in rural areas, for agricultural applications, or animal or fire monitoring in forests where solar energy nor RF signals are abundant. We prove that by using either one of these energy harvesting

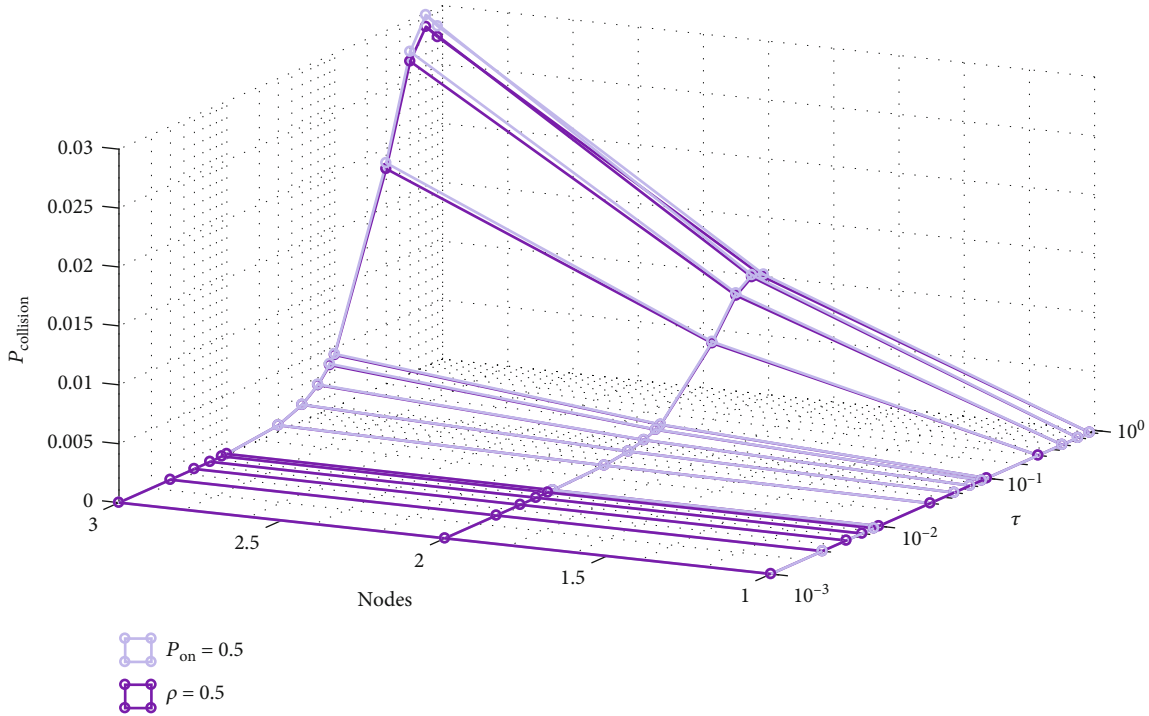


FIGURE 24: Probability of collision with $P_{\text{on}} = 0.5$ and $\rho = 0.5$.

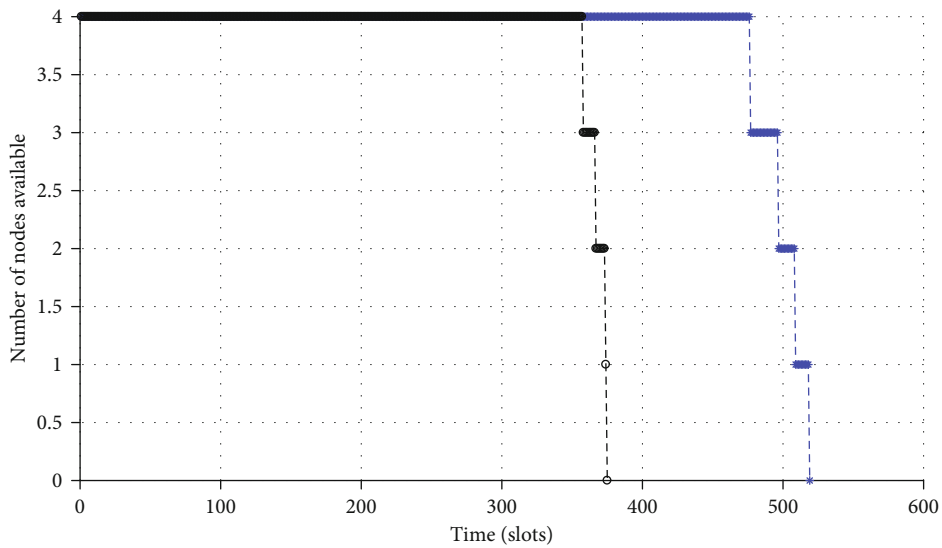


FIGURE 25: Available nodes in the network vs. time. $\tau_{\text{fixed}} = 0.05$ and τ_{variable} depends of the energy available in the node and a $\gamma = 0.05$

systems, the nodes in the network can operate without depleting their energy. Also, we propose a node design for these applications and schemes.

According to Table 6, the harvested energy is of the order of few Joules; nonetheless, such small energy values can sustain a wireless transmission if correctly adapted to drive a wireless sensor. For instance, let us consider the lowest mean harvested energy from Table 6, namely, $E_{\text{mean},1} = 0.1093$ J, corresponding to plant pot 1. Such energy can be used to transmit up to 259,564 bits, 32,452 bytes, and 3375 ms-

slots; this energy can also be used to receive up to 301,036 bits, 37,637 bytes, and 391 slots of 5 ms. On the other hand, let us consider the greatest mean harvested energy from Table 6, namely, $E_{\text{mean},5} = 1.0084$ J, corresponding to plant pot 5. This energy can be used to transmit up to 2,394,737 bits, 299,406 bytes, and 3,118 slots of 5 ms; it can also be used to receive up to 2,777,349 bits, 347,245 bytes, and 5 ms-3,616 slots. Note that these amounts of data can be used to transmit not only the payload from the sensors but also the stack of protocols involved in the networking functions.

However, note that in this mathematical model, when we consider 2 nodes in the network, there is 36 possible valid states, and with 4 nodes, there are 1296 possible valid states. Hence, computational complexity and running times greatly increase with the number of nodes. Hence, the model is not scalable. In future work, we plan to develop a new model that can be scalable considering the energy of the entire network and not of each node.

Data Availability

The simulations, tables, and figures data used to support the findings of this study are available from the corresponding author upon request.

Conflicts of Interest

The authors declare that they have no conflicts of interest.

References

- [1] I. F. Akyildiz, W. Su, Y. Sankarasubramaniam, and E. Cayirci, "A survey on sensor networks," *IEEE Communications Magazine*, vol. 40, no. 8, pp. 102–114, 2002.
- [2] T. Ajmal, D. Jazani, and B. Allen, "Design of a compact RF energy harvester for wireless sensor networks," in *IET Conference on Wireless Sensor Systems (WSS 2012)*, pp. 1–5, London, 2012.
- [3] A. Obaid and X. Fernando, "Wireless energy harvesting from ambient sources for cognitive networks in rural communities," in *2017 IEEE Canada International Humanitarian Technology Conference (IHTC)*, pp. 139–143, Toronto, ON, 2017.
- [4] T. Huynh, D. Do, H. Nguyen, and T. Nguyen, "Design of energy harvesting protocol for relay mobile node in WLAN," in *2015 17th International Conference on Advanced Communication Technology (ICACT)*, pp. 304–308, Seoul, 2015.
- [5] T. Ruan, Z. J. Chew, and M. Zhu, "Energy-aware approaches for energy harvesting powered wireless sensor nodes," *IEEE Sensors Journal*, vol. 17, no. 7, pp. 2165–2173, 2017.
- [6] S. Kim, R. Vyas, J. Bito et al., "Ambient RF energy-harvesting technologies for self-sustainable standalone wireless sensor platforms," *Proceedings of the IEEE*, vol. 102, no. 11, pp. 1649–1666, 2014.
- [7] C. R. Valenta and G. D. Durgin, "Harvesting wireless power: survey of energy-harvester conversion efficiency in far-field, wireless power transfer systems," in *IEEE Microwave Magazine*, vol. 15, no. 4, pp. 108–120, 2014.
- [8] M. M. Warriar and A. Kumar, "Energy efficient routing in wireless sensor networks: a survey," in *2016 International Conference on Wireless Communications, Signal Processing and Networking (WiSPNET)*, pp. 1987–1992, Chennai, 2016.
- [9] X. Lu, P. Wang, D. Niyato, D. In Kim, and Z. Han, "Wireless networks with RF energy harvesting: a contemporary survey," *IEEE Communications Surveys & Tutorials*, vol. 17, no. 2, pp. 757–789, 2015.
- [10] G. Ahmed, J. Zou, X. Zhao, and M. M. S. Fareed, "Markov chain model-based optimal cluster heads selection for wireless sensor networks," *Sensors*, vol. 17, no. 3, p. 440, 2017.
- [11] H. Cheng, Z. Su, N. Xiong, and Y. Xiao, "Energy-efficient node scheduling algorithms for wireless sensor networks using Markov Random Field model," *Information Sciences*, vol. 329, pp. 461–477, 2016.
- [12] A. Pughat and V. Sharma, "A review on stochastic approach for dynamic power management in wireless sensor networks," *Human-centric Computing and Information Sciences*, vol. 5, no. 1, p. 4, 2015.
- [13] R. R. Rout, M. S. Krishna, and S. Gupta, "Markov decision process-based switching algorithm for sustainable rechargeable wireless sensor networks," *IEEE Sensors Journal*, vol. 16, no. 8, pp. 2788–2797, 2016.
- [14] F. K. Shaikh and S. Zeadally, "Energy harvesting in wireless sensor networks: a comprehensive review," *Renewable and Sustainable Energy Reviews*, vol. 55, pp. 1041–1054, 2016.
- [15] G. Abdul-Salaam, A. H. Abdullah, M. H. Anisi, A. Gani, and A. Alelaiwi, "A comparative analysis of energy conservation approaches in hybrid wireless sensor networks data collection protocols," *Telecommunication Systems*, vol. 61, no. 1, pp. 159–179, 2016.
- [16] W. Liu, X. Zhou, S. Durrani, H. Mehrpouyan, and S. D. Blostein, "Energy harvesting wireless sensor networks: delay analysis considering energy costs of sensing and transmission," *IEEE Transactions on Wireless Communications*, vol. 15, no. 7, pp. 4635–4650, 2016.
- [17] P.-V. Mekikis, E. Kartsakli, A. Antonopoulos, L. Alonso, and C. Verikoukis, "Connectivity analysis in clustered wireless sensor networks powered by solar energy," *IEEE Transactions on Wireless Communications*, vol. 17, no. 4, pp. 2389–2401, 2018.
- [18] J. Ren, Y. Zhang, K. Zhang, A. Liu, J. Chen, and X. S. Shen, "Lifetime and energy hole evolution analysis in data-gathering wireless sensor networks," *IEEE Transactions on Industrial Informatics*, vol. 12, no. 2, pp. 788–800, 2016.
- [19] H. Tran, J. Åkerberg, M. Björkman, and H.-V. Tran, "RF energy harvesting: an analysis of wireless sensor networks for reliable communication," *Wireless Networks*, vol. 25, no. 1, pp. 185–199, 2019.
- [20] L. Cohen, *Time-Frequency Analysis*, Upper Saddle River, Prentice Hall PTR, 1995.
- [21] I. D. Mayergoyz and W. Lawson, *Basic Electric Circuit Theory: A One-Semester Text*, Academic Press, San Diego, 1997.
- [22] H. Jung, Y. J. Chang, and M. A. Ingram, "Experimental range extension of concurrent cooperative transmission in indoor environments at 2.4GHz," in *2010 - MILCOM 2010 Military Communications Conference*, pp. 148–153, San Jose, CA, 2010.
- [23] Y. Li-Hsing and T. Wei-Ting, "The room shortage problem of tree-based ZigBee/IEEE 802.15.4 wireless networks," *Computer Communications*, vol. 33, no. 4, pp. 454–462, 2010.
- [24] I. Ahmed, S. Orfali, T. Khatlab, and A. Mohamed, "Characterization of the indoor-outdoor radio propagation channel at 2.4 GHz," in *2011 IEEE GCC Conference and Exhibition (GCC)*, pp. 605–608, Dubai, 2011.
- [25] Digi International Inc, *XBee./ XBee-PRO. RF Modules*, Product Manual v1.xEx-802.15.4 Protocol, 2009.
- [26] Atmel Corporation, *ATmega16U4/ATmega32U4. 8-bit Microcontroller with 16/32K bytes of ISP Flash and USB Controller*, Data sheet, 2015.
- [27] H. Huo, Y. Xu, C. C. Bilen, and H. Zhang, "Coexistence issues of 2.4GHz sensor networks with other RF devices at home," in *2009 Third International Conference on Sensor Technologies and Applications*, pp. 200–205, Athens, Glyfada, 2009.

- [28] V. Iyer, F. Hermans, and T. Voigt, "Detecting and avoiding multiple sources of interference in the 2.4 GHz spectrum," in *Wireless Sensor Networks. EWSN*, T. Abdelzaher, N. Pereira, and E. Tovar, Eds., vol. 8965 of Lecture Notes in Computer Science, Springer, Cham, 2015.
- [29] P. Jin-A, P. Seung-Keun, K. Dong-Ho, C. Pyung-Dong, and C. Kyoung-Rok, "Experiments on radio interference between wireless LAN and other radio devices on a 2.4 GHz ISM band," in *The 57th IEEE Semiannual Vehicular Technology Conference, 2003. VTC 2003-Spring.*, vol. 3, pp. 1798–1801, Jeju, South Korea, 2003.
- [30] A. Kamerman and G. Aben, "Throughput performance of wireless LANs operating at 2.4 and 5 GHz," in *11th IEEE International Symposium on Personal Indoor and Mobile Radio Communications. PIMRC 2000. Proceedings (Cat. No.00TH8525), Vol. 1*, pp. 190–195, London, UK, 2000.
- [31] S. Sundaresan, N. Feamster, and R. Teixeira, "Measuring the performance of user traffic in home wireless networks," in *Passive and Active Measurement*, J. Mirkovic and Y. Liu, Eds., vol. 8995 of Lecture Notes in Computer Science 2015, Springer, Cham, 2015.
- [32] T. Srisooksai, K. Kaemarungsi, J. Takada, and K. Saito, "Radio propagation measurement and characterization in outdoor tall food grass agriculture field for wireless sensor network at 2.4 GHz band," *Progress In Electromagnetics Research*, vol. 88, pp. 43–58, 2018.
- [33] S. Aust, R. V. Prasad, and I. G. M. M. Niemegeers, "Outdoor long-range WLANs: a lesson for IEEE 802.11ah," *IEEE Communications Surveys & Tutorials*, vol. 17, no. 3, pp. 1761–1775, 2015.
- [34] Digi International Inc, *XBee-PRO 900HP/XSC RF Modules, S3 and S3B*, User guide, 2018.
- [35] M. Rawashdeh, "RF 315/433 MHz transmitter-receiver module and Arduino," *Instructables*, vol. 3, 2013 <http://volthauslab.com/datasheets/433Mhz-RF-tx-rx/RF-315433-MHz-Transmitter-receiver-Module-and-Ardu.pdf>.
- [36] T. Instruments, *CC1101, Low-Power Sub-1 GHz RF Transceiver*, Datasheet, 2019.
- [37] Microchip Technology Inc, *MRF49XA ISM Band Sub-GHz RF Transceiver*, Preliminary datasheet 2009, 2011.
- [38] M. M. Weiner, *Monopole Antennas*, Marcel Dekker Inc., New York, 2003.
- [39] Q. Chong, J. Yang, Z. Bote et al., "Nickel-based pillared MOFs for high-performance supercapacitors: design, synthesis and stability study," *Nano Energy*, vol. 26, pp. 66–73, 2016.
- [40] A. C. Forse, C. Merlet, J. M. Griffin, and C. P. Grey, "New perspectives on the charging mechanisms of supercapacitors," *Chemical Society*, vol. 138, no. 18, pp. 5731–5744, 2016.
- [41] P. Lee, Z. A. Eu, M. Han, and H. Tan, "Empirical modeling of a solar-powered energy harvesting wireless sensor node for time-slotted operation," in *2011 IEEE Wireless Communications and Networking Conference*, pp. 179–184, Cancun, Quintana Roo, México, 2011.
- [42] F. Meder, I. Must, A. Sadeghi et al., "Energy conversion at the cuticle of living plants," *Advanced Functional Materials*, vol. 28, no. 51, p. 1806689, 2018.
- [43] P. K. Narahariseti, P. Das, and P. N. Sharratt, "Critical factors in energy generation from microalgae," *Energy*, vol. 120, pp. 138–152, 2017.
- [44] M. K. Sarma, S. Kaushik, and P. Goswami, "Cyanobacteria: a metabolic power house for harvesting solar energy to produce bio-electricity and biofuels," *Biomass and Bioenergy*, vol. 90, pp. 187–201, 2016.
- [45] X. Yan, Z. Wang, L. Huang et al., "Research progress on electrical signals in higher plants," *Progress in Natural Science*, vol. 19, no. 5, pp. 531–541, 2009.
- [46] A. Christmann and E. Grill, "Electric defence," *Nature*, vol. 500, no. 7463, pp. 404–405, 2013.
- [47] J. Fejér, D. Grul'ová, and V. De Feo, "Biomass production and essential oil in a new bred cultivar of peppermint (*Mentha x piperita* L.)," *Industrial Crops and Products*, vol. 109, pp. 812–817, 2017.
- [48] M. G. Figueroa-Pérez, I. F. Pérez-Ramírez, J. A. Enciso-Moreno, M. A. Gallegos-Corona, L. M. Salgado, and R. Reynoso-Camacho, "Diabetic nephropathy is ameliorated with peppermint (*Mentha piperita*) infusions prepared from salicylic acid-elicited plants," *Journal of Functional Foods*, vol. 43, pp. 55–61, 2018.
- [49] E. Antignac, "Safety of botanical ingredients in personal care products/cosmetics," *Food and Chemical Toxicology*, vol. 49, no. 2, pp. 324–341, 2011.
- [50] E. H.-J. Kim, D. Paredes, L. Motoi et al., "Dynamic flavor perception of encapsulated flavors in a soft chewable matrix," *Food Research International*, vol. 123, pp. 241–250, 2019.
- [51] M. Maffei, "Sustainable methods for a sustainable production of peppermint (*Mentha x piperita* L.) essential oil," *Journal of Essential Oil Research*, vol. 11, no. 3, pp. 267–282, 1999.
- [52] U. N. Food and Agriculture Organization, *Peppermint Production in 2014; Crops/Regions/World List/ Production Quantity (Pick Lists)*, Corporate Statistical Database (FAOSTAT), 2017.
- [53] R. Girsowicz, I. Moroonyane, and Y. Steinberger, "Bacterial seed endophyte community of annual plants modulated by plant photosynthetic pathways," *Microbiological Research*, vol. 223–225, pp. 58–62, 2019.
- [54] N. P. A. Huner, A. G. Ivanov, K. E. Wilson, E. Miskiewicz, M. Krol, and G. Öquist, "Energy sensing and photostasis in photoautotrophs," in *Cell and Molecular Response to Stress*, vol. 3, pp. 243–255, Elsevier, 2002.
- [55] C. Peterhansel, I. Horst, M. Niessen et al., "Photorespiration," *The Arabidopsis Book*, vol. 8, article e0130, 2010.
- [56] H. M. Liddy, S. J. Feakins, F. A. Corsetti et al., "Photosynthetic pathway of grass fossils from the upper Miocene Dove Spring Formation, Mojave Desert, California," *Palaeogeography, Palaeoclimatology, Palaeoecology*, vol. 490, pp. 131–140, 2018.
- [57] C. W. Treesubstorn, W. Chaiworn, W. Surareungchai, and P. Thiravetyan, "Increasing of electricity production from *Echinodosus cordifolius* -microbial fuel cell by inoculating *Bacillus thuringiensis*," *Science of the Total Environment*, vol. 686, pp. 538–545, 2019.
- [58] U. Kiran and D. D. Patra, "Influence of natural essential oils and their by-products as nitrification retarders in regulating nitrogen utilization for Japanese mint in sandy loam soils of subtropical Central India," *Agriculture, Ecosystems & Environment*, vol. 94, no. 2, pp. 237–245, 2003.
- [59] R. A. Barbato, K. L. Foley, J. A. Toro-Zapata, R. M. Jones, and C. M. Reynolds, "The power of soil microbes: sustained power production in terrestrial microbial fuel cells under various temperature regimes," *Applied Soil Ecology*, vol. 109, p. 14e22, 2017.
- [60] L. De Schampelaire, L. Van den Bossche, H. Son Dang et al., "Microbial fuel cells generating electricity from rhizodeposits

of rice plants,” *Environmental Science & Technology*, vol. 42, no. 8, pp. 3053–3058, 2008.

- [61] Y.-B. Jiang, W.-H. Zhong, C. Han, and H. Deng, “Characterization of electricity generated by soil in microbial fuel cells and the isolation of soil source exoelectrogenic bacteria,” *Frontiers in Microbiology*, vol. 7, p. 1776, 2016.
- [62] K. Omine, V. Sivasankar, and S. D. Chicas, “Bioelectricity generation in soil microbial fuel cells using organic waste,” in *Microbial Fuel Cell Technology for Bioelectricity*, V. Sivasankar, P. Mylsamy, and K. Omine, Eds., Springer, Champions, 2018.

Research Article

An Improved Triggering Updating Method of Interest Message with Adaptive Threshold Determination for Directed Diffusion Routing Protocol

Jun Wang ¹, Xiaohang Liu ², Zhitao He ², Yadan Zhang ² and Song Gao ²

¹School of Electrical Engineering, Henan University of Science and Technology, Luoyang, Henan 471000, China

²School of Agricultural Equipment Engineering, Henan University of Science and Technology, Luoyang, Henan 471003, China

Correspondence should be addressed to Jun Wang; wangjun_haust@163.com

Received 30 September 2020; Revised 21 December 2020; Accepted 16 January 2021; Published 25 January 2021

Academic Editor: Mario E. Rivero-Angeles

Copyright © 2021 Jun Wang et al. This is an open access article distributed under the Creative Commons Attribution License, which permits unrestricted use, distribution, and reproduction in any medium, provided the original work is properly cited.

Although some progress has been made in studying the triggering updating methods of interest message for reducing node energy consumption in directed diffusion routing protocols, they do not consider the anisotropy of sensing areas of nodes and the requirement of diversity of interest message exchange rates within real-time performance, which makes these studies unable to accurately adapt to the characteristics of interest message update. In this work, we proposed an improved triggering updating method (ITUM) consisted of adaptive threshold determination based on the analytic hierarchy process and update judgement by similarity comparison of interest messages. Meanwhile, the network model and the sensing model are presented to describe actual network scenarios. We analyze the impact of critical parameters and evaluate the performance of ITUM with several interest message updating methods from the aspect of lowering the number of information exchanges. The simulation results prove that ITUM can improve the adaptability to scene changes while decreasing the number of information exchanges compared with the existing methods. Furthermore, it is shown that ITUM is a highly effective solution for determining the triggering updating conditions of various information exchange rates in directed diffusion routing protocol.

1. Introduction

Query routing technique is undoubtedly one of the most typical routing protocols for wireless sensor networks (WSNs) [1], which is concretely composed by interest message diffusion, data transmission, and path enhancement in the implementation process [2–5]. The routing method has several remarkable highlights in data-oriented monitoring applications, such as direct transmission of interested data, information screening [6], and local communication [7], resulting in the advantages of less redundant information and long network lifetime. Moreover, the query routing protocol can be explicitly classified into rumor routing, directed diffusion routing, disjoint multipath routing, and braided multipath routing [8–11]. Directed diffusion routing exhibits excellent energy efficiency compared with other query routing methods [12] and can effectively lessen network data stream by query-driven data transmission and local data aggregation

[13]. For example, Intanagonwiwat et al. explored the use of directed diffusion for a simple remote-surveillance sensor network and enabled diffusion to achieve energy savings by selecting empirically good paths and by caching and processing data in-network [14]. Mu et al. inquired a directional diffusion routing protocol to improve the reliability of data transmission and extend the network life in wireless body area networks (WBANs) [15]. Directed diffusion routing is made up of three independent stages: interest diffusion, data transmission, and path enhancement [16–19]. During the application of directed diffusion routing, the query request is sent to nodes in the target area in the form of interest message, and the routing path is established in turn. Afterwards, the nodes start to execute the corresponding monitoring tasks according to the description of the interest message. Among them, the spread of interest message is named as interest message diffusion. Besides, since the network is not static, the nodes in the target area may move out, and on

the contrary, the nodes outside the target area can also move in. These mobile nodes unavoidably require to communicate with surrounding nodes for timely exchanging or achieving interest messages in this phase, which is defined as interest message update.

In order to diminish energy consumption and extend network lifetime, various studies have been performed to optimize directed diffusion routing. For instance, Eghbali and Dehghan addressed a load-balancing method based on multipath directed diffusion to prolong the lifetime of nodes by establishing a multihop path between receivers and sensor nodes [20]. Li and Shi enhanced energy utilization rate and extended network lifetime by optimizing data transmission path and data aggregation [21]. Liu et al. investigated DDBC, a clustering-based directed diffusion routing protocol, to decrease network topology and hence improve energy efficiency by clustering and suppressing redundant messages in flooding [22]. However, these developed protocols solely pay attention to explore energy conservation strategies during data transmission and path enhancement stages in terms of data fusion, load balancing, and optimization path, less considering the energy consumption generated by interest message update. Nevertheless, the number of interest message exchanges in the stage of interest message update likewise directly influences node energy consumption [23–25], which is tightly associated with triggering updating method of interest message. It is necessary to take into account the message exchange requirement and communication cost of the target area for a triggering updating method.

Some triggering updating methods have been reported to improve the routing performance in interest message update. The current triggering updating methods can be separated into two categories: conventional triggering updating method (TUM) and energy-saving triggering updating method. The first method is that the mobile node accomplishes update through periodically broadcasting the update request of interest message to the neighbor nodes during its movement [26]. This behavior based on periodic triggering may substantially increase the number of interest message exchanges and cannot adapt to the movement path of mobile node due to the blindness of triggering. Meanwhile, the possible simultaneous responses of neighbor nodes are probable to induce information redundancy and network congestion. For overcoming the weaknesses of the classic triggering updating method, a series of energy-saving triggering updating methods are probed by refining the trigger and response patterns. Yu and Zhang and Cui and Cao investigated a method to effectively decrease the frequency of interest message updates by spreading interest messages only between cluster heads [27, 28]. Krishnamachari and Ahn proposed an extending ring query approach that can implement adaptive adjustment of query radius [29]. Niu et al. recommended an interest message updating method based on update triggering, delayed response, and incremental update to decrease update frequency [30]. Although the propagation between cluster heads or the limitation of update request range can restrain the surge of update frequency due to the flooding mode, the problem that updating operation and movement path are difficult to adapt to has not been solved, and there is an increased possi-

bility of premature death of cluster heads. Moreover, these studies are all based on the ideal node model and do not consider the variations in sensing scope for different directions. Additionally, compared with the other methods, the incremental update proposed by Niu et al. can decrease update number while multiple nodes are within the sensing area of mobile node during the update phase. However, it will inevitably boost the amount of response inhibition messages transmitted and cannot prevent nodes with high proximity of interest message content from acting void updates.

The ideal sensing area of node is approximately circular. Though in the actual scene, the path attenuation of signal transmission in different directions is varied as a consequence of the influence of wireless device properties and other environmental factors such as obstacles, leading to the anisotropy of sensing area. On the other side, choosing the improper threshold based on previous experience is a crucial problem to the triggering updating method. This may cause a direct impact on the real time, adaptability, and timeliness of interest information update. It is additionally a vital concern to avoid updating between a mobile node and multiple fixed nodes with high-similarity message content.

Based on the above introduction, this paper proposes an improved triggering updating method for interest message update in directed diffusion routing protocol, which is constituted by adaptive threshold determination using the analytic hierarchy process (AHP) and trigger judgement adopting similarity comparison of interest messages. The contribution of this paper covers four aspects:

- (1) We develop a network model based on different overlapping patterns of sensing areas between a mobile node and various fixed nodes and establish a sensing model considering time-varying anisotropy of wireless signal transmission
- (2) We propose an improved triggering updating method comprised of threshold determination and update judgement to minimize the number of information exchanges under different information exchange rates
- (3) We use the Gauss-Markov mobility model to describe the mobile node movement in the target area and investigate the performance of reducing the number of information exchanges for diverse network and mobility parameters
- (4) Simulation results demonstrate that the proposed triggering updating method can significantly decrease the number of information exchanges due to the combination of advantages of two factors. The analytic hierarchy process can dynamically obtain the proper threshold of interest messages of multifixed nodes, and the similarity comparison is capable of avoiding unnecessary updates

The outline of this paper is organized as follows. Section 2 provided the network model and sensing model. Section 3

depicts the proposed method. In Section 4, we conduct the performance analysis of the proposed method under different network and mobility parameters. Finally, we summarize our work and draw conclusions in Section 5.

2. Network and Sensing Model

In this section, aiming to describe the scenario of interest message update precisely, we propose several assumptions of network model and two categories of overlapping pattern of sensing areas to imply the preconditions of update triggering in consideration of the bidirectional links between nodes and use a time-varying standard normal distribution to indicate the difference of sensing area of node in each direction.

2.1. Network Model. Considering the distribution of fixed nodes, the moving path of mobile node, and the capacity of node interest messages, we concretely define network model as follows.

(1) Every node has the same communication ability, each communication link between nodes is bidirectional, and all fixed nodes in WSNs are randomly distributed in a rectangular target area

(2) The total number of nodes in the target area is Q , and each node can utilize the existing wireless location technology to provide location information

(3) The number of interest messages carried within each sensor node is L . These interest messages vary and are sorted by importance in descending order. The characters $1, 2, \dots, K$ are used to depict different monitoring tasks, respectively. Additionally, it is assumed that K is greater than L . Meanwhile, the interest message in a mobile node is empty at the initial stage

(4) The overlapped sensing areas of fixed nodes manifest that there are common interest messages (monitoring tasks) between them and vice versa. The fixed nodes overlapping with a mobile node can be abstracted as a fixed node

(5) A mobile node can enter or leave from any boundary of the target area and move according to the Gauss-Markov mobility model. The update is triggered by simultaneously satisfying the two conditions that the sensing areas of the mobile node and fixed nodes overlap, and the similarity of interest messages is higher than threshold value

(6) The overlaps can be divided into two kinds by the number of fixed nodes overlapped with a mobile node, as illustrated in Figure 1. The first category is that the sensing area of mobile node overlaps with that of a single fixed node, and triggering updating is settled by both. The second category is that the sensing area of mobile node overlaps with that of multiple fixed nodes at the same time, which can be classified into the following three cases:

(a) The sensing areas of fixed nodes are entirely overlapped, that is, the interest messages are the same, and the triggering updating is decided by the mobile node and any node together

(b) The sensing areas of fixed nodes do not overlap with each other at all. Namely, the interest messages are entirely different, and the mobile node needs to make the judgment of triggering updating with each fixed node, respectively

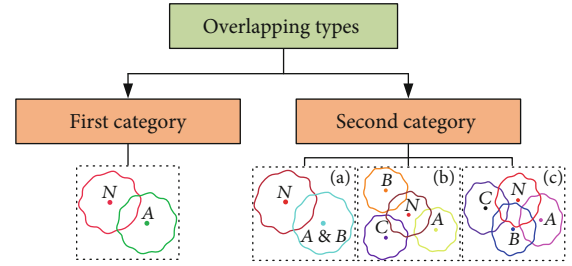


FIGURE 1: Overlapping patterns. N represents the mobile node; A , B , and C express fixed nodes, respectively.

(c) The sensing areas of fixed nodes are partially intersected, and the interest messages of these nodes are supposed to be not exactly the same. In this case, common messages of these fixed nodes are firstly arranged in random order, and the remaining messages are further sorted in descending order of importance of interest message content until the message capacity of a fixed node is reached. The triggering updating assessment is eventually carried out between the reorganized interest message and the interest message of mobile node

(7) The query request is strictly restricted in the target area, and the sink node locates outside the target area. Each request by the user is time-limited and expires after the corresponding validity duration

2.2. Sensing Model. Radio irregularity originated by the heterogeneous properties of devices and the anisotropic properties of propagation media is a common and nonnegligible phenomenon in WSNs [31]. It results in irregularity in radio range and variations in packet loss in different directions for sensor node. The sensing model we put forward here is inspired by three properties of radio signals: anisotropy, continuous variation, and heterogeneity. In addition, the degree of influence of factors such as residual energy of nodes and neighboring environment on the perceived distance of nodes in various directions is random, time varying, and has the characteristics of normal distribution. Therefore, for the convenience of description and application, the standard normal distribution is used to demonstrate the random influence degree of multiple independent factors on the perceived distance of nodes in each direction, and the time-varying process of the influence is expressed by introducing the time variable.

A time-varying irregular circle with the node as the center is proposed to depict the sensing area of node in the deployment scenario. The variable perceived distance $R_s(R_s = (1 - \sigma')R)$ is used as its radius, where R denotes the radius as the sensing area of node is a regular circle [32, 33] and σ' ($0 < \sigma' < 0.2$) is anisotropic influence factor.

The anisotropy influence factor σ' is represented by an integral function of the standard normal distribution with time and angle as variables and can be calculated by Eq. (1).

$$\sigma' = \int_{1/4|\sin(\theta+t)|}^{1/4|\sin(\theta+t)|} \frac{1}{\sqrt{2\pi}} e^{-u^2/2} du, \quad (1)$$

where θ ($\theta \in [0, 2\pi]$) and u ($u \in (-0.25, 0.25)$) are direction coefficient and adjustment coefficient, l represents a random number greater than 1, t ($t > 0$) indicates time, and the product of t and l is an adjustable time-varying parameter.

3. Triggering Updating Method

The interest message update process has varied requirements on the degree of information exchange between a mobile node and several fixed nodes with overlapped sensing areas, corresponding to different information exchange rates. The high information exchange rate indicates that the update sensitivity of interest message of mobile node and fixed nodes is at a high level and vice versa. For the information exchange requirements, relying only on the previous experience to artificially set the update threshold, it will inevitably lead to the decline of necessity and adaptability of update. Therefore, we build an improved triggering updating method in this section. In this method, the update threshold of fixed nodes is solved adaptively based on AHP for evaluating the difference of interest message content in light of information exchange rate, and then the similarity of interest message contents between the mobile node and fixed nodes is computed and compared with the update threshold to judge whether to update or not.

3.1. Threshold Determination. AHP proposed by Saaty in the early 1970s is a multicriteria decision method that uses hierarchical structures to represent a problem and makes decisions based on importance scales [34, 35]. Because of the effective combination of qualitative and quantitative approaches, it has been popularly practiced in the fields of performance evaluation, engineering planning, program sequencing, economic management, etc. [36]. In this paper, the complex correlation and subordination between interest messages and information exchange rates are combined into a three-level analysis structure model by AHP, and the threshold determination can be converted into computing the relative weights of information exchange rates to the update threshold. The specific steps are listed as follows:

(1) *Establishing Hierarchical Threshold Model.* The information exchange rate and message priority are arranged into an ordered hierarchy model based on membership relations, as shown in Figure 2. The update threshold z is referred to as the overall target layer, the priorities (B_1, B_2, \dots, B_L) of interest message content are employed as the criterion layer for achieving the overall goal, and three information exchange rates are selected as the solution layer in which A_1, A_2, A_3 express high, medium, and low information exchange rates, respectively. In the constructed model, the update threshold z is jointly determined by priorities B_1, B_2, \dots, B_L . A priority B_j ($1 < j < L$) is mutually affected by the three information exchange rates and the priorities in turn act on the same information exchange rate.

(2) *Constructing Importance Matrix.* According to the importance of priority levels of interest message content in the criterion layer, the criteria scale is evenly subdivided into nine levels from equal importance (lowest priority) to extreme importance (highest priority), and the values are

assigned 1 to 9. Each value signifies that the importance of the former over the latter of two priorities compared, and the corresponding value should be reciprocal with the positions of two priorities interchange. Moreover, $B_{j1}, B_{j2}, \dots, B_{jL}$, the importance comparison results of B_j ($1 < j < L$) and B_1, B_2, \dots, B_L are added as the j th row element of importance matrix of criterion layer B using the update threshold z as the evaluation criterion, and the importance matrix B is set up as follows:

$$B = \begin{bmatrix} b_{11} & \cdots & b_{1L} \\ \vdots & \ddots & \vdots \\ b_{L1} & \cdots & b_{LL} \end{bmatrix}. \quad (2)$$

As a result of the identical hierarchical model, the importance matrix of solution layer and criterion layer is assembled by the same method. Through the steps above, the importance matrix of solution layer with priority B_j ($1 < j < L$) as evaluation criteria is described by Eq. (3).

$$A_{B_j} = \begin{pmatrix} a_{11} & a_{12} & a_{13} \\ a_{21} & a_{22} & a_{23} \\ a_{31} & a_{32} & a_{33} \end{pmatrix}. \quad (3)$$

(3) *Sorting and Validation of Single-Layer Weight.* The eigenvectors of importance matrices B and A_{B_j} can be obtained by the square root method. The relative weights W^{B_j} among A_1, A_2, A_3 and the relative weights W^z among B_1, B_2, \dots, B_L can be collected after normalization, respectively. In this paper, we use the calculation process of W^{B_j} as an example, to illuminate the same implement process of the two weights as follows.

(a) Compute the cubic root of product of elements of each row in the importance matrix A_{B_j} by $W_i = (\prod_{j=1}^3 a_{ij})^{1/3}$, ($i = 1, 2, 3$) and normalize W_i by the following:

$$W_i^{B_j} = \frac{W_i}{\sum_{i=1}^3 W_i}, \quad (4)$$

where $W_i^{B_j}$ represents the weight of A_i by the use of B_j as evaluation criteria. $W^{B_j} = (W_1^{B_j}, W_2^{B_j}, W_3^{B_j})^T$ is the relative weight, namely, the normalized vector, and each component is the weight value of different information exchange rates relative to the priority B_j .

(b) Calculate the largest characteristic root of importance matrix A_{B_j} by Eq. (5).

$$\lambda_{\max} = \sum_{i=1}^3 \frac{C_i}{3W_i^{B_j}}, \quad (5)$$

where C_i is the i th element of vector C ($C = A_{B_j} W^{B_j}$).

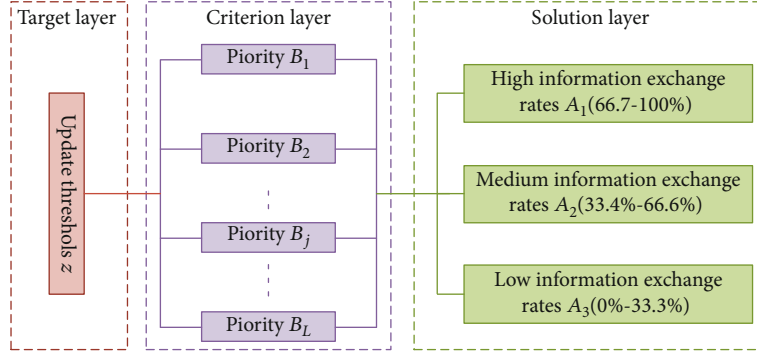


FIGURE 2: Hierarchical threshold model.

(c) As the elements of importance matrix are quantitatively assigned, in order to avoid the influence of change of characteristic roots caused by data contradiction on calculation result and decision accuracy, the consistency validation on its elements can be done through Eq. (6).

$$CR = \frac{CI}{RI} = \frac{\lambda_{\max} - n/n - 1}{RI} = \frac{\lambda_{\max} - 3}{1.16}, \quad (6)$$

where CR is the consistency ratio, RI is the random consistency index, CI is the consistency index, and n is the order of matrix A_{B_j} with a value of 3. CR is used to indicate the degree to which the constructed importance matrix deviates from the ideal completely consistent matrix, which can effectively detect the logical errors in judgement and improve the reliability of the final decision. The threshold value of 0.1 is recommended by Saaty and has been widely accepted as a general setting used to assess whether the matrix has satisfactory consistency. In case consistency ratio $CR = CI/RI < 0.1$, it shows that importance matrix A_{B_j} has satisfactory consistency. The normalized eigenvector W^{B_j} can be applied as the weight vector representing relative weight. Otherwise, the element a_{ij} should be adjusted through the reconstruction of A_{B_j} by the most inconsistent element (MICE) iteration algorithm, which is recommended by Yuan and Liang [37].

(d) *Weight Sorting and Threshold Determination.* Based on consistency validation, the total weight of each information exchange rate can be computed by Eq. (7).

$$W_{A_i}^Z = \sum_{j=1}^L W_{ij}^{B_j} W_j^Z, \quad i = 1, 2, 3, \quad (7)$$

where $W_{A_i}^Z$ is the total weight of A_i relative to z , $W_{ij}^{B_j}$ is the weight of A_i relative to B_j , and W_j^Z denotes the weight of B_j relative to z . To ensure the reliability of the total weights obtained, the consistency validation can be designed:

$$CR' = \frac{\sum_{j=1}^L W_j^Z CI_j'}{\sum_{j=1}^L W_j^Z RI_j'}, \quad (8)$$

where CR' is the final consistency ratio and CI_j' and RI_j' are the sorting consistency index and random consistency index of hierarchical weights of solution layer to the criterion layer B_j . In the case of $CR' < 0.1$, it is concluded that the weight sorting has satisfactory consistency. Then, the optimal threshold z' at the current information exchange rate can be gained by Eq. (9) and Eq. (10).

$$z' = z_{\min} + (z_{\max} - z_{\min}) \times (1 - W_{A_i}^{z'}), \quad (9)$$

$$z_{\max} = \begin{cases} 2\sqrt{\frac{2\sum_{i=1}^{L/2} (K - (2i - 1))^2}{L}} & (L \text{ is even}), \\ \sqrt{\frac{2\sum_{i=0}^{(L-1)/2} (K - (2i + 1))^2 - (K - L)^2}{L}}, \\ \times \left(2 - \sqrt{\frac{2(K - L)/K + 1}{\sum_{i=0}^{(L-1)/2} (K - (2i + 1)) - (K - L)}} \right) & (L \text{ is odd}), \end{cases} \quad (10)$$

where z_{\max} is the maximum threshold, z_{\min} is the minimum threshold with the value of zero, and $W_{A_i}^{z'}$ is the weight of the current information exchange rate relative to the update threshold z achieved by Eq. (7).

3.2. Update Judgement. After obtaining the update threshold of fixed nodes overlapped with a mobile node, the similarity can be adopted to assess whether the interest messages of mobile and fixed nodes satisfy the update condition under the current information exchange rate. Distance measurement methods are widely used to signify the similarity between data. However, such methods often show more reliable measurement results in low-dimensional space and weak performance in high-dimensional space by the cause of the sparsity of data [38]. Hence, the application of the distance-based method to the similarity comparison of multidimensional interest messages will unavoidably lead to a sharp increase in update times with the growing number of deployed nodes, forming a dimensional disaster. The predicament of the distance-based method results in the ignorance of similarity difference for high-value data and low-value

data in various dimensions, which directly generates the underestimate of similarity outcomes. To solve this problem, we propose a modified distance-based similarity function by using the absolute average of each dimension to balance the similarity discrepancy of high-value data and low-value data. This function evaluates the similarity of each dimension of data, and its value is between 0 and z_{\max} . The larger the value, the higher the difference between the two information messages. The similarity of interest message contents between a mobile node and multiple fixed nodes is defined by the following:

$$D(M, N) = \sqrt{\frac{\sum_{i=1}^L (M_i - N_i)^2}{L}} \times \left(2 - \frac{\sum_{i=1}^L (M_i - N_i) / m_i}{\sum_{i=1}^L |M_i - N_i|} \right), \quad (11)$$

where M represents a mobile node and N is the fixed node abstracted by the fixed nodes overlapped with M ; $M = (M_1, M_2, \dots, M_j, \dots, M_L)$ and $N = (N_1, N_2, \dots, N_j, \dots, N_L)$, respectively, indicate the interest message contents of M and N , $M_i, N_i \in (1, K)$; m_i is the absolute average of M_i and N_i .

The introduction of parameter m_i can make the similarity analysis based on distance depends not only on the difference between M_i and N_i but also on the size of the dimension data, for intensifying the similarity measurement performance of dimension with large value in the case of high dimension. For example, suppose $M = (1, 4, 7)$ and $N = (3.6, 9)$, if m_i in $D(M, N)$ is removed, then the similarity of M and N in these three dimensions is 2, respectively, and the overall similarity is 2. However, based upon data comparison, the similarity of the second dimension should be higher than that of the first dimension, and the similarity of the third dimension should be higher than that of the second dimension. According to the $D(M, N)$, the similarity of the two messages in the three dimensions is 3, 3.6, and 3.75, respectively, and the overall similarity is 3.45. It is easy to find that the similarity comparison function proposed in this paper has high-grade discrimination performance.

We decide whether to do the update operation following the similarity calculation. If the similarity is higher than the update threshold, the update operation will be enabled. Otherwise, the update will be abandoned, and the mobile node continues to move and prepares for the next update as requested by the query.

4. Results and Discussion

In the simulations, we make use of Gauss-Markov mobility model to depict the mobile node movement in the target area, which was initially presented for the simulation of a personal communication service network. It can be described as

$$\begin{aligned} v_k &= \beta v_{k-1} + (1 - \beta) v_{\text{avg}} + \left(\sqrt{1 - \beta^2} \right) w_{v_{k-1}}, \\ d_k &= \beta d_{k-1} + (1 - \beta) d_{\text{avg}} + \left(\sqrt{1 - \beta^2} \right) w_{d_{k-1}}, \end{aligned} \quad (12)$$

where v_k and d_k are the new velocity and direction of mobile node at time interval k ; v_{avg} and d_{avg} are constants representing the mean value of velocity and direction as $k \rightarrow \infty$; β ($0 \leq \beta \leq 1$) is the tuning parameter used to vary the randomness; $w_{v_{k-1}}$ and $w_{d_{k-1}}$ are random variables from a Gauss distribution. At each time interval, the next location is calculated based on the current location, velocity, and direction of movement. Specifically, at time interval k , the location of mobile node is given by

$$\begin{aligned} x_k &= x_{k-1} + v_{k-1} \times \cos(d_{k-1}), \\ y_k &= y_{k-1} + v_{k-1} \times \sin(d_{k-1}), \end{aligned} \quad (13)$$

where (x_k, y_k) and (x_{k-1}, y_{k-1}) are the x and y coordinates of mobile node at the k th and $(k-1)$ th time intervals, respectively, and v_{k-1} and d_{k-1} are the velocity and direction of mobile node, respectively, at the $(k-1)$ th time interval. We set the target area to be 200 m \times 100 m. All the simulation results are the average values of 50 simulations. The simulation parameters are shown in Table 1.

With the change of simulation parameters, the ITUM proposed in this paper is compared with traditional updating method (TUM) and TURIR [30], by using the number of information exchanges as the indicator.

Figure 3 depicts the relations of ITUM, TUM, and TURIR between the number of information exchanges and the deployment density of fixed nodes m . It is easy to observe that the number of information exchanges can increase significantly with the growth of m . When $m \in [1/1000 \text{ m}^2, 1/200 \text{ m}^2]$, the number of information exchanges of these three methods will rise slowly, with average growth rates of 21.58%, 23.73%, and 21.72%, respectively. When $m \in (1/200 \text{ m}^2, 1/100 \text{ m}^2]$, the number of information exchanges of these three methods will proliferate, with the growth rates of 101.72%, 104.56%, and 162.81% separately. Apparently, TUM is the most sensitive to the deployment density of fixed nodes, and ITUM has the minimum increase in the number of information exchanges, with the m rising from $1/1000 \text{ m}^2$ to $1/100 \text{ m}^2$. The triggering methods of three methods lead this phenomenon. The timing update mechanism of TUM is associated with time and deployment density of fixed nodes. Under a certain time, the deployment density directly impacts the number of information exchanges, and the higher the m is, the faster the increase will be. TURIR merely updated while the node displacement is higher than the fixed threshold value. Compared to TUM, the method can efficiently decrease the number of information exchanges, and the number of information exchanges will slowly increase with the increment of m affected by mobility model and threshold value. However, if the node density increases to a specific value, the node displacement becomes the chief influencing factor, which will drive to the sharp increase in the number of information exchanges. ITUM can lessen the number of information exchanges by avoiding blind and invalid updates as a consequence of the triggering updating conditions recommended in this paper. Influenced by the anisotropy, update threshold, and similarity in the initial

TABLE 1: Simulation parameters.

Parameter	Symbol	Initial value	Variation range
Deployment density of fixed nodes	m	$1/200 \text{ m}^2$	$[1/1000 \text{ m}^2, 1/100 \text{ m}^2]$
Sensing radius of nodes	R	10 m	[10 m, 55 m]
Tuning parameter	β	0.3	[0, 1]
Average velocity of mobile node	v_{avg}	1 m/s	(0, 1.25 m/s)
Average direction of mobile node	d_{avg}	$\pi/2$	$(0, \pi)$
Dimension of interest message	L	1	[1, 9]
Information exchange rate	H	50%	(0, 100%)

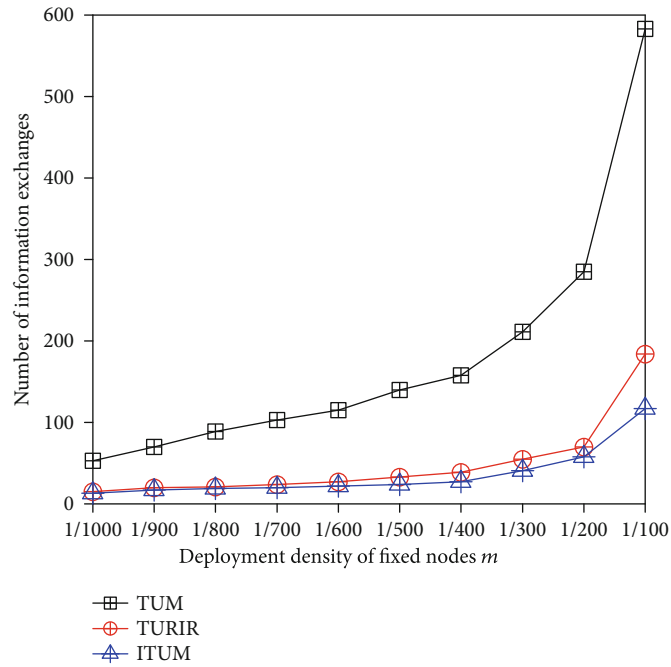


FIGURE 3: Number of information exchanges of three methods in different deployment densities.

phase, the number of information exchanges rises moderately with the increase of m . As the deployment density continues to grow, the anisotropy converts to the principle aspect and will cause an abrupt jump in the number of information exchanges.

As shown in Figure 4, with the increase of R , the average number of information exchanges of ITUM is lowered by 75.72% and 41.00%, respectively, compared to that of TUM and TURIR. When $R \in [10 \text{ m}, 30 \text{ m}]$, the number of information exchanges of ITUM and TURIR has an approximate trend with a slow growth rate. In particular, when $R \in [30 \text{ m}, 55 \text{ m}]$, ITUM can dramatically decrease the number of information exchanges, compared with the other two kinds of methods. As a whole, the rate of change, the number of information exchanges, and the increment of ITUM are significantly lower than the other two methods produced by the anisotropy of sensing area and the triggering updating conditions, which diminishes the probability of the update judgment. Furthermore, it is easy to understand that the bigger the R is, the more the number of information exchanges

are, which means that more updates will be triggered. Therefore, in order to reduce the update times, designers should set reasonable sensing radius for network nodes.

Figure 5 demonstrates the relation between the dimension of interest message L and the number of information exchanges. With the increase in L , the average number of information exchanges of these three methods is raised by 3.19%, 6.81%, and 4.55%, respectively. Compared with TUM, TURIR, and ITUM, it has better performance in reducing the number of information exchanges and decreases by 20.68% and 2.93% on average. When $L < 4$, affected by the number of monitoring tasks, priority, and threshold range, TURIR is the most effective in cutting down the number of information exchanges by reason of the fixed threshold mechanism. When $4 \leq L \leq 7$, the number of information exchanges of ITUM can be stable at 38, which has a prominent advantage over the other two methods. In the case of $L > 7$, although the impact of L will lead to sudden increases in quantities, contrasted to the other two methods, the number of information exchanges of ITUM is still

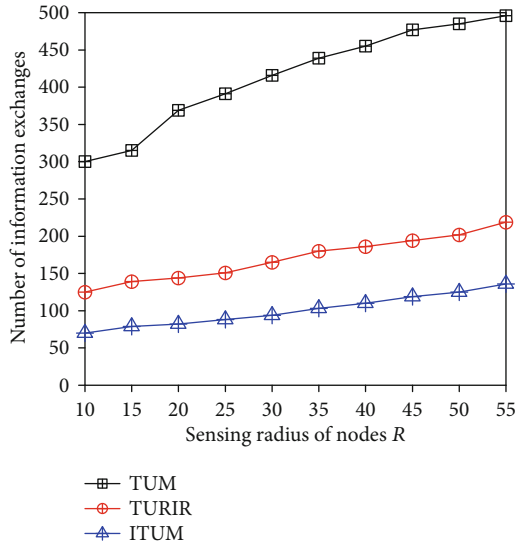


FIGURE 4: Relation between R and number of information exchanges for different methods.

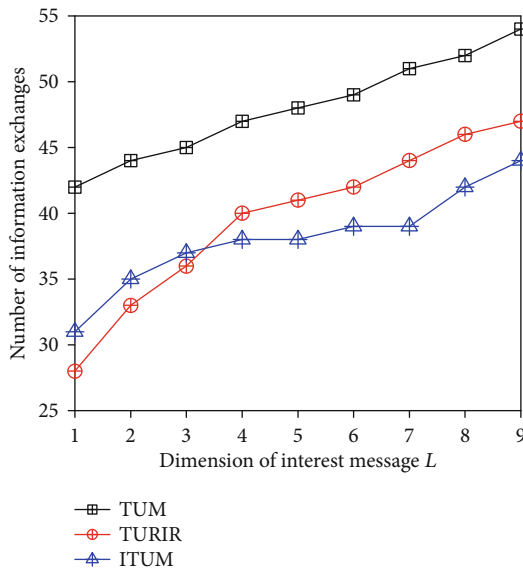


FIGURE 5: Influence of L on number of information exchanges for three methods.

reduced by 20.38% and 8.76%, respectively. Therefore, to lower the update times by ITUM, we need to limit the number of L within a reasonable scale ($4 \leq L \leq 7$).

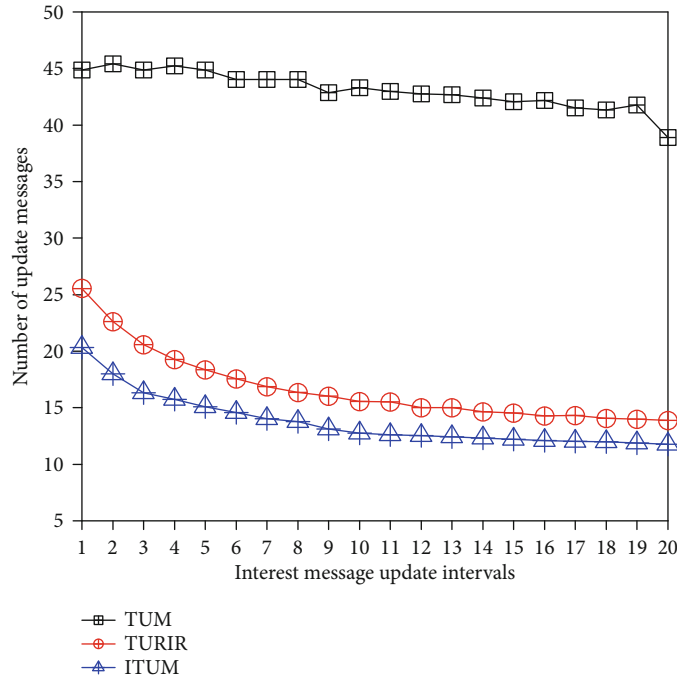
As shown in Figure 6, with the increase in number of interest message update intervals from 1 minute to 20 minutes, ITUM is the least in the number of update messages in comparison with that of TUM and TURIR. The average number of update messages is reduced by 68.03% and 17.47%, and the average amount of update data declined by 78.41% and 41.35%, respectively. In Figure 6(a), the number of update messages in TUM is linked to the number of neighbor nodes, depending on the triggering way. In the condition of a definite deployment density of fixed nodes, the number

of update messages decreases insignificantly with the increase of interest message interval, primarily induced by the decrease of the number of messages used for interest message propagation. The variance in the number of update messages between ITUM and TURIR is affected by the triggering updating mode, with the condition that the frequency of query request, the scope of target area, and the validity period of request remain unchanged.

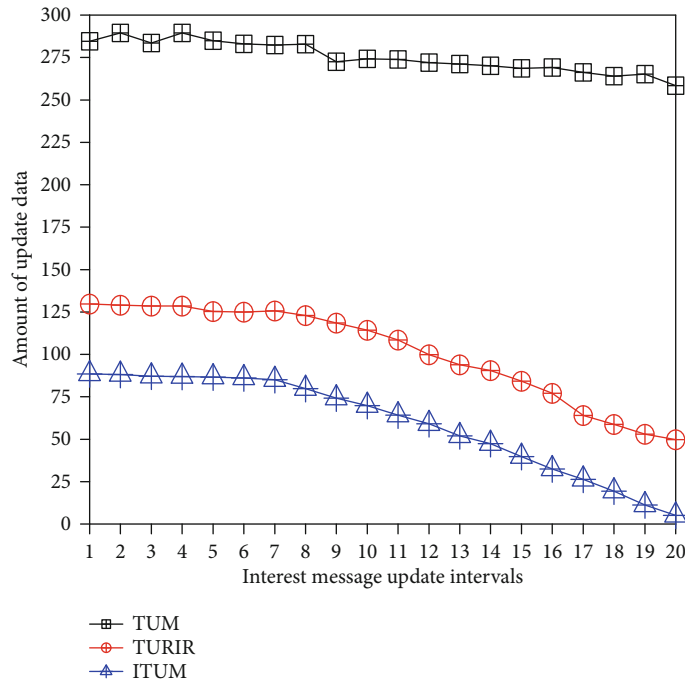
Two main factors interlock with the amount of update data: whether to adopt incremental update and the number of messages in the update process, as exhibited in Figure 6(b), as TUM does not use the incremental update, the number of messages in the update process and message format bring about that its data quantity varies little and is much larger than the other two methods. In the case that ITUM and TURIR both utilize incremental update pattern, the amount of update data of both has direct relevance to the number of messages generated by respective triggering updating methods and message formats. In summary, ITUM can not only reduce the number of update messages in the update process but also match the update messages with user queries, which is particularly suitable for data-centric WSNs with low network bandwidth requirements.

Figure 7 shows the performances under various parameters of Gauss-Markov mobility model in terms of d_{avg} , v_{avg} , and β . With the growth of d_{avg} , the average growth rates of the three methods are 1.581%, 1.089%, and 0.744%, respectively; When v_{avg} boosts, the average growth rates of the three methods are 1.803%, 1.427%, and 1.082%, respectively; with the increase in β , the average growth rates of the three methods are 0.441%, 0.401%, and 0.211%, respectively. We can effortlessly note that the increase of model parameters has the greatest impact on TUM and the least impact on ITUM. By comparison, we can observe that the β is not the critical factor in the three parameters. The update operation of TUM is easily influenced by the number of fixed nodes within the sensing area and movement path of mobile node. TURIR triggers an update once the displacement of mobile node is higher than the fixed threshold value, and the displacement of mobile node is mainly ascertained by v_{avg} and d_{avg} , as presented in Figures 7(a) and 7(b). The trigger updating mode of ITUM can adjust to the movement path and circumvent unnecessary updates within high similarity messages according to the adaptive dynamic threshold. Moreover, due to the anisotropic sensing model of ITUM, the sensing area of nodes is susceptible to the influence of d_{avg} in mobility model, as shown in Figure 7(a).

From Figure 8, we can find that TUM and TURIR are both little affected by changes in information exchange rate H , as a result of the influence of timing updating mechanism and fixed threshold updating pattern, respectively. Specifically, the timing update mechanism applied by TUM has nothing to do with H , and the fixed threshold mode of TURIR is independent of H . The variation coefficients of the two methods are 0.308% and 0.415%, respectively. The number of information exchanges of ITUM is positively correlated with H , and its variation coefficient is 41.475%. It is



(a) Number of messages



(b) Number of data

FIGURE 6: Number of update messages and data of three methods varying interest message update interval.

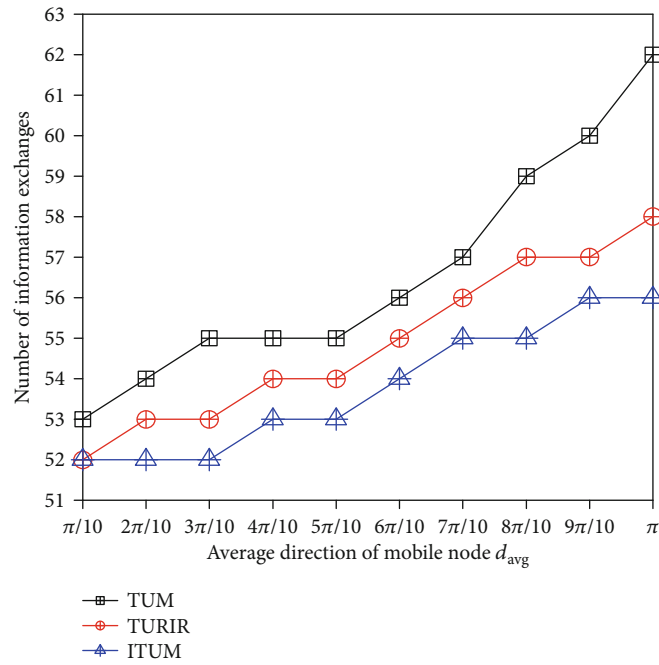
because the probability of triggering updating increases with the growth of H , resulting in the increment of number of information exchanges.

In Figure 9, we can note that m , H , and R have strong positive correlation with the number of information exchanges ($p < 0.05$). Although L , v_{avg} , and d_{avg} are also positively correlated with the number of information exchanges,

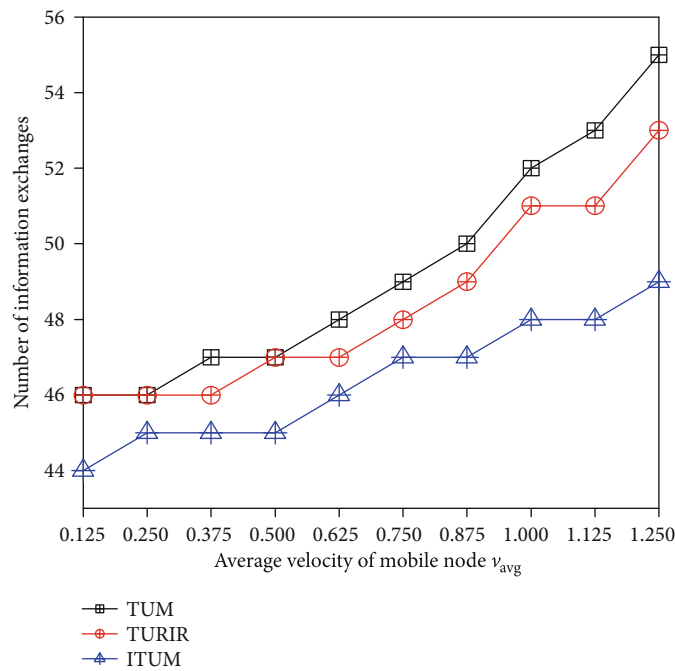
the correlation is weaker compared with m , H , and R . β has no concern with the number of information exchanges.

5. Conclusion

Energy efficiency is an essential concern in WSNs based on directed diffusion routing protocols. In this paper, after

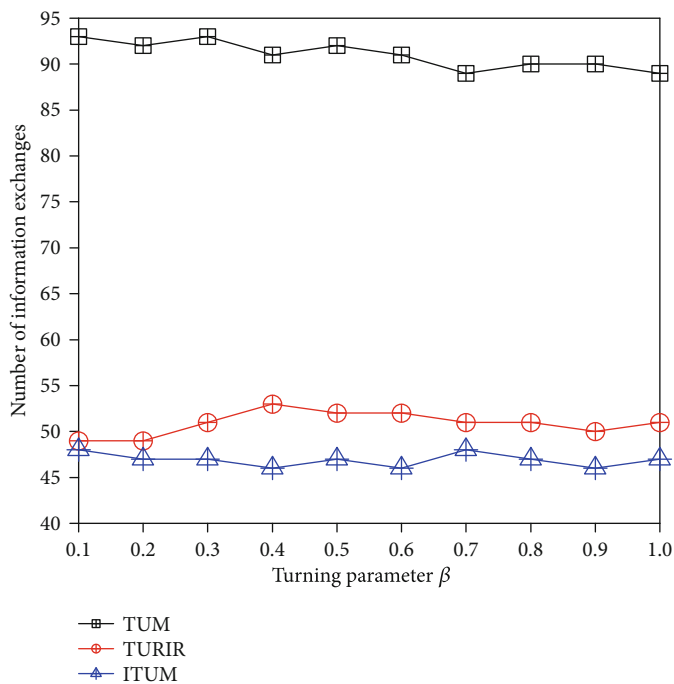


(a) Parameter d_{avg}



(b) Parameter v_{avg}

FIGURE 7: Continued.



(c) Parameter β

FIGURE 7: Number of information exchanges of three methods varying movement model parameters.

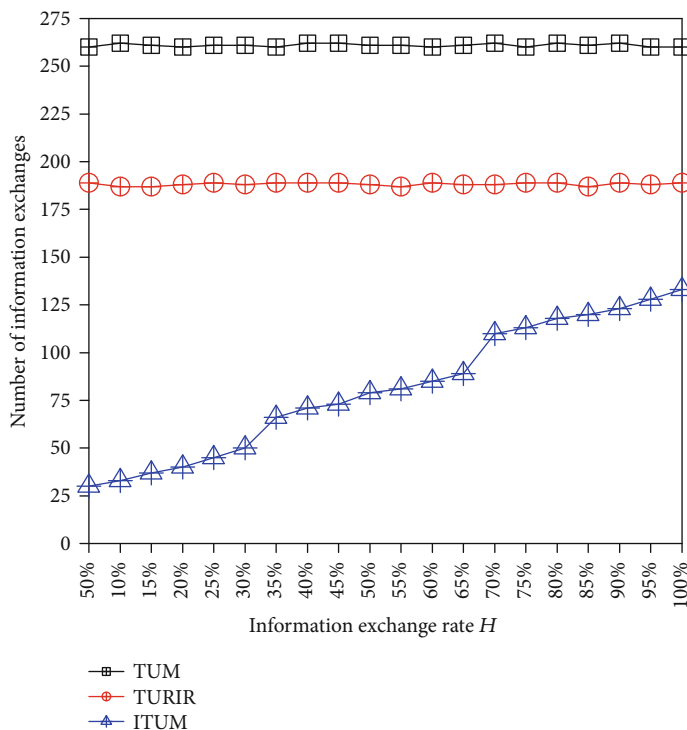
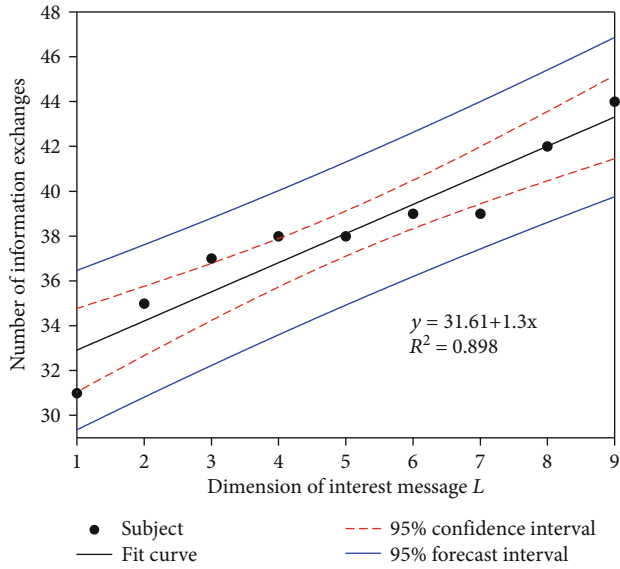


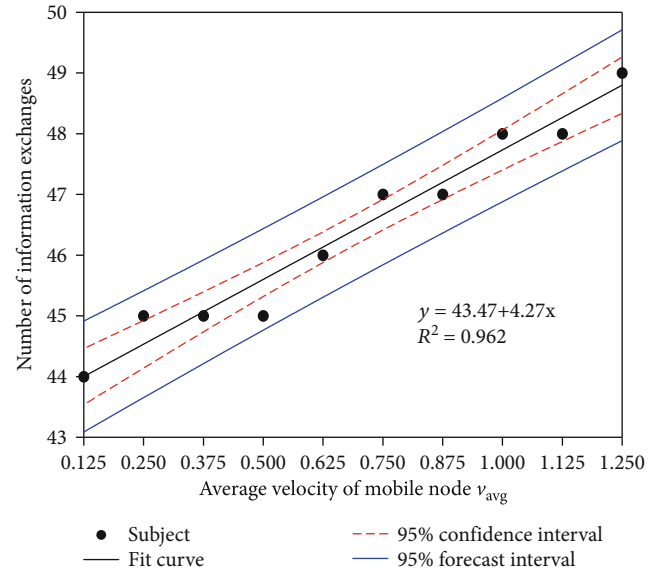
FIGURE 8: Relation between H and number of information exchanges in different methods.

defining the network model and the sensing model, we established an improved triggering updating method of interest message to reduce the number of information exchanges through threshold determination based on AHP and update judgement using similarity calculation. The most significant

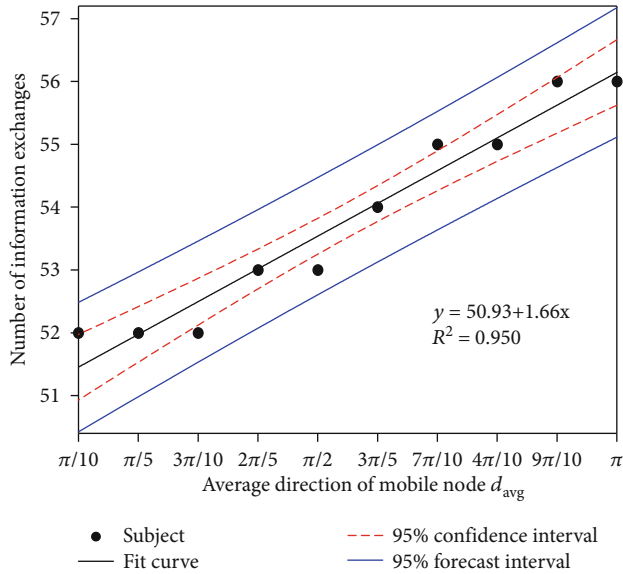
advantage of this method is that it can better adapt the requirement of information exchange rate, according to the triggering updating mechanism composed of dynamic hierarchical threshold adjustment and message similarity comparison. Besides, we analyzed the impact of key parameters



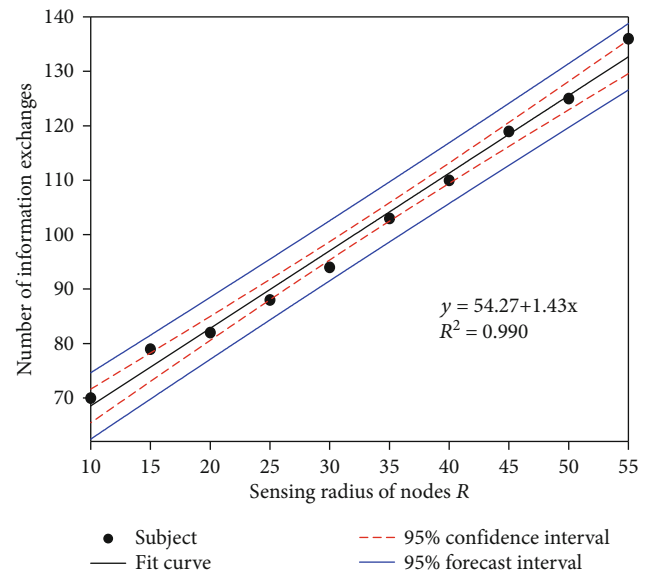
(a)



(b)



(c)



(d)

FIGURE 9: Continued.

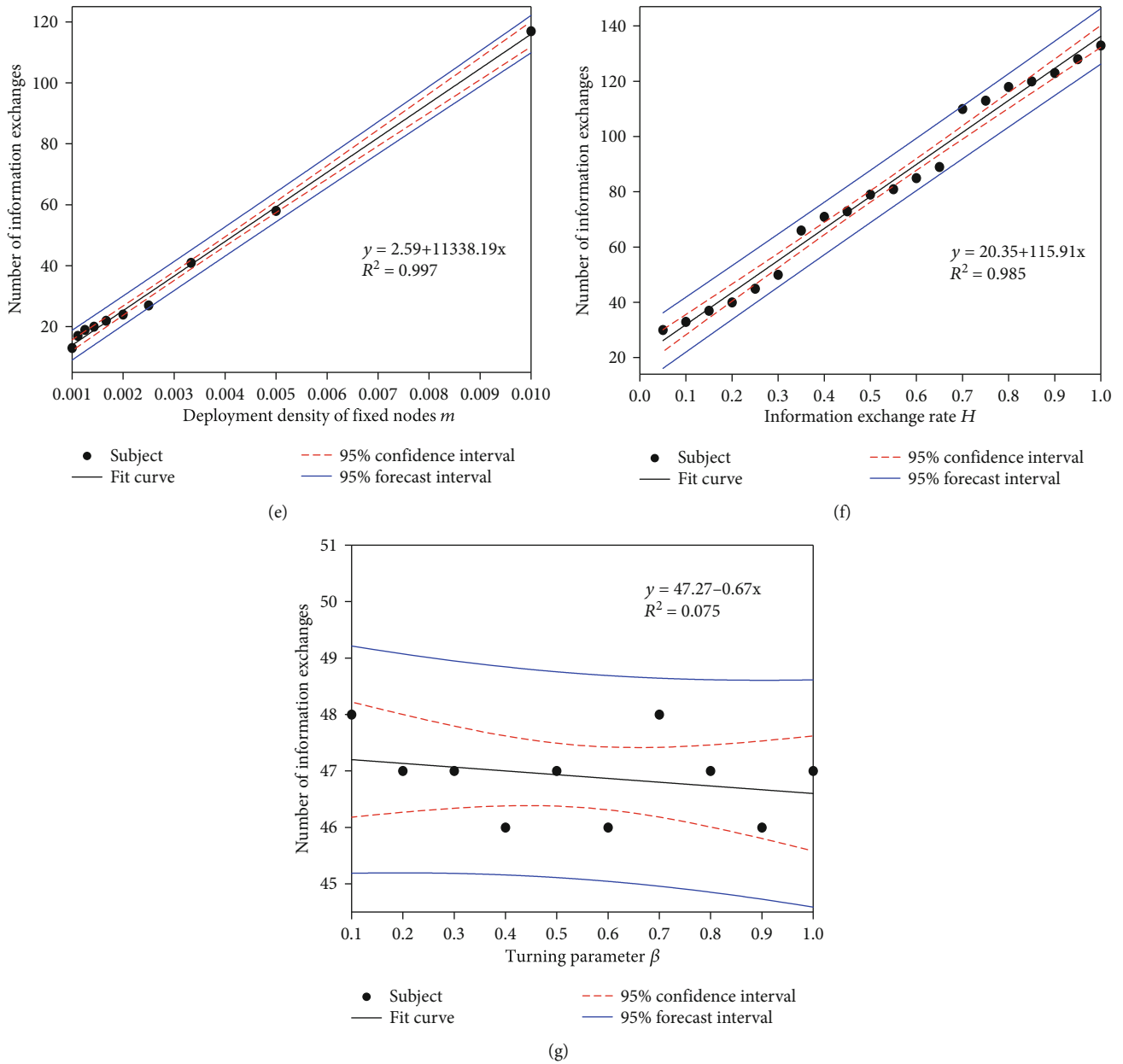


FIGURE 9: Linear correlation analysis of number of information exchanges and its influencing factors. (a–g) Represent linear relations between L , v_{avg} , d_{avg} , R , m , H , and β , respectively, and number of information exchanges.

and evaluated the performances of reducing update times with two interest message updating methods. The simulation results show that ITUM has a distinct advantage compared with the exiting interest message updating methods, and the proposed method can improve the adaptability to scene changes while lowering the number of information exchanges. Finally, other network constraints in real scenes, such as channel noise and packet loss, are not considered. It is this need in the next work to further test and improve the proposed method. Also, the paper provided the weight calculation method in threshold determination scheme is relatively complicated; in future works, the weight-decision method should be investigated to automatically get the recommended settings under the requirements imposed by a specific range of information exchange rates.

Data Availability

The authors declare that the data used to support the findings of this study are available from the corresponding author upon request.

Conflicts of Interest

The authors declared that they have no conflicts of interest to this work.

Acknowledgments

This work is supported by the National Natural Science Foundation of China (Grant no. 61771184), Program for

Science & Technology Innovation Talents in University of Henan Province (Grant no. 20HASTIT029), Program for Innovative Research Team (in Science and Technology) in University of Henan Province (Grant no. 19IRTSTHN021), and Science and Technology Major Project of Henan Province (Grant no. 181100110100).

References

- [1] R. Kolcun, D. E. Boyle, and J. A. McCann, "Efficient distributed query processing," *IEEE Transactions on Automation Science and Engineering*, vol. 13, no. 3, pp. 1–17, 2016.
- [2] S. G. El-Esawy, N. M. Elshennawy, and N. A. Elfishawy, "An improved energy-efficient directed diffusion routing protocol for wireless sensor network," in *2018 14th International Computer Engineering Conference (ICENCO)*, pp. 64–67, Cairo, Egypt, Egypt, December 2018.
- [3] M. M. Khaing and T. M. Naing, "Energy aware data-centric routing in wireless sensor network," in *International Conference on Advances in Engineering and Technology (ICAET'2014)*, pp. 80–83, Singapore, March 2014.
- [4] S. Kaushal, N. Gupta, and R. Sandhu, "Comparative study of flooded and directed diffusion protocol in WSN," *International Journal of Advanced Research in Electronics and Communication Engineering*, vol. 5, no. 5, pp. 1213–1218, 2016.
- [5] B. M. Mohammad el-Basioni, S. M. Abd el-kader, and H. S. Eissa, "Designing a local path repair algorithm for directed diffusion protocol," *Egyptian Informatics Journal*, vol. 13, no. 3, pp. 155–169, 2012.
- [6] Y. Miao and Z. Tan, "Directed diffusion routing protocol based on cluster-head path transformation in wireless sensor network," *Journal of Jilin University (Science Edition)*, vol. 55, no. 4, pp. 957–963, 2017.
- [7] M. Omar, S. Yahiaoui, and A. Bouabdallah, "Reliable and energy aware query-driven routing protocol for wireless sensor networks," *Annals of Telecommunications*, vol. 71, no. 1-2, pp. 73–85, 2016.
- [8] Y. Cui and H. Qin, "A novel rumor routing for wireless sensor network," in *2010 Fourth International Conference on Genetic and Evolutionary Computing*, pp. 795–797, Shenzhen, China, December, 2010.
- [9] J. N. Al-Karaki and A. E. Kamal, "Routing techniques in wireless sensor networks: a survey," *IEEE Wireless Communications*, vol. 11, no. 6, pp. 6–28, 2004.
- [10] L. García Villalba, A. Sandoval Orozco, A. Triviño Cabrera, and C. Barenco Abbas, "Routing protocols in wireless sensor networks," *Sensors*, vol. 9, no. 11, pp. 8399–8421, 2009.
- [11] S. Li, S. Duan, F. Li, and A. Liu, "An effective event query access strategy based on WSN," *Journal of Central South University (Science and Technology)*, vol. 45, no. 7, pp. 2223–2230, 2014.
- [12] K. P. K. Rao and K. Kalaiarasi, "Data-centric routing protocols in wireless sensor networks: a survey," *European Journal of Advances in Engineering and Technology*, vol. 2, no. 6, pp. 62–69, 2015.
- [13] K. A. Rasbi, H. Shaker, and Z. Sharef, "Survey on data-centric based routing protocols for wireless sensor networks," *International Journal of Electrical, Electronics and Computers*, vol. 2, no. 2, pp. 9–16, 2017.
- [14] C. Intanagonwiwat, R. Govindan, D. Estrin, F. Silva, and F. Silva, "Directed diffusion for wireless sensor networking," *IEEE/ACM Transactions on Networking*, vol. 11, no. 1, pp. 2–16, 2003.
- [15] J. Mu, X. Yi, X. Liu, and L. Han, "An efficient and reliable directed diffusion routing protocol in wireless body area networks," *IEEE Access*, vol. 7, pp. 58883–58892, 2019.
- [16] U. Rawat and M. Sharma, "Directed diffusion: features, current developments, issues and analysis," *International Journal of Computer Applications*, vol. 50, no. 12, pp. 31–35, 2012.
- [17] Y. Xu, Y. Yang, Y. Xin, and H. Zhu, "An improved directed diffusion protocol based on opportunistic routing," *Journal of Networks*, vol. 9, no. 5, pp. 1163–1168, 2014.
- [18] M. Chen, T. Kwon, and Y. Choi, "Energy-efficient differentiated directed diffusion (EDDD) in wireless sensor networks," *Computer Communications*, vol. 29, no. 2, pp. 231–245, 2006.
- [19] K. E. Kannammal and T. Purusothaman, "Performance of improved directed diffusion protocol for sensor networks under different mobility models," *Journal of Computer Science*, vol. 8, no. 5, pp. 694–700, 2012.
- [20] A. N. Eghbali and M. Dehghan, "Load-balancing using multipath directed diffusion in wireless sensor networks," *Mobile Ad-Hoc and Sensor Networks. MSN 2007*, H. Zhang, S. Olariu, J. Cao, and D. B. Johnson, Eds., pp. 44–55, Springer, Berlin, Heidelberg, Berlin, German, 2007.
- [21] Z. Li and H. Shi, "Design of gradient and node remaining energy constrained directed diffusion routing for WSN," in *2007 International Conference on Wireless Communications, Networking and Mobile Computing*, pp. 2600–2603, Shanghai, China, September 2007.
- [22] X. Liu, F. Li, H. Kuang, and X. Wu, "The study of directed diffusion routing protocol based on clustering for wireless sensor network," in *2006 6th World Congress on Intelligent Control and Automation*, pp. 5120–5124, Dalian, China, June 2006.
- [23] F. Semchedine, L. Bouallouche-Medjkoune, M. Tamert, F. Mahfoud, and D. Aïssani, "Load balancing mechanism for data-centric routing in wireless sensor networks," *Computers and Electrical Engineering*, vol. 41, pp. 395–406, 2015.
- [24] N. S. Samaras and F. S. Triantari, "On direct diffusion routing for wireless sensor networks," in *2016 Advances in Wireless and Optical Communications (RTUWO)*, pp. 89–94, Riga, Latvia, November 2016.
- [25] A. Merlo, M. Migliardi, D. Raso, and E. Spadacini, "Optimizing network energy consumption through intrusion prevention systems," in *International Joint Conference SOCO'14-CISIS'14-ICEUTE'14*, pp. 505–515, Bilbao, Spain, June 2014.
- [26] N. Mehta and N. V. Doohan, "An energy efficient approach for highly data-centric directed diffusion in wireless sensor networks," *International Journal of Electrical, Electronics and Computer Engineering*, vol. 1, no. 1, pp. 11–14, 2012.
- [27] J. Yu and H. Zhang, "Directed diffusion based on clustering and inquiry for wireless sensor networks," in *2010 3rd International Conference on Computer Science and Information Technology*, pp. 291–294, Chengdu, China, July 2010.
- [28] Y. Cui and J. Cao, "An improved directed diffusion for wireless sensor networks," in *2007 International Conference on Wireless Communications, Networking and Mobile Computing*, pp. 2380–2383, Shanghai, China, September 2007.
- [29] B. Krishnamachari and J. Ahn, "Optimizing data replication for expanding ring-based queries in wireless sensor networks," in *2006 4th International Symposium on Modeling and Optimization in Mobile, Ad Hoc and Wireless Networks*, pp. 1–10, Boston, USA, March 2006.

- [30] L. Niu, L. Liu, and Q. Xia, "TURIR: energy efficient interest message update protocol for mobile wireless sensor networks," *Chinese Journal of Sensors & Actuators*, vol. 22, no. 4, pp. 511–519, 2009.
- [31] G. Zhou, T. He, S. Krishnamurthy, and J. A. Stankovic, "Models and solutions for radio irregularity in wireless sensor networks," *ACM Transactions on Sensor Networks*, vol. 2, no. 2, pp. 221–262, 2006.
- [32] H. Saito, "Theoretical optimization of sensing area shape for target detection, barrier coverage, and path coverage," *IEICE Transactions on Communications*, vol. E99.B, no. 9, pp. 1967–1979, 2016.
- [33] A. Wei, F. Shao, and H. Meng, "The coverage-control optimization in sensor network subject to sensing area," *Computers and Mathematics with Applications*, vol. 57, no. 4, pp. 529–539, 2009.
- [34] T. L. Saaty, "How to make a decision: the analytic hierarchy process," *European Journal of Operational Research*, vol. 48, no. 1, pp. 9–26, 1990.
- [35] M. T. Mastura, S. M. Sapuan, and M. Noryani, "Material selection of natural fibers for composite automotive component using analytic hierarchy process/analytic network process in concurrent engineering approach," *Key Engineering Materials*, vol. 801, pp. 53–58, 2019.
- [36] R. M. Czekster, H. J. De Carvalho, G. Z. Kessler, L. M. Kipper, and T. Webber, "Decisor: a software tool to drive complex decisions with analytic hierarchy process," *International Journal of Information Technology and Decision Making*, vol. 18, no. 1, pp. 65–86, 2019.
- [37] J. Yuan and X. Liang, "Consistency improvement of judgment matrix in analytic hierarchy process," *Statistics & Decisions*, vol. 30, no. 12, pp. 15–17, 2014.
- [38] S. Huang and Q. Chen, "On clustering algorithm of high dimensional data based on similarity measurement," *Computer application and software*, vol. 26, no. 9, pp. 102–105, 2009.